HALOGEN-ELEMENT (F, Cl, AND Br) BEHAVIOUR IN APATITES, SCAPOLITE, AND SODALITE: AN EXPERIMENTAL INVESTIGATION WITH FIELD APPLICATIONS

A Thesis Submitted to the College of

Graduate Studies and Research

in Partial Fulfillment of the Requirements

for the Degree of Doctor of Philosophy

in the Department of Geological Sciences

University of Saskatchewan

Saskatoon

By

Ping Dong

© Copyright Ping Dong, August, 2005. All Rights Reserved

Permission to use

In presenting this thesis in partial fulfillment of the requirements for a Postgraduate degree from the University of Saskatchewan, I agree that the Libraries of this University may make it freely available for inspection. I further agree that permission for copying of this thesis in any manner, in whole or in part, for scholarly purposes may be granted by the professor or professors who supervised my thesis work or, in their absence, by the Head of the Department or the Dean of the College in which my thesis work was done. It is understood that any copying or publication or use of this thesis or parts thereof for financial gain shall not be allowed without my written permission. It is also understood that due recognition shall be given to me and to the University of Saskatchewan in any scholarly use which may be made of any material in my thesis.

Requests for permission to copy or to make other use of material in this thesis in whole or part should be addressed to:

Head of the Department of Geological Sciences
University of Saskatchewan
114 Science Place
Saskatoon, Saskatchewan
Canada S7N 5E2

Abstract

Halogens (F, Cl, Br, and I) are common constituents in igneous, metamorphic, and sedimentary rocks, and are particularly important in the transport of many ore-forming metals. Detailed knowledge about the abundance of halogens in melts/fluids and minerals can help to interpret many geological processes. However, most hydrothermal fluids and melts cannot be directly sampled. Halogen-bearing minerals, such as apatites, scapolite and sodalite, can provide reliable information about the halogen concentrations in their parental fluids/melts provided that the partition coefficients between those minerals and fluids/melts are known.

This is the first systematic experimental investigation of partitioning of Br between apatites and coexisting melts and the uptake of Br by scapolite and sodalite. Twenty-nine partitioning experiments between fluorapatite (FAP) /chlorapatite (ClAP) and coexisting melts were conducted in the system of CaO-P_2O_5-CaF_2-$CaCl_2$–NaBr at 1120°C to 1400°C and atmospheric pressure. The partition coefficients (D) with errors of 1δ in parentheses are as follow:

$D^{F}_{ClAP/melt}$	3.59(64)	at 1120 °C	to 4.13(22)	at 1330 °C
$D^{F}_{FAP/melt}$	1.05(4)	at 1220 °C	to 1.07	at 1400 °C
$D^{Cl}_{ClAP/melt}$	1.07(1)	at 1120 °C	to 0.83	at 1330 °C
$D^{Cl}_{FAP/melt}$	0.127(2)	at 1250 °C	to 0.115	at 1400 °C
$D^{Br}_{ClAP/melt}$	0.32(9)	at 1120 °C	to 0.42(5)	at 1330 °C
$D^{Br}_{FAP/melt}$	0.020(3)	at 1220 °C	to 0.016	at 1400 °C

Seven exchange experiments at one atmospheric pressure and 800 to 1000 °C yield the following distribution coefficients for Br-Cl exchanges between marialitic scapolite or sodalite and coexisting hydrous NaCl-NaBr melts: $K_D^{marialite\text{-}melt} = 0.92\pm0.10$ and $K_D^{sodalite\text{-}melt} = 1.18\pm0.10$. Therefore, the Cl/Br values in marialitic scapolite and sodalite closely reflect the halogen proportions of their coexisting melts or fluids.

The second part of this thesis project analyzes the halogen (F, Cl, Br) contents in natural fluorapatite and scapolite by X-ray fluorescence microprobe (XRF) for Br and electron microprobe (EMPA) for other elements. All selected localities and environments are interesting, because the origins of the parental fluids/melts are controversial. The halogen compositions of 29 natural apatite grains from the Aoshan fluorapatite-magnetite deposit (China), the Oka carbonatite complex (Quebec), and Chinese mantle xenoliths and 36 scapolite samples from the Tieshan Fe-Cu skarn deposit (China), the Nickel Plate gold deposit (British Columbia), and the Grenville pegmatite/skarn/vein deposits (Ontario and Quebec) have been analyzed by electron microprobe (EMPA) and

X-ray fluorescence microprobe (XRF). Twenty six whole-rock samples from the Aoshan deposit have also been analyzed by XRF for major and trace elements.

Fluorapatite from the Aoshan fluorapatite-magnetite deposit is Cl-bearing with 0.38-0.98 wt% Cl, 1.83-3.45 wt% F, and 0-52 ppm Br. Fluorapatite from Chinese mantle xenoliths has similar halogen compositions to the Aoshan fluorapatite. Fluorapatite from the Oka carbonatite has trace amounts of chlorine (up to 0.052 wt%) and bromine (from 9 to 57 ppm). Applications for the experimental results suggest that the Aoshan Fe-Cu deposit has Cl/Br values comparable to those of mantle sources and that the anomalously low Cl/Br values in Oka fluorapatite require Br-enriched sources.

The Cl/Br values (weight) of marialitic scapolite from the Tieshan Fe-Cu deposit cluster around 626±92, supporting an origin involving hydrothermal brines from associated evaporites. Scapolite-group minerals in the exoskarns of the Nickel Plate Au skarn deposit have Cl/Br from 560 to 570, higher than those (110 to 180) of their counterparts in the endoskarns and vuggy cavities. This variation is attributable to an increased involvement of magmatic water from distal to proximal zones. Similarly, scapolite-group minerals in the Grenvillian U-Th-Mo-REE pegmatite-skarn-vein deposits vary widely in Cl/Br from 80 to 380, indicative of mixed sources of hydrothermal fluids from magmatic sources and from associated sedimentary rocks.

The experimentally determined partition coefficients of halogens between minerals (apatites, scapolite, and sodalite) and fluids/melts of this

study have wide applications in the interpretation of source and evolution of hydrothermal fluids in mineralization processes and other geological systems. Applications of those partition coefficients to selected mineral deposits and mantle xenoliths confirm their significance.

Acknowledgements

It is my pleasure to gratefully acknowledge the guidance, encouragement, and patience of my supervisor, Dr. Yuanming Pan. Sincere thanks to all the members of my advisory committee for constructive advice and patience (Drs. Kevin Ansdell, Jim Basinger, Robert Kerrich, Doug Milne, Steve Reid, and Mel Stauffer). Dr. D. Lentz (external examiner) is greatly appreciated for valuable suggestions and comments. Special thanks are extended to the technical staff, Tom Bonli, Blaine Novakovski, and Lloyd Litwin, at the Department of Geological Sciences, University of Saskatchewan.

Grenvillian scapolite separates were kindly supplied by Dr. D. Lentz, Department of Geology, University of New Brunswick and apatites from Chinese mantle xenoliths were provided by Prof. Jianping, Zheng of Chinese University of Geosciences at Wuhan, Hubei, China.

This thesis was partly supported by a Natural Sciences and Engineering Research Council (NSERC) grant to Dr. Pan, an University of Saskatchewan graduate scholarship and graduate teaching fellowship.

I also would like to thank my friend, Peter Fehr, for proof reading of thesis draft, my wife, Jian Liu, and my son, Anqi, for their understanding and support.

Table of Contents

List of Figures

List of Tables

1. Introduction

In this Ph.D. thesis project, the distribution characteristics of halogens, especially F, Cl, and Br in apatites, scapolite, and sodalite, have been investigated. The first major part of this project investigates the partitioning of halogen elements between these mineral phases and coexisting melts/fluids by well-constrained laboratory experiments. Twenty-nine synthetic experiments have been successfully executed in the CaO-P_2O_5-CaF_2-$CaCl_2$–NaBr system at 1120 to 1400 °C and atmospheric pressure. The partition coefficients of F, Cl, and Br between fluorapatite/chlorapatite and coexisting melts have been determined, and results are interpreted. Seven exchange experiments have been carried out to investigate the Br distribution characteristics between scapolite/sodalite and coexisting hydrous NaCl-NaBr melts.

The second part of this thesis project analyzes the halogen (F, Cl, Br) contents in natural apatite and scapolite by X-ray fluorescence microprobe (XRF) for Br and electron microprobe (EMPA) for other elements. All selected localities and environments are interesting, because the origins of the parental fluids/melts are controversial: 1) twenty-two fluorapatite-bearing samples from the Aoshan fluorapatite-magnetite deposits, Middle-Lower Changjiang metallogenic belt (MLCMB), China; 2) five apatite separates from the Oka carbonatite complex, Quebec, Canada; 3) two apatite separates from mantle xenoliths in alkaline basalt and kimberlite from China; 4) seventeen scapolite-

bearing samples from the Tieshan Fe-Cu skarn deposit, MLCMB, China; 5) five scapolite-bearing samples from the Nickel Plate gold deposit, British Columbia, Canada; 6) fourteen separates of scapolite from Grenville pegmatite/skarn/vein deposits, Quebec and Ontario, Canada. The halogen contents in those mineral samples are then interpreted in light of the new experimental data.

Halogens (F, Cl, Br, and I) are common constituents in igneous, metamorphic, and sedimentary rocks, and are particularly important in the transport of many ore-forming metals, e.g., gold and copper in hydrothermal fluids. Chlorine is a dominant complexing agent for ore metals such as Au, Ag, Cu, Fe, Mn, Pb, Zn, Sn, and REE, in magmatic-hydrothermal systems. The Cl concentration of fluids in granitic magmas is known to strongly affect the solubility of Fe, Mg, Mn, alkali, and alkaline earth elements in the fluids (Webster and Holloway, 1988 and reference therein).

The importance of halogens in metal transport through the formation of aqueous metal halide complexes in magmatism and metasomatism has led to considerable effort to establish the halide contents in magmas, source rocks as well as hydrothermal fluids associated with magmatic, metamorphic, and ore-forming processes (Zhu and Sverjensky 1991; and reference herein). Detailed knowledge about the abundance of halogens in hydrothermal fluids and minerals can help to reconstruct paleo-environments (e.g., compositions of ancient seawaters; Channer et al., 1997), to deduce the sources and evolution of hydrothermal fluids, and to provide constraints on the petrogenesis of magmatic, metamorphic, and sedimentary processes. Moreover, Markl and

Paizolo (1998) had indicated that halogens may be used to infer the direction of fluid flow. The halogen abundances in the mantle may provide information about the origin and evolution of Earth and other planets.

However, most hydrothermal fluids cannot be directly sampled and analyzed, except for those from a few low-temperature and low-pressure sources such as modern geothermal fluids, hot springs, and oilfield brines. To date, the most useful data of halogen composition of hydrothermal fluids come from the studies of fluid inclusions in minerals, but this kind of data is ambiguous due to the multicomponent nature of the systems and multiple generations of inclusions (Zhu and Sverjensky 1991).

Direct determination of halogen abundances in the mantle is impossible at present. Conventional attempts are through the analysis of halogens from mantle materials, such as diamond (Turner et al., 1990; Johnson et al., 2000; Burgesss et al., 2002; and reference herein) and Mid Ocean Ridge basalts (MORB; Schilling et al., 1980; Deruelle et al., 1992; Jambon et al., 1995). But halogens in the MORB are highly variable due to contamination with seawater and fractionation during shallow magma degassing (Jambon et al., 1995; Villemant and Boudon, 1999).

The direct determination of volatile components (e.g., F, Cl, Br, etc.) in magmas before eruption is also difficult, because they easily escape from the magma through degassing during intrusion and eruption. Consequently, the concentrations of volatiles in solid igneous rocks are usually different from the primary contents of these components in their parental melts.

Fortunately, volatile components, such as F and Cl, can form their own mineral phases, e.g., fluorite and halite, or are dispersed in various rock-forming minerals, e.g., apatite, scapolite, sodalite, biotite, and amphibole. These volatile-bearing minerals can then provide more reliable information about the halogen concentrations in parental melts provided that the partition coefficients between those minerals and melts are known (Bushlyakov, 2000). Similarly, the halide concentrations in hydrothermal fluids can be estimated from the halogen contents of coexisting minerals, if the partition coefficients of halogens between minerals and fluids are known.

Apatite is a common accessory mineral group in almost all geological environments from igneous, metamorphic, and sedimentary rocks to biomass, soils, and extraterrestrial materials (Fleet and Pan, 1997). It also can be accumulated to high concentrations in cumulates and other rocks such as nelsonites (Piccoli and Candela, 2002). In addition, apatite is abundant in some mineral deposits (e.g., the Kiruna-type high-phosphorous Fe deposits; Hildebrand, 1986; Nystrom and Henriquez, 1994; and references therein); the Middle-Lower Changjiang Cu-Fe-Au deposits of China; Pan and Dong, 1999).

Fluorapatite is the most common member in the igneous systems, where it commonly contains minor amounts of chlorine, hydroxyl, and carbonate. Other halogens (Br and I) are also present in apatite, but at much lower concentrations compared to Cl and F (Pan and Fleet, 2003).

Importantly, igneous apatite is stable and is known to retain its original compositional character (e.g., the halogens) during subsequent low-grade

metamorphism and/or hydrothermal alteration. For example, studies of magmatic apatite and biotite demonstrate that consistently high Cl contents occur in apatite from Cu-mineralized intrusions, whereas the Cl content in biotite is much more variable, apparently due to post-magmatic alteration (Roegge et al., 1974; Candela, 1986).

Scapolite is another major halogen-bearing mineral group; most has formed during hydrothermal alteration, metasomatism, and metamorphism. It has a wide field of stability (Goldsmith and Newton, 1977; Pan and Fleet, 1994 and references herein) and has been suggested to be an important host for Cl, CO_2, and SO_3 in the lower crust and upper mantle (Lovering and White, 1964; Goldsmith and Newton, 1977).

The common occurrence of scapolite in some metasedimentary rocks (e.g., Mora and Valley, 1989; Moecher and Essene, 1990; Oliver et al., 1992) is controlled by layers that may have originally contained halite/evaporite (e.g., the Wallace Formation, northwest of the Idaho batholith; Mora and Valley, 1989). Scapolite is also a common mineral in a variety of ore deposits related to Ca-enriched metamorphic/metasomatic processes, especially in skarn deposits, such as calcic and magnesian iron skarn deposits (Sangster, 1969; Ettinger and Ray, 1988; Webster and Ray, 1990; Podlessky et al., 1991; Ettinger et al., 1992; Pan and Dong, 1999) and gold skarn deposits (Ettlinger et al., 1992; Pan and Fleet, 1994; Pan, 1998). Scapolite has also been reported to occur in some tungsten skarn deposits (Lowell, 1991), molybdenum skarn deposits (Webster et al., 1992), and uranium and REE-bearing skarn deposits

related to radioactive pegmatites (Shaw, 1960; Shaw et al., 1963, 1982; Lentz, 1991, 1992, 1998). In addition, scapolite has been documented in skarn-like alteration assemblages associated with porphyry copper deposits (Hodgson et al., 1976).

Numerous experiments have been carried out to investigate the stability and composition of scapolite in hydrothermal systems, including partitioning of Cl, CO_2, and SO_3 between scapolite and coexisting fluids (e.g., Orville, 1975; Goldsmith and Newton, 1977; Ellis, 1978; Vanko and Bishop, 1982; Aitken, 1983; etc.). These experimental results have been applied to studies of metamorphism and mineral deposits (e.g., Mora and Valley, 1989; Moecher and Essene, 1990, 1991; Oliver et al., 1992).

Therefore, apatite and scapolite are two important sinks of fluorine and chlorine in various geological environments, and have long been used as indicators of volatile fugacities in magmatic, metamorphic, and hydrothermal systems (Korzhinskiy, 1981; Zhu and Sverjensky, 1992; Pan, 1998). Similarly, bromine is expected to be elevated in apatite and scapolite. But this has not been well documented and only limited attention had been paid to bromine in apatite (Ionov et al., 1997; O'Reilly and Griffin, 2000) and there is no information about bromine in scapolite.

Sodalite is a chlorine-bearing, rock-forming mineral in silica undersaturated rocks, such as nepheline syenites or phonolites. It is associated with calcite, cancrinite, and other silica-deficient minerals, such as nepheline and leucite.

The experimentally determined partition coefficients of halogens between minerals (apatites, scapolites, and sodalites) and fluids/melts of this study have been applied to interprete the source and evolution of hydrothermal fluids in selected mineral deposits and mantle xenoliths, and their significances are confirmed.

The approximate time spent for preparation of synthetic and exchange experiments (more than 45 experiments), mineral crystal separation, and XRF and EMPA analyses for both synthetic minerals and natural minerals (more than 65 natural samples) is about 2,100 hours.

This thesis research produced two abstracts in national conferences and four manuscripts for publication in refereed international journals (two already published and two in preparation; see below). In addition, I participated in the early stages of laboratory experiments on the partitioning of rare-earth elements between fluorapatite and melts, which appeared in a paper entitled "Non-Henry's law behavior of REE partitioning between fluorapatite and CaF_2-rich melts; controls of intrinsic vacancies and implications for natural apatites" (Pan, Dong, and Chen 2003). This study discovered a non-Henry's Law behavior of rare-earth-element (REE) partitioning between fluorapatite and CaF_2-rich melts at low REE concentrations and provided the first structural evidence for intrinsic Ca^{2+} vacancies as a cause of this behavior. The partition coefficients are shown to be important in understanding the REE geochemistry in natural apatites. However, I did not participate in either the data analysis or the manuscript preparation and, therefore, did not include the results of this

paper in my thesis. Details of my contributions to the two conference abstracts, two published papers in refereed journals, and two manuscripts in preparation are discussed below.

Yangzi-type Cu-Fe-Au deposits in eastern China; complex exhalative-porphyry-skarn systems (Dong and Pan, 1998, Program with Abstracts - Geological Association of Canada, Mineralogical Association of Canada, Canadian Geophysical Union, Joint Annual Meeting Vol. 23, A47) is an overview of a major metallogenic belt in China, based on Chinese literature and my own field observations and geochemical analyses.

The Lower Changjiang (Yangzi/ Yangtze River) metallogenic belt, east central China; intrusion- and wall rock-hosted Cu-Fe-Au, Mo, Zn, Pb, Ag deposits (Pan and Dong, 1999, Ore Geology Reviews 15, 177-242) provided a comprehensive review and proposed a genetic model for more than 200 mineral deposits in the Lower Changjiang metallogenic belt in China. The author did field works for two summers and compiled Chinese literature data. Dr. Pan noted the similarities between these Chinese deposits and those in western USA and Mexico and wrote the manuscript. Parts of this paper (i.e., Geological background) appear in Chapter 7.

F-Cl-Br partitioning in apatite: experimental studies and applications (Dong and Pan, 2002, Program with Abstracts - Geological Association of Canada, Mineralogical Association of Canada Joint Annual Meeting Vol. 27, P. 29) is a summary of my experimental results on the partitioning of F, Cl, and Br between apatites and melts. Results are included in Chapters 5 and 7, and are

being reorganized into a manuscript for publication in a refereed journal (see below).

Bromine in scapolite-group minerals and sodalite; XRF microprobe analysis, exchange experiments, and application to skarn deposits (Pan and Dong, 2003, Canadian Mineralogist 41, 529-540) reports on: 1) an evaluation of XRF microprobe for *in situ* analysis of Br in Cl-rich minerals, 2) experimental determination of the uptake of Br by scapolite and sodalite, and 3) application of experimental results to skarn deposits. I participated in the exchange experiments, carried out all Br analyses by XRF microprobe, and participated in data analysis and manuscript preparation. Results of this paper appear in Chapters 6 and 7.

F-Cl-Br partitioning between apatites and melts: experimental results and applications (Dong and Pan, in preparation). For explanation see Dong and Pan (2002) above.

Halogen compositions of fluorapatite in the Aoshan fluorapatite-magnetite deposit, Anhui, China (Dong and Pan, in preparation) constraints on the sources and composition of mineralization fluids. Comprehensive analyses (whole-rock X-ray fluorescence, X-ray fluorescence microprobe, and electron microprobe) have been made on fluorapatite and host lithologies from the Aoshan fluorapatite-magnetite deposit. The halogen compositions of fluorapatite and host rocks are used to constrain the sources and composition of mineralization fluids in this deposit. Results of this manuscript appear in Chapter 7.

2. Review on Halogens in Geological Environments

2.1 Chemical Properties of Halogen Elements

Halogen elements including F, Cl, Br, and I have similar structures of their outer electron shell, $(n\text{-}1)d^{10}\ ns^2\ np^5$. This electron configuration, just one electron short of the corresponding noble gas configuration, causes the halogen atoms to be powerful electron-acceptors, with electron affinities higher than those known for any other atomic species and exceptionally high electronegativity values (Table 2.1).

2.2 Literature Data of Halogens in Geological Samples

A large proportion of halogen elements are presently trapped at the Earth's surface, as the ocean is the biggest reservoir of Cl and Br, and modern sediments are the biggest reservoirs for I. Tables 2.2 and 2.3 summarize available data on the halogen contents in water and rock samples. Table 2.4 gives some analytical results of halogens in fluid inclusions from quartz and galena of hydrothermal deposits including the Mississippi Valley Type Pb-Zn deposits (MVT) of the USA.

Table 2.1 Chemical properties of halogen elements and some other common ionic species

(Data from Huheey, 1978)

Element	F	Cl	Br	I	O^{2-}	S^{2-}	OH^{-}	As
Effective ionic radius (pm)*	119	167	182	206	126	170	123	60
Ionization energy**	1.681	1.2511	1.1394	1.0084	1.314	0.9996	-	0.944
Electron affinity ***	322	348.7	324.5	295	141	200.4	177	77
Electro-negativity****	3.90	2.95	2.62	2.52	3.04	2.28	2.3-3.9	1.59

*The effective ionic radius is for six-fold coordination

** MJ mol^{-1}

*** KJ mol^{-1}

**** Pauling units

Table 2.2 Average halogen contents in some fluids (ppm)

Fluid type and description	F	Cl	Br	I	References
Spring, Yellowstone N. Park, WY	25	405	1.5	0.3	Brownlaw, 1979
River and lake water	<1	7.8	0.02	2	Henderson, 1982
Brine from Salton Sea	15	155000	120	18	Henderson, 1983
Seawater	1.3	19400	67	0.06	Henderson, 1984
Ocean water	1.4	19000	65	0.05	Yasushi, 1975
Oil-field brine	0.6-1.8	4960-93900	16-817	10-35	Yasushi, 1975
Volcanic hot spring	1.5-21.5	307-2430	0.1-0.8	0.1	Yasushi, 1975
Thermal/connate/metamorphic water	0.4-8.0	58-11800	15-78	0.7-39	Yasushi, 1975

Muramatsu and Wedepohl (1998) analyzed a large series of samples representing the major units and subunits of the Earth's crust using the Inductively Coupled Plasma Mass Spectrometry (ICP-MS) technique. Their results show that crustal iodine is greatly concentrated in the sedimentary shell of the Earth (Table 2.3).

In sedimentary environments, bromine and iodine are commonly associated with organic materials. In fresh-water lakes, bromide accumulates in mud, and the concentration is normally proportional to that of the organic-matter. Martin et al. (1993) also showed that organic-bearing argillaceous sediments contain more iodine than red clays and calcareous sediments. Bromine and iodine contents in sediments generally decrease with increasing depth of burial, due to more complete decomposition of organic bromine and iodine compounds and the release of Br and I into pore fluids (Table 2.5). Processes such as trapping of pore fluids in thick, organic-rich sediments can lead to extreme Br and I enrichment (Martin et al., 1993; Channer et al., 1997).

Table 2.3 Average halogen contents in some igneous and sedimentary rocks

Rock type and description	F (ppm)	Cl (ppm)	Br (ppm)	I (ppb)	References
Alkali basalt		171	0.5	29	Shinonaga et al., 1994
Tholeiitic basalt		302	0.8	59	Shinonaga et al., 1994
Augite-hypersthene andesite		44	0.41		Shinonaga et al., 1994
Olivine andesite		29	0.336		Shinonaga et al., 1994
Obsidian		992	2.3	75	Shinonaga et al., 1994
Rhyolite		1000	2.2	72	Shinonaga et al., 1994
Peridotite (dunite)		84	0.29	86	Shinonaga et al., 1994
Gabbro		68	0.28	74	Shinonaga et al., 1994
Biotite granodiorite		56	0.073	10	Shinonaga et al., 1994
Biotite granite		44	0.17	32	Shinonaga et al., 1994
Granite		421	2.92		Shinonaga et al., 1994
Average of igneous rocks	700	314	1.6	300	Yasushi, 1975
Granite, granodiorite, basalt				4-9	Muramatsu and Wedepohl, 1998
Shales, carbonates				260-6150	
Shales	740	180	4	2.2	Mason, 1966
Sandstones	270	10	1	1.7	Mason, 1966
Carbonates	330	150	6	1.2	Mason, 1966
Primitive mantle	25	17	0.05	0.010	McDonough and Sun, 1995
CI carbonaceous chondrites	60	680	3.57	0.450	
Lithosphere		180	2.5	0.5	Taylor, 1964
Solar system		704	3.57	0.433	Anders and Grevesse, 1989

Chlorine commonly substitutes for F or OH in mineral lattices (e.g., apatite and biotite). By analogy, bromine may substitute for F or OH as well as Cl in mineral lattices. However, iodine, which is considerably larger than Cl

Table 2.4 Halogen contents in some fluid inclusions from quartz and galena (ppm)

Minerals	Sample Description	F	Cl	Br	I	References
Quartz	Quartz-Au vein	208-586	18276-21389	70-104	0.16-4.78	Yardley et al., 1993
Quartz	Metamorphic hematite-quartz vein	3581-6523	6035-20853	68-251		Boiron et al., 1999
Quartz	Metamorphic sulfide-quartz vein	944	15047	195		Boiron et al., 1999
Quartz	Archean hydrothermal Fe-oxide deposits		26871	193	7.49	Channer et al., 1997
Galena	MVT deposits from the Viburnum Trend		0.653-808	0.002-1.75		Crocetti & Holland, 1989

Table 2.5 Bromine and iodine in recent shelf and slope sediments and pore fluids (data from Channer et al., 1997)

Depth (m)	Sediments (ppm)		Pore fluids (*u* M)	
	Br	I	Br	I
Slope				
0-10	121	123	780	15
30-40	79	94	1170	356
80-90	79	109	1340	487
140-190	79	101	1360	548
190-270	4	35	1365	433
300-330	7	43	1485	478
330-380	92	68	1860	890
380-400	45	44	1760	830
430-460	9	10	1910	740
Shelf				
0-10	61	62	390	8
10-30	74	84	365	5
30-50	88	108	947	449
70-90	2	17	683	217
90-110	3	18	1060	90
160-170	18	7	1110	34
260-270	17	8	1200	41

(Table 2.1) may not easily replace F or OH in common silicates, and is probably bonded on crystal surfaces and defects or in fluid inclusions (Correns, 1956; Fuge and Johnson, 1986). The halogen contents in igneous rocks are well correlated for Cl and Br, but less for Cl and I. For example, bromine correlates well with chlorine in Mid Ocean Ridge Basalt (MORB) glasses at a constant Cl/Br value of 430 ± 130 (1σ) over the full range of Br concentration from 62 to 1320 ppb. This ratio is independent of Cl abundance or basalt type (Jambon et al., 1995).

2.3 Review of Previous Work

2.3.1 General Research about Halogens in Geological Processes

Chlorine and bromine partition strongly into aqueous fluids compared to solid phases. Therefore, minerals that concentrate Cl and Br, e.g., apatite, scapolite, and sodalite, may be particularly sensitive indicators of fluid-rock interactions, fluid compositions, and fluid origin.

Halogens in Hydrothermal Systems

Fluid inclusions trapped in minerals are widely used to study the origin and composition of hydrothermal fluids from which the host minerals precipitated. The typical analytical method used to determine the compositions of fluid inclusions in minerals is that the fluid inclusions are released by crushing, and then analyzed. This methodology cannot be used to measure the

amount of water in the fluid inclusions nor the total dissolved solutes in the fluid inclusions. Therefore, the ions in the fluid inclusions are reported as molar ratios.

Irwin and Roedder (1995) investigated fluid inclusions in three quartz vein samples in a potassic zone from the Bingham porphyry copper deposit, Bingham Canyon, Utah, by use of the laser ablation ICP-MS technique. Two of their samples have a range of Br/Cl values from 1.01×10^{-3} to 1.97×10^{-3} (M), with mean values of 1.2×10^{-3} and 1.4×10^{-3} (M), respectively. The third sample has higher Br/Cl values from 1.7×10^{-3} to 3.9×10^{-3} (M) with a mean of 2.5×10^{-3} (M). Kendrick et al. (2001) reported variable Br/Cl values from 0.5×10^{-3} to 1.5×10^{-3} (M) with a mean of 1.1×10^{-3} (M) of fluid inclusions from Bingham quartz vein samples, which are close to those of Irwin and Roedder's (1995) first two samples.

Most brines are formed by evaporation of seawater or dissolution of marine evaporites. These processes produce flluids which fall along various trends on Na/Br-Cl/Br plots (Figure 2.1). So the Na-Cl-Br compositions provide a simple way to discriminate different sources of brines (Kesler et al., 1995).

Comparison of the Cl/Br and Na/Br values obtained from geological samples with those observed during seawater evaporation was used to determine whether solutes in the fluids were derived from evaporited seawater or dissolution of halite (Figure 2.1). The comparison of Cl/Br with Ca/Cl, Mg/Cl, (Ca+Mg)/Cl, K/Cl, etc., has also been used to identify fluid-rock reactions, such

as dolomitization of limestone, albitization of plagioclase, and reactions with K-silicates, clays, and organic matter.

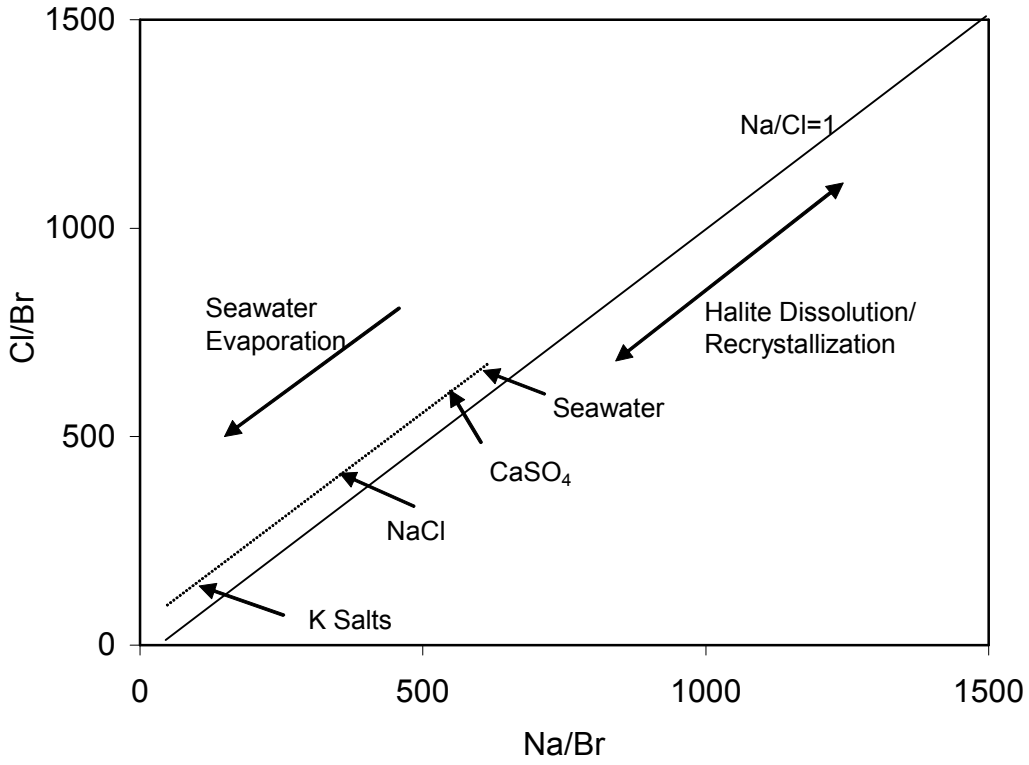

Figure 2.1 Cl/Br VS Na/Br molar ratios of fluids. The most left under arrow indicates the direction of Cl/Br and Na/Br change as sea-water evaporates and precipitates evaporite minerals along the dashed line. The long right arrows indicate the Cl/Br and Na/Br ratios of fluids with dissolved halite or recrystallized halite. The short arrows mark the point of the first appearance of evaporite minerals (after Viets et al., 1996)

The characteristics of dissolved halide chemistry of fluid inclusions have been widely applied to the study of Mississippi Valley type (MVT) Pb-Zn deposits to obtain information on the sources of solutes in the ore-forming brines, to evaluate the brine evolution processes, and to establish genetic linkages among different deposits (Viets et al., 1996; Nesbitt and Prochaska, 1998). The high salinities of MVT fluids were thought to be derived mainly from evaporited seawater sources (Crocetti and Holland, 1989; Viets et al., 1996), and the values of Cl/Br and other solutes can indicate the origin of the ore-forming fluids (Viets et al., 1996).

Appel (1997) reported anomalously high concentrations of Br (up to 418 ppm) in stratabound scheelite mineralization in Archean greenstone belts of West Greenland. These stratabound scheelite occurrences are associated with tourmalinites and massive to semi-massive sulphide (pyrrhotite, pyrite, and chalcopyrite) mineralization, and have been proposed to have originated from submarine exhalation. Appel (1997) attributed the high bromine contents and low Cl/Br values of 1.6, compared with 60-1300 ppb Br and 430 of Cl/Br values in mid-ocean ridge basalts (Jambon et al., 1995), to the alteration and serpentinization of komatiitic and tholeiitic volcanic rocks by hypersaline brines on the seafloor.

Heating during the metamorphism of sedimentary rocks can cause the loss of iodine and other halogens; these escaping halogens would be evolved into hydrothermal fluids. Campbell and Edmond (1989) observed extremely high iodine concentrations (7.4 to 11.0 ppm) in submarine hydrothermal fluids

hosted in sediment systems.

However, Boneß et al. (1991) analyzed halogens in metapelites, and did not observe any correlation between halogen contents and metamorphic grades. Boneß et al. (1991) suggested that Cl, Br and I contents are independent of metamorphic grade.

Based on their research about the halogen-rich scapolite and biotite in the Wallace Formation, northwest of the Idaho batholith, Mora and Valley (1989) determined that the abundance of Cl-rich scapolite and biotite indicates high chlorine activities during greenschist- to amphibolite-facies regional metamorphism of sedimentary rocks. The strict stratigraphic control on the occurrence of scapolite and B-rich minerals, e.g., tourmaline, in the Wallace Formation suggests the scapolite crystallized in layers that originally contained halite/evaporitic sediments (Mora and Valley, 1989). Similarly, Vanko and Bishop (1982) suggested that the likely source of Na and Cl for scapolitization (in the Humboldt lopolith) is pre-existing evaporites, evaporitic brines derived from the wallrocks, or primary magmatic Na and Cl.

The variations of scapolite composition are also related to rock types and metamorphic grade. Scapolite compositions in low grade biotite zone are more NaCl-rich than those in garnet and kyanite-sillimanite zones, from average 34.8 EqAn [equivalent anothite content=100(Al-3)/3] and 0.71 X_{Cl} [=Cl/(Cl+CO_3)] in biotite-carbonate granofels to 52.7 EqAn and 0.21 X_{Cl} in kyanite-sillimanite zone (Mora and Valley, 1989); there is a general decrease in the X_{Cl} and increase in EqAn with increasing metamorphic grade. But the

composition variation within each metamorphic grade suggests that local rock and/or local fluid compositions exert an important control on scapolite compositions (Mora and Valley, 1989).

Halogens in Mantle Materials/Fluids

Jambon et al. (1995) analyzed Mid Ocean Ridge Basalt (MORB) glasses from the Mid-Atlantic Ridge and the East Pacific Rise for Cl by electron microprobe, and Cl and Br by neutron activation analysis (NAA). The Cl and Br concentrations range from 20 to 2800 ppm and 62 to 1320 ppb, respectively. The Cl contents vary significantly (by a factor of 140), consistent with other published data from similar samples, and may be the result of interaction with seawater (Jambon et al., 1995). Bromine is well correlated with Cl at a constant Cl/Br value of 430 ± 130 (1σ) over the full range of Br concentration from 62 to 1320 ppb (Figure 2.2), and is independent of Cl abundance or basalt type. They also estimated primitive mantle Cl and Br abundances are 35±5 ppm and 100±15 ppb, respectively.

Meurer and Natland (2001) analyzed the major-element compositions of apatite from mid-ocean ridges (Hess Deep near the East Pacific Ridge, Mid-Atlantic Ridge, and Southwest Indian Ridge) by electron microprobe analysis. Apatite from the Hess Deep shows the greatest variability for both $X_{F\text{-}Ap}$ and $X_{Cl\text{-}AP}$ (from 0.1 to 0.85), but a more limited range for $X_{OH\text{-}Ap}$ (from 0.15 to 0.30). Most samples of apatite from the Mid-Atlantic Ridge are F-OH apatite with low $X_{Cl\text{-}Ap}$ (<0.10), in which the total halogen ($X_{F\text{-}Ap}$+$X_{Cl\text{-}Ap}$) is from 0.5 to 0.6. Apatite

from the Southwest Indian Ridge has a maximum $X_{Cl\text{-}Ap}$ of 0.30 and a limited range of $X_{OH\text{-}Ap}$ from 0.3 to 0.4.

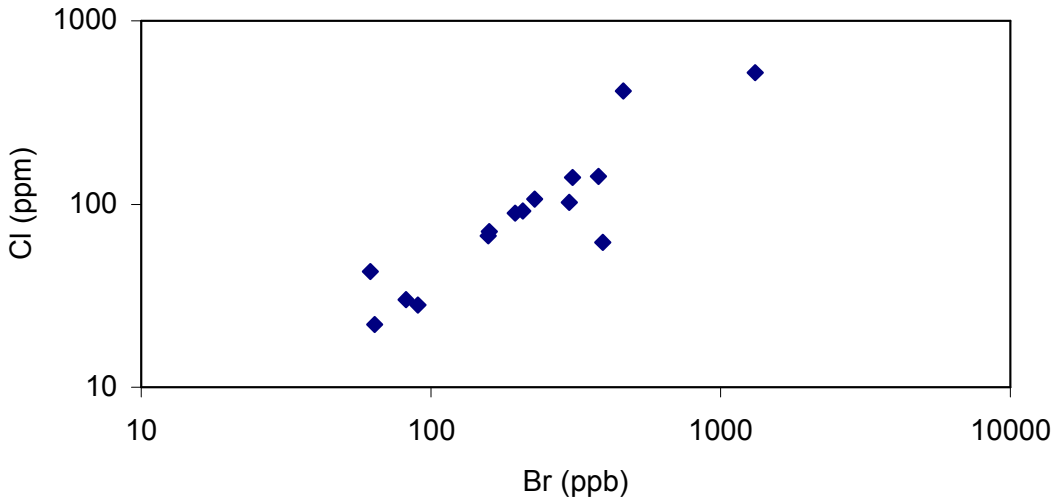

Figure 2.2 The correlation between Cl and Br in MORB glasses
(data from Jambon et al., 1995 and reference therein)

Burgess et al. (2002) analyzed the halogen composition of mantle fluids trapped as fluid inclusion in seven grains of diamond from Aikhal kimberlite, Siberia (Russia) and obtained Br/Cl values of $1.74\pm0.18\times10^{-3}$ (M) and I/Cl values of $22.0\pm3.4\times10^{-6}$ (M). These compositions are consistent with those estimated from African diamond samples ($Br/Cl=1.56\pm0.25x10^{-3}$ (M), I/Cl=20-70×10^{-6} (M)) and from the analysis of MORB ($Br/Cl=1.03\pm0.29\times10^{-3}$ (M), I/Cl=15-25×10^{-6} (M)). The close similarity in composition of mantle fluids with regard to the Br/Cl and I/Cl values for Siberian and African diamonds led them to the conclusion that there may be a wide-scale homogeneity of halogen

composition in the sub-continental mantle. Burgess et al. (2002) also estimated that the sub-continental mantle has 3 ppm Cl, 11 ppb Br, and 0.4 ppb I and that the bulk Earth has 27 ppm Cl, 108 ppb Br, and 7 ppb I.

Schrauder et al. (1996) analyzed the trace-element contents (including Br) of 13 micro-inclusion-bearing fibrous diamonds from Botswana using neutron activation analysis (NAA). The Br concentrations in the bulk fluids range from 14 to 471 ppm, and the Br concentrations in the corresponding bulk fibrous diamond samples are 1.43 to 98.7 ppb, except for one high value of 1131 ppb.

Apatite commonly occurs as an accessory mineral in xenoliths within volcanic rocks from the Phanerozoic lithospheric mantle. Its composition, especially the halogen content, is important to understand the mantle residence of volatiles such as F, Cl, and Br.

Ionov et al. (1997) reported the halogen compositions of 9 apatite samples hosted in peridotite from mantle xenoliths in alkali basalts from Siberia, Mongolia, and Spitsbergen. Moderate to high Cl contents of 2 to 3.3 wt% Cl with low F/Cl values of 0.1 to 0.3 are characteristic for apatites in the continental mantle such as Siberia, Mongolia, SE Australia, and Yemen. High F (4.4-5.5 wt%) and low Cl (0.2-0.3 wt%) apatites had been reported by Hauri et al. (1993) in peridotite xenoliths from two Pacific islands.

The Cl-rich apatites in the peridotite xenoliths from Spitsbergen, Mongolia, and SE Australia contain significant amounts of Br (12 to 74 ppm). No bromine was detected in low Cl (<1 wt%) apatites from Siberia (Ionov et al.,

1997).

Fifteen samples of apatite from mantle-derived xenoliths from Victoria, Australia; Kiama, NSW, Australia; Alaska, USA; Eifel, Germany; and Massif Central, France, had been analyzed by proton microprobe and laser ablation ICP-MS (O'Reilly et al., 2000). These samples belong to two distinct types, A and B, with different origins based on the halogen contents, and the occurrence of structural CO_2, Sr, and other trace elements (Figure 2.3). Apatite A, hosted in sheared/metasomatized mantle spinel lherzolites, is a group of carbonate-bearing hydroxyl-chlorapatite with high Cl (1.5-2.5 %), Br (6-50 ppm), and Sr and low F (<1.0%) contents. Apatite B, of magmatic origin associated with the pyroxenite-series xenoliths or related to veins in Cr-diopside peridotites, is a group of hydroxyl-fluorapatite with low Cl (0.1-0.5 %), Br (1-2 ppm), and Sr contents.

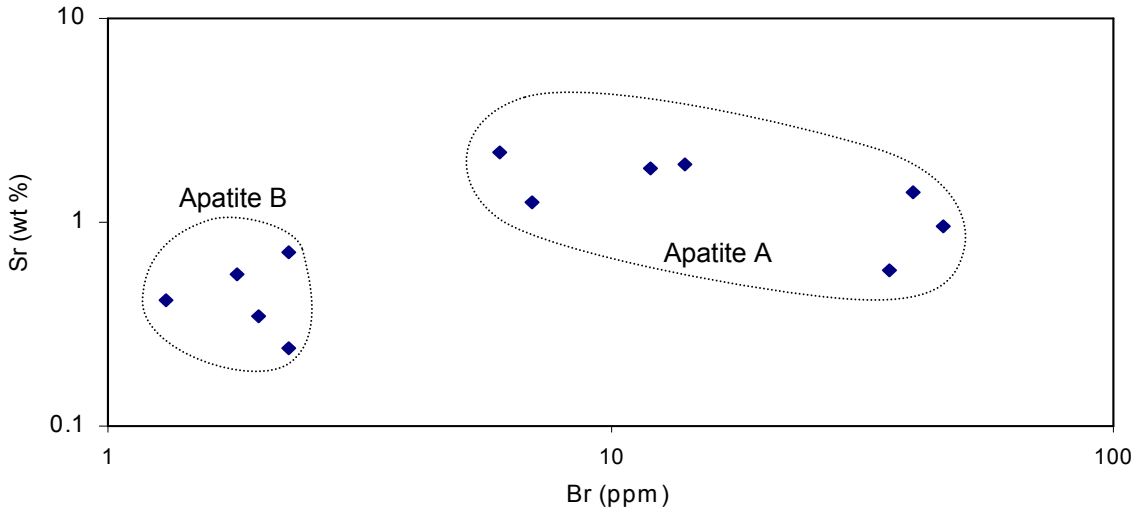

Figure 2.3 Sr VS Br in mantle apatite
(data from O'Reilly et al., 2000)

2.3.2 Terminology/Definition of the Partition Coefficient and Henry's Law

Partition Coefficient: Simple concentration ratios between two phases are termed partition coefficients (Denbigh, 1966; Beattie et al., 1993). Traditionally, partition coefficients are determined by analysis of coexisting crystals and glass/melts in natural volcanic rocks or high temperature experimental products (Purton et al., 1996). Generally there are several different ways to express the partition coefficient. The simple and widely used one is the weight (concentration) ratio between two phases (e.g., mineral and melt/liquid), which is termed the Nernst partition coefficient (D_i):

$$D_i = \frac{C_i^{xl}}{C_i^{liq}} \qquad (2.1)$$

where the subscript (i) refers to the element/species of interest, and superscripts refer to the phases concerned (xl, crystal; liq, liquid). D_i is the partition coefficient of element i, and C_i^{xl} and C_i^{liq} are the weight concentrations of i in crystal and liquid/melt phases, respectively.

Another one is the molar partition coefficient (D_i^*):

$$D_i^* = \frac{X_i^{xl}}{X_i^{liq}} \qquad (2.2)$$

where X_i^{xl} and X_i^{liq} are the molar fractions of species i in the crystal and its coexisting liquid/melt, respectively. The molar partition coefficients provide the closest reflection of thermodynamics that control the partitioning (Beattie et al., 1993). When a partition coefficient is normalized by the value of the partition coefficient for another component, the result is the exchange/distribution coefficient (K_D):

$$K_{D_{\frac{i_1}{i_2}}} = \frac{D_{i_1}}{D_{i_2}} = \frac{D^*_{i_1}}{D^*_{i_2}} \qquad (2.3)$$

where i_1 and i_2 are two species of interest. K_D is less sensitive to temperature and composition (Beattie et al., 1993; Jones, 1995; Blundy et al., 1996).

Henry's Law: Henry's Law can be stated that the activity (α) and concentration (X) of infinitely dilute species (i) are linearly related ($\alpha_i=K_iX_i$, where K_i is Henry's Law constant). Henry's Law is obeyed if the partition coefficient is constant and does not depend upon the concentration of the tracer (Jones, 1995). In that case, trace elements act as solid solution components in host minerals. Previous trivalent rare earth element (REE^{3+}) partitioning studies have demonstrated the adherence to the Henry's Law (behaviour) at concentrations from 100 ppm to 2 wt% (Gaetani and Grove, 1995). There could be up to 5 wt % Sm, 2.7 wt % Ba, and 2.5 wt % Sr in the liquid phase coexisting with plagioclase before the Nernst's distribution law (if

the solute follows Henry's Law in both phases, then the ratio of its concentrations in these phases will be constant) was violated (Drake and Weill, 1975).

At relatively higher concentrations, partition coefficients are generally constant, sometimes to a level as high as several wt % in crystals (Drake and Weill, 1975; Lindstrom and Weill, 1978; Drake and Holloway, 1978; Mysen, 1978; Hoover, 1978; Harrison and Wood, 1980; Harrison, 1981; Watson, 1985). But there exists a low concentration range (usually <20 ppm in crystals) over which the values of partition coefficients decrease with increasing concentration of the trace elements during altervalent substitutions (Mysen, 1978; Pan et al., 2003).

The extent of the non-Henry's concentration range (where Henry's law is violated) is variable even among chemically similar elements in a single mineral; this is probably related not to the concentration of a single element but rather to the sum of all elements involved in the same substitution (Harrison and Wood, 1980; Watson, 1985).

Crystal defects also play a role in the failure of Henry's law at very low concentration through either occupying the sites or producing ionic vacancies in order to balance the charges (Navrotsky, 1978; Harrison and Wood, 1980; Watson, 1985).

According to Henry's law, the concentration ranges of trace elements in minerals with (solid) solution behaviour, can be positively correlated with the difference of ionic radii between trace element and the host element for which

the tracer is assumed to substitute. If the difference is less than about 10 % (relative to the host) the solid solution is ideal (Raoult's Law). With larger differences there is an excess free energy of mixing, although Henry's law could still be obeyed in the low concentration ranges where the crystal/fluid partition coefficients are independent of element concentration (Mysen, 1978).

The concentration ranges of constant partition coefficients are extended with increased temperature. At higher concentration, the values of partition coefficients decrease with increasing concentration of the trace elements (Mysen, 1978).

Crystal Chemical Control: The ability of a crystalline or melt phase to incorporate a given trace element into its structure is controlled by the size of the available crystallographic sites and the ability of the phase to charge balance the incorporated ion. Increased ionic distance (bond length) for a specific crystallographic site will allow the incorporation of larger ions possible (Gaetani and Grove, 1995).

2.3.3 Previous Partitioning Research

Knowledge of partition coefficients between halogen-bearing minerals/ materials and fluids/melts is essential to understand various processes involved in hydrothermal mineralization, magmatism, metamorphism, and metasomatism, to evaluate the fluid-rock interaction, fluid composition, and

fluid origin, and to reveal the evolution of fluids and magmas through the examination of halogen compositions in minerals.

Siemann and Schramm (2000) estimated the average Br partition coefficient of 0.033 between aqueous solution and halite.

Anfilogov et al. (1977) experimentally studied the partitioning behaviour of F between minerals (biotite and amphibole) and granitic melts at 780 ^{o}C and 1000 atm, at a F content in melt ranging from 0.25 to 0.5 wt%. The results are 7.4 and 6.1 for biotite-melt and amphibole-melt, respectively (Table 2.6). The partition coefficient of F between biotite and melt has also been reported to decrease with increased F content in the melt, e.g., the D values change from 1.13 to 0.7, whereas the F contents in the melt increased from 3.0 wt% to 4.0 wt% (Bushlyakov, 2000).

Bernem (1970) experimentally studied the partition coefficient of F (3.0) and Cl (0.20) between melt and fluid (Table 2.6). Bushlyakov (2000) used available experimental data to calculate the partition coefficient of F (37) and Cl (2.4) between apatite and melt (Table 2.6). The initial melts of the adamellite-granite, granite-leucogranite association originated from continental-type crust contain the higher F contents (0.10 to 0.28 wt%) and lower Cl (0.01 to 0.03 wt%). The initial melts of gabbro-granite, gabbro-syenite, gabbro-plagiogranite association with magnetite skarn deposits from the island-arc type crust, are characterized by lower F (0.04 to 0.07 wt%) and higher Cl (0.26 to 0.60 wt%). The estimated highest F and Cl contents in magmatic melts parental for Uralian granites are 0.7 to 1.0 wt% F (from biotite) and 1.0 to 1.5 wt% Cl (from apatite),

respectively (Bushlyakov, 2000).

Table 2.6 Selected partition coefficients of halogens from the literature

Halogen Element	F	Cl	Br	I	Reference
Apatite-biotite	5.0	8.0			Bushlyakov, 2000
Apatite-amphibole	6.0	15.0			Bushlyakov, 2000
Apatite-fluid	111.0	0.48			Bushlyakov, 2000
Apatite-melt	37.0	2.4			Bushlyakov, 2000
Melt-fluid	3.0	0.20			**Bernem, 1970**
Melt-fluid	5.56	0.123	0.0571	0.0096	Bureau et al., 2000
Biotite-melt	7.4				Anfilogov et al., 1977
Amphibole-melt	6.1				Anfilogov et al., 1977

Webster and Holloway (1988) experimentally studied the partition coefficient (wt) of Cl between superliquidus melts of topaz rhyolite composition and fluid made up of distilled deionized water, with variable fluid/melt ratios, at the pressures of 0.5 to 5 kbar and temperatures of 725^{o} to 950^{o}C. Their results show that Cl is favorably partitioned into the fluid phase at all experimental conditions. Within the natural range of Cl concentration in magmatic systems,

e.g.,+ ≤2000 ppm Cl in the melt and ≤4 wt% Cl in fluids, the Cl partition coefficient between fluid and melt ranges from 2 to 20. The Cl partition coefficient increases with an increase of Cl content in fluid or melt (see Fig.3-b in Webster and Holloway, 1988) and with increasing temperature (see Fig. 2 in Webster and Holloway, 1988). The Cl partition coefficient is linearly correlated to the concentration of Cl in the fluids (Fig.3-b in Webster and Holloway, 1988). At similar fluid/melt ratios and concentration of Cl in the fluid and at the same pressure conditions, e.g., 2 kbar, there is a significant dependence of the partition coefficient on the run temperature (Fig. 2 in Webster and Holloway, 1988). These observations are consistent with Holland's (1972) experimental results at 822 ^{o}C to 855 ^{o}C and 1.9 to 2.3 kbar. The effect of pressure on the Cl partitioning behaviour is somewhat equivocal, but generally the partition coefficient increases with increasing pressure. The increased fluid/melt ratio also causes increased partition coefficient of Cl between fluid and melt. More fluid will permit more Cl to be dissolved in the fluid from the melt, then lowers the Cl concentration in the melt while the Cl concentration in the fluid remains unchanged.

If the Cl concentration increases to higher than 4 wt% in the fluid and 2000 to 2500 ppm in the melt, the partition coefficient will increase to greater than 20 (20 to 130). High Cl contents in the starting materials result in high concentrations of Cl in the run product glass and fluid. But if Cl in the fluid is higher than 3.5 M, the Cl concentration in the melt will remain constant at 2500±100 ppm (Fig. 3-a in Webster and Holloway, 1988), which is the solubility

limit for Cl in granitic melts. This explains why the partition coefficient is not independent on the Cl concentration in the fluid or melts.

Using natural Durango fluorapatite and aqueous fluids of HCl, NaCl, NaOH, Na_2CO_3, and mixture of CO_2-H_2O, Brenan (1993) experimentally investigated the partitioning of fluorine and chlorine between apatite and fluids at 950-1050 ^oC and 1.0-2.0 GPa. His experimental results demonstrate a proportional correlation between the X_{ClAp}/X_{OHAp} values in apatite with the chlorine concentration in the coexisting fluids with up to 15 wt%, 5 wt%, and 1 wt% of chlorine in the NaCl fluid, HCl fluid, and CO_2 fluid, respectively. While the X_{FAp}/X_{OHAp} values are also proportional to the fluorine concentration in the coexisting fluids, but only to about 0.4 wt% and 0.15 wt% of fluorine in the NaCl fluid and the HCl fluid, respectively. Apatite is more sensitive to F relative to Cl consistent with the results of partitioning experiments in this study (see Chapter 5).

On the basis of Brenan's (1993) experimental data, the following molar partition coefficients of F and Cl, respectively, between apatite (F-apatite) and fluids have been calculated: 1.59-85.9 and 0.022 for NaCl fluid, 1.54-16.96 and 0.055 for HCl fluid, and 1.25-1.82 and 0.045 for CO_2 fluid. The large variation of D^*_F may imply that equilibrium was not achieved in Brenan's (1993) experiments.

The composition of the gas phase released from an explosive volcanic eruption is usually controlled by equilibrium processes between hydrous fluids and the silicate melt in the magma chamber beneath the volcano (Bureau et

al., 2000 and references within). Bureau et al. (2000) had experimentally studied the distribution of Cl, Br, and I between silicate melts and aqueous fluids at 900 ^{o}C and 2 kbar with run duration of 7 days. The concentrations of Cl, Br, and I in the silicate melt are proportional to their concentrations in the aqueous fluids. Their data yield tightly constained partition coefficients (wt%) between the aqueous fluids and silicate melts ($D_{fluid/melt}$) of 8.1 (±0.2), 17.5 (±0.6) and 104 (±7) for Cl, Br, and I, respectively; these D values are close to the results of Bernem (1970). Based on their experimental results, the authors tried to constrain the potential effects of volcanic-derived heavy halogens (Cl, Br, and I) on stratospheric processes; they also estimated the amount of bromine injected into the stratosphere by the 1991 Mount Pinatubo eruption, which is approximately 11 to 25 kT (Cl+Br+I) as minimum. This single eruption is probably responsible for the massive ozone depletion observed after the 1991 Mount Pinatubo eruption (Bureau et al., 2000).

All experimental element partitioning studies are undertaken using simplified (ideal model) systems. The partition coefficients measured in a simple model system, such as the albite-water-alkali halogenide of Bureau et al. (2000), may not be directly applicable to natural systems. The various factors that affect the partitioning behaviour of elements, such as halogens, likely function in a similar way. The relative fractionation of F, Cl, Br, and I obtained from these simplified experimental systems can probably be used as a first order approximation of natural systems (Bureau et al., 2000), and applied in detail to further understanding magmatic-hydrothermal processes.

3. Review on Crystal Chemistry, Stabilities and Experimental Studies of Apatite, Scapolite, and Sodalite

Halogen-bearing minerals can provide reliable information about the halogen concentrations in their parental melts/fluids. Apatite, scapolite, and sodalite are common halogen-bearing mineral groups selected for this study.

3.1 Crystal Structure of Apatite-Group Minerals

The apatite-group minerals with a general chemical formula, $Ca_{10}(PO_4)_6X_2$, include three accepted species: fluorapatite (where *X*=F), chlorapatite (Cl), and hydroxylapatite (OH). The crystal structure of the apatite-group minerals is characterized by tetrahedral (PO_4) groups that are linked to two different Ca sites (Ca*1*, irregular 9-coordination; Ca*2*, irregular 7-coordination) to form a hexagonal network (Figure 3.1). Each *X* anion lies in a triangle connected to three calcium atoms with different Ca-*X* bond lengths: 2.311, 2.759, and 2.385 Å for F, Cl, and OH, respectively (Hughes et al., 1989). The F anions lie in a special position (0, 0, 1/4) at the intersection of the hexads with mirror planes at z=0.25 and 0.75, and the F-Ca triangle is within the mirror plane. The larger sizes of OH^- (1.35 Å) and Cl^- (1.81 Å) and longer bond lengths of Ca-OH (2.385 Å) and Ca-Cl (2.759 Å) relative to F (1.30 Å) and Ca-F (2.311 Å) cause both the OH and Cl ions to be displaced from the special

position on the mirror plane (Hughes et al., 1989). The structural variation caused by the different sizes and bond lengths results in a symmetry reduction from hexagonal for fluorapatite to monoclinic for chlorapatite and hydroxylapatite (Hughes et al., 1989).

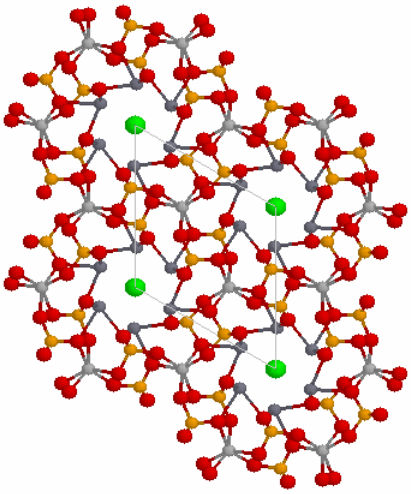

Figure 3.1 The crystal structure of apatite group minerals. There is a series of tetrahedral (PO_4) groups that are linked to two different Ca sites (Ca*1*, irregular 9-coordination; Ca*2*, irregular 7-coordination) to form a hexagonal network. The anions (F, Cl, OH) occupy the central space of the hexagonal channel. The green spheres are anions, surrounded by calcium ions (Ca2, dark grey spheres). The light grey spheres are Ca1, the red spheres are oxygen anions, and the phosphorus atoms are orange (http://www.minweb.co.uk).

3.2 Experimental Studies of Apatite-Group Minerals

Prener (1967) reported the growth of single crystals of fluorapatite and chlorapatite by slowly cooling melts of polycrystalline apatites in fused CaF_2 or $CaCl_2$ at atmospheric pressure. The phase diagrams of the pseudobinary systems CaF_2-$Ca_5(PO_4)_3F$ and $CaCl_2$-$Ca_5(PO_4)_3Cl$ are shown in Figure 3.2. Crystal growth experiments usually include the following steps: 1) mixtures of apatite and halide soaked at temperatures some 50 ^oC above the liquidus temperature for 10 to 20 hours in order to ensure complete homogenization, and 2) cooling at constant rates of 2-4 ^oC/hr. Prener (1967) obtained mm-sized crystals of fluorapatite and chlorapatite from this method. Chen (2002) confirmed that this method is effective in the synthesis of large fluorapatite crystals from a CaF_2-$Ca_5(PO_4)_3F$ mixture at a 45:55 weight ratio and a temperature range from 1325 ^oC to 1220 ^oC and chlorapatite crystals from a $CaCl_2$-$Ca_5(PO_4)_3Cl$ mixture at 72.3:27.7 weight ratio and a temperature range of from 1280 ^oC to 1060 ^oC .

Argiolas and Baumer (1978) reported hydrothermal syntheses of chlorapatite from an aqueous saturated solution of calcium chloride and orthophosphoric acid in the ranges of 200-850 ^oC and 1-3 kbar. Using this method, Baumer and Argiolas (1981) obtained chlorapatite crystals of 50-500 μm in diameter at 400 ^oC and 3 kbar. Shaw et al. (1993) synthesized fluorapatite, chlorapatite, and their intermediate members at 640-900 ^oC and 8-12 kbar. Fleet and Pan (1997) reported synthesis of single crystals of

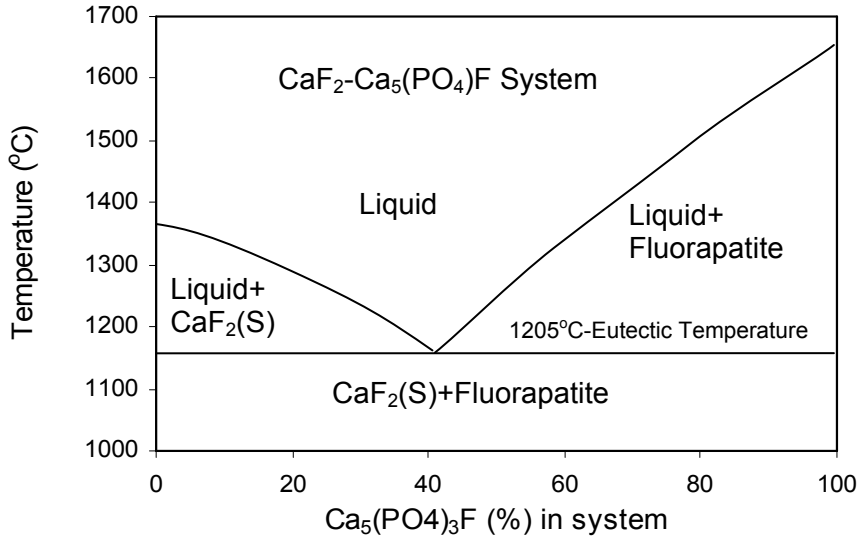

Figure 3.2a Phase diagram of CaF_2-$Ca_5(PO_4)_3F$ system at 1 atm (after Prener, 1967)

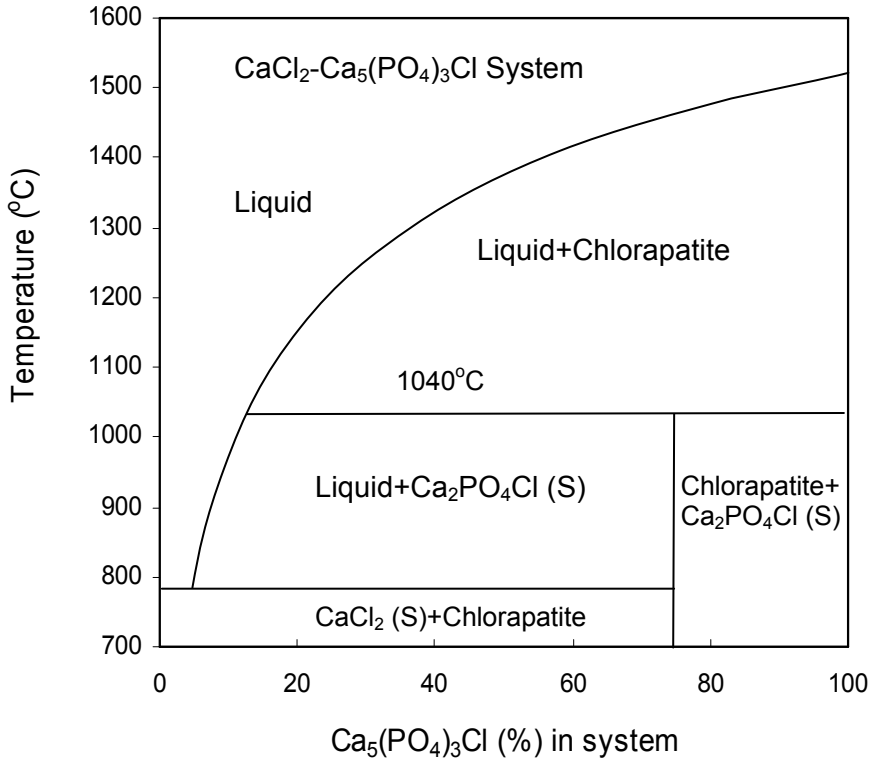

Figure 3.2b Phase diagram of CaCl2-Ca5(PO4)3Cl system at 1 atm (after Prener, 1967)

fluorapatite, chlorapatite, and hydroxylapatite from hydrous melts at 700-800^{o}C and 1-2 kbar. The growth of fluorapatite and hydroxylapatite by precipitation from artificial seawater has been described by Cappellen and Berner (1991). This method generally produces extremely fine-grained crystals of apatite.

3.3 Crystal Structure of Scapolite-Group Minerals

Scapolite-group minerals are tetragonal framework aluminosilicates and have a general formula of $M_4T_{12}O_{24}A$, where M = Na and Ca, T = Si and Al, and A = Cl, CO_3, and SO_4 (Teerstra and Sherriff, 1997; Pan, 1998). Marialite and meionite have idealized anhydrous end-member formulas of $Na_4Al_3Si_9O_{24}{\cdot}Cl$ and $Ca_4Al_6Si_6O_{24}{\cdot}CO_3$.

Scapolite is characterized by two types of four-membered rings of Si-Al tetrahedra. Type 1 rings consist of *T1* tetrahedra that point in the same direction, and type 2 rings consist of both *T2* and *T3* tetrahedra that point alternately up and down (Figure 3.3). Type 2 rings are joined into multiple chains oriented parallel to the c axis, and are linked by type 1 rings to form five-membered rings. A large subspherical cage resulting from the five-membered tetrahedral rings is surrounded by four oval-shaped channels parallel to the c axis. The large cage is occupied by the anion groups, and the channels host Na and Ca ions.

The composition of the scapolite-group minerals varies mainly between marialite and meionite (Teerstra and Sherriff, 1997; Pan, 1998), but the

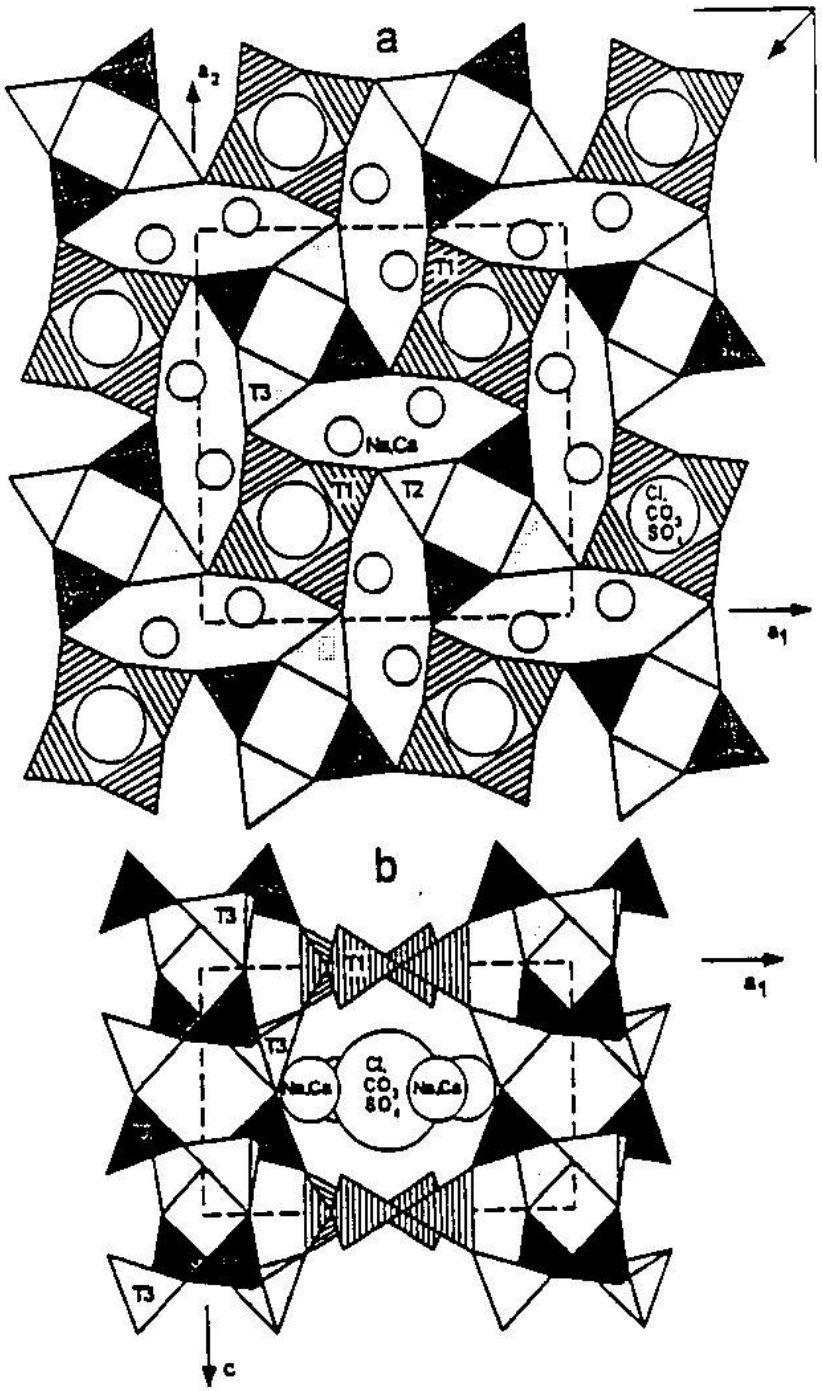

Figure 3.3 The crystal structure of scapolite group minerals viewed along (a) the a axis and (b) the c axis (Levien and Papike, 1976). There are two types of four-membered rings of Si-Al tetrahedra. Type 1 rings consist of *T1* tetrahedra that point in the same direction, and type 2 rings consist of both *T2* and *T3* tetrahedra that point alternately up and down. Type 2 rings are joined into multiple chains oriented parallel to the c axis, and are linked by type 1 rings to form five-membered rings. A large subspherical cage resulting from the five-membered tetrahedral rings is surrounded by four oval-shaped channels parallel to the c axis. The large cage is occupied by the anion groups, and the channels host Na and Ca ions.

composition of natural Cl-bearing scapolite is within the $Na_4Al_3Si_9O_{24}$·Cl - $Na_3CaAl_4Si_8O_{24}$·Cl - $NaCa_3Al_5Si_7O_{24}$·CO_3 triangle (Pan, 1998). Scapolite in skarn deposits is highly variable in chemical composition and provides important constraints on the chemical compositions of ore-forming fluids because of its variable volatile components (i.e., Cl, CO_3, SO_4, H, F, etc.; Pan, 1998). Several studies have suggested that marialitic scapolite in some skarn deposits is related to hypersaline fluids derived from pre-existing evaporites (Vanko and Bishop, 1982; Mora and Valley, 1989; Pan, 1998).

3.4 Experimental Studies of Scapolite-Group Minerals

Eugster and Protska (1960) and Eugster et al. (1962) first synthesized end-member marialite from mixtures of Al_2O_3, Na_2O, $6SiO_2$, and NaCl at 1 bar and 700-850 ^oC, although their marialite product was most likely metastable (Orville 1975; Rebbert 1995). Orville (1975) and Ellis (1978) noted that end-member marialite cannot be synthesized at 4 kbar and 750^oC. Newton and Goldsmith (1975, 1976) showed that marialite is stable relative to albite and NaCl at temperatures above 800^oC at 8-15 kbar. Other synthesis experiments involving marialite include those by Vanko (1982), Vanko and Bishop (1982), and Sokolova et al. (1996).

Newton and Goldsmith (1976) predicted the formation of jadeite + quartz + NaCl from the breakdown of marialite at high pressures. Eugster and Protska (1960) reported that marialite melts incongruently to albite-liquid at 860±10^oC

and 1 bar with the marialite-halite eutectic point lying very close to halite at about 800°C.

The stability of end-member meionite has been determined experimentally by Eugster et al. (1962), Newton and Goldsmith (1975, 1976), Goldsmith and Newton (1977), Aitken (1983), Huckenholz and Seiberl (1988, 1989), and Baker and Newton (1994). Eugster et al. (1962) synthesized meionite from a mixture of SiO_2, Al_2O_3, and $CaCO_3$ at 1-4 kbar and 850-950 °C. Goldsmith and Newton (1977) reversed the following reaction:

$$3CaAl_2Si_2O_8 + CaCO_3 = Ca_4Al_6Si_6O_{24}\cdot CO_3 \qquad (3.1)$$

and suggested that meionite is stable relative to anorthite and calcite above 850 °C and the reaction is almost independent of pressure. This observation was supported by Baker and Newton (1994), who also reported a positive dP/dT slope for this reaction. Similarly, Orville (1975) and Ellis (1978) noted that end-member meionite is not stable at 4 kbar and 750 °C. However, Huckenholz and Seiberl (1988, 1989) suggested markedly lower temperature stability limits for meionite and a steep negative dP/dT slope for this reaction. Moecher and Essene (1990) attributed this discrepancy to differences in either the starting materials (i.e., degrees of Al-Si disorder in meionite and anorthite) or the compositions of the fluids used in the different experiments. Newton and Goldsmith (1975, 1976) demonstrated that meionite is highly refractory at high pressure. The thermal breakdown curve of meionite at 15-30 kbar approaches that of anorthite (e.g., >1400 °C at 10 kbar), and the upper pressure limits for the breakdown reaction of meionite are also comparable to those of anorthite.

3.5 Sodalite

Sodalite-group minerals include sodalite, nosean, hauyne, and lazurite, and can be found in silica-undersaturated rocks, such as nepheline syenites or phonolites in association with nepheline and leucite. Sodalite-group minerals have a general formula of $C_8(T1_6T2_6O_{24})A_2$, where C = Li, Na, K, Fe, Zn, Mn, and Ca, T1 = Al, Ga, and Be, T2= Si, Ge, and Al, and A = F, Cl, Br, I, OH, S and SO_4. Sodalite has a cuboctahedral framework of (Al, Si)O_4 tetrahedral (T) units linked into four-membered and six-membered rings parallel to {100} and {111}, respectively (Figure 3.4). The cuboctahedral framework with large cavities can accommodate $ClNa_4$ tetrahedral groups, and the six-membered rings form continuous channels permitting the diffusion of interframework ions (Barrer and Vaughan, 1971; Fleet, 1989).

The sodalite structure will be affected by the accommodation of the halogen ions (Cl, Br, I) at the *A* site. The change of the sodalite structure parameters will be in proportion to the size of the halogen ions, for example the progressive increase of the unit-cell parameter and bond angles of O-Na-O and O-Na-*A* from Cl to Br and then to I (Fleet, 1989).

Powdered forms of $Na_8(Al_6Ge_6O_{24})Cl_2$ and $Na_8(Ga_6Si_6O_{24})Cl_2$ were synthesized by McLaughlan and Marshall (1970). Dodecahedral crystals of $Na_8(Al_6Ge_6O_{24})Cl_2$, $Na_8(Al_6Ge_6O_{24})Br_2$, and $Na_8(Al_6Ge_6O_{24})I_2$ were hydrothermally synthesized by Fleet (1989) through heating the mixture of $NaAlGeO_4$, sodium halide, and distilled-deionized water in sealed gold capsules.

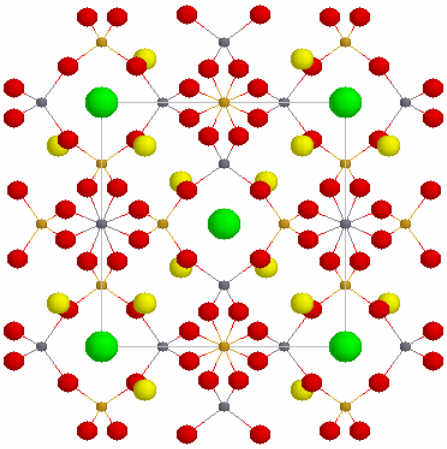

Figure 3.4 The crystal structure of sodalite group minerals. The large green spheres are Cl, small red spheres are O, yellow spheres are Na, and the smallest gray spheres are Si/Al. A cuboctahedral framework of (Al, Si)O_4 tetrahedral (T) units linked into four-membered and six-membered rings parallel to {100} and {111}, respectively. The cuboctahedral framework with large cavities can accommodate $ClNa_4$ tetrahedral groups, and the six-membered rings form continuous channels permitting the diffusion of interframework ions (http://www.minweb.co.uk).

4. Analytical Methods

There are many analytical methods available for the determination of halogens in geological samples, such as conventional X-ray fluorescence for Br (Yamada, 1968; Appel, 1997) and synchrotron X-ray fluorescence analysis for Cl, Br, and I (Frantz et al., 1988; Smith and Rivers, 1995); instrumental neutron activation analysis (INAA), and radiochemical neutron activation analysis (RNAA) for Cl, Br, and I (Deruelle et al., 1992; Ebihara et al., 1992; Shinonaga et al., 1994; Jambon et al., 1995); isotope dilution mass spectrometry (ID-MS) for Cl, Br, and I (Heumann et al., 1987; Heumann, 1988; Bone et al., 1991; Shinonaga et al., 1994); laser microprobe noble gas mass spectrometry (LMNG-MS) for Cl, Br, and I (Bohlke and Irwin, 1992); ion chromatography for halogen ion mass ratios in liquid phases of fluid inclusions (Channer and Spooner, 1994a, b; Nesbitt and Prochaska, 1998); and electron microprobe analysis (EMPA).

In this study, X-ray fluorescence (XRF) and electron microprobe analysis (EMPA) have been used to analyze most of the samples, plus a few instrumental neutron activation analysis (INAA) analyses for comparison.

4.1 X-Ray Fluorescence (XRF)

Conventional X-ray fluorescence analysis is performed on bulk specimens, such as powdered rocks or glass discs prepared by fusing rock powder with a suitable flux. Characteristic X-ray spectra are excited by illuminating the specimen with X-rays whose photon energy is higher than the binding energy of the K (or L) electrons in the elements to be determined in the sample. The detection limit is typically of the order of 0.1 to 10 ppm (e.g., 5 ppm for Cl and 2 ppm for Br; Appel, 1997).

The equipment necessary for X-ray fluorescence analysis consists of two main parts, excluding the excitation source: the spectrometer system and the measuring electronics. Two types of X-ray fluorescence spectrometers can be distinguished on the basis of the method used to isolate the individual spectral lines: wavelength dispersive and energy dispersive systems (Bacso et al., 1998).

Wavelength dispersive X-ray spectrometry is a non-destructive instrumental analytical method for chemical elements based on the measurement of wavelengths and intensities of their X-ray lines emitted after secondary excitation. The primary beam from an X-ray tube irradiates the specimen, exciting each chemical element in the specimen to emit secondary spectral lines having wavelengths characteristic to each element and intensities proportional to their concentrations. The characteristic X-ray lines of the specimen are dispersed spatially by crystal diffraction prior to detection. In

order to reduce the scattered radiation reaching the detector, apertures, and collimators are used, which also reduce the useful intensities of analysis lines. Therefore powerful X-ray tube radiation is used for excitation (Bacso et al., 1998). The spectrum measured with a wavelength dispersive system consists of peaks at different scattering angles. The elements can be identified from their specific scattering angles, while their concentrations are proportional to the peak heights. With wavelength dispersive systems, all the elements between B and U can be determined qualitatively and quantitatively. The main disadvantage of the wavelength dispersive system is that very intensive excitation source (high-power X-ray tube) is needed for excitation (Bacso et al., 1998).

For the energy dispersive spectrometer, the detector receives excited line of each element simultaneously. The total ionization of each photon is transmitted to current impulse within the solid-state detector. The amplitude of the impulse varies linearly with the energy of the incident photon. Since the primary beam is not diffracted and it is possible to reduce the source-sample-detector distance increasing the solid angle of detection, the energy dispersive X-ray fluorescence spectrometers (EDXRF) can eliminate the severe loss of intensity of secondary X-ray lines by elimination of crystal diffraction and narrow collimation. Therefore, they can be operated by use of low-power X-ray tubes, monochromatic secondary radiators, accelerated ion beams, and radioisotopes (Bacso et al., 1998). Elements with $Z>11$ are detectable with commercially available energy dispersive instrument.

In this study, most of the samples (mineral separates, melts, and solutions) are analyzed for Br by an energy-dispersive miniprobe multielement analyzer (EMMA or XRF microprobe) at the Department of Geological Sciences, University of Saskatchewan. This XRF microprobe consists of a conventional 2.0 kW X-ray generator with a Mo anode, a concave (Johansson) LiF (220) (R=250mm) monochromator, a sample holder attached to a conventional optical microscope, a 28 mm^2 Si (Li) detector, and an energy-dispersive X-ray spectrometer. The spectrometer consists of a pulse amplifier, a 12-bit analog-to-digital converter, an interface card, and an IBM-compatible computer. The X-ray generator is operated at a voltage of 40 kV and a current of 20 mA. The excitation X-ray beam (0.1 x 0.5 mm) is focused from the LiF monochromator and collimated by a conical collimator of 0.2 x 0.5 mm in dimension. The analytical data are collected and processed by the in-house software (Cheburkin et al., 1997).

This XRF microprobe has been calibrated for elements of As, Br, Cr, Cu, Fe, Ga, Ge, Hf, Mn, Ni, Rb, Se, Sr, Th, U, Zn by using selected international reference materials (Govindaraju, 1994; Pan and Dong, 2003). The calibration curve for Br was established on the basis of four international reference materials (LKSD-1, 11ppm; LKSD-4, 49 ppm; NBS1646, 117 ppm; and MAG-1, 252 ppm Br; Govindaraju, 1994; Pan and Dong, 2003). A set of Cl-rich minerals (apatite, scapolite, and sodalite from the reference mineral collection, University of Saskatchewan) were used to evaluate this calibration. All these minerals are in form of large single crystals and were selected on the basis of

quantitative electron-microprobe analyses for their homogeneity in Cl and other major elements. The crushed crystal fragments, sized between 100 to140 mesh (106-125 μm), were handpicked under a binocular microscope to minimize mineral impurities and fluid inclusions. The selected mineral separates (~0.5 g each) were sent to the Activation Laboratories of Ancaster, Ontario, for instrumental neutron activation analysis (INAA) for Br (Table 4.1; Pan and Dong, 2003).

Besides these minerals, a series of standard solutions with a wide range of concentrations of Br, from 2 ppm to as high as 6714 ppm, prepared volumetrically from NaBr (Aldrich #22, 988-1) and ultra-pure, deionized water, were analyzed by the XRF microprobe (Table 4.1).

For the analyses of mineral samples, single mineral grains are placed in the sample holders which are made of 4 μm thick Prolene films. The counting times are from 10 to 60 minutes dependent on the Br concentration in the grain and the grain size, e.g., for grains that contain less than 10 ppm Br or are smaller than 200 μm in diameter, the counting time is about 45 to 60 minutes. The analyses of solution samples are carried out by dropping the solution on the sample holders, with counting times of 10 and 45 minutes for Br concentrations above and below 10 ppm, respectively.

The precision, accuracy, and detection limit of the XRF microprobe analysis for mineral grains are all dependent on a number of factors such as the grain size and the counting time. The larger the grain size, the higher the

Table 4.1 XRF analysis results of standard solutions and minerals

Sample	Standard (ppm)		XRF			RSD[b]	Difference
	KBr	Br	Br (ppm)	STDEV[a]	No. of Analyses	(%)	(%)
Water-1		2	2.9	0.2	16	7	45
Water-2		5	5.6	0.3	16	5	12
Water-3		10	9.6	0.8	16	8	-4
Water-4		50	51	1.9	16	4	2
Water-5		100	107	3.4	16	3	7
Solution 1	250	168	160	6	6	4	-5
Solution 2	500	336	338	7	6	2	1
Solution 3	1000	671	646	13	6	2	-4
Solution 4	10000	6714	6956	123	15	2	4
Ap-01	INAA	8	7.6	1	16	16	-5
Ap-02	INAA	75	64	12	16	19	-15
SCP-1	INAA	42	41	2	16	5	-2
SCP-2	INAA	115	114	9	16	8	-1
SCP-3	INAA	70	75	3	16	4	7
SOD-1	INAA	234	223	11	16	5	-5
SOD-2	INAA	301	284	13	16	5	-6
SOD-3	INAA	418	395	16	16	4	-6

a: standard deviation; b: relative standard deviation

counting rate. The longer the counting time, the better the counting statistics, hence improving the precision and lowering the detection limit.

Repeated analyses for Br in selected apatite, scapolite, and sodalite grains and standard solutions were used to demonstrate the precision of the XRF microprobe techniques (Table 4.1). Generally the relative standard deviations (RSD) are less than 5 % for Br concentrations above 10 ppm, but increase to about 10 % for Br concentrations below 10 ppm (Table 4.1). The accuracy of the XRF microprobe technique has been evaluated by the comparison with the instrumental neutron activation analysis (INAA) results for apatite, scapolite, and sodalite and with prepared standard solutions (Table 4.1). The differences between the XRF microprobe analyses and standard solutions are less than 7 % for solutions with Br concentrations higher than 10 ppm (Table 4.1, Figure 4.1). The larger differences of 45 % and 12 % for solutions with 2 and 5 ppm Br, respectively, may be the results of evaporation because the longer counting time of 45 minutes for these analyses may cause significant evaporation and result the increase of Br concentration in fluids.

The differences between the XRF microprobe analyses and INAA for Br are less than 7.1 % for all the samples of apatite, scapolite, and sodalite except 14.7 % for the chlorapatite from Bob's Lake, Ontario, which is attributed to the impurity of fluorapatite patches in this sample (Table 4.1, Figure 4.2)

These results demonstrate that the XRF microprobe technique is reliable for quantitative analysis of Br in halogen-rich (Cl or F) minerals and solutions, and that the matrix effect is negligible for the minerals and solutions

selected in this study, although the matrix effect of this XRF microprobe technique is known to be significant for some high-density minerals (e.g., monazite and zircon; Cheburkin et al., 1997).

The detection limit is defined as 3 standard deviations of the background for the XRF microprobe technique and has been established at about 1 ppm Br for solutions and mineral grains (Pan and Dong, 2003).

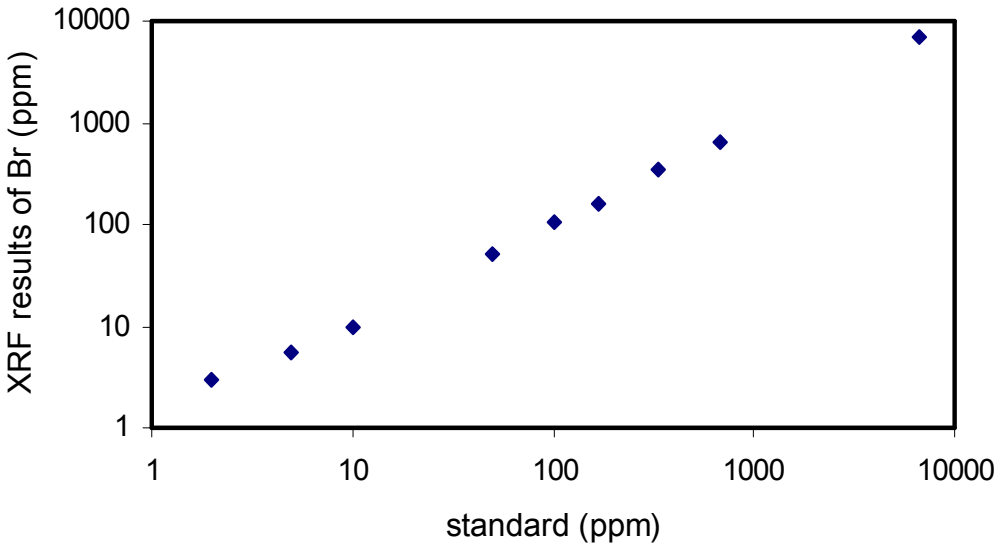

Figure 4.1 Br analyses from XRF vs in standard solutions

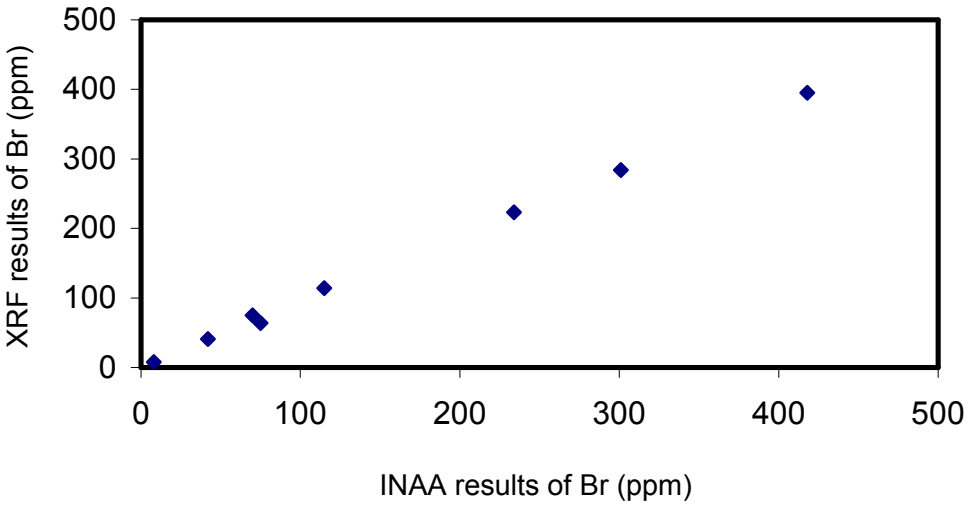

Figure 4.2 Br analyses from XRF vs from INAA

4.2 Instrumental Neutron Activation Analysis (INAA)

A few selected samples have been analyzed for Br by instrumental neutron activation analysis (INAA) at the Activation Laboratories of Ancaster, Ontario. This technique enables the analysis of all the halogen elements on the same specimen. About 150 mg powdered samples are first irradiated with thermal neutrons, then pyrohydrolyzed at 1000 ^{o}C in a quartz extraction line to ensure quantitative extraction of all the halogens from the samples. The irradiated samples are then mixed with V_2O_5 and heated in a platinum crucible. A dilute sodium hydroxide (NaOH) solution is used to absorb the volatile halogen compounds at room temperature. If needed, the NaOH solution may be subsequently split into two aliquots. One of them is used for iodine determination, and the other one is used for repeated counting of the gamma-ray spectra of ^{38}Cl and ^{82}Br using a Ge (Li) detector (Jambon et al., 1995).

The detection limit is affected by factors such as the matrix composition and geometry, counting times, sample size, and detector characteristics. But typical detection limits are from 10^{-3} to 10^{-9} g/g for different elements (Koeberl, 1993). Because the half-lives of ^{38}Cl and ^{82}Br are 37 minutes and 35.5 hours, respectively, the INAA technique is time consuming.

4.3 Electron Microprobe Analysis (EMPA)

Electron microprobe analysis (EMPA) is a common technique widely used to analyze major elements in geological samples (Reed, 1996). All the EMPA was performed on a JEOL JXA-8600 Superprobe equipped with three automated wavelength-dispersion and one energy-dispersion spectrometers at the Department of Geological Sciences, University of Saskatchewan. The analyses were obtained at 15 kV accelerating voltage, 10 nA beam current, 1 to 5 μm beam diameter, and 20-30 seconds counting time (except 60 seconds for Fe and Sr, 90 seconds for Br). Standards are quartz (Si), corundum (Al), diopside (Ca), jadeite (Na), sanidine (K), fayalite (Fe), celesite (Sr), tugtupite (Cl), anhydrite (S), and a synthetic crystal of KBr (Br). A natural scapolite (ON-70 of Shaw, 1960) was used as an independent standard.

After the XRF microprobe analysis, the grains of apatite, scapolite, and sodalite were mounted on Pyrex plugs, polished, and carbon-coated for electron microprobe (EMPA) analysis, except the scapolite grains in polished thin sections from the Nickel plate deposit (samples of 401-9, 401-12, 263-13, and 73-1-8), which were analyzed by EMPA before their removal for XRF microprobe analysis.

Electron microprobe analyses of scapolite and sodalite from the exchange experiments were executed at 10 kV accelerating voltage, 10 nA beam current, ~1 μm beam diameter, and 30 second counting time. The lower accelerating voltage was used to reduce the beam size.

5. Experimental Study on the Partitioning of F, Cl, and Br between Apatites and Melts

Many geological processes, such as crystallization of magmas, involve element partitioning between coexisting crystal phases and liquid phases. However, it has not always been possible to predict quantitatively the partition coefficients of elements between different phases, based on thermodynamic principles. In the absence of a consistent theoretical model for element partitioning with predictive capabilities, most geochemists continue to take an empirical approach, adopting constant values for partition coefficients for individual elements over a restricted *P-T-X* range (Purton et al., 1996) for the purpose of general modelling of elemental behaviour.

The partitioning of F, Cl, and Br between apatites and melts was experimentally inverstigated.

5.1. Experimental and Analytical Procedures

The starting materials used for partitioning experiments were prepared by mixing CaO-P_2O_5-CaF_2, and CaO-P_2O_5-$CaCl_2$ for fluorapatite and chlorapatite, respectively, and were doped with NaBr at various concentrations. The Br concentration in the starting materials ranges from 0.36 to 19.40 wt%

for the fluorapatite experiments and from 0.01 to 5.60 wt% for the chlorapatite experiments. Also, fluorapatite with minor amounts of the chlorapatite component and chlorapatite with minor amounts of the fluorapatite component have been investigated (Table 5.1). When the Br concentration is very low, a NaBr solution is used instead of the NaBr solid. The mixtures are thoroughly ground, then sealed in Pt capsules by the cold-welding technique. Each experiment contains approximately 40 to 50 mg of starting materials.

Experiments are conducted in a THERMOLYNE high-temperature Muffle furnace at atmospheric pressure at the Department of Geological Sciences, University of Saskatchewan. The experimental temperatures were selected by using Prener's (1967) phase diagrams (Figure 3.2). The capsules were first heated to 50 ^{o}C above the liquidus temperature for 4 to 10 hours in order to ensure complete melting and homogenization, then cooled down at a rate of 1 to 5 ^{o}C per hour to the run temperature (i.e., 50 ^{o}C below the liquidus temperature), and held there for a few hours to 7 days. The duration of each experiment was about 6 to 10 days. Several reversal experiments were conducted by heating directly to the run temperature, then held there for 7 to 12 days. The detailed experimental conditions are summarized in Table 5.1 and Appendix 1.

Table 5.1 Summary of halide compositions for apatite synthesis experiments

Run No.	Run T(°C)	Duration	Starting matrial (wt%)			Apatite[a]			Melt (wt%)[b]			Molar ratios in apatite			Molar ratios in melt			Partition coefficient		
		Days	Cl	Br	F	Cl (wt%)	Br (ppm)	F (wt%)	Cl	Br	F	X^*_{Cl}[d]	X^*_{Br}	X^*_F	X^*_{Cl}	X^*_{Br}	X^*_F	D_{Cl}*	D_{Br}*	D_F*
dp-ap-28e	1350-1120	9	40.06	2.54	0.93	5.00(102)	800(159)		50.7	3.29	1.21	0.993	0.007		0.932	0.027	0.041	1.066	0.258	
dp-ap-28h	1350-1120	9	39.19	3.35	1.11	5.20(74)	1600(277)		49.5	4.31	1.45	0.986	0.014		0.915	0.035	0.050	1.078	0.386	
average																		1.072	0.322	
stdev[c]																		0.009	0.091	
dp-ap-28g	1350-1120	9	38.62	3.22	1.90	3.40(96)	1400(157)	0.60(32)	49.3	4.15	2.30	0.744	0.013	0.243	0.889	0.033	0.077	0.836	0.406	3.140
dp-ap-28f	1350-1120	9	35.45	9.06	2.17	2.40(18)	1800(199)	0.70(46)	45.5	11.7	2.61	0.624	0.021	0.355	0.818	0.094	0.088	0.763	0.226	4.044
average																		0.799	0.316	3.592
stdev																		0.052	0.128	0.639
dp-ap-28c	1350-1220	6	37.41	0.01	0.00	5.50(24)	6(2)		43.0	0.01	0.00	1.000	0.000		1.000	0.000		1.000	0.486	
dp-ap-28b	1350-1220	6	37.44	0.09	0.00	5.70(85)	66(9)		43.0	0.10	0.00	0.999	0.001		0.999	0.001		1.001	0.485	
dp-ap-28bR	1220	12	35.70	0.12	0.00	5.30(72)	90(13)		41.0	0.13	0.00	0.999	0.001		0.999	0.001		1.001	0.493	
dp-ap-28a	1350-1220	6	41.73	0.97	0.00	5.00(180)	330(28)		65.6	1.54	0.00	0.997	0.003		0.990	0.010		1.007	0.302	
dp-ap-28aR	1220	12	36.76	0.97	0.00	5.40(86)	450(37)		42.3	1.13	0.00	0.996	0.004		0.988	0.012		1.008	0.318	
dp-ap-35a	1300-1220	6	43.39	5.60	0.00	4.00(115)	2000(167)		45.4	5.88	0.00	0.979	0.021		0.946	0.054		1.035	0.388	
average																		1.009	0.412	
stdev																		0.013	0.088	
dp-ap--36a	1420-1330	6	37.21	0.59	1.11	4.90(78)	430(29)	0.70(17)	39.3	0.63	1.14	0.780	0.003	0.217	0.943	0.007	0.051	0.827	0.454	4.285
dp-ap--36b	1420-1330	6	34.59	1.14	4.08	2.20(15)	720(88)	2.60(93)	36.7	1.21	4.18	0.309	0.005	0.686	0.815	0.012	0.173	0.379	0.384	3.966
average																		0.603	0.419	4.125
stdev																		0.317	0.050	0.226
dp-ap-29b	1350-1220	6	0.30	0.36	22.53	0.01(2)	3.2(4)	5.00(85)	0.35	0.42	25.84	0.001	0.000	0.999	0.007	0.004	0.989	0.134	0.005	1.010
dp-ap-33b	1300-1220	6	0.00	0.45	24.80	0.02(2)	60(60)	5.00(41)	0.00	0.47	26.00	0.002	0.000	0.997	0.000	0.004	0.996		0.089	1.002
dp-ap-29h	1360-1220	8	0.00	0.95	22.22		40(7)	4.90(84)	0.00	1.11	25.48	0.000	0.000	1.000	0.000	0.010	0.990		0.025	1.010
dp-ap-29a	1350-1220	6	1.84	2.22	23.86	0.03(1)	46(5)	4.70(73)	2.16	2.61	27.41	0.004	0.000	0.996	0.040	0.021	0.939	0.092	0.014	1.061
dp-ap-33a	1300-1220	6	0.00	4.25	26.49		130(59)	5.50(67)	0.00	4.49	27.79	0.000	0.001	0.999	0.000	0.037	0.963		0.022	1.038
dp-ap-29c	1360-1220	8	0.00	4.92	23.71	0.01(0)	160(62)	5.60(20)	0.00	5.78	27.23	0.000	0.001	0.999	0.000	0.048	0.952		0.021	1.049
dp-ap-29cR	1220	8	0.00	4.93	23.71		160(71)	3.90(59)	0.00	5.80	27.23	0.000	0.001	0.999	0.000	0.048	0.952		0.021	1.050
dp-ap-29d	1350-1220	10	0.00	10.04	22.04		400(101)	500(103)	0.00	11.81	25.26	0.000	0.002	0.998	0.000	0.100	0.900		0.022	1.109
dp-ap-29dR	1220	8	0.00	10.04	22.04		300(182)	4.60(62)	0.00	11.81	25.26	0.000	0.002	0.998	0.000	0.100	0.900		0.021	1.109
dp-ap-29e	1360-1220	10	0.00	19.40	18.99		600(136)	4.30(47)	0.00	22.81	21.68	0.000	0.004	0.996	0.000	0.200	0.800		0.019	1.245
average																		0.113	0.021	1.048
stdev																		0.029	0.003	0.040
dp-ap-30a	1320-1250	5	1.18	1.75	24.94	0.02(1)	44(2)	4.50(102)	1.25	1.86	26.23	0.003	0.000	0.997	0.025	0.016	0.959	0.128	0.017	1.039
dp-ap-30aR	1250	5	1.18	1.75	24.94	0.02(1)	40(8)	4.40(69)	1.25	1.86	26.23	0.003	0.000	0.997	0.025	0.016	0.959	0.126	0.015	1.039
dp-ap-30b	1320-1250	5	2.25	3.08	23.83	0.04(1)	70(22)	4.00(112)	2.38	3.27	25.05	0.006	0.000	0.993	0.047	0.029	0.924	0.129	0.014	1.075
dp-ap-30bR	1250	5	2.25	3.08	23.83	0.04(1)	100(72)	4.00(148)	2.38	3.27	25.05	0.006	0.001	0.994	0.047	0.029	0.924	0.124	0.022	1.075
dp-ap-30c	1320-1250	5	3.99	5.70	21.84	0.04(1)	50(12)	3.70(65)	4.23	6.05	22.95	0.006	0.000	0.993	0.085	0.054	0.861	0.073	0.006	1.154
dp-ap-30cR	1250	5	3.99	5.70	21.84	0.05(1)	50(34)	4.40(30)	4.23	6.05	22.94	0.007	0.000	0.993	0.085	0.054	0.861	0.080	0.006	1.153
average																		0.127	0.017	1.057
stdev																		0.002	0.004	0.021
dp-ap-32a	1450-1400	6	1.55	2.15	18.19	0.03(2)	60(42)	3.40(60)	1.58	2.19	18.49	0.005	0.000	0.995	0.043	0.026	0.931	0.115	0.017	1.068

a: the contents of Cl and F are from EMPA, and Br is from XRF except some very fine-grained apatites, to avoid the influnces from bromine-rich melts, EMPA results are used (dp-ap-29c, 29cR, 30bR, 30cR, 32a, 33a, and 33b); **b**: halogen contents in melts are calculated based on mass balance method, detailed in text; **c**: standard deviation;
d: X^*_i=i/(F+Cl+Br) in molar, where i=F, Cl, or Br. One standard deviation (1δ) is in the parentheses.

At the end of each experiment, the capsules are quenched by dropping them into water. Most of the experimental products are composed of millimeter-sized crystals of apatite and quenched melts, which were separated under a binocular microscope. The apatite crystals were analyzed by using an X-ray Fluorescence (XRF) Microprobe for Br, and a JEOL-JXA 8600 electron microprobe for major elements. The XRF analyses were performed at 40 kV and 20 mA, and counting time of 900 to 1800 seconds depending on the Br concentration. The electron microprobe analyses included an accelerating potential of 15 kV, beam current of 10 nA, beam size of 1 to 5 μm in diameter. The counting times are 20 seconds for Ca, Na, K, P, Cl, F and 90 seconds for Br.

Approach to Equilibrium

The approach to equilibrium was demonstrated by the reversed experiments. Both the forward and reversed experiments yielded apatite crystals and gave similar partition coefficients for Br, Cl, and F, confirming that chemical equilibrium was attained during the present experiments.

Melt Composition Calculation

Because the electron microprobe analyses for the quenched melts were not successful and the quenched melts of the chlorapatite experiments were

quickly dissolved when exposed to air, the melt composition was calculated on the basis of mass balance. The amounts of apatite and melt for each run were calculated on the basis of their phase relationships. This is the equation used to calculate the melt composition:

$$C_i^{melt} = \frac{C_i^{total} - X^{apatite} C_i^{apatite}}{X^{melt}} \qquad (5.1)$$

where the C_i^{melt} is the content of i (Cl, F, or Br) in the melt, C_i^{total} is the total content of i in the starting material, $C_i^{apatite}$ is the content of i in the apatite, $X^{apatite}$ and X^{melt} are the mass fractions of apatite and melt, respectively, where $X^{apatite} + X^{melt} = 1$.

At high halide-melt to mineral-crystal ratios, the composition of the melt is almost unchanged, while the mineral composition may be significantly changed.

5.2. Experimental Results

Most of the experimental products consist of apatite crystals and quenched melts. The separated apatite crystals were analyzed by an X-ray Fluorescence (XRF) Microprobe for Br, and a JEOL-JXA 8600 electron microprobe for major elements. Summarized analytical results are listed in

Table 5.1 and the detailed XRF and EMPA data are listed in Table 5.2 and Table 5.3, respectively.

5.2.1 Halogens in Apatite

The Br contents in fluorapatite are in direct proportion to the Br concentrations in the starting materials up to ~20 wt % of Br in the latter (Figure 5.1) and are fitted by a line started at the origin. The Br, Cl, and F contents in the apatite from the reversed experiments are close to their contents of the forward counterparts (Figure 5.1, Table 5.1), confirming the proximity to equilibrium at the experimental conditions of this study.

Similarly, the Br contents in chlorapatite are linearly correlated to the Br concentrations (at least to ~6 wt % Br) in the starting materials. The analytical data are fitted to a line starting from the origin, but with a much steeper slope in comparison with that from the fluorapatite experiments (Figure 5.2). The Br contents in chlorapatite are much higher (1 order of magnitude) than those in

Table 5.2 Summary of XRF results for Br content in synthetic apatite separates

Run No.	Starting Materials			Apatite
	Br %	Cl %	F %	Br (ppm)*
Chlorapatite				
ap-28-a	0.97	41.73	0.00	330(28)
ap-28-a(R)	1.09	41.39	0.00	450(37)
ap-28-b	0.10	42.25	0.00	66(9)
ap-28-b (R)	0.14	41.91	0.00	90(13)
ap-28-c	0.01	42.25	0.00	6(2)
ap-28-e	2.54	40.06	0.93	800(159)
ap-28-f	9.06	35.45	2.17	1800(199)
ap-28-g	3.22	38.62	1.90	1400(157)
ap-28-h	3.35	39.19	1.11	1600(277)
ap-35-a	5.60	43.39	0.00	2000(167)
ap-36-a	0.59	37.21	1.11	430(29)
ap-36-b	1.14	34.59	4.08	720(88)
Fluorapatite				
ap-29-a	2.20	1.84	23.86	46(5)
ap-29-b	0.40	0.33	25.05	3(0)
ap-29-h	1.06	0.00	24.96	40(7)
ap-29-c	4.92	0.00	23.71	400(180)
ap-29-c(R)	4.92	0.00	23.71	500(231)
ap-29-d	10.04	0.00	22.04	400(101)
ap-29-d(R)	10.04	0.00	22.04	300(182)
ap-29-e	19.40	0.00	18.99	600(136)
ap-30-a	1.75	1.18	24.94	44(2)
ap-30-a(R)	1.75	1.18	24.94	40(8)
ap-30-b	3.08	2.25	23.83	60(22)
ap-30-c	5.70	3.99	21.84	50(12)
ap-32-a	2.15	1.55	18.19	200(38)
ap-33-a	4.25	0.00	26.49	4900(985)
ap-33-b	0.45	0.00	24.80	200(39)

*One standard deviation (1δ) in the parentheses

Table 5.3 EMPA results of synthetic apatites (wt%)

Run No.	CaO	P_2O_5	Na_2O	K_2O	F	Cl	Br	Total
Chlorapatite								
ap-28-a	55.40(56)	40.20(43)	0.00	0.01(1)	0.00	5.00(180)	0.011(7)	100.62
ap-28-a(R)	55.90(51)	39.10(61)	0.00		0.00	5.40(86)	0.020(11)	100.42
ap-28-b	55.00(113)	39.80(70)	0.00	0.03(4)	0.00	5.70(85)	0.020(16)	100.55
ap-28-b(R)	55.80(48)	39.70(37)	0.00	0.01(1)	0.00	5.30(72)	0.009(3)	100.82
ap-28-c	54.90(86)	39.40(54)	0.00		0.00	5.50(24)	0.007(5)	99.81
ap-28-e	53.00(211)	42.00(202)	0.05(2)	0.02(2)	0.00	5.00(102)	0.060(18)	100.13
ap-28-f	53.00(134)	44.00(231)	0.05(2)	0.01(1)	0.70(46)	2.40(18)	0.110(26)	100.27
ap-28-g	51.00(191)	42.00(160)	0.10(2)	0.01(1)	0.60(32)	3.40(96)	0.080(19)	97.19
ap-28-h	51.00(198)	41.00(269)	0.10(2)	0.01(1)	0.00	5.20(74)	0.120(22)	97.43
ap-35-a	55.80(87)	40.10(79)	0.02(2)	0.02(1)	0.00	4.00(115)	0.080(17)	100.02
ap-36-a	51.70(43)	41.90(97)	0.06(2)	0.01(1)	0.70(17)	4.90(78)	0.030(10)	99.30
ap-36-b	52.90(46)	42.70(91)	0.03(2)		2.60(93)	2.20(15)	0.020(11)	100.45
Fluorapatite								
ap-29-a	56.00(166)	42.20(41)	0.00	0.01(2)	4.70(73)	0.03(1)	0.010(10)	102.95
ap-29-b	55.30(87)	42.30(39)	0.00	0.01(2)	5.00(85)	0.01(1)	0.020(11)	102.64
ap-29-c	54.20(20)	42.20(51)	0.00	0.00	5.60(20)	0.01(0)	0.016(6)	102.03
ap-29-c(R)	57.00(121)	41.00(269)	0.10(11)	0.00	3.90(59)	0.00	0.016(7)	102.02
ap-29-d	55.00(117)	43.00(76)	0.02(4)	0.01(1)	5.00(103)	0.00	0.020(12)	103.05
ap-29-d(R)	56.00(177)	41.50(41)	0.01(3)	0.00	4.60(62)	0.01(1)	0.006(5)	102.13
ap-29-e	56.60(91)	41.10(82)	0.00	0.00	4.30(47)	0.01(1)	0.015(6)	102.03
ap-29-h	56.00(145)	41.00(59)	0.00	0.00	4.90(84)	0.01(1)	0.009(5)	101.92
ap-30-a	54.00(223)	44.00(289)	0.01(1)	0.01(1)	4.00(102)	0.02(1)	0.011(6)	102.05
ap-30-a(R)	54.00(213)	45.00(300)	0.01(1)	0.10(10)	4.40(69)	0.02(1)	0.010(8)	103.54
ap-30-b	52.00(173)	45.00(202)	0.02(2)	0.04(5)	4.00(112)	0.04(1)	0.004(3)	101.10
ap-30-b(R)	53.00(164)	45.00(214)	0.01(1)	0.04(4)	4.00(148)	0.04(1)	0.010(7)	102.10
ap-30-c	54.80(99)	43.50(58)	0.01(3)	0.02(1)	3.70(65)	0.04(1)	0.006(4)	102.08
ap-30-c(R)	54.00(31)	43.30(25)	0.01(2)	0.01(1)	4.40(30)	0.05(1)	0.005(3)	101.78
ap-32-a	58.00(210)	40.00(235)	0.02(2)	0.01(1)	3.40(60)	0.03(2)	0.006(4)	101.47
ap-33-a	55.50(89)	41.40(50)	0.03(5)	0.01(1)	5.50(67)	0.00	0.013(6)	102.45
ap-33-b	54.10(81)	43.20(51)	0.02(2)	0.00	5.00(41)	0.02(2)	0.006(6)	102.35

One standard deviation (1δ) is in the parentheses [e.g., 0.011(7)=0.011± 0.007]

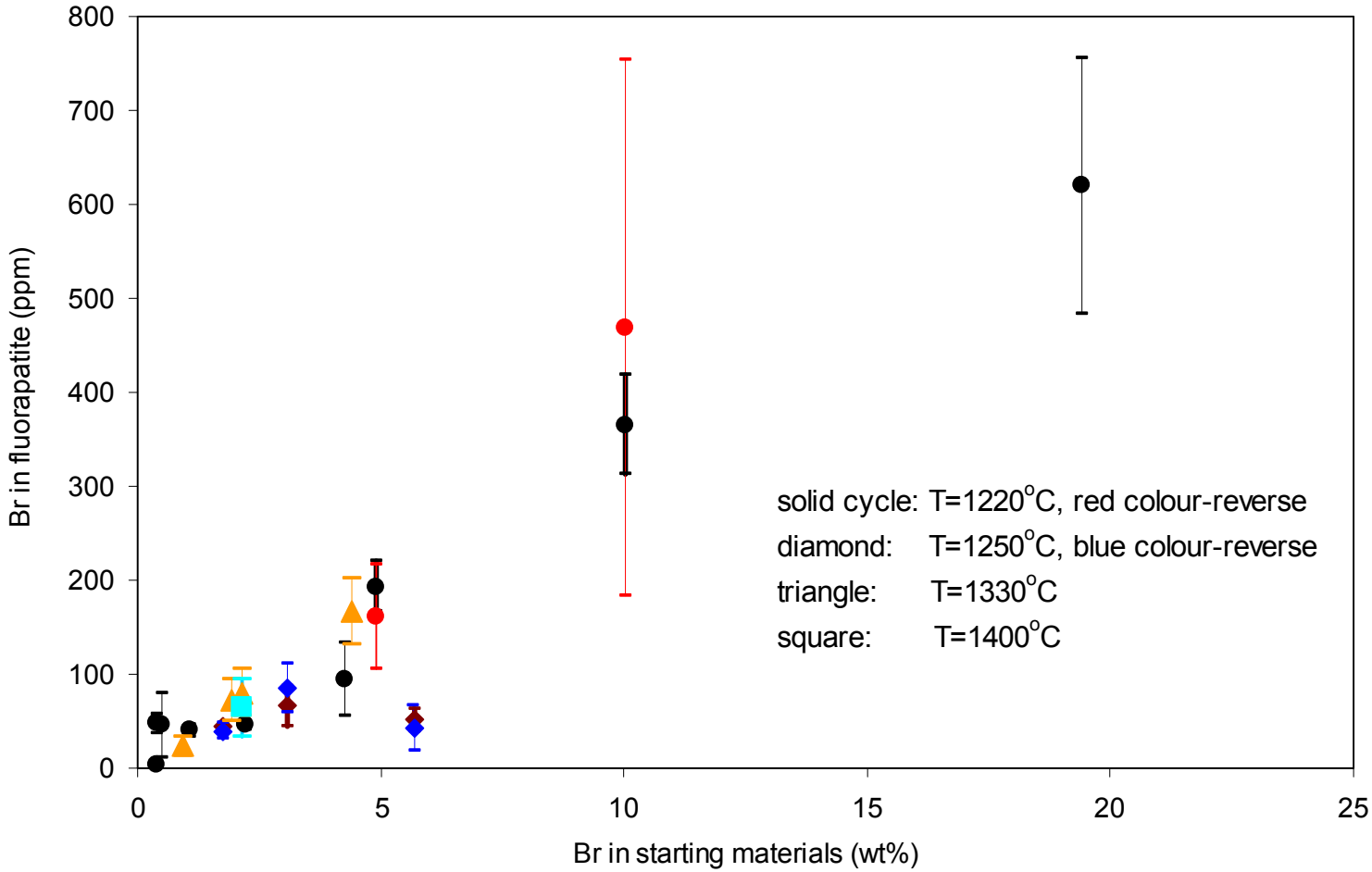

Figure 5.1 Bromine in fluorapatite (ppm) vs bromine in starting materials (wt%)

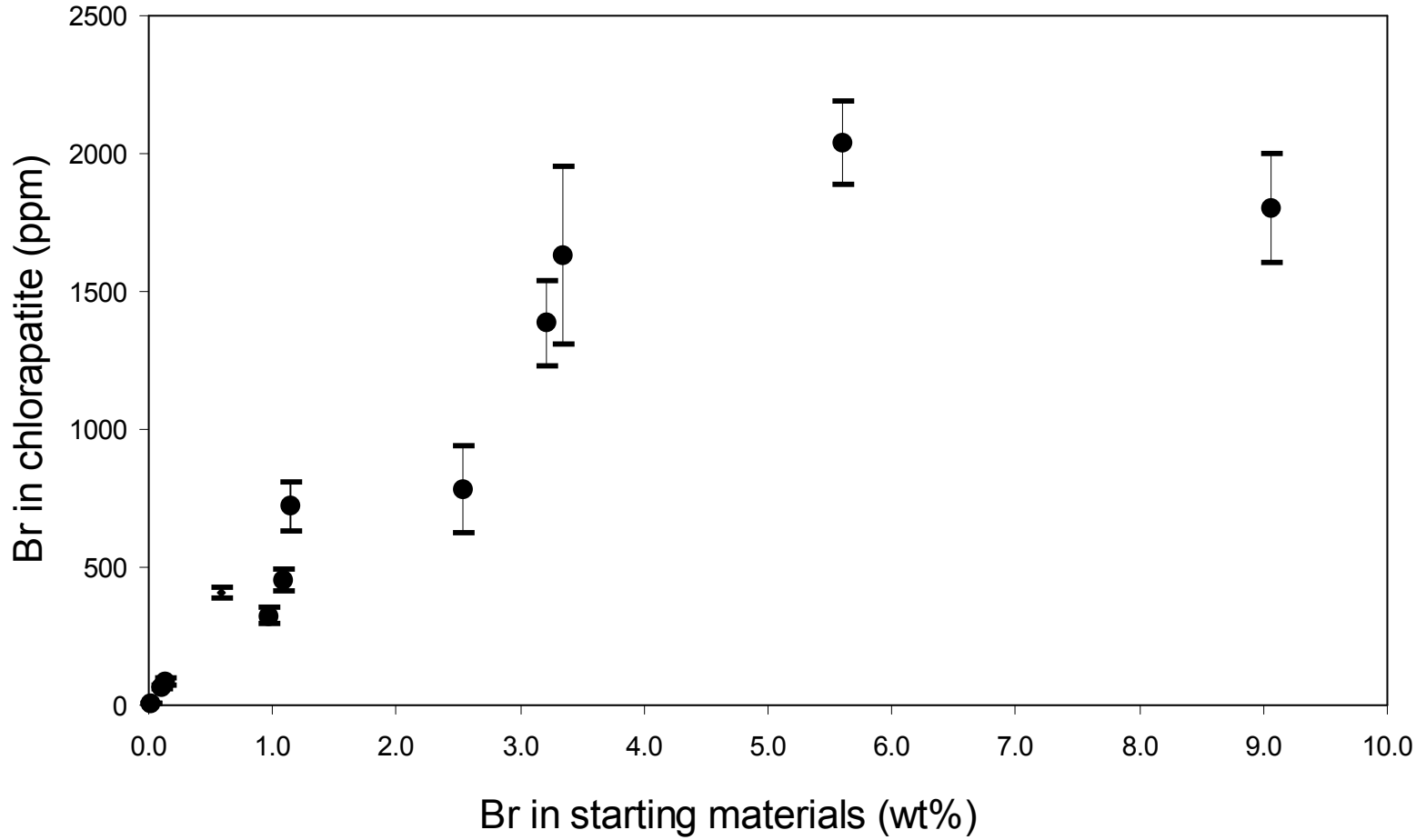

Figure 5.2 Br in chlorapatite(ppm) vs Br in starting materials(wt%)

fluorapatite (Figures 5.1 and 5.2, also Figure 5.7) with similar Br concentration in the starting materials. The anomalous lower Br content of 1800 ppm in the chlorapatite from an experiment of run dp-ap-28f with 9.06 wt % Br in the starting material (Figure 5.2, Table 5.1) probably is due to the analytical uncertainties. However, similar partitioning behavior of halogens (F and Cl) in apatites was reported by Brenan (1993).

In addition, the Cl content in fluorapatite is linearly correlated to the Cl concentration in the starting materials to at least 2.25 wt % Cl in the latter (Figure 5.3). However, the Cl content in fluorapatite from experiments with higher Cl concentrations in the starting materials (e.g., 3.99 wt % at run dp-ap-30) remains unchanged (Figure 5.3), a non-Henry's law behaviour.

The F contents in chlorapatite increase with increasing F concentration in the starting materials at least to 4.08 wt % F in the latter (Figure 5.4). The temperature dependence of the F partitioning between chlorapatite and melt is apparent: the partition coefficient of F between chlorapatite and melt increases with increased temperature (Figure 5.4, also Figure 5.11d).

5.2.2 The Molar Ratios of Halogens in Apatite Compared with those in the Melt

In geological environments, the apatite compositions, namely the variations of F-Cl-Br-OH, are controlled by the relative concentrations of F, Cl, Br, and OH in the parent melts/liquids from which the apatites are crystallized.

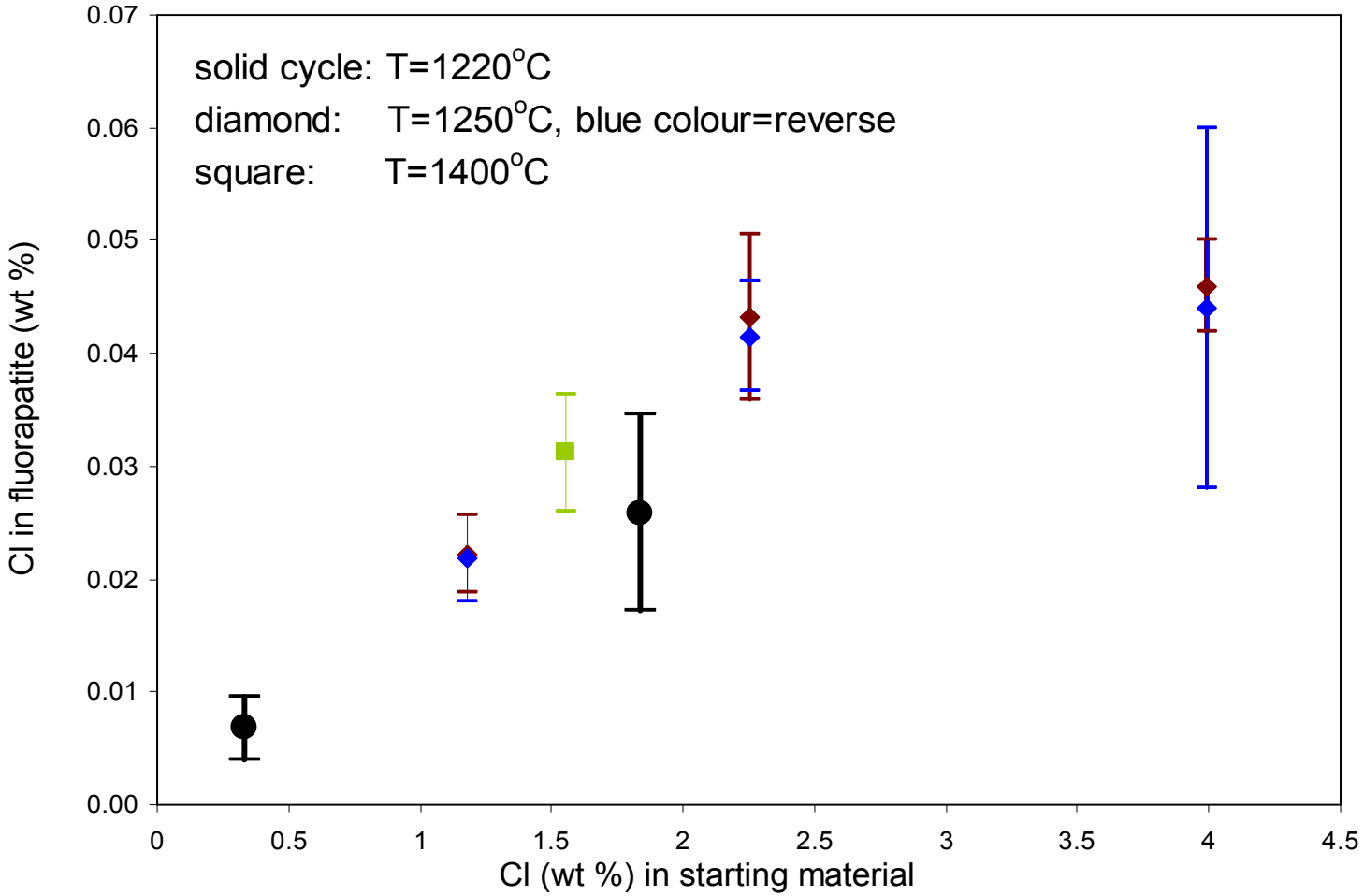

Figure 5.3 Chlorine in fluorapatite vs chlorine in starting materials (wt%)

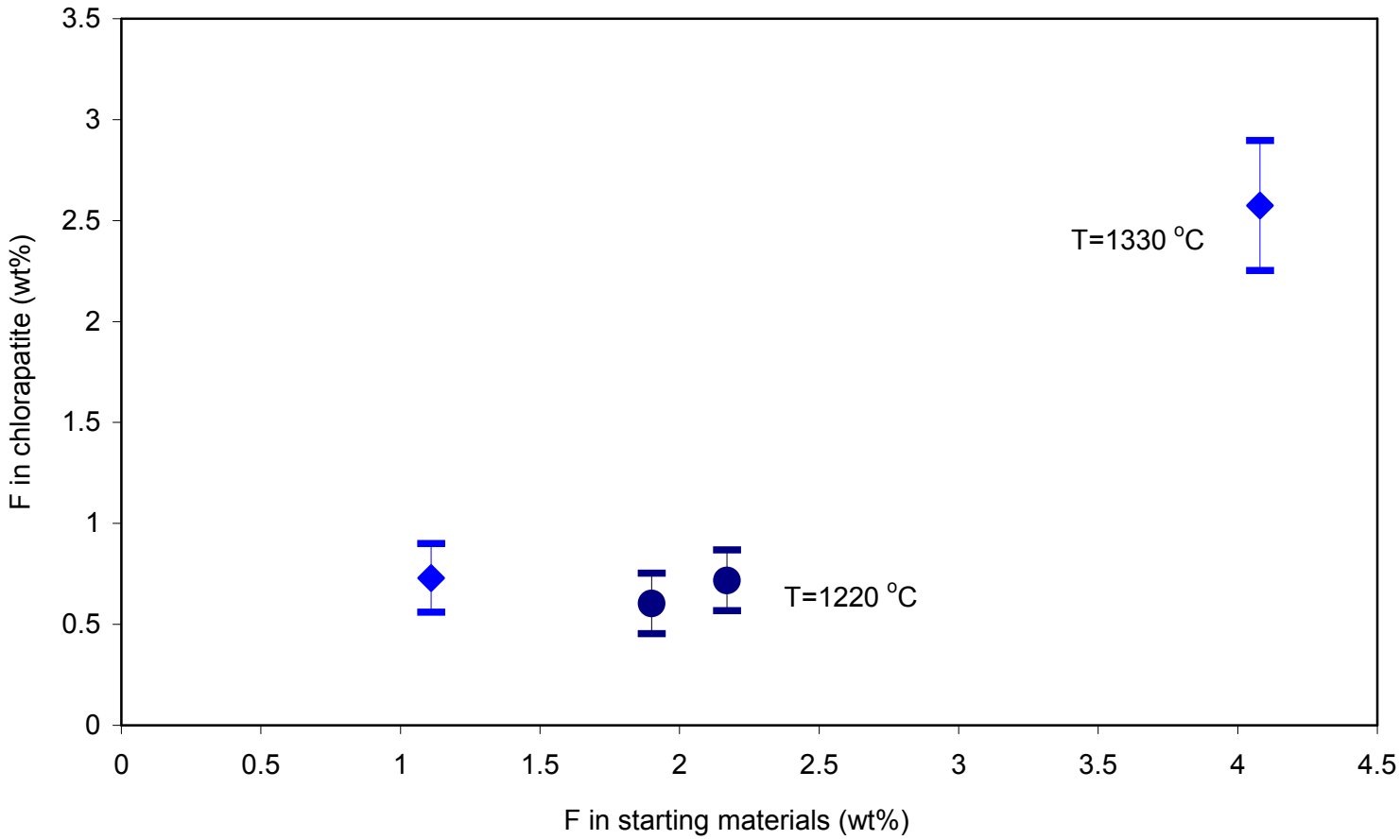

Figure 5.4 Fluorine in chlorapatites vs fluorine in starting materials

For example, it is expected that the partitioning of Cl, F, and Br into apatites is a function of the Cl/F ratio (independent of the OH concentration) in melts/liquids (Meurer and Natland, 2001). Therefore, the halogen ratios in apatites are functionally related to the halogen ratios in the melts/liquids.

The molar ratios of Cl/(Cl+F+Br) between apatites and coexisting melts are illustrated in Figure 5.5. There are two distinct areas with different Cl partitioning behavior corresponding to the differences in Cl concentrations in the melts/liquids. When the Cl/(Cl+F+Br) molar ratio is less than 0.085 in the melt (i.e., fluorapatite experiments), the Cl/(Cl+F+Br) molar ratio in the coexisting apatite is less than 0.007. Moreover, the molar ratios of Cl/(Cl+F+Br) in the melt correlate positively with those in fluorapatite (Figures 5.3 and 5.5). Consequently, the molar partition coefficient of Cl (D^*_{Cl}) between fluorapatite and melt is about 0.11 to 0.13. When the molar ratios of Cl/(Cl+F+Br) in the melt/liquid are larger than 0.82 (i.e., chlorine-rich apatite experiments), the molar ratios of Cl/(Cl+F+Br) in chlorine-rich apatite vary from 0.62 to 1.00 and increase with increasing Cl/(Cl+F+Br) molar ratios in the melt (Figure 5.5). Therefore, the molar partition coefficient of Cl (D^*_{Cl}) between chlorapatite and melt is close to unity (e.g., 1.035).

The partitioning of F between fluorapatite and melt is distinct from that between chlorapatite and melt. For example, the F/(Cl+F+Br) molar ratios in apatite from F-poor experiments increase abruptly from 0.00 to 0.69 with increasing F/(Cl+F+Br) molar ratios from 0.00 to 0.17 in the melt, yielding an overall slope of 3.85 (Figure 5.6). In the F-rich experiments with

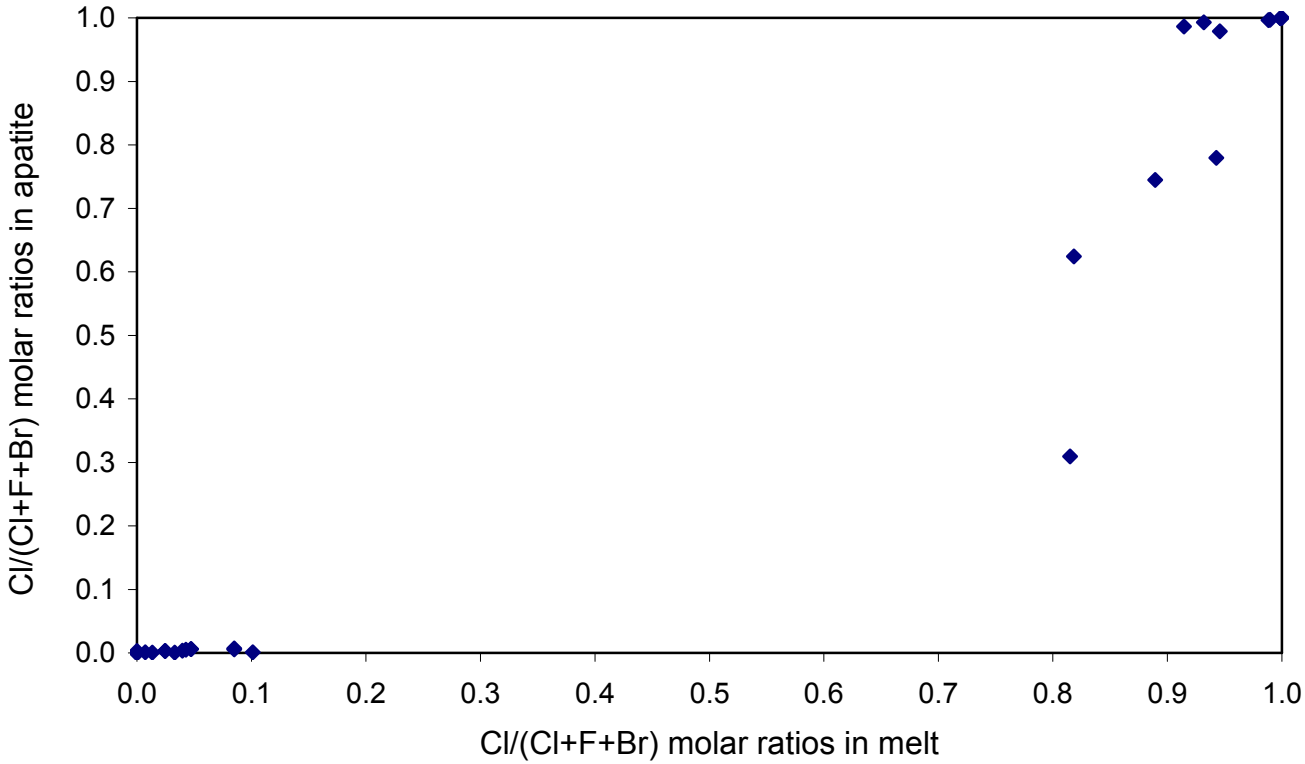

Figure 5.5 Cl/(Cl+F+Br) molar ratios in apatite vs in melt

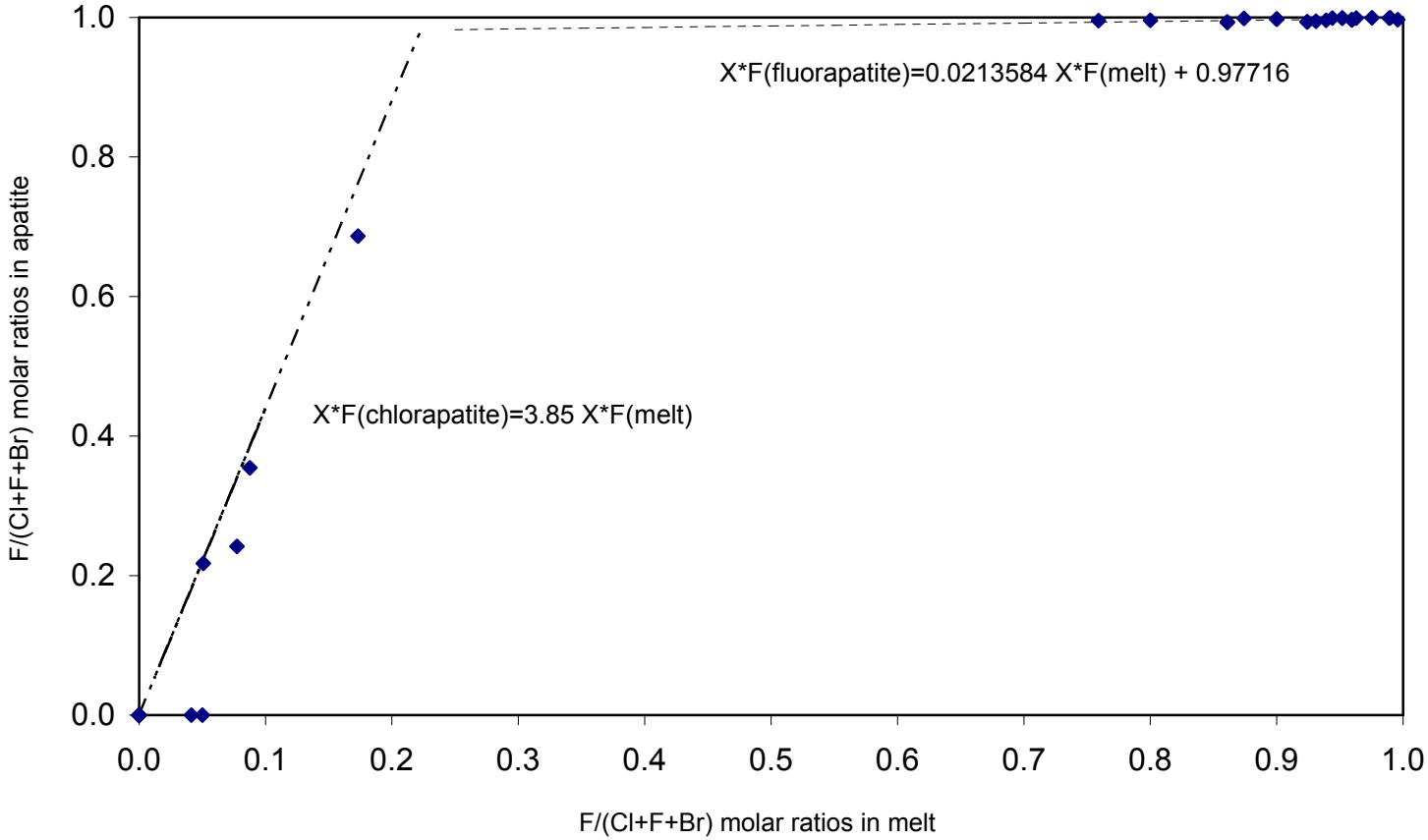

Figure 5.6 F/(Cl+F+Br) molar ratios in melt vs in apatite

F/(Cl+F+Br) molar ratios higher than 0.80 in the melt, the molar ratios of F/(Cl+F+Br) in apatite are close to 1 (0.993 to 0.999). For the fluorapatite endmember, the F/(Cl+F+Br) molar ratio in apatite increases minimally with increasing F/(Cl+F+Br) molar ratio in the melt.

The molar ratio of Br/(Cl+F+Br) in apatites is positively correlated to the molar ratio of Br/(Cl+F+Br) in the corresponding melts. Also, the uptake of Br by fluorapatite is distinct from that of chlorapatite (Figure 5.7). It is expected that Br readily replaces Cl in chlorapatite owing to their similarity in ionic radius, whereas Br is much larger than F and thus is difficult to enter the F site in fluorapatite.

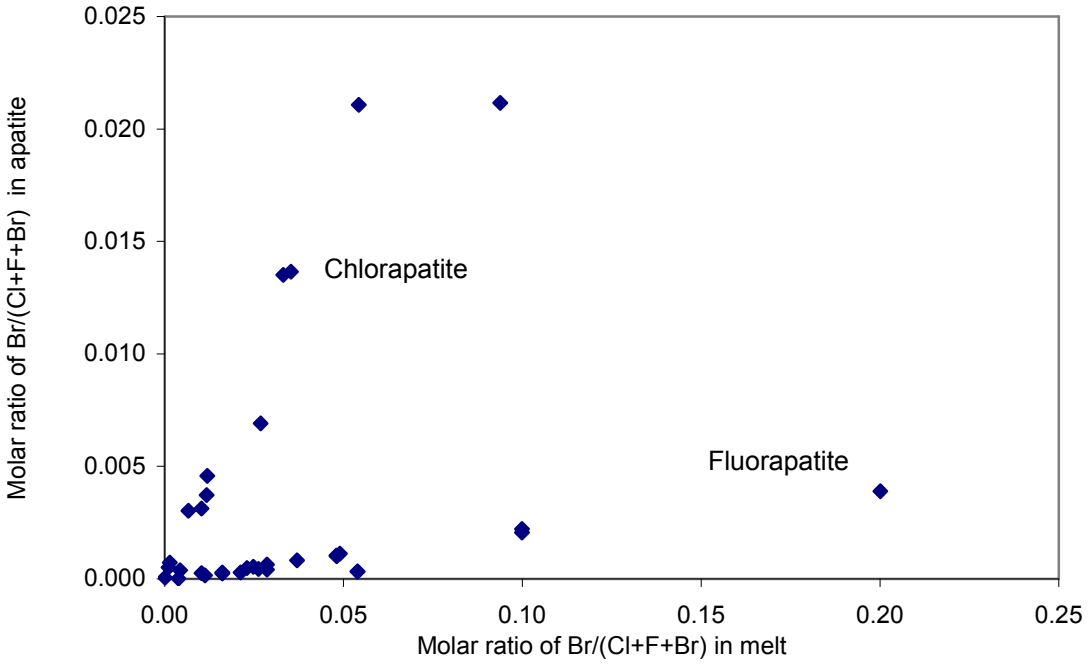

Figure 5.7 Br/(Cl+F+Br) molar ratio in apatite vs in melt. There are two different trends representing the chlorapatite and fluorapatite, respectively.

5.2.3 The Molar Partition Coefficients of F, Cl, and Br between Apatites and Melts

The molar partition coefficient of Cl (D^*_{Cl}) between apatite and melt is in positive linear correlation with the molar ratio of Cl/(Cl+Br+F) in apatites (Figure 5.8a) or in positive correlation (not linearly) with the molar ratios of Cl/(Cl+Br+F) in the melts (Figure 5.8b). The value of D^*_{Cl} between the fluorapatite and melt with trace $CaCl_2$ [<0.09 of the molar ratios of Cl/(Cl+Br+F) in melts] is about 0.113 (± 0.029) at a run temperature of 1220 ^oC, 0.127 (± 0.002) at 1250 ^oC, and 0.115 at 1400 ^oC, respectively. Meanwhile, the value of D^*_{Cl} between the chlorapatite and $CaCl_2$-rich melt [>0.9 of the molar ratios of Cl/(Cl+Br+F) in the melts] is about 1.072 (± 0.009), 1.009 (± 0.013), and 0.827 at run temperatures of 1120 ^oC, 1220 ^oC and 1330 ^oC, respectively. The results of D^*_{Cl} are apparently temperature dependent (detailed in 5.2.4).

Oppositely, the molar partition coefficient of fluorine (D^*_F) between apatite and melt is in negative correlation with the molar ratios of F/(Cl+Br+F) in apatites, except in the special situation when there is no fluorine in the apatite (Figure 5.9a, 5.9b). If the molar ratio of F/(Cl+Br+F) in apatite is less than 0.7, the D^*_F is about 4.125 (± 0.226) and 3.592 (± 0.639) at run temperatures of 1330 ^oC and 1120 ^oC, respectively. With increased F/(Cl+Br+F) molar ratios in apatites (>0.69), D^*_F drops to 1.049 (± 0.040), 1.057 (± 0.021), and 1.068 at run temperatures of 1220 ^oC, 1250 ^oC, and 1400 ^oC, respectively.

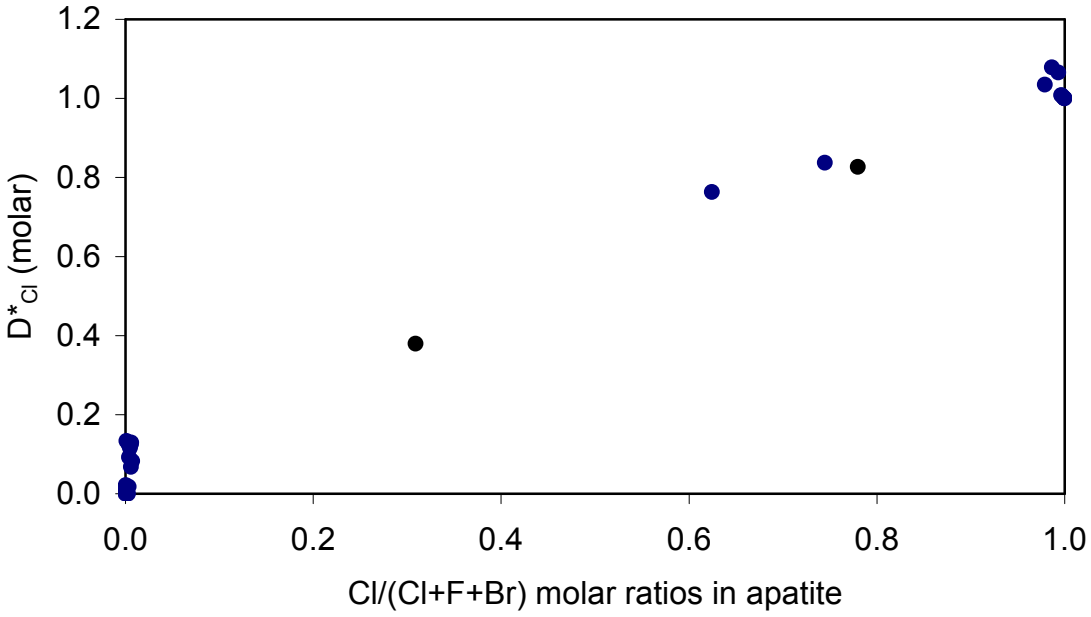

Figure 5.8a D^*_{Cl} vs molar ratios of Cl/(Cl+F+Br) in apatite
$D^*_{Cl}=0.95846\ X^*_{Cl}{}^{Apt}+0.081398$, r=0.9898, sigma=0.00214

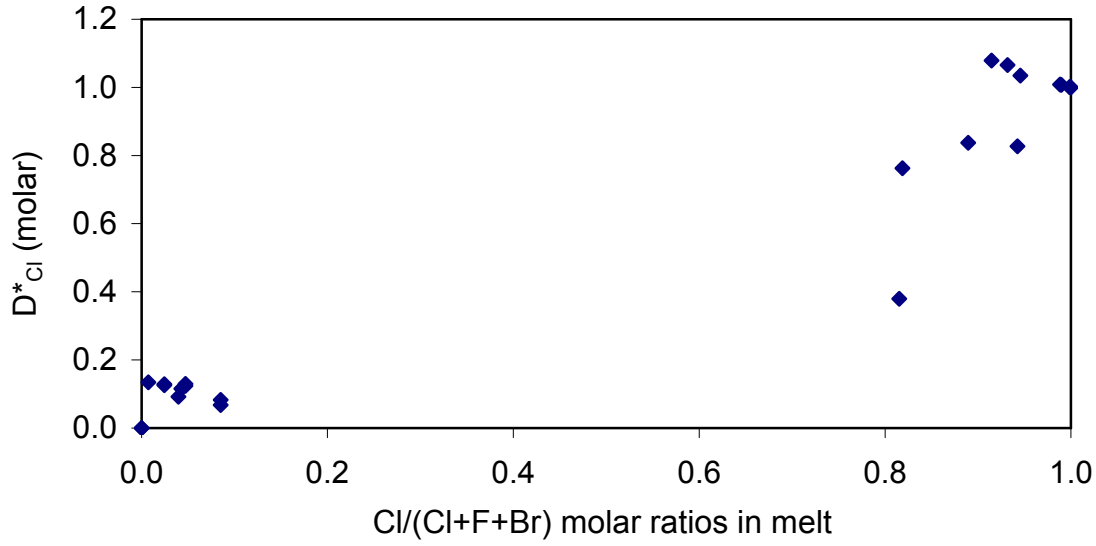

Figure 5.8b D^*_{Cl} vs molar ratios of Cl/(Cl+F+Br) in melt

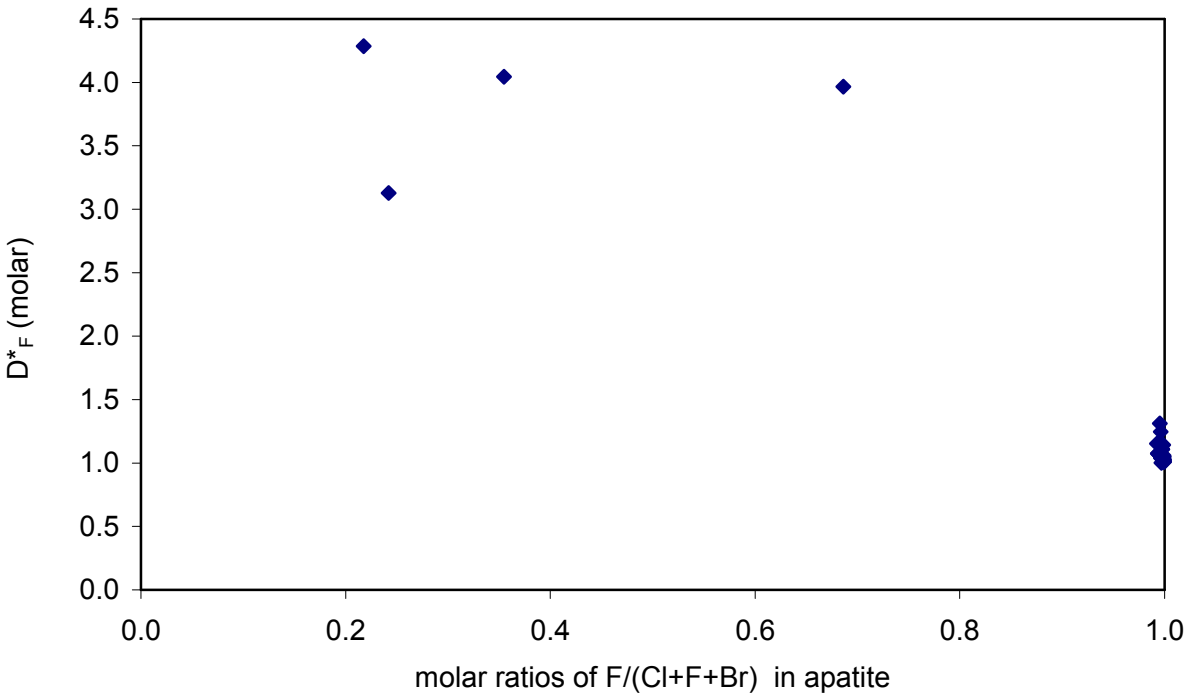

Figure 5.9a D^*_F vs molar ratios of F/(Cl+F+Br) in apatite

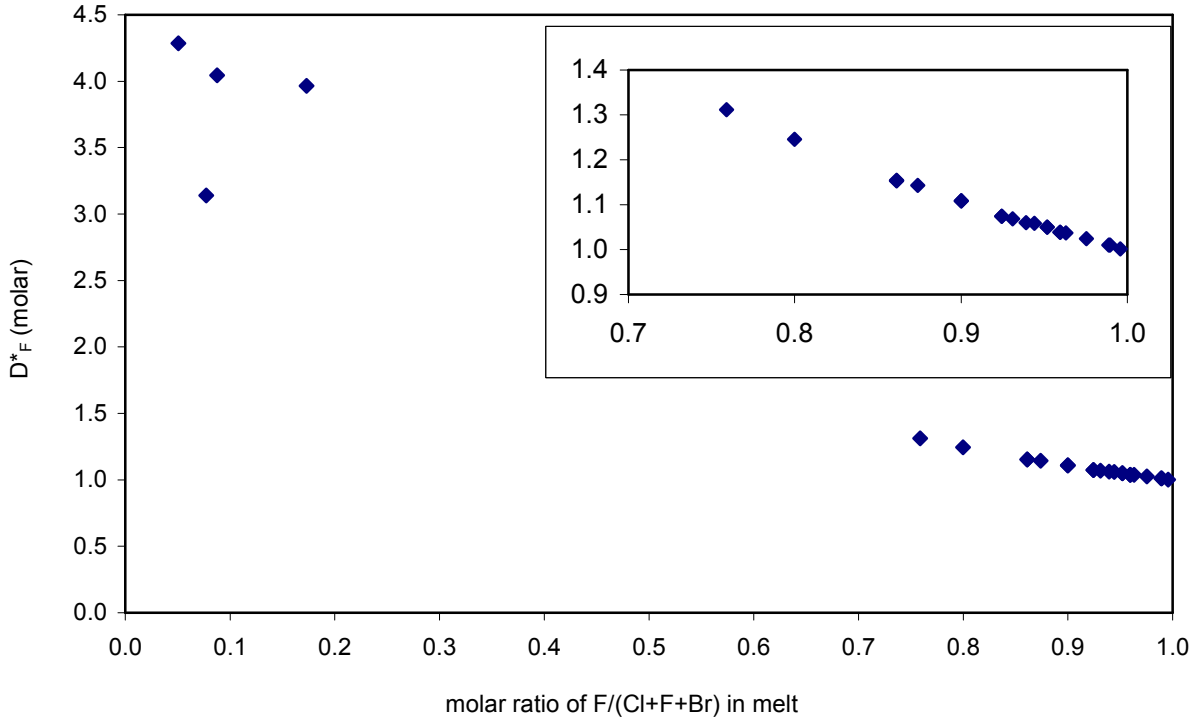

Figure 5.9b D^*_F vs molar ratio of F/(Cl+Br+F) in melt

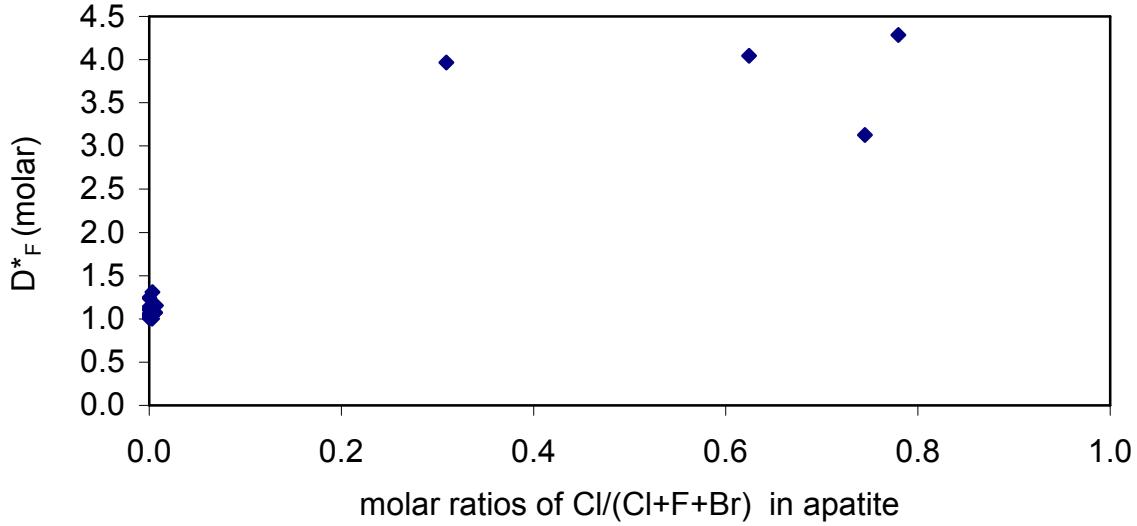

Figure 5.9c D^*_F vs molar ratios of Cl/(Cl+F+Br) in apatite

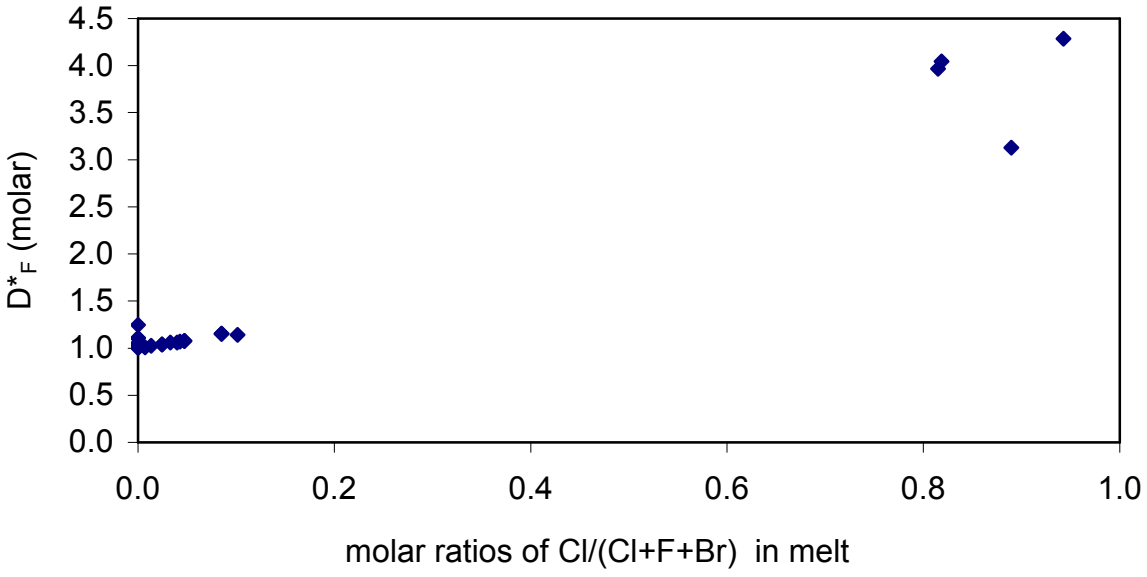

Figure 5.9d D^*_F vs molar ratios of Cl/(Cl+F+Br) in melt

Using the molar ratio of F/(Cl+Br+F) in the melt as reference (Figure 5.9b), trace amount of fluorine in the melt (e.g., less than 0.173 molar ratio of F/(Cl+Br+F)) results in a higher D^*_F value (3.14 to 4.29); this value drops to near 1.0 when the molar ratio of F/(Cl+Br+F) in the melt is higher than 0.80 (Table 5.1).

Bromine behaves differently from chlorine and fluorine. The molar partition coefficient of bromine (D^*_{Br}) is independent of the molar ratios of Br/(Cl+Br+F) in apatite or in melt (Figure 5.10a and 5.10b). Instead, the values of D^*_{Br} are stable at two different levels, corresponding to chlorapatite and fluorapatite, respectively. The Br molar partition coefficients (D^*_{Br}) are about 0.316-0.322, 0.412 (±0.088), and 0.419 (±0.050) for chlorapatite (X^*_{Cl} >0.31 in apatite) at the run temperatures of 1120 ^oC, 1220 ^oC, and 1330 ^oC, respectively (Table 5.1). For fluorapatite, the Br molar partition coefficients (D^*_{Br}) are about 0.0207 (±0.0033), 0.0174 (±0.0035), and 0.0168 at the run temperatures of 1220 ^oC, 1250 ^oC, and 1400 ^oC, respectively (Table 5.1; Figures 5.10a, c; also Figures 5.11a, b). Obviously, the values of D^*_{Br} are positively correlated to the molar ratios of Cl/(Cl+Br+F) in apatite or melt (Figure 5.10c, d).

Since there have been no experiments carried out with Cl/(Cl+Br+F) molar ratios between 0.085 and 0.815 in the melt (Table 5.1 and Figure 5.10d), it is not clear how the bromine partitioning changes from fluorapatite-style to chlorapatite-style, i.e., does it change gradually or abruptly? More experiments with Cl/(Cl+Br+F) molar ratios in the melt between 0.085 and 0.815 are required to resolve the transition.

5.2.4 Temperature Dependence of the Molar Partition Coefficient

The molar partition coefficients for halogens between apatites and melts are temperature dependent (Figure 5.11). With increased temperature, the values of D^*_{Br} between chlorapatites and melts are increased as well, for example, from 0.316-0.322 at 1120 ^oC, to 0.412 at 1220 ^oC, and to 0.419 at 1330 ^oC *(*Figures 5.2 and 5.11a). In contrast, the values of D^*_{Br} between fluorapatites and melts gently decrease with increasing temperature, for example from 0.0207 at 1220 ^oC, 0.0174 at 1250 ^oC, to 0.0168 at 1400 ^oC (Figure 5.11b).

The values of D^*_F increase with increasing temperature. For example, the values of D^*_F between chlorapatites and melts and between fluorapatites and melts increase from 3.592 at 1120 ^oC to 4.125 at 1330 ^oC and from 1.049 at 1220 ^oC to 1.057 at 1250 ^oC, and 1.068 at 1400 ^oC, respectively (Figure 5.11c). Contrary to D^*_F, the values of D^*_{Cl} between chlorapatites and melts decrease with an increase in temperature, e.g., from 1.072 at 1120 ^oC, 1.009 at 1220 ^oC, to 0.827 at 1330 ^oC (Figure 5.11d).

Higher temperature favors the formation of fluorapatites and also causes more bromine to replace the chlorine in chlorapatites, whereas lower temperature favors the formation of chlorapatite.

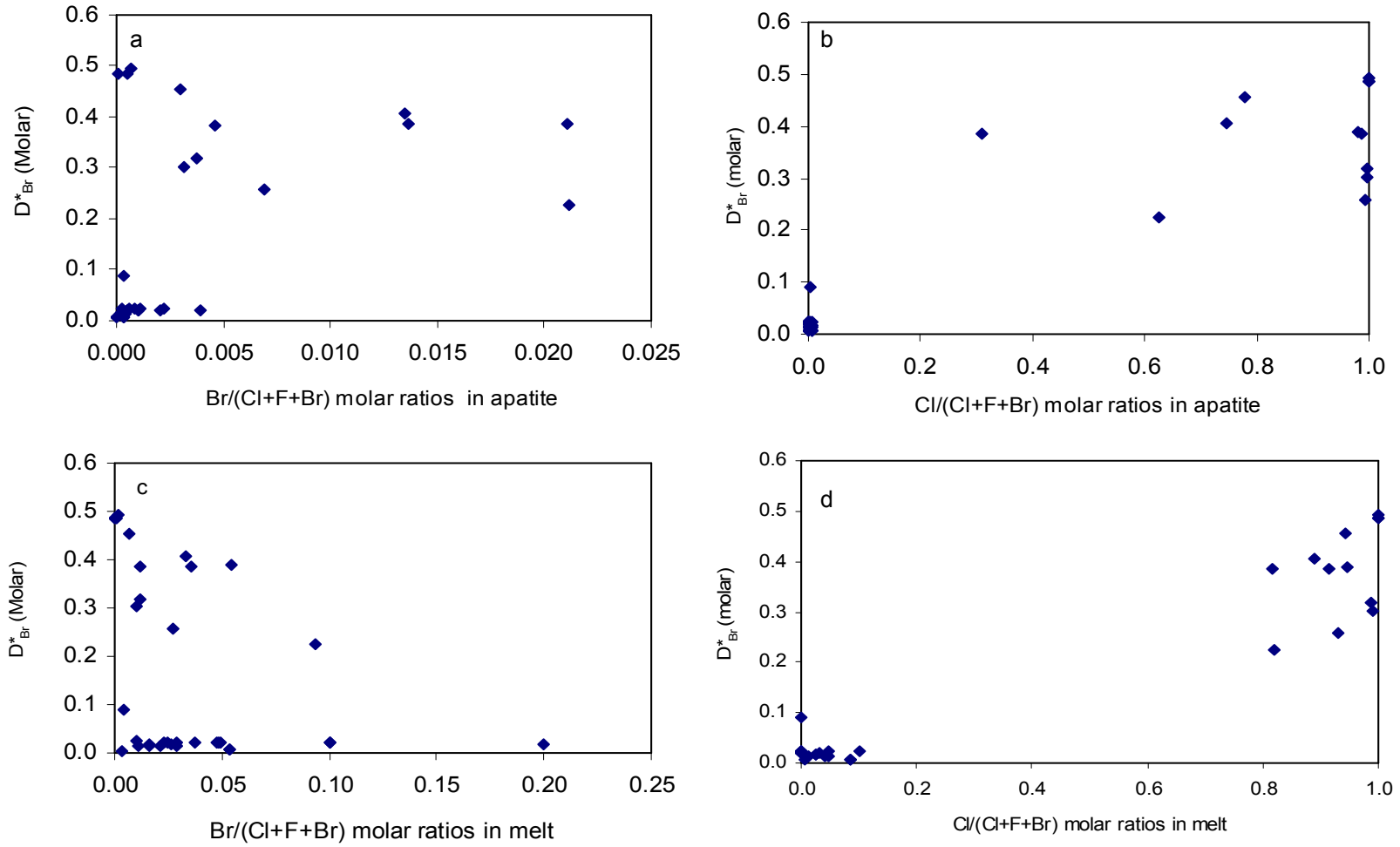

Figure 5.10 D*Br vs molar ratios of Br/(Cl+F+Br) in apatite (a), molar ratios of Cl/(Cl+F+Br) in apatite (b), molar ratios of Br/(Cl+F+Br) in melt (c), and molar ratios of Cl/(Cl+F+Br) in melt (d)

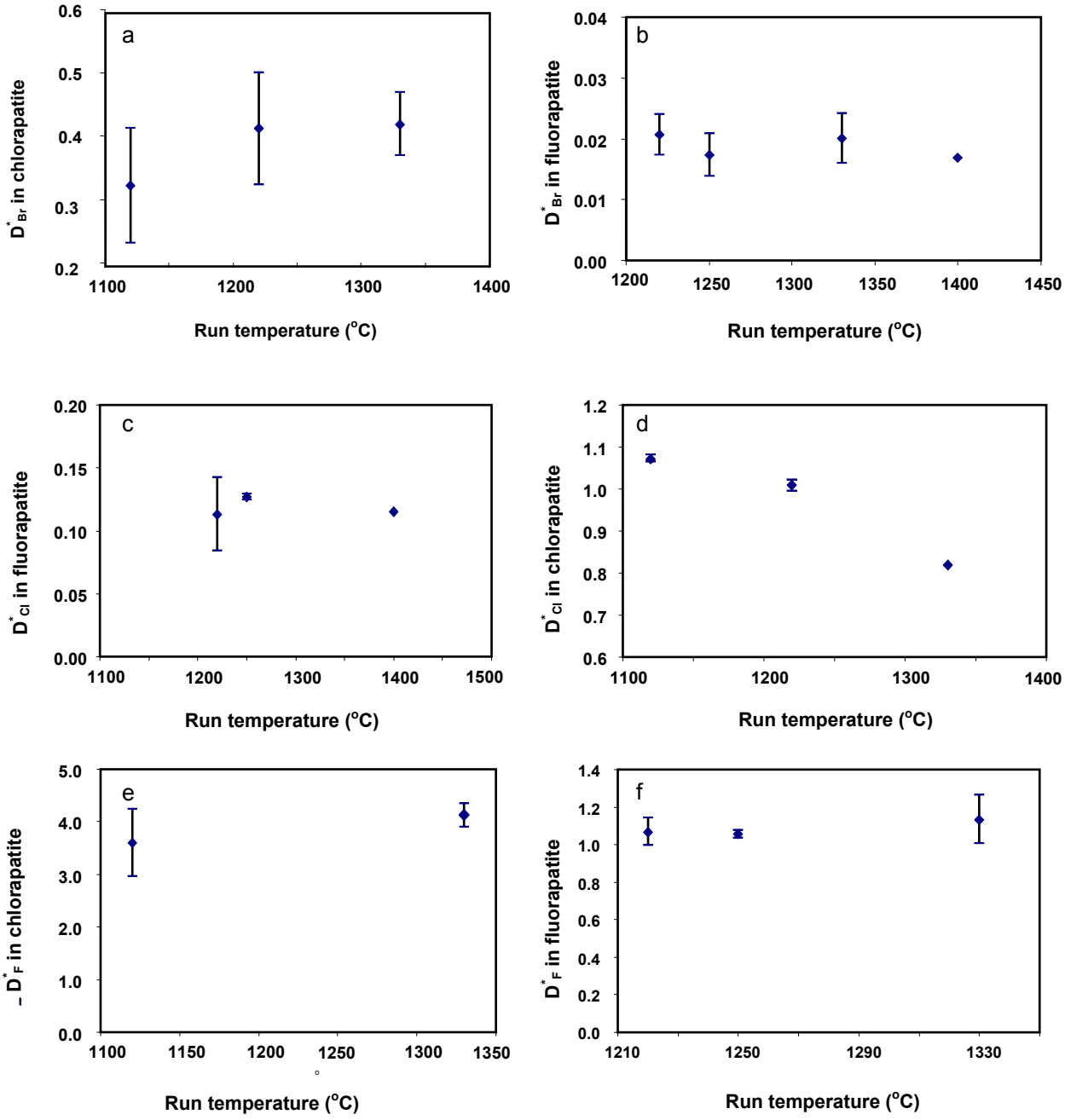

Figure 5.11 Temperature dependence of D^*_{Br} in chlorapatite (a), D^*_{Br} in fluorapatite (b), D^*_{Cl} in fluorapatite (c), D^*_{Cl} in chlorapatite (d), D^*_{F} in chlorapatite (e), and D^*_{F} in fluorapatite (f).

5.3. Thermodynamic/Crystal-Chemical Approach

The partitioning of chlorine/fluorine between fluorapatite/chlorapatite and melt can be expressed as an exchange equilibrium:

$$Ca_5(PO_4)_3F + 0.5\ CaCl_2 = Ca_5(PO_4)_3Cl + 0.5\ CaF_2 \qquad (5.2)$$

fluorapatite melt chlorapatite melt

The equilibrium constant (K) for equilibrium 5.2 is

$$K = \frac{X^{Xtl}_{Cl\text{-}Ap}}{X^{Xtl}_{F\text{-}Ap}} \times \left[\frac{X^{melt}_{CaF_2}}{X^{melt}_{CaCl_2}} \right]^{0.5} \qquad (5.3)$$

For equation 5.3, the $X^{melt}_{CaF_2} = X^{melt}_{F}$ and $X^{melt}_{CaCl_2} = X^{melt}_{Cl}$, so the

$$K = \frac{D^*_{Cl}}{D^*_{F}} \times \left[\frac{X^{melt}_{Cl}}{X^{melt}_{F}} \right]^{0.5} \qquad (5.4)$$

Table 5.4 summarizes the available standard state thermodynamic properties for apatites and some other materials. Based on the available thermodynamic properties, the Gibbs Free Energy (ΔG_T) and the equilibrium constants for equation 5.2 at different experimental temperatures were calculated and are listed in Table 5.5. The positive values of Gibbs Free Energy and much less than 1 of the equilibrium constants (0.143 to 0.167) demonstrate the strong tendency to crystallize fluorapatite from reaction 5.2.

For all of these partitioning experiments, the distribution coefficients (Kd) for Cl compared to F between apatite and melt range from 0.11 to 0.22, consistent with the above thermodynamic results (Table 5.5).

Table 5.4 Summary of the standard state thermodynamic properties for apatites and some other relevant materials (25°C, 1 atm)

Materials	Formula	S^o (cal/mole.k)	ΔG^o (cal/mole)	ΔH^o (cal/mole)	C_p^o
Chlorapatite	$Ca_5(PO_4)_3Cl$	95.58 [1]	-1486000 [1]	-1576783 [1]	158.67 [1]
Chlorapatite	$Ca_5(PO_4)_3Cl$	109.23 [9]	-1605266 [9]	-1565016 [9]	
Fluorapatite	$Ca_5(PO_4)_3F$	92.7 [2]	-1539926 [4]	-1630843 [1]	159.84 [6]
			-1542968 [2]	-1629986 [2]	
Hydroxyapatite	$Ca_5(PO_4)_3OH$	95.3 [1]	-1505187 [1]	-1600069 [1]	181.36 [7]
		93.3 [2]	-1502412 [2]	-1593991 [2]	
Calcium chloride	$CaCl_2$	25 [2]	-178791.3 [2]	-190200.8 [2]	17.35 [4]
	$CaCl_2$	27.2 [5]	-179300 [5]	-190000 [5]	
$CaCl_2$ melt	$CaCl_2$	21.04 [3]		-184071 [3]	
Fluorite	CaF_2	16.38 [4]	-280968 [4]	-293500 [4]	25.48 [8]
		16.46 [2]	-281290.6 [2]	-293800 [2]	
CaF_2 melt	CaF_2	12.48 [3]		-285982 [3]	

1-Zhu and Sverjensky, 1991; 2-Robie et al., 1979; 3-Tacker and Stormer, 1993; 4-Garvin et al., 1987 (CODATA); 5-Weast (ed), 1972/1973; 6-Egan et al., 1951; 7-Egan et al., 1950; 8-Todd, 1949; 9-Korzhinskiy, 1981

Table 5.5 Calculated ΔG_T and K results for equilibrium 5.2 at high temperature

T (°C)	ΔG_T (cal/mole)	K
1120	5384.07	0.143
1220	5536.55	0.155
1250	5580.62	0.158
1330	5694.65	0.167

The thermodynamic data indicate an increase of the equilibrium constant with increased temperature (high temperature favors the formation of chlorapatite), which contrasts with the experimental results in this study; this discrepancy is possibly due to the inaccuracy of the estimated thermodynamic data.

Based on the empirical observations, Onuma et al (1968) found that: (1) trace elements occupy lattice sites on or within a crystal; (2) for trace elements with the same charge as the host ion, the difference between the ionic radius of the trace and host ions is the most important factor controlling the partition coefficient. The Onuma Diagram plots the logarithm of partition coefficient versus the ionic radius for a particular lattice site. There are sub-parallel curves for different valences, parabolic near the optimum ionic radius with the maximum logD values corresponding to optimum radius of the lattice sites, linear elsewhere, and mirror images on opposite sides of optimum (Onuma et al., 1968; Philpotts, 1978). It indicates the crystal structure control of both the major and trace elements. Partition coefficients for isovalent series cations show a parabolic dependence on the ionic radius (Onuma et al., 1968; Blundy and Wood, 1994; Purton et al., 1996; and references within).

Nagasawa (1966) and Brice (1975) derived expressions relating partition coefficients to the mechanical strain (energy) around a misfit ion in an isotropic perfectly elastic crystal lattice. The strain energy is expressed in terms of the mismatch between the ionic radius of the substituent ion (r_i) and the

optimum radius of the lattice site of interest (r_o), and the rigidity of the lattice around the defect as expressed by its elastic modulus. Brice's expression is:

$$\Delta G^{xl}_{strain} = 4\pi Y N_A [\frac{1}{2} r_o (r_i - r_o)^2 + \frac{1}{3}(r_i - r_0)^3] \qquad (5.5)$$

where ΔG^{xl}_{strain} is the strain energy (per mole) due to the size mismatch between r_i and r_o, N_A is the Avagadro's Number, and Y is the Young's Modulus of the interested site.

Blundy and Wood (1994), and Wood and Blundy (1997) have expressed the correlation between partition coefficient and ionic radius:

$$D_i = D_0 \exp\left(\frac{-\Delta G^{xl}_{strain}}{RT}\right) = D_0 \exp\left\{\frac{-4\pi Y N_A [\frac{1}{2} r_o (r_i - r_o)^2 + \frac{1}{3}(r_i - r_0)^3]}{RT}\right\} \qquad (5.6)$$

where D_0 is the partition coefficient for the strain-free substitution ($r_i = r_o$), R is the gas constant, and T is the temperature in Kelvin (K). Based on this equation, we can obtain a parabolic dependence of D_i on the ionic radius (Figure 5.12). The maximum value of D is D_0, and the corresponding radius is r_0. The tightness of the parabola corresponds with the Young's modulus of the particular site. This theoretical dependence of D_i on ionic radius corresponds quite closely with the observed partition coefficient values for the 2^+ cation substitution in plagioclase and clinopyroxene (Blundy and Wood, 1994; Wood

and Blundy, 1997). That means the homovalent trace-element substitution for Ca^{2+} in pyroxene and plagioclase follows the Brice equation.

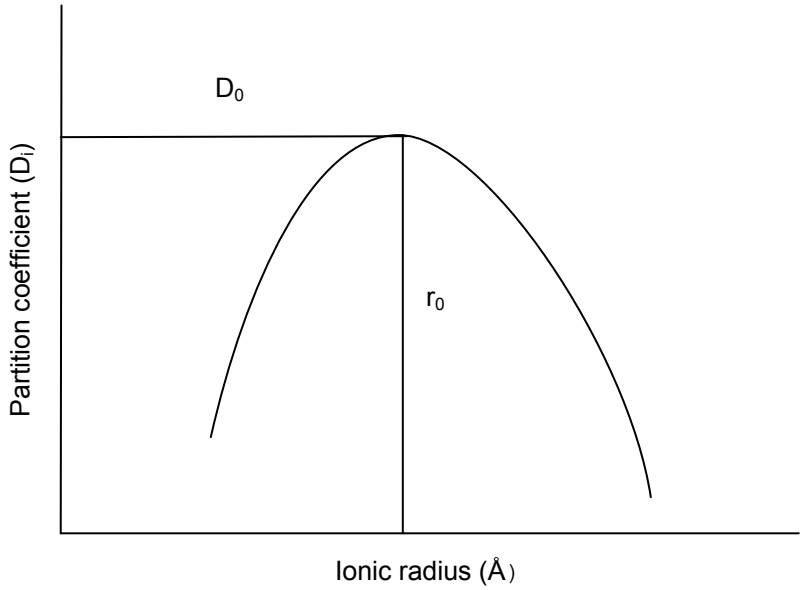

Figure 5.12 The schematic diagram showing the dependence of D_i on the ionic radius (after Wood and Blundy, 1997)

Detailed analysis of the parabola has shown that, for ions of the same valence, the curvature of the parabola often varies from crystal to crystal in a fashion consistent with the elastic modulus of the host crystal (Blundy and Wood, 1994). Crystals with higher elastic modulus are often characterized by tighter parabolae than those with lower elastic modulus, which accommodate misfit cations more easily (Purton et al., 1996). Liquids and melts have zero shear modulus and therefore are more tolerant of misfit cations.

Based on the quantitative relationship between the elastic property of a crystal and its element partitioning behavior, the partition coefficients of other similar ions (closed-shell ions and lanthanides), can be predicted, although there is some deviation from the Brice curve, for example the Pb^{2+}, Mn^{2+}, Ni^{2+}, Hg^{2+}, and Cd^{2+}, where the electronic effects may be important (Blundy and Wood, 1994; Wood and Blundy, 1997).

The equation used by Wood and Blundy (1997) to predict unknown partition coefficient of similar elements from some known partition coefficients is adopted from the Brice equation:

$$D_a = D_b \exp\left\{\frac{-4\pi Y N_A\left[\frac{1}{2} r_o (r_b^2 - r_a^2) + \frac{1}{3}(r_a^3 - r_b^3)\right]}{RT}\right\} \qquad (5.7)$$

where the D_a and D_b are the partition coefficients of elements a and b, respectively.

The experimental results of the partition coefficients between apatites and melts display a parabolic curve similar to the Onuma Diagram (Figure 5.12), i.e., the values of D* (F, Cl, and Br) are dependent on the ionic radius (Figure 5.13). By applying the experimentally determined D* values for F, Cl, and Br, at an experimental temperature of 1220 ^{o}C, into equation 5.6, the values of r_o =1.2776 Å and 1.343 Å, D_0=1.0902 and 3.568, and Y=158.43 and 113.325 kbar were obtained for fluorapatite and chlorapatite, respectively. Through substitution of the ionic radius into equation 5.7, the D* value of

interested elements can be obtained. For iodine, the D^*_I is approximately 0.000459 and 0.0277 between fluorapatite/melt and chlorapatite/melt, respectively, at a temperature of 1220 ^oC. Also, the predicted D^*_{OH} is approximately 0.0135 and 0.551 between fluorapatite/melt and chlorapatite/melt, respectively, at a temperature of 1220 ^oC (Figures 5.14a, b).

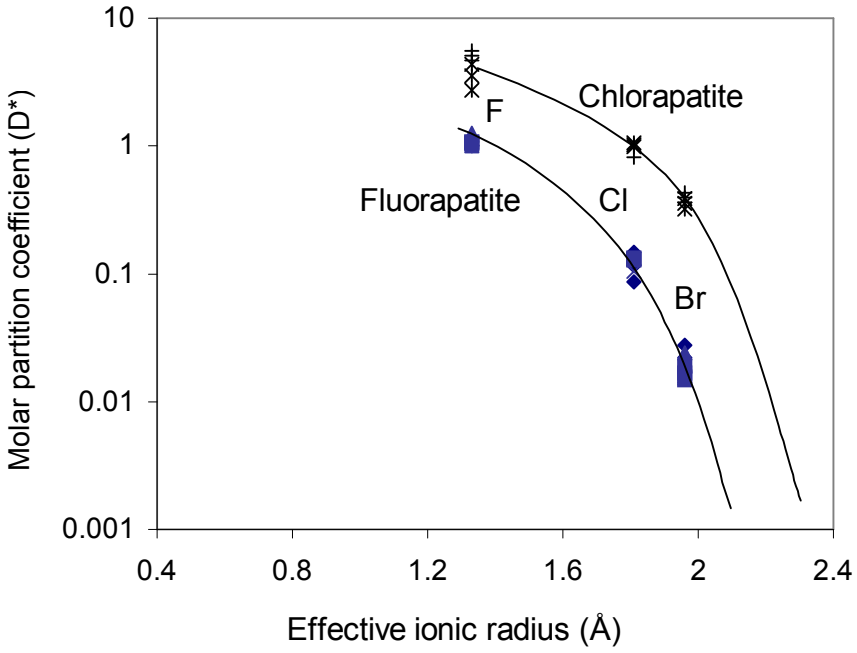

Figure 5.13 Molar partition coefficients of halogens in synthetic apatites and coexisting melts compared to their ionic radius

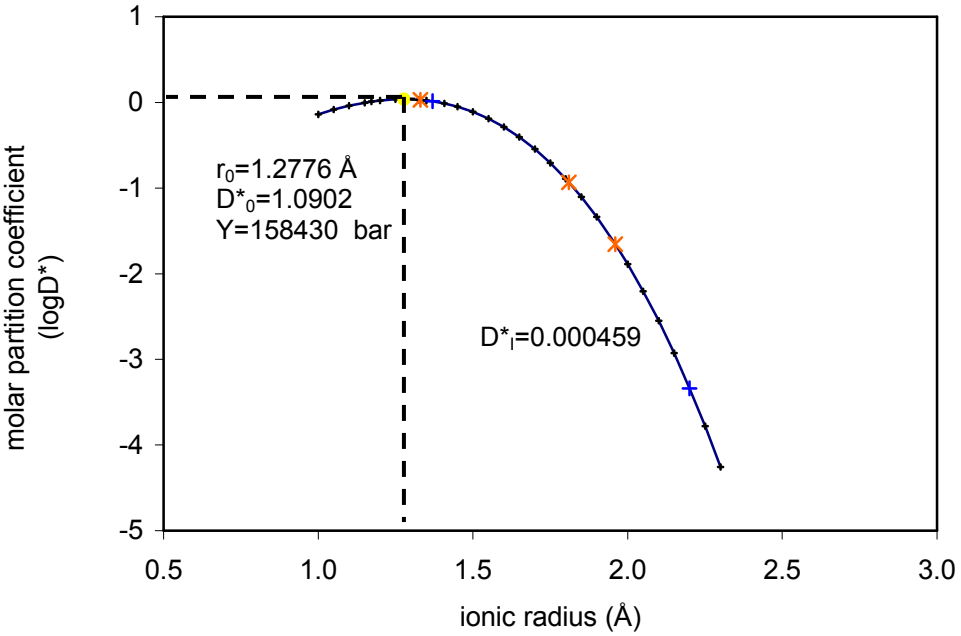

Figure 5.14a Plot of ionic radius vs partition coefficient for fluorapatite at T=1220°C

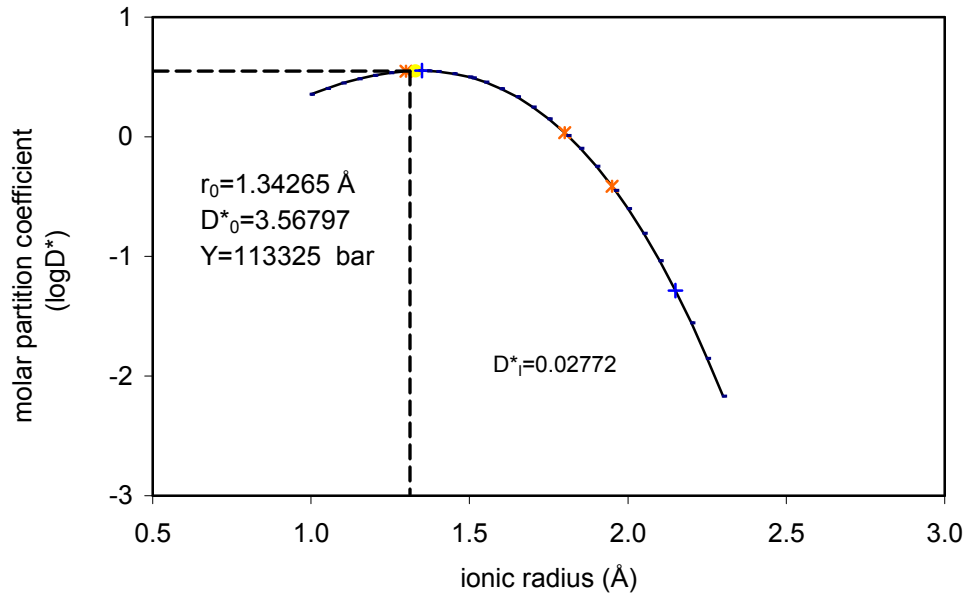

Figure 5.14b Plot of ionic radius vs partition coefficient for chlorapatite at T=1220 °C

5.4 Summary

The results of the halogen partitioning experiments demonstrate that the partition coefficients for halogens between apatite and melts are principally controlled by the ratios of Cl/F or Cl/(Cl+F+Br) in the melts. The Cl/F ratio will control the formation of chlorapatite or fluorapatite. For each halogen element (F, Cl, Br, or I), there are distinct partition coefficients for chlorapatite-melt and fluorapatite-melt. With specific Cl/F ratio, the partition coefficient is stable and independent on the halogen concentrations in the melts.

Consistent distribution coefficients (0.11 - 0.22) for Cl compared to F between apatite and melt demonstrate a pronounced distribution codependancy for Cl and F. For example, fluorine enters the apatite crystals more easily than does chlorine, forming fluorapatite, which is consistent with the thermodynamic results.

The results of molar partition coefficient for halogens between apatite and melt are temperature dependent. Higher temperature is in the favor of the formation of fluorapatites and also causes more bromine to substitute for chlorine in the chlorapatite, whereas lower temperature favors the formation of chlorapatite.

6. Experimental Investigation on the Uptake of Br by Scapolite and Sodalite

It is expected that Br content is elevated in Cl-rich minerals based on similarity of anionic radii. The presence of significant Br in halite and sylvite is well documented (e.g., Stoessell and Carpenter, 1986; Berndt and Seyfried, 1997). Appel (1997) reported high Br contents (up to 418 ppm) and low Cl/Br values (down to 1.6) in hydrothermally altered Archean komatiitic rocks from West Greenland and suggested that Br may originally reside in hydroxychlorides (e.g., hibbingite) or in fluid inclusions. It remains unclear whether the trace amounts of Br in nominally anhydrous silicate minerals (e.g., feldspars; Shinonaga et al., 1994) are related to the presence of fluid inclusions in these minerals. O'Reilly and Griffin (2000) reported up to 54 ppm Br in fluorapatite from mantle xenoliths by laser ablation - inductively coupled plasma-mass spectrometry (LA ICP-MS). INAA and XRF microprobe analyses in this study showed that the Durango fluorapatite contains ~8 ppm Br, whereas chlorapatite from Bob's Lake, Ontario has a notably higher Br content (~75 ppm).

Scapolite-group minerals and sodalite of this study contain up to 114 and 395 ppm Br, respectively (Table 4.1). To the best of our knowledge, this is the first report of significant Br in natural Cl-rich aluminosilicates. Bromine is

known to partition strongly into aqueous fluids/melts rather than coexisting minerals (Seyfried et al., 1986), similar to Cl (Carroll and Webster, 1994). Therefore, the presence of any fluid inclusions in selected mineral grains could significantly affect the Br analytical results. During the initial stage of this study, anomalously high (and variable) Br contents were encountered in a few grains of halite and were subsequently found to be related to the presence of fluid inclusions. Fortunately, fluid inclusions are generally rare in grains of scapolite-group minerals (Pan et al., 1994). Also, care was taken in our selection of the mineral grains to minimize the effect of fluid inclusions and other impurities. On the basis of the mostly homogeneous distribution of Br in scapolite-group minerals, as evidenced by the small standard deviations (Table 8.6), we suggest that the Br contents in scapolite-group minerals and sodalite of this study (Tables 4.1 and 7.4) represent a substitution for Cl in these minerals. This suggestion is supported by a correlation between the Br contents from the XRF microprobe analyses and the Cl contents from EMPA analysis in sample DL-70K (Table 7.6).

6.1. Experimental and analytical procedures

Exchange experiments for Br between Cl-rich minerals (scapolite, SCP-1; sodalite, SOD-3) and hydrous halide-rich melts have been carried out at temperatures of 800 ^{0}C and 1000 ^{0}C and 1 atmospheric pressure. Scapolite (SCP-1) selected in this study is marialite (Me=12.2) from Gooderham, Ontario (Shaw, 1960; Teerstra and Sherriff, 1997); and sodalite (SOD-3) is from South

Africa. These minerals were crushed to 100-140 mesh (106-125 μm in diameter), then hand-picked under a binocular microscope. The hand-picked mineral grains were grounded to less than 200 mesh (75 μm in diameter).

The starting materials were mixtures of about 30 mg powdered mineral (scapolite or sodalite) grains and 120 mg NaCl-NaBr mixtures that are prepared from NaCl and NaBr with weight ratios of 1:1 and 2:1 (Table 6.1). These mixtures of starting materials were thoroughly ground to ensure homogenization. Each charge containing about 40 mg of the starting materials plus variable amounts of deionized water (Table 6.1) was sealed in Au or Pt capsules by the cold-seal technique.

The 800 ^{o}C experiments in Au capsules were performed in a Thermolyne 47900 furnace for 30 days and quenched in water. The 1000 ^{o}C experiments in Pt capsules using a Thermolyne 46100 furnace were originally set for 14 days, but terminated after 12 days due to a power failure. The experimental products were washed with deionized water, then mounted and polished in Pyrex plugs for EMPA analyses.

The EMPA analytical conditions are of 10 kV accelerating voltage, 10 nA beam current, ~1 μm beam diameter, 30 seconds counting time. The peak-overlap interference between Al and Br was manually corrected and was monitored by analyzing a synthetic crystal of end-member $Na_8(Al_6Ge_6)O_{24}Br_2$ (Fleet, 1989).

Table 6.1 Exchange experiments of Br between minerals and melts

Sample No.	Starting Material (mg)				Charge (mg)		Run		
	Scapolite	Sodalite	NaCl	NaBr	Mixture	DI Water	T (^{0}C)	Time (Days)	Products
scp2002-1	29.5		59.5	59.8	40.8	2.9	800	30	Scapolite+glass+water
scp2002-2	30.1		81.2	41.4	41.6	4.8	800	30	Scapolite+glass+water
scp2002-3	29.5		59.5	59.8	49.0	18.0	1000	12	Wollastonite+albite
sod-2002-1		29.3	60.7	60.3	42.2	4.5	800	30	Sodalite+glass+water
sod-2002-2		30.4	79.8	40.8	41.2	1.2	800	30	Sodalite+glass+water
sod-2002-3		29.3	60.7	60.3	55.3	18.5	1000	12	Sodalite+glass+water
sod-2002-4		30.4	79.8	40.8	54.0	12.2	1000	12	Sodalite+glass+water

6.2. Experimental results

The products of all sodalite experiments consist of sodalite, glass, and water at room temperature. In the scapolite experiments, scapolite was well preserved after the experiments at 800 ^{o}C, but completely broken down to form wollastonite and albite in the experiments at 1000 ^{o}C (Table 6.1). Most grains of sodalite and scapolite in the experimental products are angular in morphology, suggesting that dissolution and re-precipitation were negligible in these experiments. The decomposition of scapolite at 1000 ^{o}C is consistent with the experimental results of Rebbert (1995) who reported that marialite is stable only at temperatures up to ~900 ^{o}C.

The grains of sodalite and scapolite after the exchange experiments contain Br-rich rims of ~1 to ~6 μm wide around the original Br-poor core (Figure 6.1). The Br-rich rims are uniform in width in most sodalite and scapolite grains, except for grains with well-developed fractures and/or cleavages. For example, Br-rich rims are less than 2 μm in width in both sodalite and scapolite from the 800 ^{0}C experiments.

The concentration profiles of Br across the Br-rich rims and the original cores of sodalite and scapolite have been obtained from EMPA traverses. For narrow rims, the Br profiles are constructed from multiple EMPA traverses (Figure 6.2a and 6.2b).

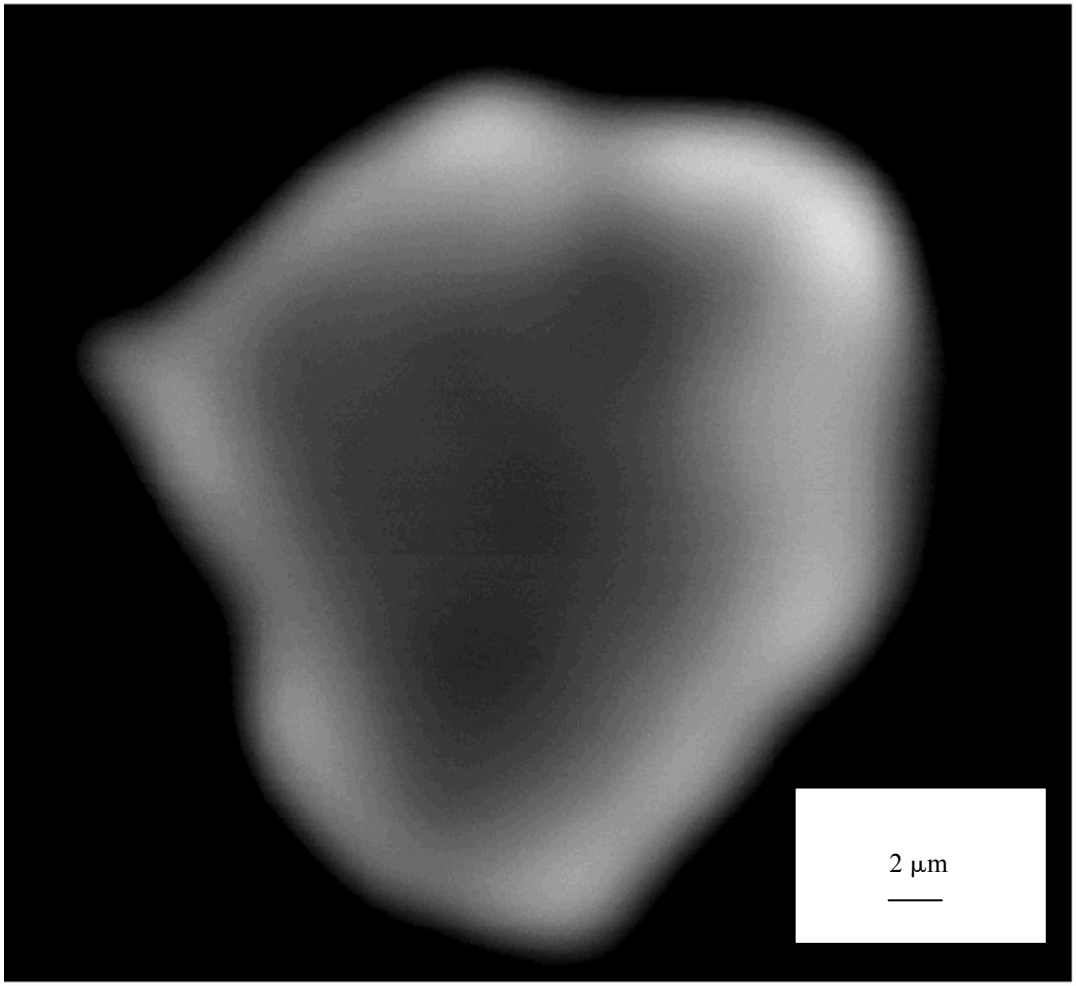

Figure 6.1 SEM-back-scattered electron image illustrating a Br-rich rim around the original (Br-poor) core of a sodalite grain from experiment SOD-3-1.

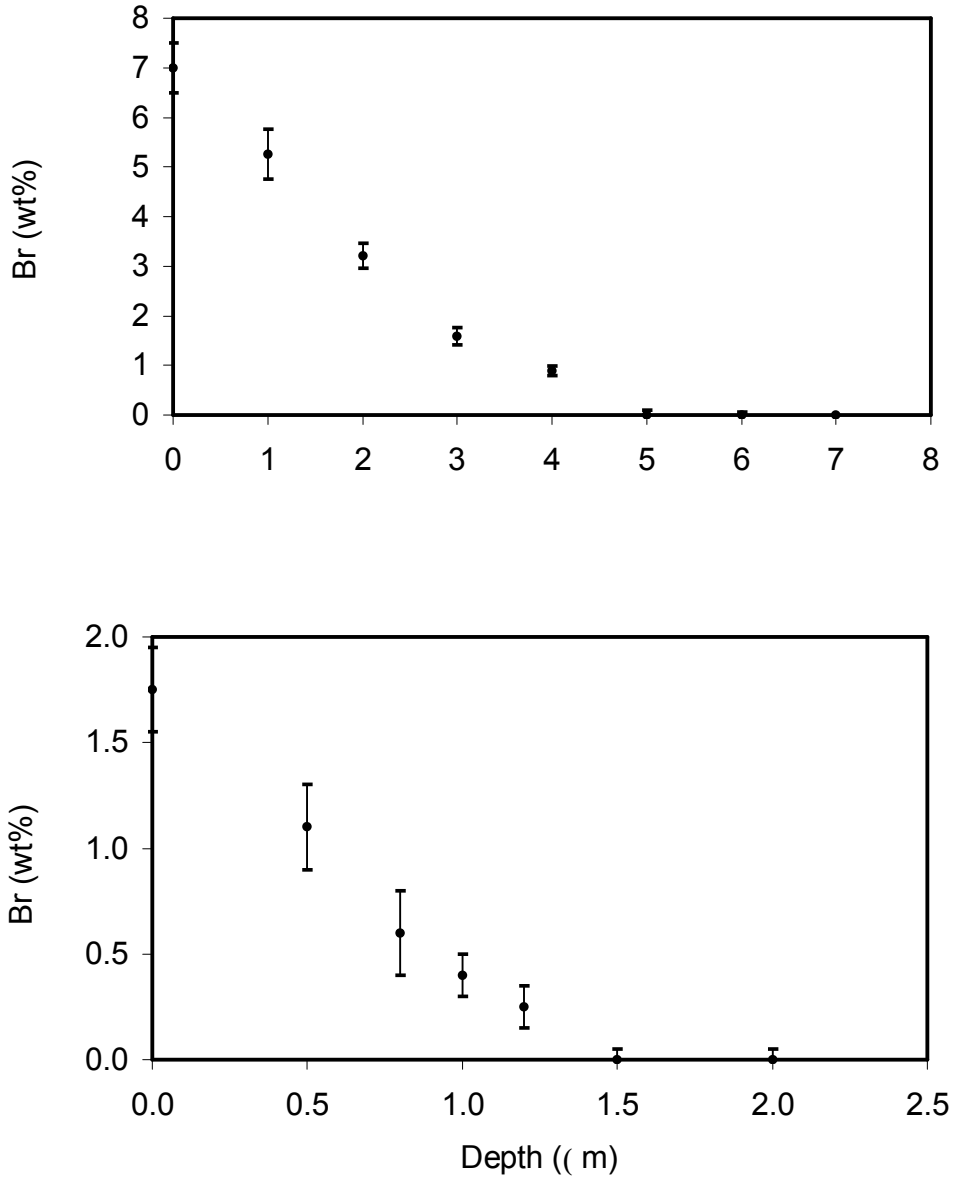

Figure 6.2 Representative Br profiles across the rims of a) marialite from experiment SCP-1-1 (average of spot analyses from 6 different traverses) and b) sodalite from experiment SOD-3-1. The Br contents at the surface (depth=0) of mineral grains cannot be determined by EMPA and are extrapolated from individual traverses.

6.3. Diffusion and Partition of Br between Scapolite/Sodalite and Melt

6.3.1 Diffusion of Br between Scapolite/Sodalite and Melt

The Br concentration profiles of scapolite and sodalite (Figure 6.2) have been fitted to a non-steady-state diffusion equation:

$$C_{x,t} = C_0[1 - \mathrm{erf}(\frac{x}{2\sqrt{D_d t}})] \qquad (6.1)$$

where Cx,t is the concentration of Br at depth x from the surface after time of t, C_0 is the surface concentration of Br, and D_d is the diffusion coefficient (m^2/s; Crank, 1975). Here, the surface Br values of marialite and sodalite cannot be determined directly by EMPA owing to unavoidable edge effects (e.g., interference from melts, and epoxy resin), and hence are extrapolated from the concentration profiles (Figure 6.2).

The calculated diffusion coefficient of Br in scapolite and sodalite, based on the exchange experiments, are listed in Table 6.2. The diffusion coefficients of Br in scapolite and sodalite seem to have a compositional dependence: *i.e.*, increase in D_d with increasing surface concentrations of Br at a given temperature (Table 6.2). Also, the D_d values of Br in marialite and sodalite at 800ºC are similar. A least-squares fit to the data from the sodalite experiments (Table 6.2, Figure 6.3) yields an Arrhenius relation: $D_d = 6.5 \times 10^{-7} \exp(-270 \pm 10$ kJ/mol/RT) m^2/s, over the temperature range from 800 to 1,000ºC.

Table 6.2 Results of scapolite and sodalite Br-Cl exchange experiments

Run#	T (°C)	Melt			Mineral			D^*_{Cl}	D^*_{Br}	K_D	$LogD_d$
		X_{Cl} (M)	X_{Br} (M)	Br/Cl (M)	X_{Cl} (M)	X_{Br} (M)	Br/Cl(M)			(Br/Cl)	(m^2/s)
scp2002-1	800	0.636	0.364	0.572	0.643	0.357	0.555	1.011	0.981	0.97	-18.70
scp2002-2	800	0.775	0.225	0.290	0.802	0.198	0.247	1.035	0.880	0.85	-18.83
sod2002-1	800	0.639	0.361	0.565	0.575	0.425	0.739	0.900	1.177	1.31	-19.09
sod2002-2	800	0.775	0.225	0.290	0.759	0.241	0.318	0.979	1.071	1.09	-19.38
sod2002-3	1000	0.639	0.361	0.565	0.575	0.425	0.739	0.900	1.177	1.31	-17.06
sod2002-4	1000	0.775	0.225	0.290	0.771	0.229	0.297	0.995	1.018	1.02	-17.32

X_{Cl} (M)=Cl/(Cl+Br), X_{Br} (M)=Br/(Cl+Br), all in moles

Figure 6.3 shows that the diffusion rates of Br in marialite and sodalite are significantly lower than those of F-Cl-OH along the *c*-axis, broadly similar to those of F-Cl-OH parallel to the *a*-axis and of Sr, but are much higher than those of Nd (and other rare-earth elements) in the apatite-group minerals (Brenan, 1993; Cherniak and Ryerson, 1993; Cherniak, 2000). The rapid rate of diffusion of F-Cl-OH along the *c*-axis direction in apatite-group minerals has been attributed to the location of these anions in the *c*-axis channels (Brenan, 1993). The Cl^- and Br^- ions in scapolite-group minerals and sodalite are located in large cages surrounded by rings of (Al,Si) tetrahedra (Papike and Zoltai, 1965; Fleet, 1989) and, unlike F-Cl-OH in apatite-group minerals, are not confined to channels. Also, the Br^- ion (1.96 Å) is significantly larger than F^-, OH^-, and Cl^- (1.33, 1.37, and 1.81 Å, respectively; Table 2.1). These differences are most likely responsible for the considerably slower diffusivities

of Br in scapolite-group minerals and sodalite than those of F-Cl-OH parallel to the *c* axis in apatite-group minerals.

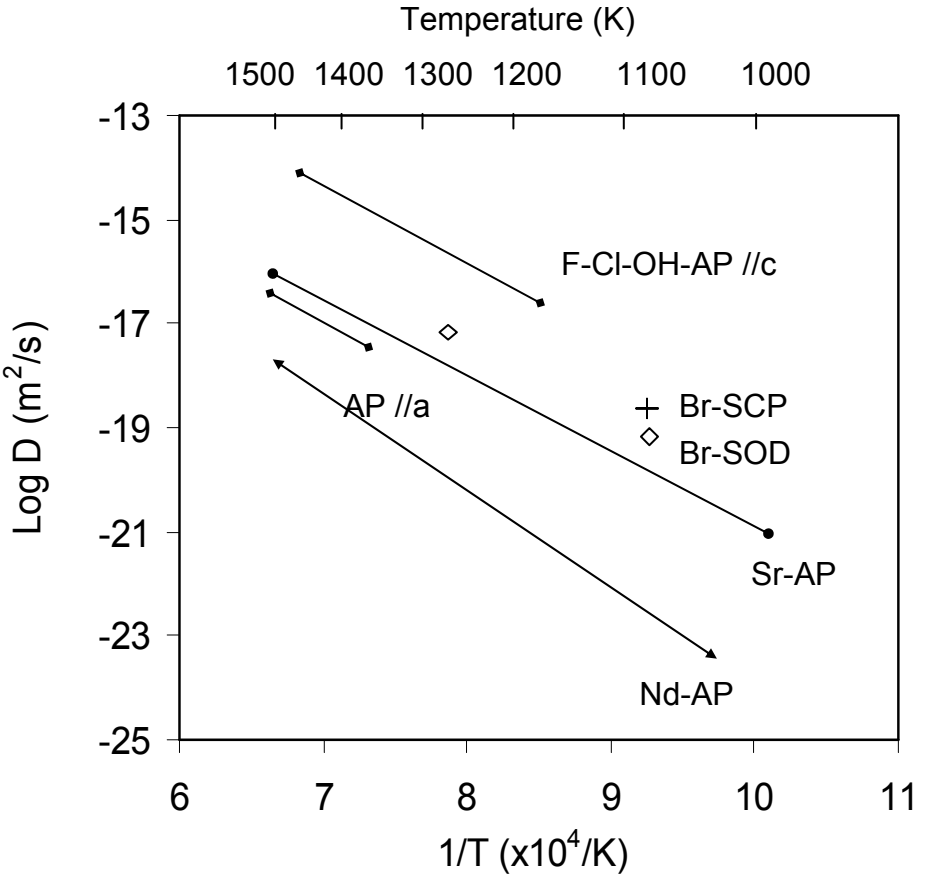

Figure 6.3 Arrhenius plot illustrating Br diffusivities in marialite and sodalite. Also show are the diffusivities of F-Cl-OH (//c and //a at 1 atm), Sr, and Nd in apatite-group minerals (data from Brenan, 1993; Cherniak and Ryerson, 1993; and Cherniak, 2000)

The relatively rapid rates of diffusion of F-Cl-OH in apatite-group minerals led Brenan (1993) to express caution about the application of the halogen chemistry of these minerals to infer melt/fluid compositions, because of possible modification during subsequent thermal events. Dobson (1973)

formulated the closure temperatures (T_c) of slowly diffusing species in mineral grains as follows:

$$T_C = \frac{E_a/R}{\ln\left(\frac{ART_c^2 D_o/a^2}{E_a dT/dt}\right)} \qquad (6.2)$$

where E_a is the activation energy of diffusion, R is the gas constant, D_o is the pre-exponential term, A is a geometric factor, a is the grain radius, and dT/dt is the cooling rate. Ganguly and Tirone (1999) pointed out that Dobson's (1973) formulation is applicable only to minerals that have undergone large extents of diffusion, i.e., even the composition at the core of individual grains is affected. Figure 6.4 shows that the closure temperatures of Br in sodalite are significantly higher than those of F-Cl-OH in apatite-group minerals, but are close to those of Sr in apatite-group minerals. The closure temperatures of Br in marialite are probably similar to those of this element in sodalite, because of similarities in the experimentally determined D_d at 800ºC (Table 6.2) and the structural environments of Br in these minerals.

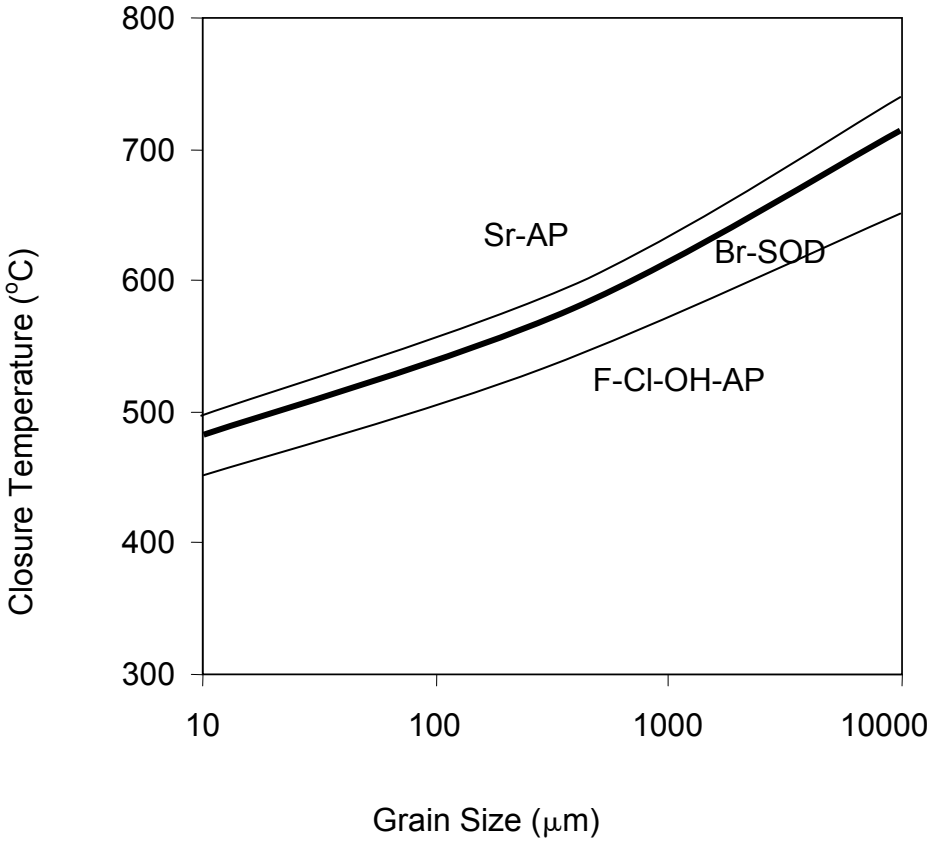

Figure 7.4 Closure temperatures for Br in sodalite (Br--SOD, heavy line) as a function of grain sizes at assumed cooling rate of 2°C/Ma and a spherical geometry, using the formulation of Dobson (1973). Also show for comparison are values for F-Cl-OH and Sr in grains of apatite group minerals (F-Cl-OH-AP and Sr-AP, light lines) under similar assumptions (diffusivity data from Brenan, 1993; Cherniak and Ryerson, 1993).

6.3.2 Distribution Coefficients and Partition Coefficients

The Br-Cl exchange between marialite or sodalite and hydrous halide melts can be represented by the following reaction:

$$Cl^-_{mineral} + Br^-_{melt} = Br^-_{mineral} + Cl^-_{melt} \qquad (6.3)$$

The expression for the distribution coefficient of this exchange equilibrium is:

$$K_D^{mineral\text{-}melt} = (X_{Br}/X_{Cl})^{mineral}/(X_{Br}/X_{Cl})^{melt} \qquad (6.4)$$

The Br/Cl values of the ion-exchanged sodalite at the surface (Figure 6.2) are higher than those of the starting materials or residual melts, giving $K_D^{sodalite\text{-}melt}$ from 1.02±0.10 to 1.31±0.10 with an average of 1.18±0.10 (Table 6.2). The Br/Cl values of the ion-exchanged marialite at the surface are marginally lower than those in the starting materials, yielding Br-Cl $K_D^{marialite\text{-}melt}$ close to unity (0.85±0.10 and 0.97±0.10; Table 6.2). There is no significant difference in the estimated Br-Cl $K_D^{sodalite\text{-}melt}$ values from experiments at 800ºC and 1,000ºC (Table 6.2).

These Br-Cl $K_D^{mineral\text{-}melt}$ values for marialite and sodalite, indicating no significant Cl-Br fractionation, are distinct from those for halides (Stoessell and Carpenter, 1986; Berndt and Seyfried, 1997; Siemann and Schramm, 2002) and apatite-group minerals (Chapter 5), all of which have marked preference for Cl over Br. This approximately equal uptake of Cl and Br by scapolite-group minerals and sodalite is probably attributable to their accommodation in the large structural cages of these framework aluminosilicates (Papike and Zoltai, 1965; Fleet, 1989). Fleet (1989) successfully synthesized $Na_8(Al_6Ge_6)O_{24}Cl_2$, $Na_8(Al_6Ge_6)O_{24}Br_2$ and $Na_8(Al_6Ge_6)O_{24}I_2$, with the still larger I^- ion (2.20 Å,

Table 2.1) accommodated in the cage of sodium alumino-germanate sodalite.

The molar partition coefficients for Br and Cl between scapolite or sodalite and hydrous halide-rich melt have been calculated on the basis of the molar ratios of Br/Cl on the grain surface, which were obtained from the extrapolation of EMPA traverses and the molar ratios of Br/Cl in the residual melts calculated by the mass balance method (assuming 1% Br in scapolite and 0.5% Br in the sodalite after the exchange experiment); the results are listed in Table 6.2.

The D^*_{Cl} between scapolite and melt varies from 1.011 to 1.035. Whereas the D^*_{Br} between scapolite and melt ranges from 0.88 to 0.98. Although the D* values of Cl and Br are similar, there is still a consistent fractionation between Br and Cl, with a distribution coefficient of 0.85 to 0.97.

The D^*_{Cl} between sodalite and melt varies from 0.900 to 0.995; and D^*_{Br} is from 1.018 to 1.177. The distribution coefficient for Br (compared to Cl) between sodalite and melt ranges from 1.023 to 1.308. It seems that the sodalite structure is more favorable for Br than for Cl. This is probably attributable to the accommodation ability of its large structural cages. There is no apparent affect of temperature on the partitioning of Br between sodalite and melt.

The values of molar ratio partition coefficient for Br and Cl exhibit a compositional dependence (Figure 6.5) both for scapolite and sodalite. Higher Cl or Br concentration in the melt corresponds a higher partition coefficient (D*) value.

The results from the exchange experiments have demonstrated that the Cl/Br values in scapolite-group minerals closely reflect those of its coexisting melts/fluids. Therefore, the Cl/Br values of scapolite-group minerals from the skarn deposits are useful in providing constraints on the compositions and sources of ore-forming fluids. For example, the Cl/Br values of marialite in the Tieshan Fe-Cu skarn deposit (details in section 7.2) are considerably higher than that of seawater (~280; You et al. 1994), but can be explained by hydrothermal brines derived by the dissolution of halite and sylvite, providing further support for a genetic model of this deposit involving marine evaporites (Pan and Dong, 1999).

There have been numerous applications of Cl/Br systematics from fluid inclusions in constraining the sources and evolution of hydrothermal fluids in a variety of mineral deposits (e.g., Kesler et al. 1995). The present study shows that the Cl/Br values in Cl-rich minerals are also useful tracers for the compositions and sources of ore-forming fluids, provided that the distribution coefficients of Cl and Br between minerals and coexisting melts and fluids are known. In this respect, scapolite-group minerals and sodalites are special cases in that their Cl/Br values can be used directly as tracers for the sources and evolution of hydrothermal fluids, because their K_D values are close to unity. Another advantage of scapolite-group minerals and sodalites is that the Cl/Br values in these minerals from skarn systems and medium-grade metamorphic terrains are not significantly affected during cooling processes (Figure 6.4), unlike those in fluid inclusions.

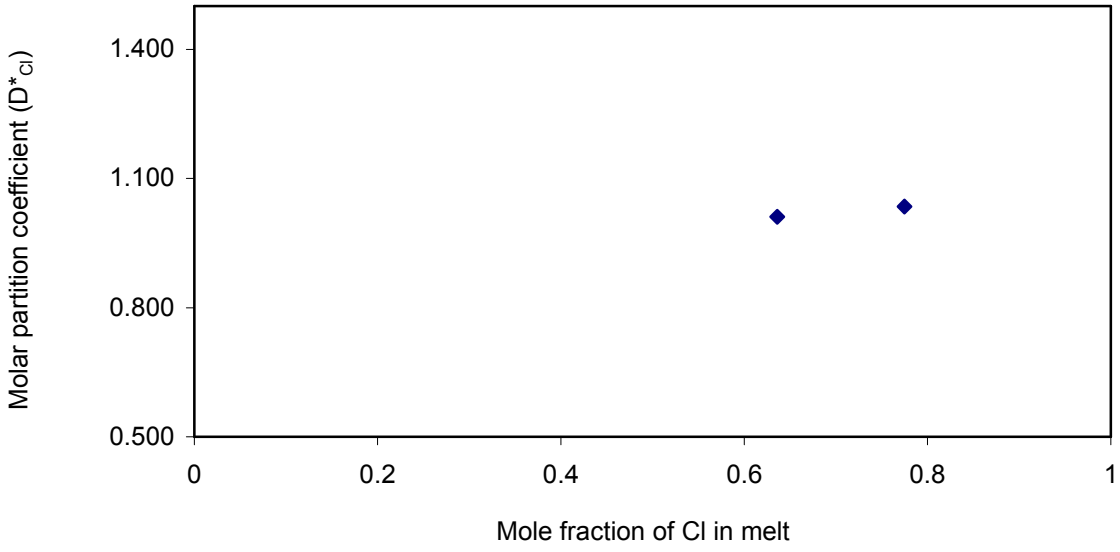

Figure 6.5a Molar partition coefficient (D^*_{Cl}) vs mole fraction of Cl in melt associated with scapolite

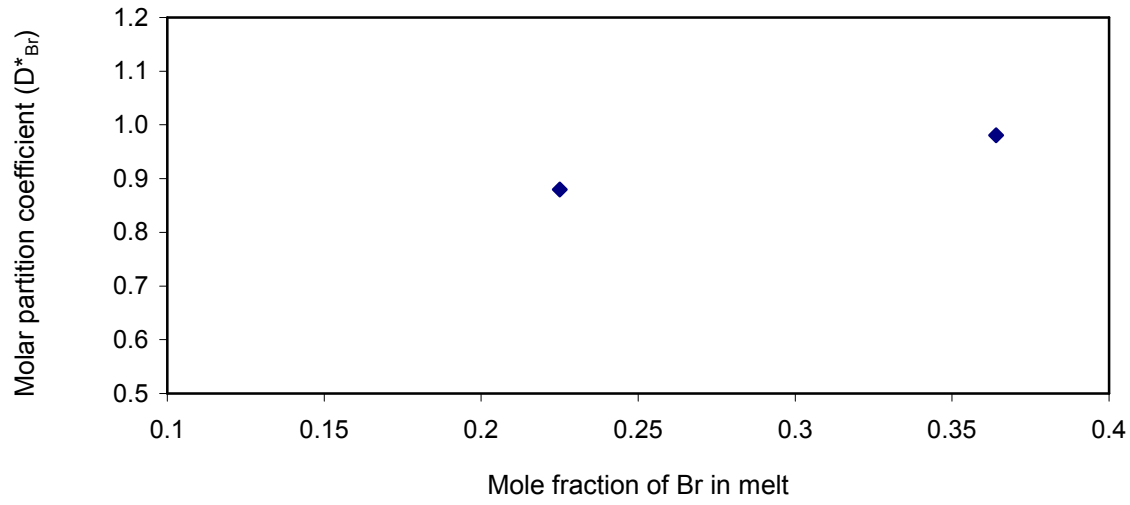

Figure 6.5b Molar partition coefficient (D^*_{Br}) vs mole fraction of Br in melt associated with scapolite

7. Applications

The experimentally determined partition coefficients of halogens between minerals (apatites, scapolites, and sodalites) and fluids/melts of this study have been applied to interprete the source and evolution of hydrothermal fluids/melts in mineralization processes and other geological systems. All selected localities and environments are interesting, because the origins of the parental fluids/melts are controversial.

7.1 Halogens in Fluorpatite and Applications

Apatites from Aoshan fluorapatite-magnetite deposit of the Middle-Lower Changjiang metallogenic belt, Eastern China; from Oka carbonatite complex, Quebec, Canada; and from Chinese mantle xenoliths were analyzed for halogen elements with the use of EMPA and XRF, and the halogen compositions of the fluids/melts equilibrated with the apatites were calculated based on the experimental results.

7.1.1 Fluorapatite from the Aoshan Fluoapatite-Magnetite Deposit of the Middle-Lower Changjiang Metallogenic Belt, Eastern China

The Middle-Lower Changjiang metallogenic belt, including more than 200 Cu-Fe-Au, Mo, and Zn-Pb-Ag deposits, is one of the most important metallogenic belts in China. Most of the polymetallic deposits in this belt are clustered in seven districts (Figure 7.1) and share many similarities. One of the most characteristic features is the occurrence of three distinct types of mineralization in close spatial association: porphyry orebodies in Late Mesozoic Yanshanian granitoid intrusions, skarn orebodies near contact

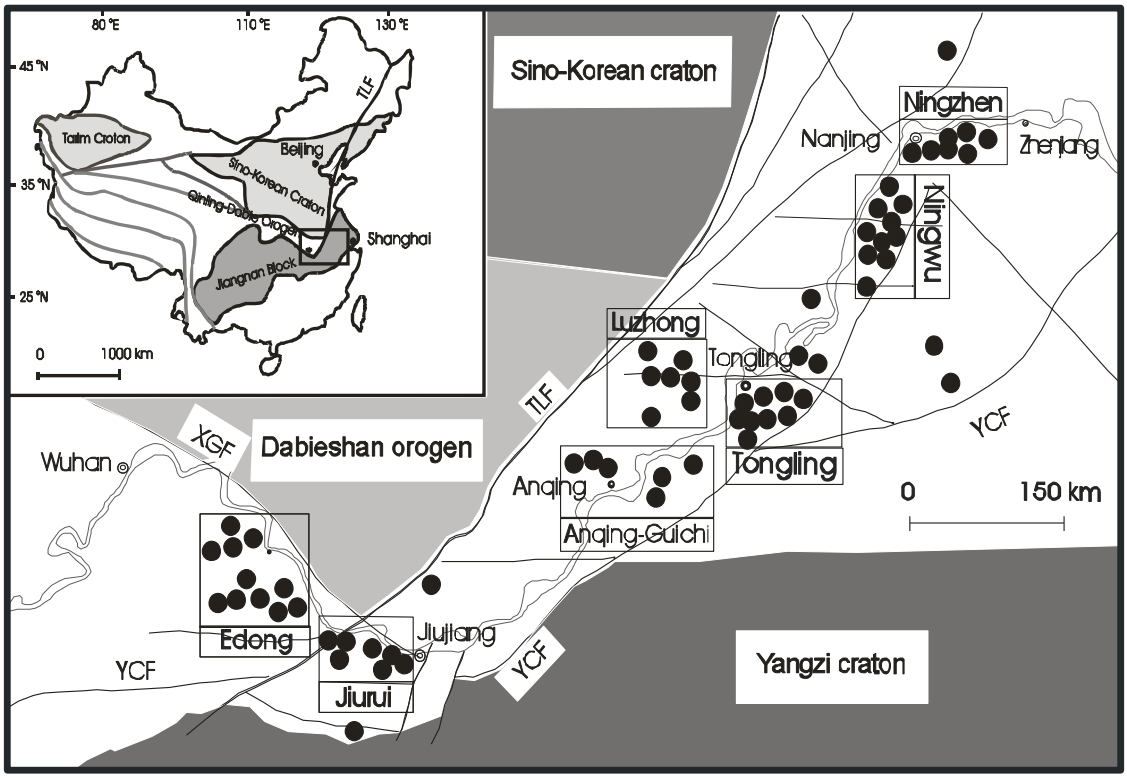

Figure 7.1 Location map of the Middle-Lower Changjiang metallogenic belt, Eastern China and the distribution of the polymetallic deposits. There are seven mineralization districts (from west to east: Edong, Jiurui, Anqing-Guichi, Luzhong, Tongling, Ningwu, and Ningzhen). XGF: Xiangfan-Guangji Fault; YCF: Yangxing-Changzhou Fault; and TLF: Tancheng-Lujiang Fault.

zones between the Late Mesozoic granitoid intrusions and Late Paleozoic-Early Mesozoic carbonates and evaporites, and “stratiform” massive sulphide orebodies in the Late Paleozoic-Early Mesozoic carbonates and evaporites (Chang et al., 1991; Pan and Dong, 1999 and references therein).

There is a general consensus that the porphyry- and skarn-type mineralization in the Middle-Lower Changjiang metallogenic belt formed during hydrothermal alteration related to the Late Mesozoic granitoid intrusions. Most Chinese researchers favoured models of syngenetic mineralization involving sedimentary, volcano-sedimentary or sedimentary-exhalative processes in the Middle Carboniferous shallow marine environments, with or without upgrading by the Late Mesozoic magmatism, for the formation of the stratiform massive sulphide deposits (e.g., Gu, 1984; Wang et al., 1987; Li, 1989; Ji et al., 1990; Chang et al., 1991; Zhu et al., 1991; Zhai et al., 1992; Yue et al., 1993; Li et al., 1996; Zhao and Zhao, 1997). Many other models have been proposed for the stratiform orebodies in the literature as well. Pan and Dong (1999) noted that the “stratiform” massive sulphide deposits in the Middle-Lower Changjiang metallogenic belt share a number of similarities to those of high-temperature, carbonate-hosted replacement deposits of northern Mexico, the Great Basin of western United States, and the Ertsberg deposit of Indonesia (Meinert, 1982; Haynes and Kesler, 1988; Megaw et al., 1988; James and Henry, 1993; Titley, 1993 and 1996; Megaw et al., 1996; Meinert et al., 1997; Rubin and Kyle, 1997; Megaw, 1998). Therefore, the stratiform massive sulphide orebodies in the Middle-Lower Changjiang metallogenic belt may represent distal parts of

large hydrothermal systems that form the porphyry orebodies within the granitoid intrusions and the proximal skarn orebodies near the contact zones.

The Aoshan fluorapatite-magnetite deposit is located in the central part of the Ningwu basin (Ningwu mineralization district), on the east part of the Middle-Lower Changjiang metallogenic belt, and is hosted in the late Yanshanian Aoshan intrusion. The exposed strata at the Aoshan deposit are mainly the Lower Cretaceous trachyandesitic volcanic rocks, which have been subjected to extensive silicification, kaolinitization, and sulphidization along fractures and faults. The Aoshan intrusion with an exposed area of 7.5 km^2 lies at the intersection between the Bijiashan-Mashan fault (BMF) and the Yanghutang-Aoshan fault (YAF; Figure 7.2), and comprises mainly a gabbro-diorite porphyry intruded by albite porphyry and quartz-albite porphyry dykes (Zhai et al., 1992).

The disk-like Aoshan main orebody (approximately 600-800 m long, 400-500 m wide, and 250-300 m thick) occurs in the northern part of the gabbro-diorite porphyry, and also extends into the contact zone and volcanic country rocks (Chang et al., 1991). The orebody is composed mainly of magnetite, fluorapatite, actinolite (after diopside), and albite. Mineralization at the Aoshan deposit is characterized by Ti- and V-bearing magnetite, and exhibits a pronounced vertical zonation from a lower zone of fine-grained, Ti- and V-poor, disseminated ores to a middle zone of massive ores in stockworks with intermediate Ti and V contents, and an upper zone of pegmatitic and brecciated ores with high Ti and V contents. Fluorapatite crystals (up to 1.2 m

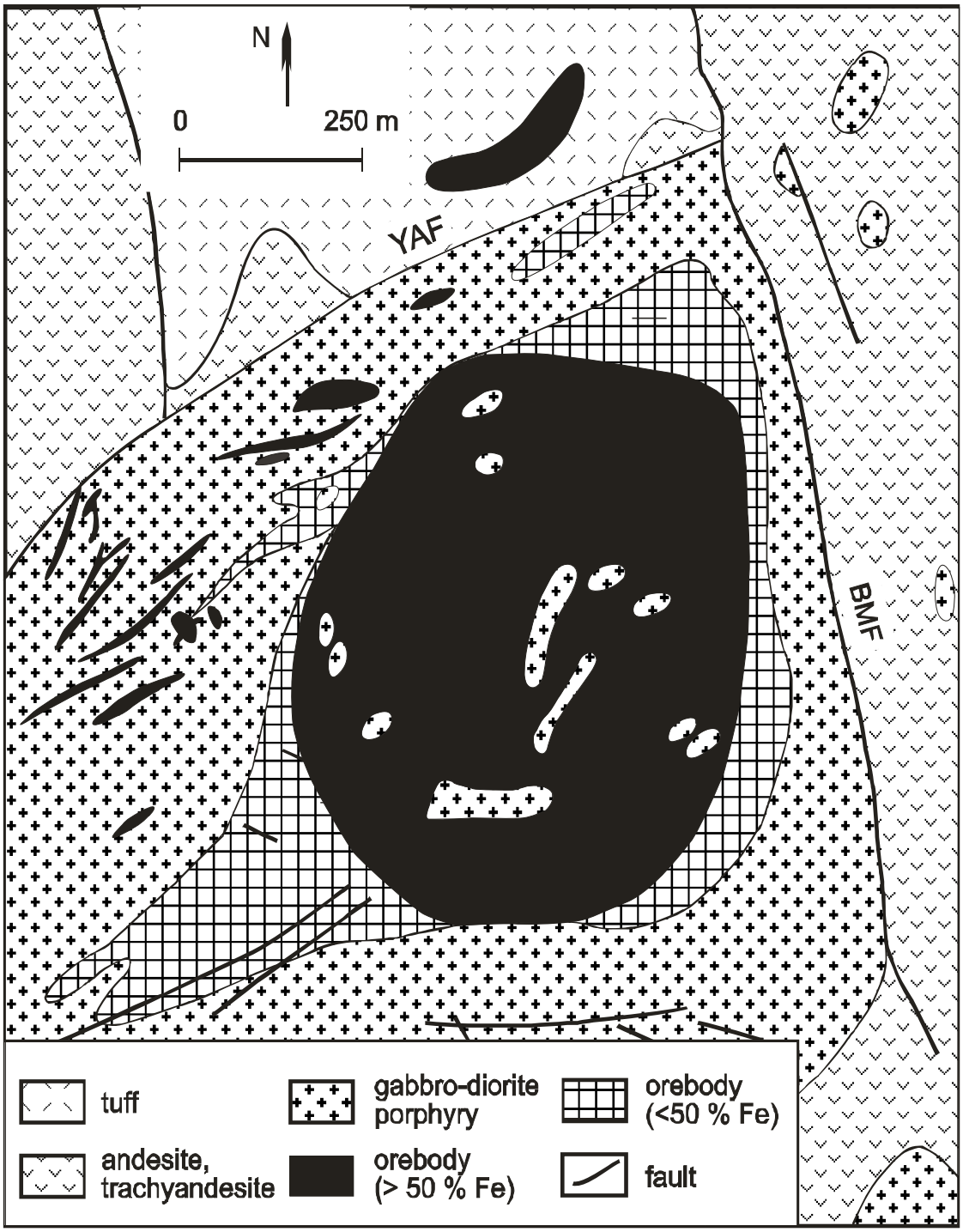

Figure 7.2 Geological map of Aoshan fluorapatite-magnetite deposit, Ningwu District, the Middle-Lower Changjiang metallogenic belt, Eastern China (Modified after Zhai et al., 1992). BMF: Bijiashan-Mashan fault; YAF: Yanghutang-Aoshan fault.

long) are particularly abundant in the upper pegmatitic zone.

There are three stages of hydrothermal alteration at the Aoshan deposit: 1) early sodic alteration including mainly albite and marialitic scapolite with minor amounts of actinolite, epidote, and magnetite, forming a light coloured zone at the lower part; 2) diopside-albite-fluorapatite-magnetite mineralization with weak epidotization and carbonatization, resulting in a dark coloured zone at the middle part; and 3) late argillization, alunitization, silicification, sulphidization, and carbonatization, forming an upper light coloured zone (Zhai et al., 1992). Supergene alteration at the Aoshan deposit averages 60 to 70 m in depth (Zhai et al., 1992).

Aoshan fluorapatite-magnetite deposit is similar to the Kiruna-type iron deposits in terms of mineral assemblage (fluorapatite-actinolite-magnetite), texture, orebody occurrences (e.g., disk-like concordant orebodies), sodium alteration, and geological setting. They are intimately associated with intermediate subvolcanic plutons in an intermediate-acid volcanic rock environment.

There are many different models for the origins of the Kiruna-type iron deposits, even after a century of studies of this deposit type. Many researchers are in favor of magmatic origin involving the emplacement of volatile-rich magmas through processes, such as magmatic differentiation or liquid immiscibility and vapor separation. Other models such as hydrothermal or post-magmatic processes, exhalative sedimentary processes, and remobilization of Fe and phosphorus from sedimentary rocks are also suggested (Hildebrand,

1986; Nystrom and Henriquez, 1994; and references therein).

Twenty-six samples including twenty-two fluorapatite-bearing samples had been collected from different parts of the Aoshan apatite- magnetite ore bodies and altered wallrock. The sample locations and mineral assemblages are summarized in Table 7.1. A small portion of each sample was grounded and fused disks were analyzed for bulk composition by XRF, except for F and Cl by ion specific electrode (ISE) and Br by INAA (basic) at SGS Lakefield Research, Ontario and the results are listed in Table 7.2.

For the Kiruna-type iron deposits, there is a large variation of the Ti content even within a same orebody. Relatively high V and very low Cr values

Table 7.1 Description of samples from Aoshan apatite-magnetite deposit

Sample #	Location	Description
99-6-1	-45m Level, west side of the open pit	Brecciated Apt-Act-Mat ore
99-6-2	-45m Level, west side of the open pit	Brecciated Apt-Act-Mat ore
99-6-3	-45m Level, west side of the open pit	Coarse grained Apt-Act-Mat ore
99-6-4	-45m Level, west side of the open pit	Pegmatitic Apt-Act
99-6-5	-45m Level, west side of the open pit	Pegmatitic Apt-Act
99-6-6	-45m Level, west side of the open pit	Pegmatitic Apt-Act-Mat ore
99-6-7	-45m Level, west side of the open pit	Pegmatitic Apt-Act
99-6-8	-45m Level, west side of the open pit	Pegmatitic Apt-Act-Mat ore
99-6-9	-45m Level, west side of the open pit	Pegmatitic Apt-Act-Mat ore
99-6-10	-45m Level, west side of the open pit	Act-Mat ore
99-6-11	-45m Level, west side of the open pit	Apt-Act-Qtz
99-6-12	-15m Level, west side of the open pit	Pegmatitic Apt
99-6-13	-15m Level, west side of the open pit	Pegmatitic Apt Mat ore
99-6-14	-90m Level, east side of the open pit	Apt (pinkish)-Act-Mat ore
99-6-15	-90m Level, east side of the open pit	Pinkih Apt
99-6-16	-90m Level, east side of the open pit	Apt (light green)-Act-Mat ore with volcanic fragments
99-6-17	-90m Level, east side of the open pit	Apt (light pinkish)-Act-Mat ore bccia
99-6-18	-90m Level, east side of the open pit	Apt (light yellowish green)-Act-Mat ore with volcanic fragments
99-6-19	-90m Level, east side of the open pit	Apt (euhedral)-Act-Mat ore
99-6-20	-90m Level, west side of the open pit	Apt (pinkish)-Act-Mat ore
99-6-21	-90m Level, west side of the open pit	Apt (light green)
99-6-22	-90m Level, west side of the open pit	Apt (pinkish)+qtz inide Act
99-6-23	-75m Level, north-west side of the open pit	Apt (light green)-Act-Mat ore
99-6-24	-60m Level, north-west side of the open pit	Apt (pink)-Act-Mat
99-6-25	-30m Level, north-west side of the open pit	Altered volcanics
99-6-26	0 m Level, west side of the open pit	Altered volcanics

Mineral abbreviations: Apt=apatite, Act=actinolite, Mat=magnetite, Qtz=quartz

Table 7.2 XRF analytical results of Aoshan whole rock samples for major elements (%) and some trace elements (ppm)

Sample No.	SiO_2	Al_2O_3	CaO	MgO	Na_2O	K_2O	Fe_2O_3	MnO	TiO_2	P_2O_5	Cr_2O_3	LOI	Total	Rb	Sr	Y	Zr	Nb	Ba	F	Cl	Br
99-6- 1	31.79	10.03	4.86	3.05	3.89	0.46	41.26	0.07	0.93	2.84	<0.01	0.85	100.1	15	141	44	72	<2	119	2280	322	<1
99-6- 2	41.19	12.76	3.13	2.4	5.98	0.25	32.26	0.07	0.6	0.78	<0.01	0.5	99.98	3	245	15	81	2	116	1210	194	<1
99-6- 3	28.02	0.64	21.62	7.89	0.2	0.07	27.07	0.24	0.61	11.64	<0.01	0.25	98.31	<2	6	434	14	<2	26	7040	2370	<1
99-6- 4	19.36	0.45	26.28	6.4	0.35	0.07	24.35	0.21	0.53	17.21	<0.01	0.5	95.81	3	<2	907	18	<2	<20	12123	3720	<1
99-6- 5	40.76	0.79	20.85	11.86	0.16	0.06	11.84	0.52	0.14	7.27	<0.01	3.75	98.08	<2	30	491	46	<2	22	5050	686	<1
99-6- 6	18.14	0.47	34.03	4.95	0.27	0.09	16.2	0.22	0.38	21.5	<0.01	1.05	97.43	<2	<2	1190	7	<2	<20	13191	3730	<1
99-6- 7	36.06	0.47	26.45	9.52	0.38	0.07	9.27	0.16	0.13	13.32	<0.01	0.9	96.85	<2	<2	1040	38	<2	<20	8490	2910	<1
99-6- 8	23.01	0.65	26.88	5.65	0.24	0.06	21.06	0.19	0.49	19.24	<0.01	0.3	97.84	<2	<2	745	7	<2	21	9770	2710	<1
99-6- 9	17.11	1.1	4.2	4.43	0.06	0.05	>70	0.33	1.73	0.72	<0.01	<0.01	100.2	<2	14	42	25	<2	84	749	145	<1
99-6-10	28.91	0.95	6.8	6.92	0.08	0.06	53.48	0.39	1.32	1.27	<0.01	<0.01	100.1	3	24	58	35	<2	74	1390	292	<1
99-6-11	66.73	0.25	14.57	1.87	0.14	0.05	1.46	0.03	0.05	11.58	<0.01	0.6	97.38	5	<2	423	4	<2	25	7190	1680	<1
99-6-12	1.59	<0.01	49.96	0.13	0.47	0.03	0.33	0.03	<0.01	44.22	<0.01	0.6	97.53	<2	<2	3210	<2	<2	<20	17118	>5000	<1
99-6-13	60.67	0.53	4.02	3.19	0.01	0.05	29.18	0.23	1.04	0.12	<0.01	0.9	99.96	<2	3	7	17	<2	76	399	129	<1
99-6-14	6.69	0.47	37.76	1.2	0.29	0.06	20.97	0.06	0.45	27.58	<0.01	0.45	96.1	<2	<2	1360	<2	<2	<20	15738	3900	<1
99-6-15	3.34	0.16	44.87	0.04	0.42	0.03	1.32	0.04	0.02	48.6	<0.01	0.75	99.77	<2	<2	2690	<2	<2	<20	17643	>5000	<1
99-6-16	19.45	5.18	10.04	3.14	1.66	0.1	52.78	0.26	1.56	5.43	<0.01	0.4	100	<2	111	145	25	<2	88	3600	985	<1
99-6-17	11.87	1.26	9.16	3.2	0.1	0.06	67.98	0.21	2.23	4.72	<0.01	<0.01	99.96	<2	54	101	11	<2	65	3300	795	<1
99-6-18	23.93	3.29	10.52	5.31	0.68	0.09	50.02	0.19	1.26	4.95	<0.01	0.35	100.6	<2	74	119	28	<2	69	3660	1020	<1
99-6-19	10.25	0.79	4.14	0.85	0.03	0.04	>70	0.16	2.03	2.79	<0.01	<0.01	100.3	<2	29	51	3	<2	39	1850	578	<1
99-6-20	6.13	0.65	13.35	0.76	0.1	0.04	69.73	0.09	1.21	9.16	<0.01	<0.01	99.76	<2	48	203	2	<2	61	6560	1530	<1
99-6-21	12.37	0.79	38.85	3.24	0.35	0.06	6.31	0.21	0.23	35.53	<0.01	2.2	100.3	<2	<2	1700	3	<2	<20	14940	4340	<1
99-6-22	56.56	0.96	11.72	15.03	0.45	0.12	10.38	0.37	0.18	1.03	<0.01	1.6	98.43	4	18	164	76	<2	30	3870	386	<1
99-6-23	11.78	0.91	12.74	3.83	0.16	0.06	61.62	0.26	1.99	6.6	<0.01	<0.01	99.39	<2	51	191	11	<2	60	4640	1260	<1
99-6-24	18.38	0.6	28.74	5.63	0.27	0.05	20.42	0.19	0.5	19.23	<0.01	0.7	94.83	2	<2	1030	8	<2	<20	10672	3270	1
99-6-25	57.45	14.98	7.54	4.76	6.32	0.13	6.62	0.18	0.08	0.05	<0.01	1.6	99.77	<2	407	23	140	<2	81	558	125	<1
99-6-26	57.91	20.02	2.47	0.44	8.2	1.3	5.53	0.03	0.28	0.59	<0.01	1.5	98.38	42	482	8	98	4	324	662	174	<1

have been reported in the magnetites (Hildebrand, 1986; Nystron and Henriquez, 1994). Similarly, the Aoshan samples exhibit highly variable Ti contents from <0.01% to 2.23% of TiO_2 and very low Cr_2O_3 contents (less than 0.01% of the detection limit). Two altered volcanic wallrock samples are with higher Na_2O values from 6.32 to 8.2%. Both the Cl and F are positively correlated to the P_2O_5 contents in all the samples (Figure 7.3) and it suggests that most of the halogens in the Aoshan orebodies are hosted in apatites.

Fluorapatite from each sample was hand-picked in order to determine the halogen contents. The hand-picked fluorapatite grains were first analyzed for Br by XRF, and then were mounted on Pyrex plugs. The plugs were polished and carbon-coated for electron microprobe analysis, except for sample 99-6-26 that was directly analyzed by EMPA from polished thin section due to the too fine-grain size of apatite.

The XRF and EMPA results of apatite crystals from Aoshan apatite-magnetite deposit are listed in Table 7.3. Detailed analytical results can be found in Appendix 3a and 3b. All the Aoshan apatites are Cl-bearing fluorapatite with 0.38 to 0.98 wt% Cl and 1.83 to 3.45 wt% F. Trace to 52 ppm bromine were detected in Aoshan apatite crystals.

Figure 7.4 illustrates the molar fraction of Br and Cl (X^*_{Br} and X^*_{Cl}) in natural apatites. Consistent with the experimental results, the values of X^*_{Br} in the mantle apatites, Aoshan apatites, and Chinese xenolith apatites, all increase with increased X^*_{Cl} values. The Aoshan apatites are similar to the mantle apatite of group B (O'Reilly and Griffin, 2000) and Chinese mantle

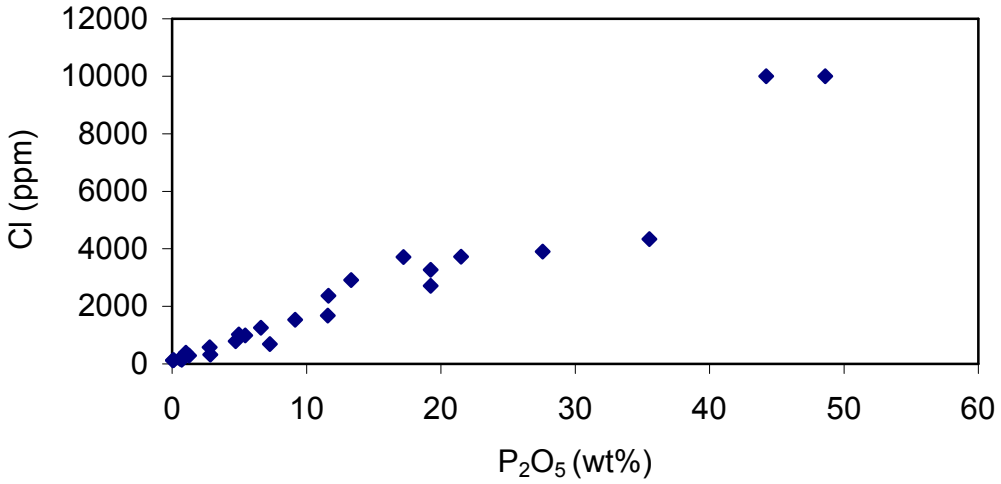

Figure 7.3a Cl vs P_2O_5 contents for bulk Aoshan samples (See Table 7.2)

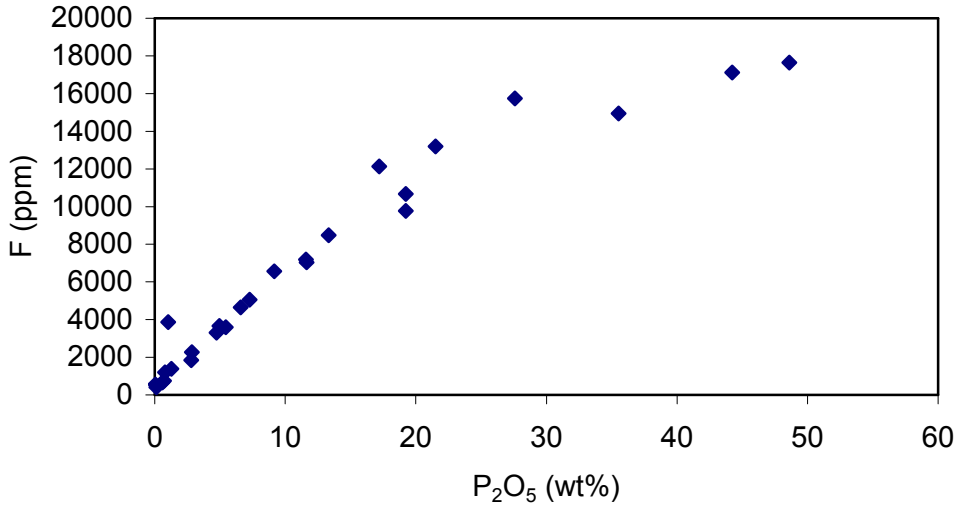

Figure 7.3b F vs P_2O_5 contentsfor bulk Aoshan samples (See Table 7.2)

Table 7.3 Compositions of apatite from Aoshan apatite-magnetite deposit, Eastern China (wt%)

Sample No.	CaO	SiO_2	MnO	FeO	Na_2O	P_2O_5	Cl	F	Br	Br^a(ppm)	O=(Cl+F)	Total
996-3	54.00(244)	0.21(4)	0.02(2)	0.13(7)	0.20(12)	43.00(235)	0.70(31)	2.80(44)	0.010(11)	0	1.33	99.74
99-6-4	53.00(172)	0.30(13)	0.03(3)	0.15(9)	0.30(11)	42.00(180)	0.90(24)	2.40(27)	0.020(14)	0	1.21	97.89
99-6-5	53.00(318)	0.24(7)	0.03(3)	0.13(6)	0.30(10)	41.00(381)	0.70(30)	2.80(56)	0.010(12)	7(4)	1.35	96.86
99-6-6	55.00(138)	0.23(8)	0.03(3)	0.08(5)	0.20(15)	41.00(124)	0.70(39)	3.20(33)	0.018(8)	0	1.51	98.95
99-6-7	54.50(55)	0.40(45)	0.03(3)	0.11(7)	0.20(11)	41.50(61)	1.00(27)	2.70(22)		0	1.35	99.09
99-6-8	54.50(87)	0.26(2)	0.02(3)	0.12(6)	0.29(3)	39.00(201)	0.90(24)	3.30(36)	0.020(19)	0	1.59	96.82
99-6-9	55.30(96)	0.19(8)	0.03(2)	0.12(7)	0.10(13)	42.20(59)	0.60(38)	2.80(36)	0.010(12)	0	1.29	100.06
99-6-11	53.00(187)	0.21(2)	0.03(3)	0.14(6)	0.20(3)	42.00(302)	0.70(16)	3.00(60)	0.020(15)	9	1.40	97.90
99-6-12	53.00(177)	0.24(3)	0.03(4)	0.20(12)	0.29(7)	43.00(193)	0.80(11)	2.60(55)	0.012(8)	50(38)	1.26	98.91
99-6-14	55.00(172)	0.20(10)	0.03(3)	0.11(8)	0.20(14)	42.00(107)	0.60(40)	2.70(41)	0.020(13)	10(10)	1.29	99.57
99-6-15	52.00(144)	0.24(3)	0.02(3)	0.16(6)	0.31(5)	44.00(233)	0.90(16)	2.40(16)	0.020(13)	4(3)	1.21	98.84
99-6-16	54.70(94)	0.23(6)	0.04(3)	0.17(4)	0.23(6)	41.00(165)	0.80(27)	2.00(55)	0.020(13)	20(10)	1.44	97.75
99-6-17	53.00(128)	0.26(3)	0.04(3)	0.16(3)	0.28(5)	41.00(244)	1.00(17)	3.00(55)	0.011(8)	9(5)	1.49	97.26
99-6-18	55.00(210)	0.10(10)	0.04(3)	0.13(8)	0.10(11)	42.00(128)	0.90(33)	2.00(102)	0.020(10)	8(3)	0.98	99.31
99-6-19	53.00(195)	0.24(5)	0.02(3)	0.20(50)	0.30(11)	44.00(214)	0.80(23)	2.50(24)	0.020(15)	6(1)	1.20	99.88
99-6-20	54.00(122)	0.20(15)	0.02(2)	0.10(11)	0.10(10)	41.00(124)	0.40(33)	3.00(30)	0.010(7)	1.1(6)	1.35	97.48
99-6-21	54.80(49)	0.15(8)	0.02(2)	0.06(6)	0.10(12)	42.00(128)	0.38(41)	3.00(34)	0.010(12)	0.6	1.35	99.17
99-6-22	55.00(150)	0.23(6)	0.01(1)	0.11(4)	0.24(4)	38.00(118)	0.77(9)	3.50(33)	0.011(8)	0.3(1)	1.62	96.25
99-6-23	55.00(121)	0.20(9)	0.02(3)	0.10(7)	0.10(12)	42.00(144)	0.60(40)	2.80(50)	0.020(14)	0.8(2)	1.29	99.55
99-6-24	53.00(131)	0.22(6)	0.02(3)	0.13(6)	0.20(12)	41.00(128)	0.90(34)	2.50(36)	0.030(19)	1.8(1.1)	1.24	96.76
99-6-26	53.40(60)	0.07(7)	0.03(3)	0.20(13)	0.21(8)	41.60(37)	0.70(14)	2.90(25)		0	1.37	97.74

a:XRF results in ppm. One standard deviation is in the parentheses.

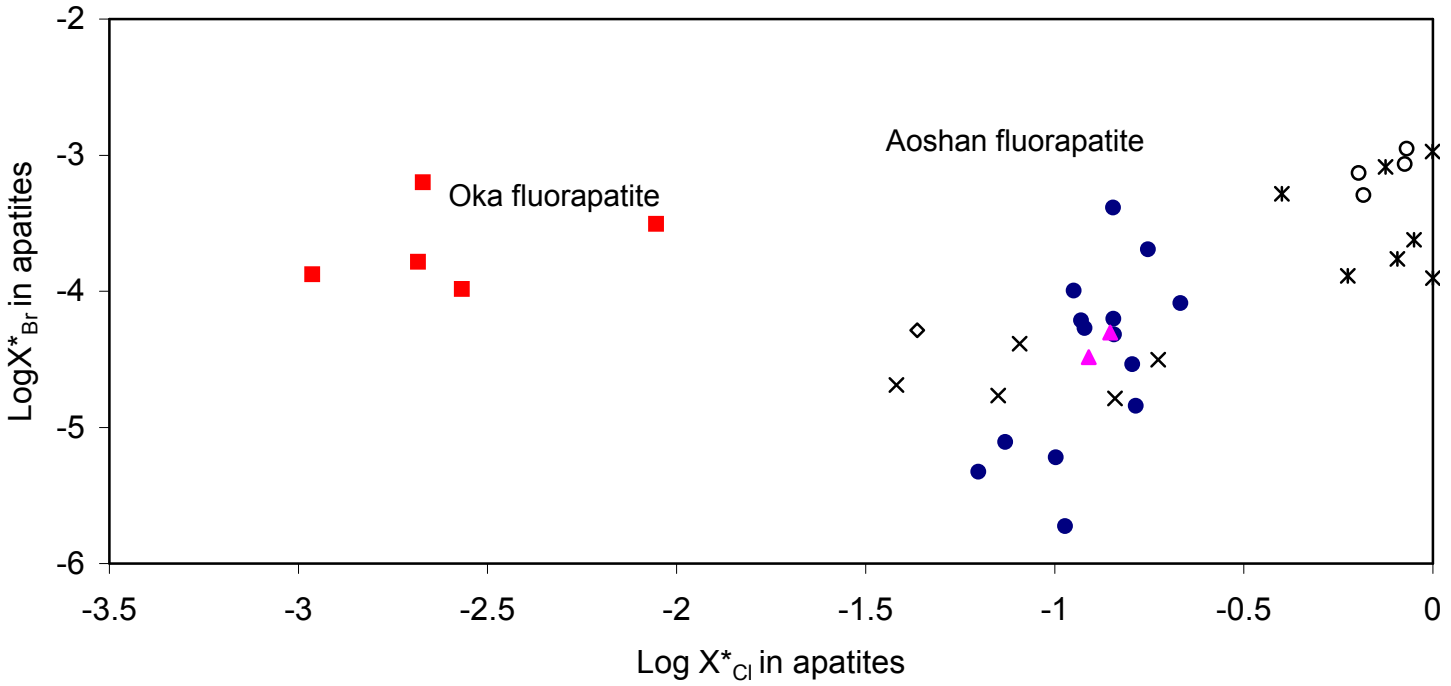

Figure 7.4 Molar fraction of Cl and Br (X^*_{Cl} vs X^*_{Br}) in apatites from Aoshan, Oka, and mantle xenoliths

The molar ratios are calculated based on partitioning experimental results (refer to text for detailes). Solid circles-Aoshan; solid squares-Oka; solid triangles-Chinese xenolith apatite; stars-mantle apatite A; crosses-mantle apatite B; open circles-other mantle apatites.

Griffin, 2000) and Chinese mantle xenolith fluorapatite (see section 7.1.3) in their Br and Cl composition. The apatite of group B was considered to be of magmatic origin and represent various stages of crystallization within a fractionating alkaline magma (O'Reilly and Griffin, 2000). By comparison, the Aoshan fluorapatite may have originated from magma as well. The halogen composition of fluorapatite supports the magmatic origin probably with a mantle source for Aoshan fluorapatite-magnetite deposit.

The partitioning experimental results of halogens between apatites and melts at run temperature of 1120^{o}C have been applied to calculate the molar ratios of halogens in the melts from that the apatites precipitated. The values of partition coefficients are adjusted based on the apatite halogen composition (e.g., the Cl/F ratio). The calculated halogen compositions of melts in equilibrium with natural apatites are listed in Table 7.4 and illustrated in Figure 7.5. The calculated halogen compositions of melts equilibrated with mantle apatites (Ionov et al., 1997; O'Reilly and Griffin, 2000) and Durango apatite are plotted as well. Also displayed are the estimated (Br/Cl) molar ratios of mantle fluid/melt (0.000533-0.00444/0.000247-0.001234; Johnson et al., 2000 and references therein). The halogen compositions of carbonates (Mason, 1966), seawater (Henderson, 1984), and metamorphic fluids (Boiron et al., 1999) are exhibited for reference. The melt from which the Aoshan fluorapatite crystallized is similar to the melts from which the mantle apatite B crystallized, implying the possibility of mantle sources for Aoshan fluorapatite and associated magnetite.

Table 7.4 Halogen compositions of apatites and melt from Aoshan, China Xenolith, and Oka

	Apatite					Apatite/Melt(liquid)						Calculated					
	EMPA			XRF	Final	Apatite molar fraction			Molar partition coefficient			Melt(liquid) molar fraction			Melt molar ratios		
Sample N	Cl %	F %	Br %	Br (ppm)	Br (ppm)	X_{Br}*[a]	X_F*	X_{Cl}*	D_F*	D_{Cl}*	D_{Br}*	X_F*	X_{Cl}*	X_{Br}*	Br/F	Cl/F	Br/Cl
996-3	0.74	2.77	0.012	0			0.875	0.125	1.049	0.201	0.021	0.835	0.620			0.743	
99-6-4	0.88	2.40	0.019	0			0.836	0.164	1.049	0.239	0.021	0.797	0.688			0.863	
99-6-5	0.72	2.82	0.014	7	7	0.0001	0.880	0.120	1.049	0.196	0.021	0.839	0.611	0.003	0.003	0.728	0.004
99-6-6	0.71	3.21	0.018	0			0.895	0.105	1.049	0.183	0.021	0.853	0.578			0.678	
99-6-7	0.98	2.68	0.013	0			0.836	0.164	1.049	0.239	0.021	0.797	0.687			0.862	
99-6-8	0.89	3.32	0.020	0			0.874	0.126	1.049	0.202	0.021	0.834	0.623			0.747	
99-6-9	0.58	2.76	0.013	0			0.900	0.100	1.049	0.178	0.021	0.858	0.565			0.659	
99-6-11	0.73	2.95	0.022	9	9	0.0001	0.883	0.117	1.049	0.194	0.021	0.842	0.605	0.003	0.004	0.719	0.005
99-6-12	0.80	2.57	0.012	52	52	0.0004	0.857	0.143	1.049	0.218	0.021	0.817	0.654	0.020	0.024	0.800	0.030
99-6-14	0.64	2.72	0.017	13	13	0.0001	0.888	0.112	1.049	0.189	0.021	0.847	0.594	0.005	0.006	0.701	0.008
99-6-15	0.86	2.42	0.019	4	4	0.0000	0.840	0.160	1.049	0.235	0.021	0.801	0.682	0.001	0.002	0.851	0.002
99-6-16	0.80	2.01	0.022	21	21	0.0002	0.824	0.176	1.049	0.250	0.021	0.785	0.704	0.010	0.013	0.896	0.014
99-6-17	0.95	3.04	0.011	9	9	0.0001	0.857	0.143	1.049	0.218	0.021	0.817	0.654	0.003	0.004	0.800	0.005
99-6-18	0.93	1.83	0.021	8	8	0.0001	0.785	0.215	1.049	0.287	0.021	0.749	0.748	0.004	0.005	0.999	0.005
99-6-19	0.76	2.45	0.023	6	6	0.0000	0.857	0.143	1.049	0.219	0.021	0.817	0.655	0.002	0.003	0.802	0.004
99-6-20	0.44	2.98	0.010	1	1	0.0000	0.926	0.074	1.049	0.152	0.021	0.883	0.485	0.000	0.000	0.549	0.001
99-6-21	0.38	3.02	0.012	1	1	0.0000	0.937	0.063	1.049	0.142	0.021	0.894	0.443	0.000	0.000	0.496	0.001
99-6-22	0.77	3.45	0.011	0	0	0.0000	0.894	0.106	1.049	0.183	0.021	0.852	0.580	0.000	0.000	0.681	0.000
99-6-23	0.58	2.77	0.016	1	1	0.0000	0.899	0.101	1.049	0.178	0.021	0.858	0.566	0.000	0.000	0.660	0.001
99-6-24	0.90	2.47	0.026	2	2	0.0000	0.836	0.164	1.049	0.238	0.021	0.798	0.687	0.001	0.001	0.861	0.001
99-6-26	0.69	2.90	0.000				0.887	0.113	1.049	0.190	0.021	0.8458	0.5961	0		0.705	
																	0.002
Ty-16	0.62	2.06	0.008	5	4.99	0.0000	0.8599	0.1401	1.0485	0.2156	0.0207	0.820	0.649	0.002	0.003	0.792	0.004
IN-49	0.91	3.48	0.007	5	5.48	0.0000	0.8770	0.1230	1.0485	0.1992	0.0207	0.836	0.617	0.002	0.002	0.738	0.003
Durango	0.30	3.53		8	8	0.0001	0.9567	0.0433	1.0485	0.1229	0.0207	0.912	0.352	0.002		0.386	
oka-9718	0.01	2.13	0.007	57	57	0.0006	0.9972	0.0021	1.0485	0.0834	0.0207	0.951	0.026	0.031	0.032	0.027	1.195
oka-9719	0.05	3.11	0.013	41	41	0.0003	0.9909	0.0088	1.0485	0.0899	0.0207	0.945	0.098	0.015	0.016	0.104	0.154
oka-9723	0.01	3.54	0.029	20	20	0.0001	0.9988	0.0011	1.0485	0.0824	0.0207	0.953	0.013	0.006	0.007	0.014	0.487
oka-9729	0.01	2.45	0.006	17	17	0.0002	0.9978	0.0021	1.0485	0.0834	0.0207	0.952	0.025	0.008	0.008	0.026	0.319
oka-9730	0.01	2.15	0.006	9	9	0.0001	0.9972	0.0027	1.0485	0.0840	0.0207	0.951	0.032	0.005	0.005	0.034	0.155

a: X_i*=i/(F+Cl+Br) in mole, i=F, Cl, or Br

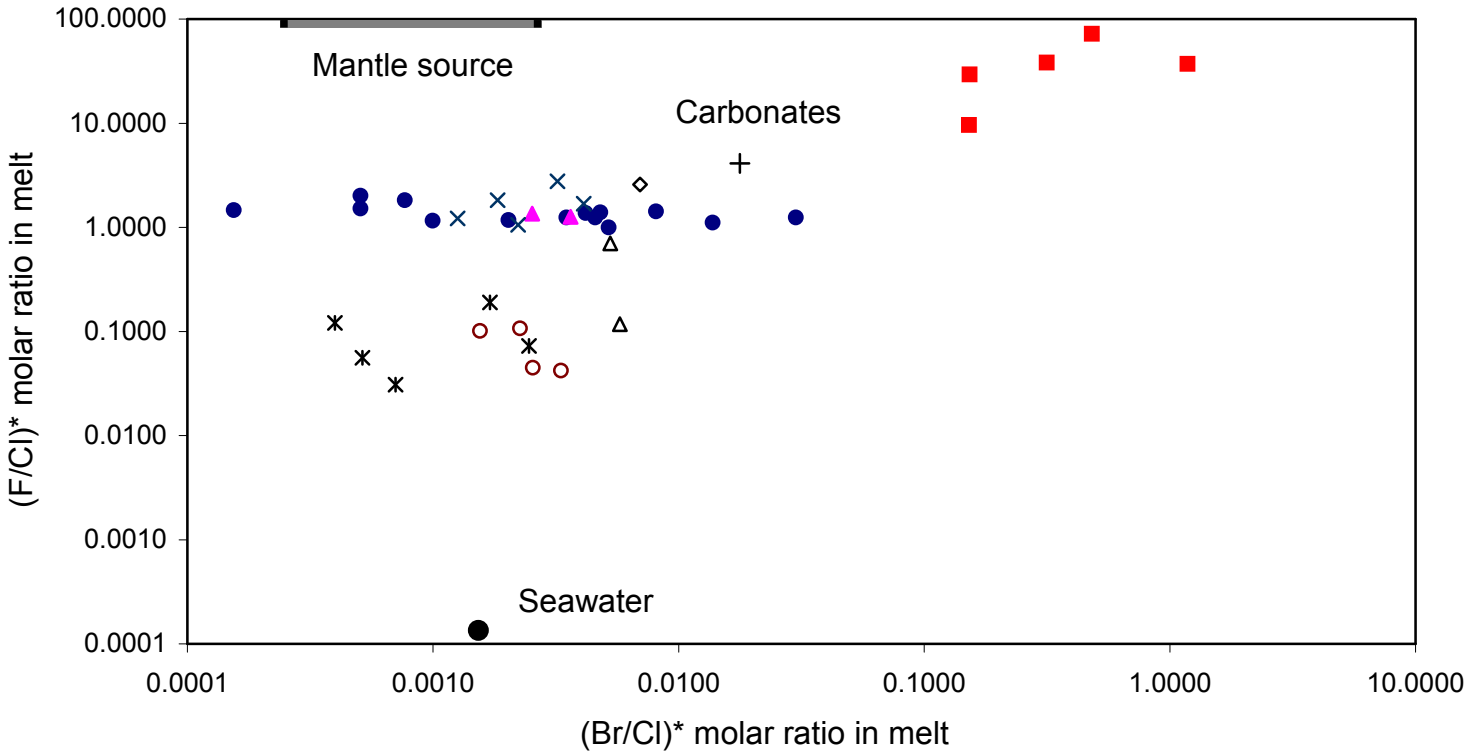

Figure 7.5 F/Cl*-Br/Cl*molar ratio in melt equilibrated with apatites

The molar ratios are calculated based on partitioning experimental results (refer to text for detailes). Solid circle-Aushan; solid square-OKA; solid triangle-Chinese xenolith; star- mantle apatite A; cross-mantle apatite B; open circle-other mantle apatites; open diamond-Durango; open triangle-metamorphic fluids; large black circle-seawater; large plus-carbonates. Estimated mantle fluids Br/Cl is displayed for reference only.

7.1.2 Fluorapatite from the Oka Carbonatite Complex, Quebec

The Oka carbonatite complex is part of the Monteregian Hills suite series of alkaline igneous intrusions, located about 32 km west of Montreal, Quebec. They intruded into the northeast-trending Precambrian gneisses, quartzite, and marble of the Grenville Series and the layered rocks of the Morin Series during the early Cretaceous. The Oka carbonatite complex represents the western end of the Monteregian Hills suite of alkaline intrusions (Fairbairn et al., 1963; Shafiqullah et al., 1970; Gold, 1972; Samson et al., 1995).

Regionally, there is a progressive change from silica-saturated plutons in the eastern part of the Monteregian Hills series, through undersaturated, nepheline-normative rocks, to highly undersaturated rocks with modal nepheline and/or melilite, and carbonatites in the west (e.g., in the Oka area). Correspondently, there is also a chemical trend of decreased silica and increased alkalis, calcium, carbon dioxide, volatile components westward (Gold, 1972).

The oval-shaped Oka complex, about 7.5 x 2.4 km^2, is comprised of two intersecting rings. Surrounding the complex is an aureole of veined and metasomatically altered rocks of fenites. The complex consists of a number of mineralogically distinct rock types: calcite-rich sovites, dolomite-rich rauhaugites, melilite and titan-augite-bearing, silica-undersaturated alkalic rocks such as okaites, jacupirangites, melteigites, ijolites, urtites, and juvites. The alkaline silicates are in the crescent-shaped masses, arcuate dykes, and discontinuous tabular bodies present only in the northern ring. The carbonatites

are interlayered by ferromagnesian minerals and magnetite concentrations of 1-5 cm thick. There are also several late lamprophyres and intrusive breccias as dykes and/or irregular pipe-like bodies (Gold, 1972).

The Oka carbonatites are usually coarse-grained sovites/calcite interlayered with minor or accessory aegirine (sodian augite), biotite, apatite, nepheline, monticellite, melilite, pyrochlore, perovskite, niocalite, richterite, pyrite, and pyrrhotite (Gold, 1963, 1972; Gold et al., 1967; Samson et al., 1995). The crystallization temperature of the carbonatites has been estimated to be about 730^{o}C for niocalite sovite, 720^{o}C for soda-pyroxene sovite, 765^{o}C for coarse-grained okaite, and 855^{o}C for calcite-rich, apatite okaite, on the basis of oxygen isotope geothermometers (e.g., calcite-magnetite; Conway and Taylor, 1969; Gold, 1972).

The minerals in the Oka carbonatite complex are characterized by the enrichment of cations with high ionic potential (high charge/small ionic radius), such as F, P, S, Sc, Ti, V, Mn, Cu, Sr, Y, Zr, Nb, Ba, La, Ce, Yb, Th, U, and alkalis, and with deficiency of SiO_2. Pyrochlore, a complex Nb oxide, is the main economic mineral and apatite, magnetite, and calcite are the main gangue minerals (Gold, 1972).

Fluorapatite is ubiquitous and occurs as small euhedral to subhedral crystals (~0.1 mm in length), disseminated at the boundary between the calcite grains, along the edges of monticellite crystals, or as inclusions in calcite and monticellite. Its concentration is mainly from 1 % to 8 %. Fluid inclusions in the apatite grains yielded a formation temperature from 183^{o} to 393^{o}C (Girault,

1966 cited from Gold, 1972). However, the acicular morphology and its association with other minerals suggest that the Oka apatite precipitated from a liquid phase enriched in CO_2 and poor in H_2O with sufficient fluid for fractional crystallization (Gold, 1972).

There are different hypotheses about the source and origin of the Oka carbonatite, including: 1) metamorphism of either the Palaeozoic or Grenville limestones by the alkalic rocks, 2) assimilation of the Palaeozoic or Grenville limestones by the alkalic magmas, 3) fractional crystallization from CO_2-bearing ultramafic magmas, and 4) directly crystallized from a primary carbonate magma (Gold, 1972).

There is a similarity between the Oka carbonatite complex and other Monteregian plutons in the initial Sr^{87}/Sr^{86} values (0.7032) and Rb-Sr and K-Ar ages of 114 ma for micas (Gold, 1972 and references therein). The initial Sr^{87}/Sr^{86} values (0.7027-0.7044; Powell et al., 1966; Bell and Blenkinson, 1989; and references therein) of the Oka carbonatite is also close to the mean Sr^{87}/Sr^{86} value of 0.7034 for typical carbonatites throughout the world (Faure and Powell, 1972). These Sr^{87}/Sr^{86} values are lower than those for oceanic and continental basalts (0.7042 to 0.7052) and sedimentary limestones and marbles (0.707 to 0.711), implying that carbonatites including the Oka carbonatites are originated from deeper parts of the mantle compared to the tholeiite magmas (Faure and Powell, 1972; Gold, 1972; Bell and Blenkinson, 1989; Wyllie, 1989). The Oka carbonatite complex has been considered to be “formed from volatile-rich differentiates of materials generated and outgassed

in the western (deeper) part of the Mongeregian belt" as "the 'pegmatitic' phase of the alkali ultramafic parent magma of probable mantle composition and origin" (Gold, 1972).

Five samples of the Oka carbonatites from the collection of the Department of Geological Sciences, Univ. of Sask., were dissolved in HCl solution to obtain fluorapatite separates. They were analyzed for Br by the XRF microprobe and major elements by the EMPA. The results are summarized in Table 7.5 and illustrated in Figures 8.3 and 8.4.

Oka fluorapatite contains trace amount of chlorine (up to 0.05 wt% Cl). Surprisingly, there are higher bromine contents in the Oka fluorapatite compared to their trace amount of chlorine. This distinguishes the Oka fluorapatite from other apatites such as Aoshan fluorapatite, mantle apatites, and apatite from Chinese mantle xenoliths (Figures 8.3 and 8.4). It may imply the Oka apatites originated from a different source and crystallized from a highly Br-enriched melt/fluid.

Apparently, the melt from which the Oka fluorapatite crystallized is different (in halogen composition) from the mantle melts and there is a possible genetic link to the carbonate (the Palaeozoic or Grenville limestones).

7.1.3 Fluorapatite from Chinese Mantle Xenoliths

Fluorapatite crystals in two samples of Chinese mantle xenoliths were provided by Prof. Jianping Zheng of Chinese University of Geosciences at Wuhan, China. LN-49 is apatite separate from Mg-Fe xenolith in Palaeozoic

Table 7.5 EMPA results of fluorapatite compositions from the Oka carbonatite complex and Chinese xenoliths (wt%)

Sample No.	Location	CaO	SrO	MnO	FeO	Na_2O	K_2O	P_2O_5	Cl	F	Br	Br[a]	O=(Cl+F)	Total
9718	Oka, Quebec	50.00(142)	0.83(5)	0.07(4)	0.03(2)	0.13(3)	0.01(1)	42.00(190)	0.01(1)	2.00(74)	0.007(6)	57(50)	0.90	94.19
9719	Oka, Quebec	51.00(214)	0.90(11)	0.08(4)	0.03(2)	0.24(4)	0.01(0)	44.00(218)	0.10(12)	3.00(61)	0.013(8)	41(25)	1.32	98.05
9723	Oka, Quebec	52.00(189)	0.46(5)	0.05(5)	0.02(2)	0.10(3)		43.00(197)	0.01(0)	4.00(53)	0.030(10)	20(13)	1.49	98.18
9729	Oka, Quebec	50.00(120)	0.83(3)	0.06(3)	0.02(2)	0.12(1)	0.02(1)	42.00(218)	0.01(1)	2.50(36)	0.006(0)	17(13)	1.03	94.54
9730	Oka, Quebec	50.00(161)	0.63(4)	0.08(2)		0.09(3)	0.01(0)	41.00(216)	0.01(1)	2.15(6)	0.006(0)	9(3)	0.90	93.08
LN-49	Chinese xenolith	52.76				0.04	0.00	42.11	0.91	3.48	0.007	5	1.67	97.62
TY-16	Chinese xenolith	51.40				0.13	0.00	42.06	0.62	2.06	0.008	5	1.00	95.27

a:XRF results in ppm. One standard deviation is in parentheses.

kimberlite in north-eastern China, and TY-16 is apatite separates from Mg-Fe xenolith in Mesozoic basalt in north-western China. Selected grains of apatite have been analyzed for Br by XRF and major elements by EMPA. The analytical results are listed in Table 7.5 and illustrated in Figures 7.3 and 7.4.

The Chinese xenolith apatite is similar to the Aoshan fluorapatite and group B mantle apatite of O'Reilly and Griffin (2000) on the basis of halogen compositions (Figures 7.3 and 7.4).

7.1.4 Discussion

Like other Kiruna-type iron deposits, there are many different models for the origins of the Aoshan fluorapatite-magnetite deposit, for example the magmatic differentiation or immiscibility separation (Chang et al., 1991; Zhai et al., 1992). The halogen composition of apatites from the Aoshan deposits suggests a magmatic origin, similar to the Group B of the mantle apatite (O'Reilly and Griffin, 2000) and Chinese xenolith apatite in the kimberlite and basalt (Figures 7.4 and 7.5).

There are several different hypotheses for the origin and source of the Oka carbonatite, such as the results of metamorphism of either the Palaeozoic or Grenville limestones by the alkalic rocks or of assimilation of the Palaeozoic or Grenville limestones by the alkalic magmas (Gold, 1972).

Oka fluorapatite is distinct from Aoshan fluorapatite and mantle apatites in terms of their halogen composition, e.g., trace amount of chlorine (up to 0.052 wt% Cl) with higher bromine content (9 to 57 ppm). The melt from which

the Oka apatite crystallized is different (in halogen composition) from the normal mantle melts and there is a possible genetic link to the carbonate (the Palaeozoic or Grenville limestones; Figure 7.5).

7.2 Halogens in Scapolite and Applications

Scapolite from Tieshan Fe-Cu skarn deposit of the Middle-Lower Changjiang Metallogenic Belt, Eastern China; from the Nickel Plate Gold skarn deposit, BC, Canada; and from the Grenvillian U, Th, Mo, and REE deposits, Ontario and Quebec, Canada has been studied for halogen compositions and interpreted with the results of exchange experiments, presented in section 6.3.2.

7.2.1 Scapolite from the Tieshan Fe-Cu Skarn Deposit of the Middle-Lower Changjiang Metallogenic Belt, Eastern China

The Tieshan Fe-Cu skarn deposit at the Edong district is located in the west part of the Middle-Lower Changjiang Metallogenic Belt and is situated in the northern limb of the Tieshan anticline. It consists of six orebodies at the contact of the Tieshan intrusion with the Triassic limestones and evaporites (Figure 7.6; Zhao et al., 1990; Shu et al., 1992). The Tieshan intrusion is a ring complex with a granodioritic porphyry at the centre, syenodiorite and quartz monzodiorite at the transitional zone, and quartz diorite, porphyritic quartz diorite, and biotite-pyroxene diorite at the marginal zone.

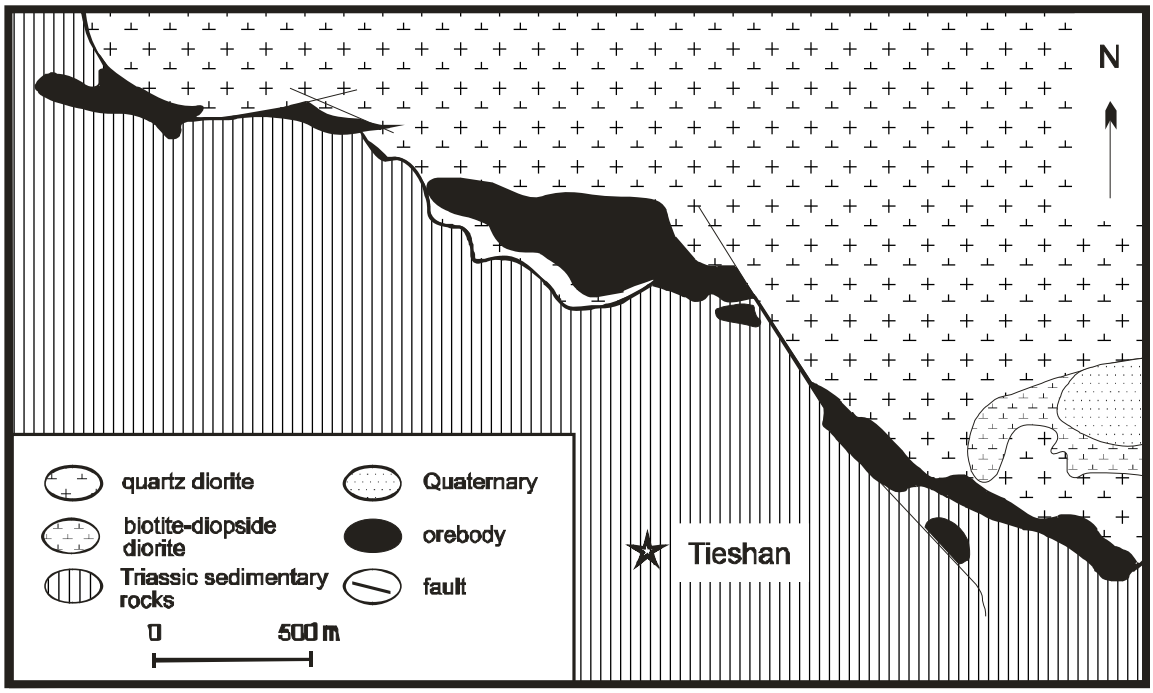

Figure 7.6 Geological map of the Tieshan Fe-Cu skarn deposit at the Edong district, west part of the Middle-Lower Changjiang Metallogenic Belt (after Shu et al., 1992). See Figure 7.1 for the location of Edong district.

There are five types of ore at the Tieshan deposit: 1) Cu-bearing magnetite skarn ores; 2) high-temperature hydrothermal magnetite ores; 3) high- to medium-temperature hydrothermal Cu-bearing magnetite-siderite ores; 4) medium- to low-temperature hydrothermal siderite ores; and 5) supergene Cu-bearing limonite ores. Types 1 and 3 are the most important Fe-Cu ores at the Tieshan deposit (Zhao et al., 1990). The individual orebodies of the Tieshan deposit are mainly lenticular or podiform in shape. Major ore minerals are magnetite, hematite, siderite, pyrite, chalcopyrite, and pyrrhotite.

The intrusive rocks and sedimentary carbonates at the Tieshan deposit have been subjected to extensive hydrothermal alteration, resulting in the

formation of a wide variety of skarn and other alteration assemblages, from internal alkaline alteration (scapolite-albite, microcline) to garnet-diopside-scapolite endoskarn, diopside skarn, grossular-andradite garnet skarn, and wollastonite-grossular-diopside skarn. The internal alkaline alteration is characterized by abundant marialitic scapolite, albite, and microcline. The skarn and alkaline alteration assemblages commonly show systematic zonation. A typical example of skarn zonation occurs at the Shizishan orebody, from the quartz diorite intrusion to marble, and includes diopside-bearing albitized diorite, diopside-scapolite-bearing albitized diorite, garnet-diopside-scapolite endoskarn, and pyroxene-biotite exoskarn that hosts the magnetite-chalcopyrite-siderite mineralization (Zhao et al., 1990). Other styles of hydrothermal alteration at the Tieshan deposit include biotitization, epidotization, actinolitization, carbonatization, chloritization, and kaolinitization, which generally overprint the early skarn and alkaline alteration assemblages.

The alkaline alteration at the Tieshan Fe-Cu skarn deposit is similar to the sodic alteration in the Cordilleran porphyry- and skarn- Cu-Au deposits (Dilles et al., 1995). Stable isotope geochemical studies on the Cordilleran deposits revealed that this sodic alteration occurred synchronously with the potassic alteration and mineralization at relatively high-temperatures, but resulted from the convection of non-magmatic hypersaline formation water in the country rocks (Dilles et al., 1995). Pan and Dong (1999) also proposed that the alkaline alteration at the Tieshan Fe-Cu skarn deposit resulted from

interactions with hypersaline fluids from the Late Paleozoic-Early Mesozoic evaporites.

Seventeen scapolite-bearing samples were collected from different parts of the Tieshan Fe-Cu skarn deposit (Table 7.6). Scapolite separates, hand-picked under a binocular microscope, were analyzed for trace elements including Br by the XRF microprobe and major elements by the electron microprobe. The results are listed in Table 7.7.

All samples of scapolite from the Tieshan Fe-Cu skarn deposit are marialite (Me_{23} to Me_{44}), with 2.0% to 3.7% Cl and 31 ppm to 102 ppm Br. There is a positive correlation between Cl and Br contents in Tieshan scapolite (Figure 7.7). The Cl/Br weight ratios of marialite from the Tieshan deposit cluster around 626±92.

The results from our exchange experiments (K_D=1.1 for Cl/Br or 0.91 for Br/Cl; Table 6.2) have shown that the Cl/Br values in scapolite-group minerals closely reflect those of its coexisting melts/fluids. Therefore, the Cl/Br values of scapolite-group minerals from the skarn deposits are useful in providing constraints on the compositions and sources of ore-forming fluids. For example, the Cl/Br values of marialite in the Tieshan deposit are considerably higher than that of seawater (280 to 294; Valyashko, 1956; You et al., 1994). Possibly the fluid with higher Cl/Br values is originated from the dissolution of halite and sylvite (Figure 2.1 and Figure 7.7), providing further support for a genetic model of this deposit involving marine evaporites in surrounding rocks (Pan and Dong, 1999).

Table 7.6 Description of scapolite-bearing samples from skarn deposits

Sample No.	Location	Description	References
99-1-3	Tieshan, Daye, Hubei, China	Endoskarn	
99-1-5	Tieshan, Daye, Hubei, China	Endoskarn	
99-1-9	Tieshan, Daye, Hubei, China	Scp-Cpx endoskarn	
99-1-12	Tieshan, Daye, Hubei, China	Scp endoskarn	
99-1-14	Tieshan, Daye, Hubei, China	Scp-Phl-Cpx-Mt endoskarn	
99-1-16	Tieshan, Daye, Hubei, China	Scp-Phl-Cpx endoskarn	
99-1-17	Tieshan, Daye, Hubei, China	Scp-Phl-Cpx-Grt endoskarn	
99-1-19	Tieshan, Daye, Hubei, China	Scp-Grt-Cpx endoskarn	
99-1-20	Tieshan, Daye, Hubei, China	Scp-Cpx endoskarn	
99-1-22	Tieshan, Daye, Hubei, China	Scp-Cpx endoskarn	
401-9	Nickel Plate, BC, Canada	Endoskarn	Pan et al., 1994
401-12	Nickel Plate, BC, Canada	Endoskarn	Pan et al., 1994
263-13	Nickel Plate, BC, Canada	Exoskarn	Pan et al., 1994
73-1-8	Nickel Plate, BC, Canada	Exoskarn	Pan et al., 1994
HD55	Nickel Plate, BC, Canada	Vuggy cavity, Copperfield breccia	Pan et al., 1994
DL-22B	Clark fluorite pegmatite/skarrn, Grenville, Canada	Fl-Cpx-Scp-Kfs skarn near pegmatite	Lentz, 1992
DL-26A	McDonald feldspar pegmatite, Grenville, Canada	Phl-Cpx-Scp-Cc skarn near pegmatite	Lentz, 1992
DL-28A	Quirk U pegmatite/skarn, Grenville, Canada	Cpx-Scp skarn near pegmatite	Lentz, 1992
DL-30A	Cardiff North Zone U skarn, Grenville, Canada	Cpx-ScpPhl-Cc skarn	Lentz, 1992
DL-45D	Belanger's Corner Zone, Grenville, Canada	Phl-Scp-Cpx skarn	Lentz, 1992
DL-60A	Matte apatite-U vein, Grenville, Canada	Cpx-Fl-Fap-Cc vein (Scp-Cpx margin)	Lentz, 1992
DL-60G	Matte apatite-U vein, Grenville, Canada	Cpx-Fl-Fap-Cc vein (Scp-Cpx margin)	Lentz, 1992
DL-61A	Camp pegmatite/skarn/vein, Grenville, Canada	Phl-Tr-Scp skarn near pegmatite	Lentz, 1992
DL-62C	Thorianite skarn, Grenville, Canada	Cpx-Phl-Cc skarn	Lentz, 1992
DL-66H	Calumet U skan/vein, Grenville, Canada	Py-Phl-Cc-Scp-Cpx skarn near dyke	Lentz, 1992
DL-70K	Litchfield Mo skarn/vein, Grenville, Canada	Ttn-Phl-Scp-Cc skarn vein	Lentz, 1992
DL-70N	Litchfield Mo skarn/vein, Grenville, Canada	Phl-Scp-Cc skarn	Lentz, 1992

Mineral abbreviations: Cc calcite, Cpx clinopyroxene, FAp fluorapatite, Grt garnet, Kfs K-feldspar, Phl phlogopite, Py pyrite, Scp scapolite, Tr tremolite, and Ttn titanit

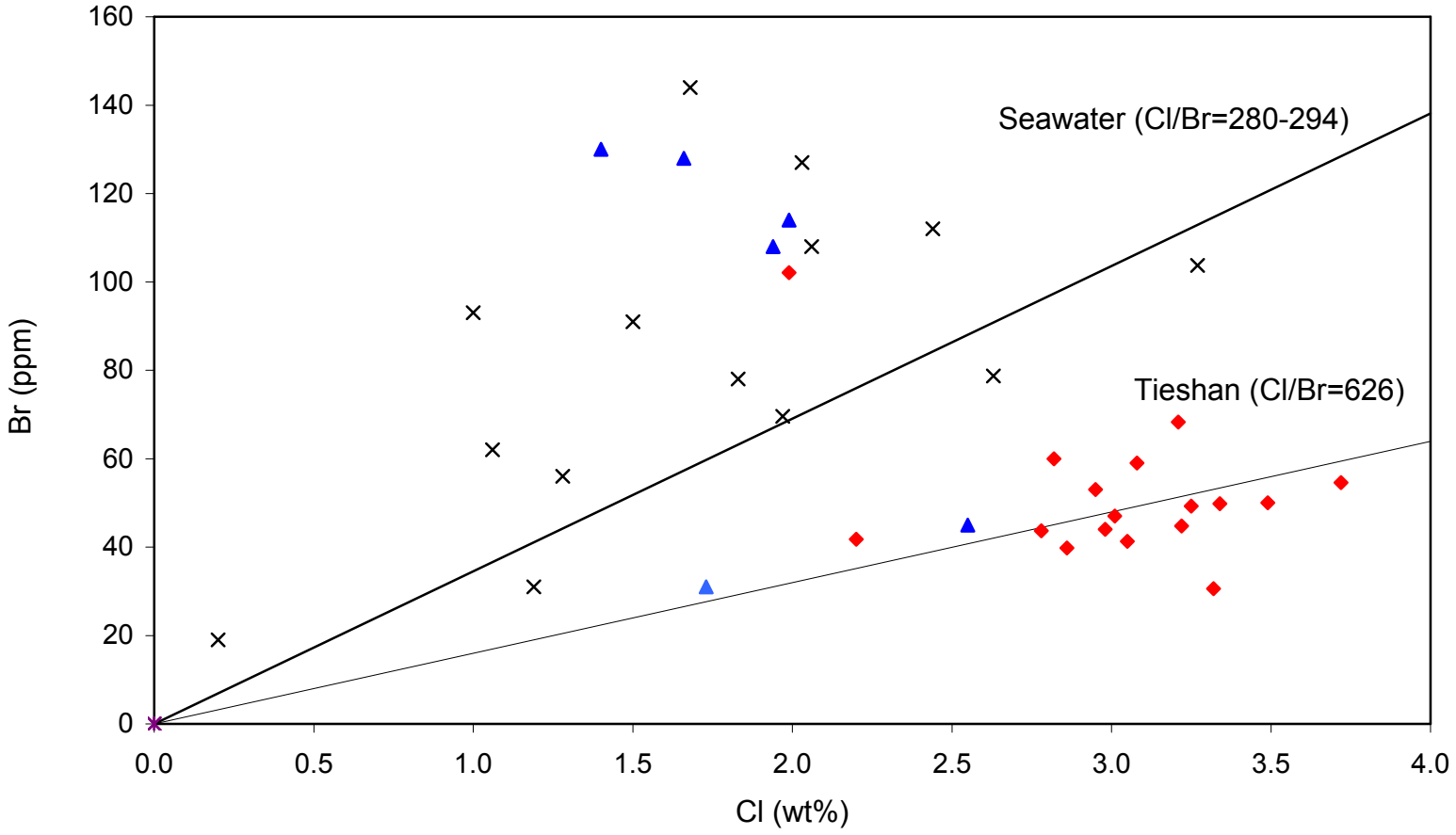

Figure 7.7 Br (ppm) vs Cl (wt%) compositions in scapolite from Tieshan (diamond), Grenville (cross), and Nickel Plate (triangle) deposits. See Table 7.7 for details.

Table 7.7 EMPA compositions of scapolite-group minerals from the Tieshan Fe-Cu deposit, Grenville U-Th-Mo-REE deposits, and Nickel Plate Au skarn deposit (wt%)

Sample No.	Location	SiO_2	Al_2O_3	FeO[a]	MnO	CaO	SrO	BaO	Na_2O	K_2O	SO_3	Cl	CO_2[b]	Br[c] (ppm)	Cl/Br	O=Cl	Total
99-1-3	Tieshan, China	54.54	23.80	0.16	0.00	8.76	0.13	0.03	8.21	0.83	0.49	2.78	1.312	44(9)	636	0.63	100.4
99-1-5	Tieshan, China	56.86	22.96	0.11	0.00	6.77	0.21	0.01	9.18	0.74	0.30	3.21	0.967	68(16)	470	0.72	100.6
99-1-6	Tieshan, China	58.08	22.67	0.13	0.00	5.58	0.12	0.04	9.92	0.76	0.27	3.34	0.882	50(12)	671	0.75	101.0
99-1-7	Tieshan, China	57.53	22.71	0.11	0.01	6.51	0.15	0.00	9.11	0.71	0.32	3.25	0.932	49(10)	659	0.73	100.6
99-1-9	Tieshan, China	52.44	24.49	0.09	0.02	10.92	0.07	0.02	7.06	0.74	0.51	2.20	1.954	42(3)	526	0.50	100.0
99-1-12	Tieshan, China	54.98	23.52	0.12	0.01	8.35	0.15	0.01	8.57	0.82	0.41	2.86	1.272	40(0)	719	0.64	100.4
99-1-13	Tieshan, China	56.94	23.18	0.12	0.02	7.23	0.14	0.05	9.13	0.80	0.27	3.22	0.993	45(5)	719	0.72	101.4
99-1-14	Tieshan, China	54.85	23.66	0.12	0.00	8.48	0.13	0.01	8.32	0.63	0.40	2.82	1.324	60(40)	470	0.63	100.1
99-1-15	Tieshan, China	55.59	23.74	0.15	0.00	8.06	0.13	0.01	8.63	0.66	0.59	3.05	0.984	41(9)	738	0.69	100.9
99-1-16	Tieshan, China	58.57	22.61	0.18	0.01	5.58	0.09	0.01	9.66	1.08	0.35	3.72	0.393	55(2)	681	0.84	101.4
99-1-17	Tieshan, China	57.78	22.83	0.14	0.01	6.30	0.13	0.02	9.70	0.78	0.26	3.49	0.687	50(9)	698	0.79	101.3
99-1-19	Tieshan, China	56.00	23.64	0.31	0.02	7.88	0.15	0.04	8.63	0.77	0.36	2.95	1.249	53(10)	557	0.66	101.3
99-1-20.	Tieshan, China	55.35	23.41	0.14	0.01	7.92	0.10	0.02	8.71	0.81	0.31	3.01	1.155	47(8)	640	0.68	100.3
99-1-21	Tieshan, China	55.68	23.26	0.10	0.02	7.87	0.12	0.01	8.66	0.75	0.34	2.98	1.174	44(14)	677	0.67	100.3
99-1-22	Tieshan, China	56.20	23.03	0.13	0.00	7.12	0.18	0.04	9.01	0.90	0.30	3.08	1.090	59(35)	522	0.69	100.4
S88-DL-22B	Grenville, Canada	52.69	24.41	0.09	0.01	11.07	0.12	0.02	6.87	1.08	0.18	2.06	2.316	108(11)	191	0.46	100.5
S88-DL-26A	Grenville, Canada	50.67	24.62	0.05	0.01	12.86	0.16	0.00	6.00	0.44	1.51	1.19	2.556	31(3)	384	0.27	99.8
S88-DL-28A	Grenville, Canada	51.10	24.89	0.06	0.02	12.00	0.16	0.05	6.31	0.94	1.15	1.68	2.187	144(15)	117	0.38	100.2
S88-DL-30A	Grenville, Canada	53.68	24.16	0.07	0.01	9.14	0.23	0.03	6.58	0.74	0.81	1.76	2.374	5(3)	3520	0.40	99.2
S88-DL-45D	Grenville, Canada	58.85	22.46	0.06	0.02	6.69	0.03	0.02	8.85	1.02	0.01	3.27	1.533	104(13)	315	0.74	102.1
S88-DL-60A	Grenville, Canada	52.39	24.24	0.08	0.01	11.30	0.25	0.00	6.68	1.01	1.07	1.83	2.089	78	235	0.41	100.5
S88-DL-60G	Grenville, Canada	53.48	24.11	0.09	0.02	10.63	0.26	0.06	6.85	0.98	1.11	1.97	1.947	70	283	0.44	101.1
S88-DL-61A	Grenville, Canada	43.16	29.32	0.02	0.01	19.05	0.39	0.01	2.40	0.07	1.78	0.20	3.506	19(13)	105	0.05	99.9

Sample No.	Location	SiO_2	Al_2O_3	FeO[a]	MnO	CaO	SrO	BaO	Na_2O	K_2O	SO_3	Cl	CO_2[b]	Br[c] (ppm)	Cl/Br	O=Cl	Total
S88-DL-62C	Grenville, Canada	50.61	25.05	0.03	0.01	12.70	0.29	0.03	6.00	0.58	1.12	1.50	2.411	91(13)	165	0.34	100.0
S88-DL-66E	Grenville, Canada	57.35	23.30	0.08	0.01	7.98	0.23	0.02	8.64	0.71	0.70	2.63	1.529	79(3)	334	0.59	102.6
S88-DL-66H	Grenville, Canada	54.56	23.11	0.35	0.02	8.67	0.21	0.02	7.87	1.00	0.53	2.44	1.670	112	218	0.55	99.9
S88-DL-70M	Grenville, Canada	48.43	26.05	0.06	0.00	14.49	0.29	0.01	4.77	0.65	1.55	1.06	2.658	62(8)	171	0.24	99.8
S88-DL-70K	Grenville, Canada	49.91	25.35	0.06	0.01	13.58	0.18	0.03	5.45	0.67	1.52	1.28	2.450	56	229	0.29	100.2
S88-DL-70K	Grenville, Canada	52.53	24.43	0.06	0	10.81	0.25	0	7.07	0.82	1.03	2.03	1.878	127	160	0.46	100.5
S88-DL-70N	Grenville, Canada	47.89	26.05	0.04	0.02	14.85	0.24	0.00	4.68	0.70	1.68	1.00	2.630	93(1)	108	0.23	99.6
HD-55	Nickel Plate, Canada	50.42	24.88	0.08	0.01	12.83	0.06	0.02	5.76	0.84	0.02	1.66	2.788	128(10)	130	0.37	99.0
GR-91-130	Nickel Plate, Canada	49.50	25.50	0.13	0.02	13.83	0.01	0	5.18	0.71	0.01	1.40	3.108	138(4)	101	0.32	99.1
401-9	Nickel Plate, Canada	52.60	23.80	0.15		11.60	0.07		6.68	0.82	0.02	1.99	2.460	114	175	0.45	99.7
401-12	Nickel Plate, Canada	52.40	24.00	0.18		11.60	0.04		6.63	0.78	0.02	1.94	2.530	108	180	0.44	99.7
263-12	Nickel Plate, Canada	50.80	26.00	0.15		12.10	0.01		6.2	1.14	0	1.73	2.800	31	558	0.39	100.6
73-1-8	Nickel Plate, Canada	53.50	24.50	0.06		9.60	0.04		8.2	0.85	0.02	2.55	1.850	45	567	0.58	100.6

a: total iron as FeO; b:calculated on the basis of stoichiometry; c:Br from XRF in ppm, one standard deviation in parentheses.

7.2.2 Scapolite from the Nickel Plate Gold Skarn Deposit, British Columbia

The Nickel Plate gold skarn deposit, Hedley district, about 240 km east of Vancouver, B.C., is one of the largest gold skarn deposits in Canada. The Hedley district is within the Quesnel terrain of the Intermontane belt, in the southern part of the Canadian Cordillera. The Intermontane belt is a collage of different terrains, bounded by faults. Lower Paleozoic to Jurassic marine volcanic and sedimentary rocks and comagmatic intrusive rocks deposited in an island-arc or marginal basin setting (Wheeler et al., 1991; Ettlinger et al., 1992).

The Quesnel terrain is mainly composed of arc-related marine volcanic and sedimentary rocks of the Upper Triassic to Lower Jurassic Nicola Group, the host of several porphyry Cu-Mo and Cu-Ag-Au deposits as well as gold skarn deposits in the Hedley district (Preto, 1977; Mortimer, 1986; Ettlinger et al., 1992 and references herein). The Nicola Group includes the Whistle Formation on the top, underlain by four sedimentary formations: French Mine, Hedley, Chuchuwayha, and Stemwinder formations, with the Oregon Claims Formation at the base.

The Whistle Formation is a thick, widely developed unit of alkalic to subalkalic tuffs and tuffaceous sedimentary rocks. The French Mine Formation is distributed in the east and composed of thin-bedded, shallow-marine, limestone dominant sedimentary rocks. In the central part of this area is the Hedley and Chuchuwayha formations of thicker, siltstone-dominant

sedimentary rocks. The Stemwinder Formation of thick, deep-marine, argillite-dominant sedimentary rocks is in the west. These sedimentary facies are separated from one another by major, long-lived synsedimentation growth faults. The Oregon Claims Formation is a poorly documented sequence of mafic tuff with minor limestone, volcanic flows, and chert pebble conglomerate (Ettlinger et al., 1992 and references therein).

The sedimentary facies have an important stratigraphic and lithological control on skarn distribution in this district. All gold skarns (e.g., the Nickel Plate, French, and Good Hope gold skarns) are hosted by the shallow-marine, carbonate-rich Hedley and French Mine formations (Ettlinger et al., 1992 and references herein).

There are several episodes of magmatism in the Hedley district and the oldest one formed the Hedley intrusions of diorite to gabbro that are associated with the regional gold skarn mineralization. Other intrusive rocks include the granodioritic Bromley Batholith and Mount Riordan stock, the granodioritic to quartz monzonitic Lookout Ridge and Cahill Creek plutons, and the youngest granitoid Verde Creek stock (Ettlinger et al., 1992 and references herein).

The Hedley intrusions exist throughout the Hedley district and include stocks (>1km in diameter) and swarms of dikes and sills (up to 200 m thick. Billingsley and Hume, 1941; Ettlinger et al., 1992 and references herein). The stocks are generally equigranular granodiorite, quartz diorite, diorite, or gabbro. The dikes and sills are porphyritic quartz diorite to diorite with minor gabbro.

The gold skarn mineralization is commonly associated with dikes and sills (Ettlinger et al., 1992 and references herein).

The Nickel Plate orebodies are hosted by the strongly altered, thinly bedded, west-dipping calcareous and tuffaceous siltstones and limestones of the Hedley Formation intruded by a swarm of semiconformable dioritic sills and dikes (Billingsley and Hume, 1941; Ettlinger et al., 1992). The exoskarn is more intense than the endoskarn and overprints a thick sequence of siltstones and limestones of the Hedley Formation, locally extending up into the overlying Copper-field breccia, a limestone-boulder-bearing unit (Ettlinger et al., 1992; Pan and Fleet, 1994).

The skarn at Nickel Plate is usually strongly banded with coarser garnet-bearing bands corresponding to the original carbonate-rich layers and pyroxene-rich bands after the clastic-rich layers (Ettlinger et al., 1992). The typical ore-grade skarn is dark green, fine-grained, hedenbergitic pyroxene with arsenopyrite. Other minerals in the skarn are quartz, calcite, K-feldspar, apatite, plagioclase, titanite, pyrrhotite, pyrite, and ilmenite (Ettlinger et al., 1992). The skarn envelope surrounding the Nickel Plate deposit encompasses an area of 4 km^2 and is up to 300 meters thick (Ray et al., 1988; Ettlinger et al., 1992).

In the Nickel Plate gold skarn deposit, scapolite is ubiquitous although with variable quantities. It is an alteration product of plagioclase phenocrysts in the sills and dikes. It is also present in the ore zone exoskarns with gold-sulphide mineralization, and in marble even beyond the outer limits of the skarn

envelope. The most abundant scapolite is found in the ore-zone exoskarn, within and adjacent to the sulphide-gold orebodies, as discrete grains in veins and interstitial of garnet and clinopyroxene (Ettlinger et al., 1992; Pan and Fleet, 1994). Scapolite in the porphyry sills is reported to be Na-rich (marialite73-meionite27; Dolmage and Brown, 1945), whereas scapolite from the marble underlying the ore zone is more calcic (Ettlinger et al., 1992).

The main stage of gold mineralization is associated with coarse-grained scapolite and arsenopyrite. There is up to 10-20 vol% of scapolite in individual specimens from the gold-bearing skarn and the scapolite occurs as coarse anhedral masses in exoskarn and finer grained replacement of igneous plagioclase phenocrysts and groundmass in the endoskarn (Ettlinger et al., 1992; Pan and Fleet, 1994).

The presence of chlorine-rich minerals, such as amphiboles, chlorite, and chlorine-rich scapolite, in some gold skarn deposits indicates the importance of chloride complexes in the transportation and precipitation of gold in some skarn-formation hydrothermal systems. Ettlinger et al. (1992) suggested that the presence of abundant scapolite may be an indicator of the potential of a gold skarn deposit.

There is a wider range of EqAn (31-52 mol%) and Cl contents (1.7 to 2.9 wt%) for scapolite in the exoskarn compared to 40-51 mol% of EqAn and 1.8 to 2.6 wt% Cl for scapolite in the endoskarn. The EqAn and Cl content are correlated to the An content of coexisting plagioclase (Pan and Fleet, 1994).

Results of combined EMPA and XRF microprobe analyses of scapolite-

group minerals from the Nickel Plate are listed in Table 7.7. The Nickel Plate scapolite minerals are chemically between the marialite and meionite with similar Me from 40 to 58.

The Cl/Br weight ratios of scapolite-group minerals from the Nickel Plate deposit are highly variable from 108 to 567 (Table 7.7; Figure 7.7). In particular, the Cl/Br values increase from endoskarn (170 to 180) to exoskarn (558 to 567), whereas the marialite crystals in the vuggy cavity of the Copperfield breccia have a Cl/Br value of 130 (Table 7.7).

Also, the Cl/Br values of scapolite-group minerals in the exoskarns of the Nickel Plate deposit are higher than that of seawater and close to those of the scapolites from the Tieshan deposit. It may indicate a similar origin of the hydrothermal fluid in Nickel Plate to the Tieshan, from the dissolution of surrounding evaporites. The increase in Cl/Br from endoskarn to exoskarn is readily attributable to an increased involvement of magmatic water in the former.

7.2.3 Scapolite from the Grenvillian U, Th, Mo, and REE Deposits, Canada

There are numerous U, Th, Mo, and REE deposits hosted in spatially, temporally, mineralogically, and geochemically related granitic pegmatites, skarns, and vein-dykes in the Central Metasedimentary Belt of the Grenville Province, Ontario and Quebec (Lentz, 1992, 1998).

The U-, Mo-, and REE-bearing granitic pegmatites are the results of

partial melting and fractional crystallization of the late-tectonic granitic plutons or the emplacement of mid-crustal anatectic melts of pegmatites (Lentz, 1992 and references herein). The pegmatites occur as dykes that cut all rocks, except the late diabase dikes. Mineralogically there are two kinds of pegmatites, simple pegmatites composed of quartz and feldspar, and complex pegmatites made up of biotite, clinopyroxene, hornblende, magnetite, pyrite, and numerous rare minerals. The mineralization of U, Th, Mo, and REE is related to the complex pegmatites (Lentz, 1992).

Scapolite-bearing skarns are usually hosted by marbles, clinopyroxenites, and amphibolites. The endoskarns are within the pegmatites and composed of Ca-pyroxene, scapolite, andradite, and titanite. The exoskarns are primary skarns characterized by a mineralogical zonation from proximal to distal: diopside or diopside-phlogopite to diopside-tremolite-phlogopite-calcite, then to tremolite-phlogopite-calcite-dolomite, and finally to the graphite-norbergite-phlogopite-calcite-dolomite marble. The mineralogy of skarns is dependent on the chemical composition of their host rocks.

The calcite-rich vein-dykes represent the distal parts of the primary skarns, and are composed of variable proportions of fluorite, apatite, silicates, sulphides, and magnetite (Lentz, 1992).

Although mineralogically and geochemically similar to each other, there is a progressive evolution from pegmatite to skarn with considerable overlap for both the major and trace elements, and the composition of the calcite-rich vein-dykes is intermediate between the proximal skarns and pegmatites (Lentz,

1992).

The granitic pegmatites probably originated from *in situ* crustal anatexis, or from partial melting and fractional crystallization of a partial melt derived at depth, or from association of granite-pegmatite, or from hydrothermal replacement. The skarns have a late metamorphic-hydrothermal origin or a late magmatic-hydrothermal origin. The calcite-rich vein-dykes are thought to be igneous carbonatite, magmatic pegmatitic-hydrothermal veins (Lentz, 1992 and references herein).

The separation of a silicate (Si, Al, Fe)-, rare metal (Ti, U, Th, Mo, REE, Nb)- and halogen (F, Cl)-rich magmatic volatile phase from the pegmatite melt is thought to be responsible for metasomatism in the dolomitic marbles, which lead to the formation of skarns. Modification of the hydrothermal fluids after metasomatism (processes of skarn formation) results in the formation of calcite-rich vein-dykes (Lentz, 1998).

The U, Th, Mo, and REE mineralization in the Grenville Province has been interpreted to be syngenetic or originated from a metamorphic-hydrothermal fluid (Karvinen, 1971; Masson and Gordon, 1981; Haynes, 1986) or has a magmatic-metasomatic origin (Lentz, 1989; 1998).

Scapolite occurs commonly in many of the gneisses, marbles, pegmatites, skarns and veins in the Grenville Province. It has been observed to replace pre-existing feldspars (K-feldspar and plagioclase). Scapolitization within the marginal skarns may happen as either deposition of scapolite directly from fluids and/or replacement of pre-existing feldspars.

Twelve scapolite separates from different localities within the Grenville Province, supplied by Dr. D.R. Lentz, have been analyzed for major elements by EMPA and Br by XRF microprobe. The sample description and analytical results are listed in Table 7.6 and Table 7.7, respectively. The Grenvillian scapolite separates are chemically variable, with the Me from 30 to 81.

Scapolite-group minerals in the Grenvillian deposits have a range of Cl/Br from 80 to 384 (Table 7.7). The wide variation in Cl/Br in Grenvillian scapolite (Figure 7.7) is consistent with varying degrees of mixing of hydrothermal fluids derived from magmatic sources and from associated sedimentary rocks (Lentz 1992, 1998).

7.2.4 Discussion

Bromine in scapolite-group minerals of these skarn deposits varies widely from 5 ppm in a sample of meionite (Me_{81}) to 144 ppm in marialite (Me_{49}; Table 7.7). The relatively small standard deviations of most samples indicate that Br in scapolite-group minerals is homogeneous in its distribution. However, marialite from sample DL-70K has two populations of different Br and Cl contents (Table 7.7). It is noteworthy that their Cl/Br values are similar (157 and 177). Bromine is positively correlated to the chlorine in scapolite group minerals (Figure 7.7).

The results of the Br-Cl distribution coefficient from our exchange experiments (K_D=0.85-0.97 for Br compared to Cl; Table 6.2) have shown that the Cl/Br values in scapolite-group minerals closely reflect those of its

coexisting melts/fluids. Therefore, the Cl/Br values of scapolite-group minerals from skarn deposits are useful in providing constraints on the compositions and sources of ore-forming fluids.

The Cl/Br systematics from fluid inclusions has been widely applied in constraining the sources and evolution of hydrothermal fluids in a variety of mineral deposits (e.g., Kesler et al. 1995). The present study shows that the Cl/Br values in Cl-rich minerals are also useful tracers for the compositions and sources of ore-forming fluids, provided that the distribution coefficients of Cl and Br between minerals and coexisting melts or fluids are known. In this respect, scapolite-group minerals and sodalite are special cases in that their Cl/Br values can be used directly as tracers for the sources and evolution of hydrothermal fluids, because their K_D values are close to unity.

In summary, it has been confirmed that the experimentally determined partition coefficients of halogens between minerals (apatites, scapolites, and sodalites) and fluids/melts of this study have wide applications in the interpretation of the source and evolution of hydrothermal fluids/melts in mineralization processes and other geological systems.

8. Conclusions

Compared to complicated geological processes, all experimental studies on elemental partitioning were carried out in simplified systems. The partition coefficients measured in simple model systems may be different from those in the natural systems. However, the various factors that affect the partitioning of elements, such as halogens, do likely function in a similar way, and the relative fractionation of F, Cl, Br, and I obtained from simplified experimental systems probably can be directly applied to natural systems (Bureau et al., 2000).

Like all other experimental studies, the partitioning experiments in this thesis research have been carried out in simplified systems, for example the halogenide-rich melt-apatite system and hydrous halide-rich melt-scapolite/sodalite systems. The partition coefficients constrained from those simplified systems may not be identical to those in natural systems. However, they may be systematically shifted from the real values, and the relative fractionation should be very close to those in the geological systems.

The present study is the first series of experiments systematically investigating the partitioning of Br between apatite/scapolite/sodalite and fluids/melts. The experimental results are then evaluated on the basis of applications to a series of mineral deposits.

Twenty-nine experiments were undertaken to study the partitioning of halogen elements between fluorapatite/chlorapatite and halogenide-rich melts at 1120 ^{o}C to 1400 ^{o}C and atmospheric pressure. Experimental results demonstrate that the F/Cl ratio in the melt/fluid is the main factor to control the crystalization of chlorapatite or fluorapatite. There is a strong tendency to form fluorapatite rather than chlorapatite at similar F or Cl concentration in the melt**,** which is consistent with the common occurrence of fluorapatite in natural environments. There is about a 0.22 molar fraction of fluorapatite ($X^{*}_{F\text{-}Ap}$) in apatite crystallized from a melt with only 0.05 molar F (X^{*}_{F}) in the melt (Table 5.1; dp-ap-36a). In comparison, there is only about 0.006 mole of the chlorapatite component ($X^{*}_{Cl\text{-}Ap}$) in apatite crystallized from a melt with a similar Cl concentration (Table 5.1; dp-ap-30b). If the X^{*}_{F} value in the melt is higher than 0.8, the resulting apatite is almost the end-member of fluorapatite with 0.996 $X^{*}_{F\text{-}Ap}$.

Partition coefficients for each halogen element (F, Cl, and Br) between chlorapatite/fluorapatite and melts are summarized in Table 8.1. These experimentally determined partition coefficients between apatites and melts fit the Brice curve (Figure 5.13) and the values of D* (F, Cl, and Br) are dependent on their respective ionic radii. The predicted partition coefficients for iodine (D^{*}_{I}) for fluorapatite/melt and chlorapatite/melt are 0.000459 and 0.0277, respectively. The predicted D^{*}_{OH} values for fluorapatite/melt and chlorapatite/melt are 0.0135 and 0.551, respectively.

Table 8.1 Partition coefficients of halogens between apatite and melt

Partition Coefficient					System
D^*_F	3.59(64) at 1120°C	to	4.13(22) at 1330°C		Chlorapatite-melt
D^*_F	1.05(4) at 1220 °C	to	1.07	at 1400 °C	Fluorapatite-melt
D^*_{Cl}	1.07(1) at 1120 °C	to	0.83	at 1330 °C	Chlorapatite-melt
D^*_{Cl}	0.127(2) at 1250 °C	to	0.115	at 1400 °C	Fluorapatite-melt
D^*_{Br}	0.32(9) at 1120 °C	to	0.42(5)	at 1330 °C	Chlorapatite-melt
D^*_{Br}	0.020(3) at 1220 °C	to	0.016	at 1400 °C	Fluorapatite-melt

The partition coefficients of halogens between apatites and melts are temperature dependent. Higher temperature favors the formation of fluorapatite and also causes more bromine to replace chlorine in chlorapatite, whereas lower temperature favors the formation of chlorapatite (Figure 5.11).

Three exchange experiments have been executed to determine the distribution coefficients of Br between scapolite and coexisting hydrous halide-rich melts. The D^*_{Cl} values are 1.011 to 1.035 and the D^*_{Br} values are 0.88 to 0.98 between scapolite and melts. Although the D^*_{Cl} values are very close to the D^*_{Br}, there is still a weak tendency of fractionation between Br and Cl, with a Br-Cl distribution coefficients from 0.85 to 0.97.

Four exchange experiments were carried out to investigate the distribution of Br between sodalite and coexisting hydrous halide-rich melts. The D^*_{Cl} values vary from 0.900 to 0.995 and the D^*_{Br} values are 1.018 to 1.177. The Br-Cl distribution coefficients range from 1.023 to 1.308.

These experimental results have been applied to selected geological systems. The halogen compositions of 22 fluorapatite samples from the Aoshan fluorapatite-magnetite deposit, 2 fluorapatite separates from Chinese

mantle xenoliths, and 5 fluorapatite separates from the Oka carbonatite complex have been analyzed by XRF for Br and EMPA for Cl and F. Aoshan fluorapatite is Cl-bearing with 0.38 to 0.98 wt% Cl and 1.83 to 3.45 wt% F. Trace to 52 ppm bromine were detected in Aoshan fluorapatite. Fluorapatite from Chinese mantle xenoliths has similar halogen composition to the Aoshan fluorapatite. Oka fluorapatite contains trace chlorine (up to 0.05 wt% Cl). High bromine contents (9 to 57 ppm) have been detected in the Oka fluorapatite only with trace amount of chlorine. These results, when interpreted on the basis of experimentally determined partition coefficients, suggest that the Oka fluorapatite crystallized from highly Br-enriched melt/fluid and that the Aoshan deposit is consistent with a magmatic fluid of mantle origin

Seventeen scapolite-bearing samples from the Tieshan Fe-Cu skarn deposit, five scapolite-bearing samples from the Nickel Plate gold deposit, and fourteen separates of scapolite from Grenville pegmatite/skarn/vein-dykes deposits, were analyzed for Br by XRF and Cl as well as other major elements by EMPA. Bromine in scapolite-group minerals varies widely from 25 ppm to 144 ppm and is positively correlated to Cl. The Cl/Br weight ratios of marialitic scapolite from the Tieshan deposit cluster around 626±92, whereas those of scapolite-group minerals from the Nickel Plate and Grenville deposits are more variable. In particular, the Cl/Br values of scapolite-group minerals in the Nickel Plate deposit increase from endoskarn (170 to 180) to exoskarn (558 to 567). Scapolite-group minerals in the Grenville deposits have a range of Cl/Br values from 80 to 384.

The Cl/Br values of marialitic scapolite in the Tieshan deposit are considerably higher than that of sea water (280 to 294; Valyashko, 1956; You et al., 1994). It is possible that the Tieshan hydrothermal fluid originated from dissolution of halite and sylvite in the surrounding marine evaporites. Similar Cl/Br values of scapolite-group minerals in the exoskarns of the Nickel Plate deposit may indicate a similar origin. The increase in Cl/Br from endoskarn to exoskarn is readily attributable to an increased involvement of magmatic water in the former. Similarly, the wide variation in Cl/Br in scapolite-group minerals from the Grenvillian deposits is consistent with varying degrees of mixing of hydrothermal fluids derived from magmatic sources and from associated sedimentary rocks.

In summary, this is the first systematic experimental investigation of partitioning of Br between apatite/scapolite/sodalite and fluids/melts. Experimental results show that the partitioning of halogens between fluorapatite and melt is different from that between chlorapatite and melt and that the partition coefficients of halogens between apatites and melts are temperature dependent**.** The results of exchange experiments demonstrate that the Cl/Br values in marialitic scapolite and sodalite closely reflect the halogen compositions of their coexisting melts or fluids. The significance of those experimentally determined partition coefficients has been confirmed by their applications to selected mineral deposits and other geological systems.

It is not clear how the F, Cl, and Br partitioning changes from fluorapatite-style to chlorapatite-style. More experiments with F/(Cl+Br+F)

molar ratios in the melt between 0.17 and 0.80 and Cl/(Cl+Br+F) molar ratios between 0.085 and 0.815 are required to resolve the transitions. Partitioning experiments at lower temperatures are also suggested.

References

Anfilogov, V.N., Bushlyakov, I.N., and Bragina, G.I., 1977. Distribution of fluorine between coexisting biotite and amphibole and granitic melt at 780 ^{o}C and 1000 atm pressure. Geochemistry International 14, 95-98.

Aitken, B.G., 1983. T-X_{CO2} stability relations and phase equilibria of a calcic carbonate scapolite. Geochimica et Cosmochimica Acta 47, 351-362.

Anders, E. and Grevesse, N., 1989. Abundances of elements: meteoritic and solar. Geochimica et Cosmochimica Acta 53, 197-214.

Appel, P.W.U., 1997. High bromine contents and low Cl/Br ratios in hydrothermally altered Archaean komatiitic rocks, West Greenland. Precambrian Research 82, 177-189.

Argiolas, R. and Baumer, A., 1978. Synthese de chlorapatite par voie hydrothermale: etude de l influence de la sursaturation sur l evolution des facies des cristaux. Canadian Mineralogist 16, 285-290.

Bacso, J., Pazsit, A., and Somogyi, A., 1998. Energy dispersive X-ray fluorescence analysis. In Nuclear Methods in Mineralogy and Geology Techniques and Applications, A. Vertes, S. Nagy and K Suvegh (Editors). Plenum Press, New York, 165-215.

Baker, J. and Newton, R.C., 1994. Standard thermodynamic properties of meionite, $Ca_4Al_6Si_6O_{24}CO_3$, from experimental phase equilibrium data. American Mineralogist 79, 478-484.

Barrer, R.M. and Vaughan, D.E.W., 1971. Trapping of inert gases in sodalite and cancrinite crystals. Journal of Physics and Chemistry of Solids 32, 731-743.

Baumer, A. and Argiolas, R., 1981. Syntheses hydrothermales et determinations RX d apatites chloree, fluoree ou hydroxylee. Neues Jahrbuch fuer Mineralogie, Monatshefte, 344-348.

Beattie, P., Drake, M., Jones, J., Leeman, W., Longhi, J., McKay, G., Nielsen, R., Palme, H., Shaw, D., Takahashi, E., and Watson, B., 1993. Terminology for trace element partitioning. Geochimica et Cosmochimica Acta 57, 1605-1606.

Bell, K. and Blenkinson, J., 1989. Neodymium and strontium isotope geochemistry of carbonatites. In: Carbonatites, Genesis and Evolution, K. Bell (Editor), Unwin Hyman, London, 278-300.

Bernem, I.V., 1970. Hydrothermal fluids in magmatic stage. In: Geochemistry of Hydrothermal Ore Deposits, Moscow: Nauka, 40-74.

Berndt, M.E. and Seyfried, W.E.Jr., 1997. Calibration of Br/Cl fractionation during phase separation of seawater: possible halite at 9º to 10ºN East Pacific Rise. Geochimica et Cosmochimica Acta 61, 2849-2854.

Billingsley, P. and Hume, C.B., 1941. The ore deposits of Nickel Plate Mountain, Hedley, British Columbia. Canadian Institute of Mining and Metallurgy Bulletin 64, 524-590.

Blundy, J.D. and Wood, B.J., 1994. Prediction of crystal-melt partition coefficients from elastic moduli (On the relationship between elastic moduli and mineral-melt partitioning). Nature 372, 452-454.

Blundy, J.D., Wood, B.J., and Davies, A., 1996. Thermodynamics of rare earth element partitioning between clinopyroxene and melt in the system CaO-MgO-Al_2O_3-SiO_2. Geochimica et Cosmochimica Acta, 60, 359-364.

Bohlke, J.K., and Irwin, J.J., 1992. Laser microprobe analyses of Cl, Br, I, and K in fluid inclusions: Implications for sources of salinity in some ancient hydrothermal fluids. Geochimica et Cosmochimica Acta 56, 203-225.

Boiron, M.C., Moissette, A., Cathelineau, M., Banks, D., Monnin, C., and Dubessy, J., 1999. Detailed determination of palaeofluid chemistry: an integrated study of sulphate-volatile rich brines and aquo-carbonic fluids in quartz veins from Ouro Fino (Brazil). Chemical Geology 154, 179-192.

Boneβ, M., Heumann, K.G., and Haack, U., 1991. Cl, Br and I analyses of metamorphic and sedimentary rocks by isotope dilution mass spectrometry. Contributions to Mineralogy and Petrology 107, 94-99.

Brice, J.C., 1975. Some thermodynamic aspects of the growth of strained crystals. Journal of Crystal Growth 28, 249-253.

Brenan, J.M., 1993. Partitioning of fluorine and chlorine between apatite and aqueous fluids at high pressure and temperature: implications for the F and Cl content of high P-T fluids. Earth and Planetary Science Letters 117, 251-263.

Bureau, H., Keppler, H., and Metrich, N., 2000. Volcanic degassing of bromine and iodine: experimental fluid/melt partitioning data and applications to stratospheric chemistry. Earth and Planetary Science Letters 183, 51-60.

Burgess, R., Layzelle, E., Turner, G., and Harris, J.W., 2002. Constraints on the age and halogen composition of mantle fluids in Siberian coated diamonds. Earth and Planetary Science Letters 197, 193-203.

Bushlyakov, I.N., 2000. Estimation of halogen content in granitoid melts. Geochemistry International 38, No. 4, 401-404.

Campbell, A.C. and Edmond, J.M., 1989. Halide systematics of submarine hydrothermal vents. Nature 342, 168-170.

Candela, P.A., 1986. Toward a thermodynamic model for the halogens in magmatic systems: an application to melt-vapor-apatite equilibria. Chemical Geology 57, 289-301.

Cappellen, P.V. and Berner, R.A., 1991. Fluorapatite crystal growth from modified seawater solutions. Geochimica et Cosmochimica Acta 55, 1219-1234.

Carroll, M.R. and Webster, J.D., 1994. Solubilities of sulfur, noble gases, nitrogen, chlorine and fluorine in magmas. Reviews in Mineralogy 30, 231-279.

Chang, Y.F., Liu, X.P. and Wu, Y.C., 1991. The copper-iron belt of the Lower and Middle Reaches of The Changjiang River. Geological Publishing House, Beijing, in Chinese, with English abstract, 379p.

Channer, D.M.DeR., and Spooner, E.T.C., 1994a. Combined gas and ion chromatographic analysis of fluid inclusions: Applications to Archean granite pegmatite and gold-quartz vein fluids. Geochimica et Cosmochimica Acta 58, 1101-1118.

Channer, D.M.DeR., and Spooner, E.T.C., 1994b. Analysis of fluid inclusion leachates from quartz by ion chromatography. Geochimica et Cosmochimica Acta 56, 249-259.

Channer, D.M.DeR., de Ronde, C.E.J., and Spooner, E.T.C., 1997. The Cl^--Br^--I^- composition of ~ 3.23 Ga modified seawater; implications for the geological evolution of ocean halide chemistry. Earth and Planetary Science Letters 150, 325-335.

Cheburkin, A.K., Frei, R., and Shotvk, W., 1997. An energy-dispersive miniprobe multielement analyzer (EMMA) for direct analysis of trace elements and chemical age dating of single mineral grains. chemical Geology 135, 75-87.

Chen N., 2002. Electron paramagnetic resonance spectroscopic study of two gadolinium centres at calcium sites in synthetic fluorapatite. Ph.D. thesis, University of Saskatchewan.

Cherniak, D.J., 2000. Rare earth element diffusion in apatite. Geochimica et Cosmochimica Acta 64, 3871-3885.

Cherniak, D.J. and Ryerson, F.J., 1993. A study of strontium diffusion in apatite using Rutherford backscattering spectroscopy and ion implantation. Geochimica et Cosmochimica Acta 57, 4653-4666.

Conway, C.M. and Taylor, H.P. Jr., 1969. O^{18} / O^{16} and C^{13}/C^{12} ratios of coexisting minerals in the Oka and Magnet Cove carbonatite bodies. Journal of Geology 77, 618-626.

Correns, C.W., 1956. The geochemistry of the halogens. In: Physics and Chemistry of the Earth 1, Ahrens, L.H., Rankama, K., Runcorn, S.K., (Editors). Pergamon, London, 181-233.

Crank, J., 1975. The Mathematics of Diffusion. 2nd Edition, Oxford Univ. Press, London, UK.

Crocetti, C.A. and Holland, H.D., 1989. Sulfur-lead isotope systematics and the composition of fluid inclusions in galena from the Viburnum Trend, Missouri. Economic Geology 84, 2196-2216.

Denbigh, K., 1966. The principles of chemical equilibrium. 4th edition, Cambridge University Press.

Deruelle, B., Dreibus, G., and Jambon, A., 1992. Iodine abundances in oceanic basalts: implications for Earth dynamics. Earth and Planetary Science Letters 108, 217-227.

Dilles, J.H., Farmer, G.L., and Field, C.W., 1995. Sodium-calcium alteration by non-magmatic saline fluids in porphyry copper deposits: results from Yerington, Nevada. In Magmas, Fluids, and Ore Deposits; Thompson, J.F.H. (Editor). Mineralogical Association of Canada Short Course Series 23, 309-338.

Dobson, M.H., 1973. Closure temperature in cooling geochronological and petrological systems. Contributions to Mineralogy and Petrology 40, 259-264.

Dolmage, V. and Brown, C.., 1945. Contact metamorphism at Nickel Plate Mountain, Hedley, British Columbia. Canadian Institute of Mining and Metallurgy Bulletin 48, 27-68.

Dong, P. and Pan, Y., 1998. Yangzi-type Cu-Fe-Au deposits in eastern China; complex exhalative-porphyry-skarn systems. Program with Abstracts - Geological Association of Canada, Mineralogical Association of Canada, Canadian Geophysical Union, Joint Annual Meeting Vol. 23, A47.

Dong, P. and Pan, Y., 2002. F-Cl-Br partitioning in apatite: experimental studies and applications. Program with Abstracts - Geological Association of Canada, Mineralogical Association of Canada Joint Annual Meeting Vol. 27, 29.

Drake, M.J. and Holloway, J.R., 1978. Henry's law behavior of Ni in an olivine/ melt system. Eos 59, 1219-1220.

Drake, M.J. and Weill, D.F., 1975. Partition of Sr, Ba, Ca, Y, Eu (super 2+) , Eu (super 3+) , and other REE between plagioclase feldspar and magmatic liquid; an experimental study. Geochimica et Cosmochimica Acta 39, 689-712.

Ebihara, M., Saito, N., Akaiwa, H., and Tomura, K., 1992. Instrumental and radiochemical neutron activation analysis of trace iodine in geological samples. Analytical Sciences 8, 183-187.

Egan, E.P., Wakefield, Z.T., and Elmore, K.L., 1950. High-temperature heat content of hydroxyapatite. American Chemical Society. Journal 72, 2418-2421.

Egan, E.P., Wakefield, Z.T., and Elmore, K.L., 1951. Low-temperature heat content and entropy of hydroxyapatite. American Chemical Society. Journal 72, 5579-5580

Ellis, D.E., 1978. Stability and phase equilibria of chloride and carbonate bearing scapolites at 750^{o}C and 4000 bar. Geochimica et Cosmochimica Acta 42, 1271-1281.

Ettlinger, A.D. and Ray, G.E., 1988. Gold-enriched skarn deposits of British Columbia. British Columbia Ministry Energy, Mines Petroleum Resources Paper 1988-1, 263-279.

Ettlinger, A.D., Meinert, L., and Ray, G., 1992. Gold skarn mineralization and fluid evolution in the Nickel Plate deposit, British Columbia. Economic Geology 87, 1541-1565.

Eugster, H.P. and Protska, H.J., 1960. Synthetic scapolites. Geological Society of America Bulletin 71, 1859-1860.

Eugster, H.P., Protska, H.J., and Appleman, D.E., 1962. Unit-cell dimensions of natural and synthetic scapolites. Science 137, 853-854.

Fair, G. and Powell, J.L., 1972. Strontium isotope geology. Springer, Berlin.

Fairbairn, H.W., Faure, G., Pinson, W.H., Hurley, P.M., and Powell, J.L., 1963. Initial ratio of strontium 87 to strontium 86, whole-rock age, and discordant biotite in the Monteregian igneous province, Quebec Journal of Geophysical Research 68, 6515-6522.

Fleet, M.E., 1989. Structures of sodium alumino-germanate sodalites [$Na_8(Al_6Ge_6O_{24})A_2$, A=Cl, Br, I]. Acta Crystallographica, C45, P843-847.

Fleet, M.E. and Pan, Y., 1997. Rare earth elements in apatite: Uptake from H_2O-bearing phosphate-fluoride melts and the role of volatile components. Geochimica et Cosmochimica Acta 61, 4745-4760.

Frantz, J.D., Mao, H.K., Zhang, Y-G, Wu, Y., Thompson, A.C., Underwood, J.H., Giauque, R.D., Jones, K.W., and Rivers, M.L., 1988. Analysis of fluid inclusions by X-ray fluorescence using synchrotron radiation. Chemical Geology 69, 235-244.

Fuge, R. and Johnson, C.C., 1986. The geochemistry of iodine- a review. Environmental Geochemistry and Health 8, 31-54.

Gaetani, G.A. and Grove, T.L., 1995. Partitioning of rare earth elements between clinopyroxen and silicate melt: Crystalal-chemical controls. Geochimica et Cosmochimica Acta 59, 1951-1962.

Ganguly, J. and Tirone, M., 1999. Diffusion closure temperature and age of a mineral with arbitrary extent of diffusion: Theoretical formulation and applications. Earth and Planetary Science Letters 170, 131-140.

Garvin, D., Parker, V.B., and White H.J., Jr, 1987. CODATA thermodynamic Tables: selections for some compounds of calcium and related mixtures: A prototype series of Tables.Hemisphere.

Gold, D.P., 1963. The relationship between the limestones and the alkaline igneous rocks of Oka and St. Hilaire, Quebec. Ph.D thesis, McGill University.

Gold, D.P., 1972. The Monteregian Hills: ultra-alkaline rocks and the Oka carbonatite complex. 24th International Geological Congress, Excursion B-11, Guidebook.

Gold, D.P., Vallee, M., and Charette, J.P., 1967. Economic geology and geophysics of the Oka alkaline complex, Quebec. Canadian Institute of Mining and Metallurgy Bulletin 60, 1131-1144.

Goldsmith, J.R. and Newton, R.C., 1977. Scapolite-plagioclase stability relations at high pressures and temperatures in the system $NaAlSi_3O_8$-$CaAl_2Si_2O_8$-$CaCO_3$-$CaSO_4$. American Mineralogist 62, 1063-1081.

Govindaraju, K., 1994. 1994 compilation of working values and sample description for 383 geostandards. Geostandards Newsletter 18, special issue.

Gu, L.X., 1984. Massive sulphide deposits in the continental fault depression troughs, South China. PhD thesis, Nanjing University, Nanjing, China, in Chinese.

Harrison, W.J., 1981. Partition coefficients for REE between garnets and liquids; implications of non-Henry's law behaviour for models of basalt origin and evolution. Geochimica et Cosmochimica Acta 45, 1529-1544.

Harrison, W.J. and Wood, B.J., 1980. An experimental investigation of the partitioning of REE between garnet and liquid with reference to the role of defect equilibria. Contributions to Mineralogy and Petrology 72, 145-155.

Hauri, E.H., Shimizu, N., Dieu, J.J., and Hart, S.R., 1993. Evidence for hotspot-related carbonatite metasomatism in the oceanic upper mantle. Nature 365, 221-227.

Haynes, S.J., 1986. Metallogeny of uranium and thorium, Grenville Supergroup Peterborough County, Ontario. In The Grenville Province, J.M. Moore, A. Davidson, and A.J. Baer (Editors). Geological Association of Canada Special Paper 31, 271-280.

Haynes, F.M. and Kesler, S.E., 1988, Compositions and sources of mineralizing fluids for chimney and manto limestone-replacement ores in Mexico. Economic Geology 83, 1985-1992.

Heumann, K.G., 1988. Isotope dilution mass spectrometry. In: Inorganic Mass Spectrometry, F. Adams, R. Gijbels, and R. van Grieken (Editors). Wiley, New York, 301-376.

Heumann, K.G., Gall, M., and Weiss, H., 1987. Geochemical investigations to explain iodine-over abundances in Antarctic meteorites. Geochimica et Cosmochimica Acta 51, 2241-2547.

Hildebrand, R.S., 1986. Kiruna-type deposits: their origin and relationship to intermediate subvolcanic plutons in the Great Bear Magmatic Zone, Northwest Canada. Economic Geology 81, 640-659.

Hodgson, C.J., Bartes, R.J., and Verzosa, R.S., 1976. Cariboo-Bell. Canadian Institute of Mining and Metallurgy Spec. Vol. 15, 388-396.

Hoover, J.D., 1978. The distribution of samarium and thulium between plagioclase and liquid in the systems An-Di and Ab-An-Di at 1300 degrees C. Year Book - Carnegie Institution of Washington, 77, 703-706.

Huckenholz, H.G. and Seiberl, W., 1988. Stability of meionite ($Ca_4Al_6Si_6O_{24}CO_3$) in the presence of (H_2O-CO_2) fluid. Terra Cognita 8, 66.

Huckenholz, H.G. and Seiberl, W., 1989. Occurrence of carbonate scapolites and their bearing on geothermometry of rocks of (high-temperature) granulite facies. Abstracts of the 28th International Geological Congress 2, 79-80.

Hughes, J.M., Cameron, M., and Crowley, K.D., 1989. Structural variations in natural F, OH, and Cl apatites. American Mineralogist 74, 870-876.

Huheey, J.E., 1978. Inorganic Chemistry. Principles of Structure and Reactivity. New York, Harper and Row.

Ionov, D.A., Griffin, W.L., O'Reilly, S.Y., 1997. Volatile-bearing minerals and lithophile trace elements in the upper mamtle. Chemical Geology 141, 153-184

Irwin, J.J. and Roedder, E., 1995. Diverse origins of fluid in magmatic inclusions at Bingham (Utah, USA), Butte (Montana, USA), St. Austell (Cornwall, UK), and Ascension Island (mid-Atlantic, UK) indicated by laser microprobe anlysis of Cl,K, Br, I, Ba + Te, U, Ar, Kr, and Xe. Geochimica et Cosmochimica Acta 59, 295-312.

Jambon, A., Deruelle, B., Dreibus, G., and Pineau, F., 1995. Chlorine and bromine abundance in MORB: the contrasting behaviour of the Mid-Atlantic Ridge and East Pacific Rice and implications for chlorine geodyamic cycle. Chemical Geology 126, 101-117.

James, E.W. and Henry, C.D., 1993. Pb isotopes of ore deposits in Trans-Pecos Texas and Northeastern Chihuahua, Mexico: basement, igneous, and sedimentary sources of metals. Economic Geology 88, 934-947.

Ji, S.X., Wang, W.B., Xing, W.C., Xue, Y.Y., Yue, W.Z., Wu, H.R., Dai, J.Y., Wei, N.Y. and Zhou, H.M., 1990. The Copper Deposits of Northwestern Jiangxi. Geological Publishing House, Beijing, 167p, in Chinese, with English abstract.

Johnson, L.H., Burgess, R., Turner, G., Milledge, H.J., and Harris, J.W., 2000. Noble gas and halogen chemistry of mantle fluids: comparison of African and Canadian diamonds. Geochimica et Cosmochimica Acta 64, 717-732.

Jones, J.H., 1995. Experimental trace element partitioning. In: Rock Physics and Phase Relations: A Handbook of Physical Constants, J.H. Ahrens (Editor). American Geophysical Union Reference Shelf 3, 73-104.

Karvinen, W.O., 1973. Metamorphogenic molybdenite deposits in the Grenville Province. Ph.D thesis, Queen's University, Kingston, Ontario.

Kendrick, M.A., Burrgess, R., Pattrick R.A.D., and Turner, G., 2001. Halogen and Ar-Ar age determinations of inclusions within quartz veins from porphyry copper deposits using complementary noble gas extraction techniques. Chemical Geology 177, 351-370.

Kesler, S.E., Appold, M.S., Martini, A.M., Walter, L.M., Huston, T.J., and Kyle, J.R., 1995. Na-Cl-Br systematics of mineralizing brines in Mississippi Valley-type deposits. Geology 23, 641-644.

Koeberl, C., 1993. Instrumental neutron activation analysis of geochemical and cosmochemical samples: a fast and reliable method for small sample analysis. Journal of Radioanalytical and Nuclear Chemistry, Articles 168, 47-60.

Korzhinskiy M.A., 1981. Apatite solid solutions as indicators of the fugacity of HCl^o and HF^o in hydrothermal fluids. Geochemistry International 3, 44-60.

Lentz, D., 1989. Petrogenesis of uranium-, and molybdenum-bearing skarns, and veins in the CMB of the Grenville Province; petrologic aspects. GAC/MAC Program with Abstracts 14, 51.

Lentz, D., 1991. Radioelement distribution in U, Th, Mo, and rare-earth-element pegmatites, skarns, and veins in a portion of the Grenville province, Ontario and Quebec. Canadian Journal of Earth Sciences 28, 1-12.

Lentz, D.R., 1992. Petrogenesis of U-, Mo-, and REE-bearing pegmatites, skarns,, and veins in the Central Metasedimentary Belt of the Southwestern Grenville Province, Ontario and Quebec. Ph.D. thesis, University of Ottawa, Ottawa, Ontario.

Lentz, D.R., 1998. Late-tectonic U-Th-Mo-REE skarn and carbonatitic vein-dyke systems in the southwestern Grenville Province: A pegmatite-related pneumatolytic model linked to marble melting (limestone syntexis). In: Mineralized Intrusion-Related Skarn Systems, D.R. Lentz (Editor). Mineralogical Association of Canada Short Course Series 26, 519-567.

Levien, L. and Papike, J.J., 1976. Scapolite crystal chemistry: Aluminum-silicon distribution, carbonate group disorder, and thermal expansion. American Mineralogist 61, 864-877.

Li, W.D., 1989. On the Yangtze type copper ore deposits and its origin. Bulletin of Nanjing Institute of Geology and Mineral Resources, Chinese Academy of Geological Sciences 10-2, 1-14, in Chinese, with English abstract.

Li, W.D., Wang, W.B., Fan, H.Y., Dong, P., Zhou, T.F., and Xie, H.G., 1996. The prospects for gigantic-supergigantic copper-gold deposits in Middle-Lower Yangzi area. Unpublished Research Report, 144p, in Chinese.

Lindstrom, D.J. and Weill, D.F., 1978. Partitioning of transition metals between diopside and coexisting silicate liquids; I, Nickel, cobalt, and manganese. Geochimca et Cosmochimica Acta 42, 817-832.

Lovering, J.F. and White, A.J.R., 1964. The significance of primary scapolite in granulitic inclusions from deep-seated pipes. Journal of Petrology 5, 195-218.

Lowell, G.R., 1991. Tungsten-bearing scapolite-vesuvianite skarns from the upper Salsha River area, east-central Alaska. In: Skarns-their genesis and metallogeny, A. Barto-Kyriakidis (Editor), Athens, Greece, Theophrastus, 385-418.

Markl, G. and Piazolo, S., 1998. Halogen-bearing minerals in syenites and high-grade marbles of Dronning Maud Land, Antarctica: monitors of fluid compositional changes during late-magmatic fluid-rock interaction processes. Contributions to Mineralogy and Petrology 132, 246-268.

Martin, J.B., Gieskes, J.M., Torres, M., and Kastner, M., 1993. Bromine and iodine in Peru margin sediments and pore fluids: Implications for fluid origins. Geochimica et Cosmochimica Acta 57, 4377-4389.

Mason, B., 1966. Principles of Geochemistry. John Wiley and Sons, New York, 329 p.

Masson, S.L. and Gordon, J.B., 1981. Radioactive mineral deposits of the Pembroke-Renfrew area. Ontario Geological Survey, Circular 23, 155p

McDonough, W.F. and Sun, S.S., 1995. The composition of the Earth. In: Chemical Evolution of the Mantle, W.F. McDonough, N.T. Arndt, and S. Shirey (Editors), Chemical Geology 120, 223-253.

McLaughlan, S.D. and Marshall, D.J., 1970. Paramagnetic resonance of F-type centers in photochromic sodalites. Physics Letters 32A, 343-344.

Megaw, P.K.M., 1998. Carbonate-hosted Pb-Zn-Ag-Cu-Au replacement deposits: An exploration perspective. In: Mineralized Intrusion-Related Skarn Systems, D.R. Lentz (Editor), Mineralogical Association of Canada Short Course Series 26, 337-357.

Megaw, P.K.M., Ruiz, J., and Titley S.R., 1988, High-temperature, carbonate-hosted Ag-Pb-Zn (Cu) deposits of Northern Mexico. Economic Geology 83, 1856-1885.

Megaw, P.K.M., Barton, M.D. and Iislas-Falce, J., 1996. Carbonate-hosted lead-zinc (Ag, Au, Cu) deposits of northern Chihuahua, Mexico. In: Carbonate-Hosted Lead-Zinc Deposits, D. Sangster (Editor). Society of Economic Geologist Special Publication 4, 277-289.

Meinert, L.D., 1982. Skarn, manto, and breccia pipe formation in sedimentary rocks of the Cananea mining district, Sorona, Mexico. Economic Geology 77, 919-949.

Meurer, W.P. and Natland, J.H., 2001. Apatite compositions from oceanic cumulates with implications for the evolution of mid-ocean ridge magmatic systems. Journal of Volcanology and Geothermal Research 110, 281-298.

Moecher, D.P. and Essene, E.J., 1990. Phase equilibria for calcic scapolite, and implications of variable Al-Si disorder for P-T, T-X_{CO2}, and a-X relations. Journal of Petrology 31, 997-1024.

Moecher, D.P. and Essene, E.J., 1991. Calculation of CO_2 activities using scapolite equilibria; constraints on the presence and composition of a

fluid phase during high grade metamorphism. Contributions to Mineralogy and Petrology 108, 219-240.

Mora, C.I. and Valley, J.W., 1989. Halogen-rich scapolite and biotite: Implications for metamorphic fluid-rock interaction. American Mineralogist 74, 721-737.

Mortimer, N., 1986. Late Triassic, arc-related, potassic igneous rocks in the North American cordillera. Geology 14, p1035-1038.

Muramatsu, Y. and Wedepohl, K.H., 1998. The distribution of iodine in the earth's crust. Chemical Geology 147, 201-216.

Mysen, B.O., 1978. Limits of solution of trace elements in minerals according to Henry's Law: review of experimental data. Geochimica et Cosmochimica Acta 42, 871-885.

Nagasawa, H., 1966. Trace element partition coefficient in ionic crystals. Science 152, 767-769.

Navrotsky, A., 1978. Thermodynamics of element partitioning; (1) Systematics of transition metals in crystalline and molten silicates and (2) Defect chemistry and "the Henry's law problem". Geochimica et Cosmochimica Acta 42, 887-902.

Nesbitt, B.E. and Prochaska, W., 1998. Solute chemistry of inclusion fluids from sparry dolomites and magnesites in Middle Cambrian carbonate rocks of the southern Canadian Rocky Mountains. Canadian Journal of Earth Sciences 35, 546-555.

Newton, R.C. and Goldsmith, J.R., 1975. Stability of the scapolite meionite ($3CaAl_2Si_2O_8 \cdot CaCO_3$) at high pressure and storage of CO_2 in the deep crust. Contributions to Mineralogy and Petrology 49, 49-62.

Newton, R.C. and Goldsmith, J.R., 1976. Stability of the end-member scapolites: $3NaAlSi_3O_8 \cdot NaCl$, $3CaAl_2Si_2O_8 \cdot CaCO_3$, $3CaAl_2Si_2O_8 \cdot CaSO_4$. Zeits. Kristallogr. 43, 333-353.

Nystrom, J. O. and Henriquez, F., 1994. Magmatic features of iron ores of the Kiruna type in Chile and Sweden: ore textures and magnetite geochemistry. Economic Geology 89, 820-839.

Oliver, N.H.S., Wall, V.J., and Cartwright, I., 1992. Internal control of fluid compositions in amphibolite-facies scapolitic calc-silicates, Mary Kathleen, Australia. Contributions to Mineralogy and Petrology 111, 94-112.

Onuma, N., Higuchi, H, Wakita, H., and Nagasawa, H., 1968. Trace element partition between two pyroxenes and the host lava. Earth and Planetary Science Letters 5, 47-51.

O'Reilly, S.Y. and Griffin, W.L., 2000. Apatite in the mantle: Implications for metasomatic processes and high heat production in Phanerozoic mantle. Lithos 53, 217-232.

Orville, P.M., 1975. Stability of scapolite in the system Ab-An-NaCl-$CaCO_3$at 4 kb and 750 ^{o}C. Geochimica et Cosmochimica Acta 39, 1091-1095.

Pan, Y., 1998. Scapolite in skarn deposits: Petrogenetic and geochemical significance. In: Mineralized Intrusion-Related Skarn Systems, D.R. Lentz (Editor), Mineralogical Association of Canada Short Course Series 26, 69-109.

Pan, Y. and Dong, P., 1999. The Lower Changjiang (Yangzi/ Yangtze River) metallogenic belt, east central China; intrusion- and wall rock-hosted Cu-Fe-Au, Mo, Zn, Pb, Ag deposits. Ore Geology Reviews 15, 177-242.

Pan, Y. and Dong, P., 2003. Bromine in scapolite-group minerals and sodalite; XRF microprobe analysis, exchange experiments, and application to skarn deposits. Canadian Mineralogist 41, 529-540.

Pan, Y., Dong, P., and Chen, N., 2003. Non-Henry's law behavior of REE partitioning between fluorapatite and CaF (sub 2) -rich melts; controls of intrinsic vacancies and implications for natural apatites. Geochimica et Cosmochimica Acta 67, 1889-1900.

Pan, Y. and Fleet, M.E., 2002. Compositions of the apatite group minerals; substitution mechanisms and controlling factors. In: Phosphates; geochemical, geobiological, and materials importance, M.J. Kohn, J. Rakovan, and J.M. Hughes (Editors). Reviews in Mineralogy and Geochemistry 48, 13-49.

Pan, Y., Fleet, M.E., and Ray, G.E., 1994. Scapolite in two Canadian gold deposits: Nickle Plate, British Columbia and Hemlo, Ontario. Canadian Mineralogist 32, 825-837.

Papike, J.J. and Zoltai, T., 1965. The crystal structure of a marialite scapolite. American Mineralogist 51, 641-655.

Philpotts, J.A., 1978. The law of constant rejection. Geochimica et Cosmochimica Acta 42, 909-920.

Piccoli, P.M. and Candela, P.A., 2002. Apatite in igneous systems. In: Phosphates; geochemical, geobiological, and materials importance. M.J. Kohn, J. Rakovan, and J.M. Hughes (Editors). Reviews in Mineralogy and Geochemistry 48, 255-292.

Podlessky, K.V., Vlasova, D.K., and Kudrja, P.F., 1991. Magnetite-bearing skarns of Mongolia. In: Skarns-their genesis and metallogeny, A. Barto-Kyriakidis (Editor), Athens, Greece, Theophrastus, 265-298.

Powell, J.L., Hurley, P.M., and Fairbairn, H.W., 1966. The strontium isotopic composition and origin of carbonatites. In: Carbonatites, O.F. Tuttle and J. Gittins (Edotors), Wiley, London, 365-378.

Prener, J.S., 1967. The growth and crystallographic properties of calcium fluor- and chlorapatite crystals. Solid State Science 114, 77-83.

Preto, V.A., 1977. The Nicola Group: Mesozoic volcanism related to rifting in southern British Columbia. Geological Association of Canada Special Paper 16, 39-57.

Purton, J.A., Allan, N.L., Blundy, J.D., and Wasserman, E.A., 1996. Isovalent trace element partitioning between minerals and melts: a computer simulation study. Geochimica et Cosmochimica Acta 60, 4977-4987.

Ray, G.E., 1988. Geology and mineral occurrences in the Hedley gold camp. British Columbia Ministry Energy, Mines Petroleum Resources, Open File Map 1988-6.

Rebbert, C.R., 1995. Studies of Volatile-bearing Silicate Minerals:Cl-CO_3 Scapolite Solution Properties and Hydrothermal Oxidation of Synthetic Iron Biotite. Ph.D. thesis, University of Oregon, Eugene, Oregon.

Reed, S.J.B., 1996. Electron microprobe analysis and scanning electron microscopy in geology. Cambridge, Cambridge University Press.

Robie, R.A., Hemingway, B.S., and Fifher, J.R., 1979. Thermodynamic properties of minerals and related substances at 298.15K and 1 bar (105 pascals) pressure and at higher temperatures. United States, Geological Survey Bulletin1452 (revised).

Roegge, J.S., Logsdon, M.J., Young, H.S., Barr, H.B., Borcsik, M, and Holland, H.D., 1974. Halogens in Apatites from the Providencia Area, Mexico. Economic Geology 69, 229-240.

Rubin, J.N., and Kyle, J.R., 1997. Precious metal mineralogy in porphyry-, skarn-, and replacement- type ore deposits of the Ertsberg (Gunung Bijih) District, Irian Jaya, Indonesia. Economic Geology 92, 535-550.

Samsom, I.M., Williams-Jones, A.E., and Liu, W., 1995. The chemistry of hydrothrmal fluids in carbonatites: evidence from leachate and SEM-decrepitate analysis of fluid inclusions from Oka, Quebec, Canada. Geochimica et Cosmochimica Acta 59, 1979-1989.

Sangster, D.F., 1969. The contact metasomatic magnetite deposits of British Columbia. Canada Geological Survey Bulletin 172.

Schilling, J.G., Bergeron, M.B., and Evans, R., 1980. Halogens in the mantle beneath the North Atlantic. In: The evidence for chemical heterogeneity in the Earth's mantle, D.K. Bailey, J. Tarney, and K. Dunham (Chairpersons). Philosophical Transactions of the Royal Society of London, Series A: Mathematical and Physical Sciences 297, 147-178.

Schrauder, M., Koeberl, C., and Navon, O., 1996. Trace element analyses of fluid-bearing diamonds from Jwaneng, Botswana. Geochimica et Cosmochimica Acta 60, 4711-4724.

Seyfried, W.E.Jr., Berndt, M.E., and Janecky, D.R., 1986. Chloride depletions and enrichments in hydrothermal fluids: constraints from experimental basalt alteration studies. Geochimica et Cosmochimica Acta 50, 469-475.

Shafiqullah, M., Tupper, W.M., and Cole, T.J.S., 1970. K-Ar age of the carbonatite complex, Oka, Quebec. Canadian Mineralogist 10, 541-552.

Shaw, D.M., 1960. The geochemistry of scapolite. Journal of Petrology 1, 218-285.

Shaw, D.M., Moxham, R.L., Filby, R.H., and Lapkowsky, W.W., 1963. The petrology and geochemistry of some Grenville skarns. Canadian Mineralogist 7, 420-452.

Shaw, R.K., Venkatesh, T.L., and Gupta, A.K., 1993. Experimental study of the system fluorapatite-chlorapatite under 10 and 12 kbar at 640, 750 and 900 ^{o}C. Natural Academical Science Letters 16, 27-35.

Shinonaga, T., Ebihara, M., Nakahara, H., Tomura, K., and Heumann, K.G., 1994. Cl, Br and I in igneous standard rocks. Chemical Geology 115, 213-225.

Shu, Q.A., Chen, P.L., and Cheng, J.R., 1992. Geology of Iron-Copper Deposits in Eastern Hubei Province, China. Ministry of Metallurgical Industry Publishing House, Beijing, 532p, in Chinese.

Siemann, M.G. and Schramm, M., 2000. Thermodynamic modelling of the Br partition between aqueous solutions and halite. Geochimica et Cosmochimica Acta 64, 1681-1693.

Siemann, M.G. and Schramm, M., 2002. Henry's and non-Henry's law behavior of Br in simple marine systems. Geochimica et Cosmohimica Acta 66, 1387-1399.

Smith, J.V. and Rivers, M.L., 1995. Synchrotron X-ray microanalysis. In: Microproble Techniques in the Earth Sciences, P.J. Potts, J.F.W. Bowles, S.J.B. Reed, and M.R. Cave (Editors), Chapman and Hall, London, 163-233.

Sokolova, E.V., Kabalov, Y.K., Sherriff, B.L., Teertstra, D.K., Jenkins, D.M., Kunath-Fandrel, G., Goetz, S., and Jager, C., 1996. Marialite: Rietveld structure-refinement and ^{29}Si MAS and ^{27}Al satellite transition NMR spectroscopy. Canadian Mineralogist 34, 1039-1050.

Stoessell, R.K. and Carpenter, A.B., 1986. Stoichiometric saturation tests of $NaCl_{1-x}Br_x$ and $KCl_{1-x}Br_x$. Geochim. Cosmochim. Acta 50, 1465-1470.

Tacker, R.C. and Stormer J.C.,Jr., 1993. Thermodynamics of mixing of liquids in the system $Ca_3(PO_4)_2$-$CaCl_2$-CaF_2-$Ca(OH)_2$. Geochimica et Cosmochimica Acta 57, 4663-4676.

Taylor, S.R., 1964. Abundance of chemical elements in the continental crust: a new table. Geochimica et Cosmochimica Acta 28, 1273.

Teertstra, D.K. and Sherriff, B.L., 1997. Substitutional mechanisms, compositional trends and the end-member formulae of scapolite. Chemical Geology 136, 233-260.

Titley, S.R., 1993. Characteristics of high temperature carbonate-hosted massive sulphide ores in the United States, Mexico and Peru. In: Mineral Deposits Modelling, R.V. Kirkham, W.D. Sinclair, R.I. Thorpe, and J.M. Duke (Editors), Geological Association of Canada Special Paper 40, 585-614.

Titley, S.R., 1996. Characteristics of high temperature carbonate-hosted replacement ores and some comparisons with Mississippi Valley-type

ores. In: Carbonate-hosted Lead-Zinc Deposits, D.F. Sangster (Editor). Society of Economic Geologist Special Publication 4, 244-254.

Todd, S.S., 1949. Heat capacities at low temperatures and entropies of magnesium and calcium fluorides. Journal. American Chemical. Society 71, 4115-4116.

Turner, G., Burgess, R., and Bannon, M., 1990. Volatile-rich mantle fluids inferred from inclusions from diamond and mantle xenoliths. Nature 334, 653-655.

Valyashko, M.G., 1956. Geochemistry of bromine in the processes of salt deposition and the use of the bromine content as a genetic and prospecting criterion. Geochemistry 1, 570-589.

Vanko, D.A., 1982. Petrology of the Humboldt Lopolith, N.W. Nevada, with Emphasis on Marialitic Scapolitization and the Synthesis of Marialitic Scapolite. Ph.D. thesis, Northwestern University, Evanston, Illinois.

Vanko, D.A. and Bishop, F.C., 1982. Occurrence and origin of marialitic scapolite in the Humbold lopolith, N.W. Nevada. Contributions to Mineralogy and Petrology 81, 277-289.

Viets, J.G., Hofstra, A.H., and Emsbo, P., 1996. Solute compositions of fluid inclusions in sphalerite from North American and European Mississippi Valley-Type ore deposits: ore fluids derived from evaporited seawater. In: Carbonate-Host Pb-Zn Deposits, D.F. Sangster (Editor), Society of Economic Geologists Special Publication 4, 465-482.

Villemant, B., and Boudon, G., 1999. H_2O and halogen (F, Cl, Br) behaviour during shallow magma degassing processes. Earth and Planetary Science Letters 168, 271-286.

Wang, D.H., Fu, D.X., and Wu, L.X., 1987. The basic characters and metallogenetic laws of copper, gold, iron, sulphur ore deposits in Middle and Lower Yangtze area. Geological Publishing House, Beijing, 196p, in Chinese, with English abstract.

Watson, E.B., 1985. Henry's law behavior in simple systems and in magmas: Criteria of discerning concentration-dependent partition coefficients in nature. Geochimica et Cosmochimica Acta 49, 917-923.

Weast, R.C., 1972-1973. Handbook of Chemistry and Physics. 53rd Edition.

Webster, I.C.L. and Ray, G.E., 1990. Geology and mineral deposits of northern Texada island. British Columbia Ministry Energy, Mines Petroleum Resources Paper 1990-1, 257-265.

Webster, I.C.L., Ray, G.E., and Pettipas, A.R., 1992. An investigation of selected mineralized skarns in British Columbia. British Columbia Ministry Energy, Mines Petroleum Resources Paper 1992-1, 235-252.

Webster, J.D. and Holloway, J.R., 1988. Experimental constraints on the partitioning of Cl between topaz rhyolite melt and H_2O and H_2O-CO_2 fluids: New implications for granitic differentiation and ore deposition. Geochimica et Cosmochimica Acta 52, 2091-2105.

Wheeler, J.O., Brookfield, A.J., Gabrielse, H., Monger, J.W.H., Tipper, H.W., and Woodsworth, G.J., 1991. Terrane map of the Canadian cordillera. Canada Geol. Survey, Map 1713 A, scale 1:2,000,000.

Wood, B.J. and Blundy, J.D., 1997. A predictive model for rare earth element partitioning between clinopyroxene and anhydrous silicate melt. Contributions to Mineralogy and Petrology 129, 166-181.

Wyllie, P.J., 1989. Origin of carbonatites: evidence from phase equilibrium studies. In: Carbonatites, Genesis and Evolution, K. Bell (Editor), Unwin Hyman, London, 500-545.

Yamada, Y., 1968. Occurrence of bromine in plants and soil. Talanta 15, 1135-1141.

Yardley, B.W.D., Banks, D.A., Bottrell, S.H., and Diamond, L.W., 1993. Post-metamorphic gold-quartz veins from N.W. Italy: the composition and origin of the ore fluid. Mineralogical Magazine 57, 407-422.

Yasushi, K., 1975. Geochemistry of Water. Dowden, Hutchinson and Ross, New York, 455p.

You, C.F., Butterfield, D.A., Spivack, A.J., Gieskes, J.M., Gamo, T., and Campbell, A.J., 1994. Boron and halide systematics in submarine hydrothermal systems: Effects of phase separation and sedimentary contributions. Earth and Planetary Science Letters 123, 227-238.

Yue, W.Z., Ye, Z.Z., Wei, N.Y., Jiang, Y.H., and Ji, S.X., 1993. Sedimentary geology and stratabound massive sulphide deposits of Late Carboniferous Weining Age in the Middle and Lower Yangtze Reaches. Geol. Publ. House, Beijing, 163p, in Chinese, with English abstract.

Zhai, Y.S., Yao, S.Z., Lin, X.D., Zhou, X.N., Wan, T.F., Jin, F.Q., and Zhou, Z.G., 1992. Fe-Cu (Au) metallogeny of the Middle-Lower Changjiang region. Geological Publishing House, Beijing, 235p, in Chinese.

Zhao, B. and Zhao, J.S., 1997. O and Sr isotopic geochemistry for massive and vein calcareous skarns from some iron- copper (-gold) deposits along the Middle-Lower Reaches of the Yangtze River. Geochemistry 26, 34-53, in Chinese, with English abstract.

Zhao, Y.M., Lin, W.W., Bi, C.S., Li, D.X. and Jiang, C.J., 1990. Skarn deposits of China. Geological Publishing House, Beijing, China, 354p, in Chinese, with English abstract.

Zhu, C. and Sverjensky, D. A., 1991. Partitioning of F-Cl-OH between minerals and hydrothermal fluids. Geochimica et Cosmochimica Acta 55, 1837-1858.

Zhu, C. and Sverjensky, D.A., 1992. F-Cl-OH partitioning between biotite and apatite. Geochimica et Cosmochimica Acta 56, 3435-3467.

Zhu, S.Q., Huang, H.S., Shi, Q.Z., Wen, C.Q., and Cui, B., 1991. On the origin and composite association of Tongguanshan copper deposit, Anhui, China. In: Skarn-Their Genesis and Metallogeny, A. Barto-Kyriakidis (Editor), Theophrastus, Athens, Greece, 15-29.

Appendix 1 Summary of Apatite Synthetic Experiments

Run No.	Description	Composition	Run Temperatures & Cooling Rate	Duration (Days)	Products
dp-ap-28	Chlorapatite mixture	CaO (18.45%), P_2O_5 (15.53%) $CaCl_2$ (66.02%)			
dp-ap-28a	Br-Chlorapatite mixture	dp-ap-28 mixture (98.75%) NaBr (1.25%)	1350 to 1220 ^oC, @ 1 ^oC/hr	6	Few coarse-grained + lots needle-shaped apatite crystals + melt
dp-ap-28b	Br-Chlorapatite mixture	dp-ap-28 mixture (88.61 %) 1 wt % NaBr solution (11.39 %)	1350 to 1220 ^oC, @ 1 ^oC/hr	6	Medium-grained apatite crystals + melt
dp-ap-28c	Br-Chlorapatite mixture	dp-ap-28 mixture (88.53 %), 0.1 wt % NaBr solution (11.47 %)	1350 to 1220 ^oC, @ 1 ^oC/hr	6	Medium-grained apatite crystals+ melt
dp-ap-28 (2)	Chlorapatite mixture	CaO(18.23%), P_2O_5 (16.17 %) $CaCl_2$ (65.60 %)			
dp-ap-28a(R)	Br-Chlorapatite mixture (Reversed)	dp-ap-28 (2) mixture (87.56%) 10 wt % NaBr solution (12.44 %) charge 37 mg	1220^oC @ 0 ^oC/hr	12	Small-sized apatite crystals + melt
dp-ap-28b(R)	Br-Chlorapatite mixture (Reversed)	dp-ap-28 (2) mixture (85.05%) 1 wt % NaBr solution (14.95%) charge 33 mg	1220^oC @ 0 ^oC/hr	12	Small-sized apatite crystals + melt
dp-ap-28 (3)	Chlorapatite mixture	CaO(18.38 %), P_2O_5 (15.59 %) $CaCl_2$ (66.03 %)			

Run No.	Description	Composition	Run Temperatures & Cooling Rate	Duration (Days)	Products
dp-ap-28d	Br-F-Chlorapatite mixture	dp-ap-28 (3) mixture (87.15%) NaBr (2.58 %), CaF_2 (10.27 %)	1350 to1220 ^oC@ 1 ^oC/hr, to 1120 ^oC @ 4 ^oC/hr	9	Failed (broken)
dp-ap-28e	Br-F-Chlorapatite mixture	dp-ap-28 (3) mixture (94.86 %), NaBr (3.25 %), CaF_2 (1.89 %)	1350 to1220 ^oC @ 1 ^oC/hr, to 1120 ^oC @ 4 ^oC/hr	9	Small-sized apatite crystals (1.5 mm) + melt
dp-ap-28f	Br-F-Chlorapatite mixture	dp-ap-28 (3) mixture (83.95 %), NaBr (11.62 %), CaF_2 (4.43 %)	1350 to 1220 ^oC @ 1 ^oC/hr, to 1120 ^oC @ 4 ^oC/hr	9	Small-sized apatite crystals (<1.0mm) + melt
dp-ap-28(4)	Chlorapatite mixture	CaO(17.78 %), P_2O_5 (16.68 %), $CaCl_2$ (65.54 %)			
dp-ap-28g	Br-F-Chlorapatite mixture	dp-ap-28 (4) mixture (92.07 %), NaBr (4.12 %), CaF_2 (3.81 %)	1350 to 1220 ^oC @ 1 ^oC/hr, to 1120 ^oC @ 4 ^oC/hr	9	Small-sized apatite crystals with a 2 mm crystal + melt
dp-ap-28h	Br-F-Chlorapatite mixture	dp-ap-28 (4) mixture (93.44 %) NaBr (4.29 %) CaF_2 (2.27 %)	1350 to 1220 ^oC @ 1 ^oC/hr, to 1120 ^oC @ 4^oC/hr	9	Small-sized apatite crystals + melt
dp-ap-29	Fluorapatite mixture	CaO (26.00 %), P_2O_5 (21.98 %), CaF_2 (52.02 %)			
dp-ap-29a	Br-Cl- Fluorapatite mixture	dp-ap-29 mixture (94.27 %), $CaCl_2$(2.88 %), NaBr (2.85 %)	1350 to 1220 ^oC @ 1^oC/hr	6	Long prismatic/ needle shaped apatite crystals + melts

Run No.	Description	Composition	Run Temperatures & Cooling Rate	Duration (Days)	Products
dp-ap-29b	Br-Cl- Fluorapatite mixture	dp-ap-29 mixture (89.07 %), $CaCl_2$ (0.47 %), NaBr (0.46 %), H_2O (10.00 %)	1350 to 1220 ^oC @ 1^oC/hr	6	Short prismatic apatite crystals + melt
dp-ap-29c	Br-Fluorapatite mixture	dp-ap-29 mixture (93.67 %), NaBr (6.33 %), charge 42.4 mg	1360 to 1220 ^oC @ 1^oC/hr	8	Many apatite fragments + melt
dp-ap-29c (R)	Br-Fluorapatite mixture (Reversed)	Same as dp-ap-29c, charge 42.2 mg	1220 ^oC @ 0 ^oC/hr	8	Apatite fragments +melt
dp-ap-29d	Br-Fluorapatite mixture	dp-ap-29 mixture (87.07 %), NaBr (12.93 %), charge 66.8 mg	1350 to 1220 ^oC @ 1^oC/hr	10	One long apatite, some fine grained apatite crystals + melt
dp-ap-29d (R)	Br-Fluorapatite mixture (Reversed)	Same as dp-ap-29d, charge 42.0 mg	1220 ^oC @ 0 ^oC/hr	8	Apatite fragments + melt
dp-ap-29e (1)	Br-Fluorapatite mixture	dp-ap-29 mixture (75.02 %), NaBr (24.98 %), charge 67.9 mg	1350 to 1220 ^oC @ 1 ^oC/hr	10	Leaked, totally empty
dp-ap-29e (2)	Br-Fluorapatite mixture	dp-ap-29 mixture (75.02 %), NaBr (24.98 %), charge 46.5 mg	1360 to 1220 ^oC @ 1 ^oC/hr	8	One large and lots fine grained apatite crystals + melt
dp-ap-29h	Br-Fluorapatite mixture	dp-ap-29 mixture (87.82 %), 10 % NaBr solution (12.18 %), charge 43.4 mg	1360 to 1220 ^oC @ 1^oC/hr	8	Apatite fragments + melt
dp-ap-30	Fluorapatite mixture	CaO (24.97 %), P_2O_5 (21.04 %), CaF_2 (53.99 %)			
dp-ap-30a	Br-Cl-Fluorapatite mixture	dp-ap-30 mixture (95%), KCl (2.5%), KBr (2.5%)	1320 to 1250 ^oC @ 5 ^oC /hr	4	Medium-fine-grained apatite crystals + melt
dp-ap-30b	Br-Cl-Fluorapatite mixture	dp-ap-30 mixture (90%), KCl (5%), KBr (5%)	1320 to 1250 ^oC @ 5 ^oC /hr	4	Fine-grained apatite crystals + melt

Run No.	Description	Composition	Run Temperatures & Cooling Rate	Duration (Days)	Products
dp-ap-30c	Br-Cl-Fluorapatite mixture	dp-ap-30 mixture (84%), KCl (8%), KBr (8%)	1320 to 1250 ^{o}C @ 5 ^{o}C /hr	4	Medium-fine-grained apatite crystals + melt
dp-ap-30a (R)	Br-Cl-Fluorapatite mixture (Reversed)	dp-ap-30 mixture (95%), KCl (2.5%), KBr (2.5%)	1250 ^{o}C	7	Medium-grained, needle shaped apatite + melt
dp-ap-30b (R)	Br-Cl-Fluorapatite mixture (Reversed)	dp-ap-30 mixture (90%), KCl (5%), KBr (5%)	1250 ^{o}C	7	Needle-shaped apatite crystals + melt
dp-ap-30c (R)	Br-Cl-Fluorapatite mixture (Reversed)	dp-ap-30 mixture (84%), KCl (8%), KBr (8%)	1250 ^{o}C	7	Medium-grained, needle shaped apatite + melt
dp-ap-31	Fluorapatite mixture	CaO (21.67 %), P_2O_5 (18.43 %) CaF_2 (59.90 %)			
dp-ap-31a	Br-Cl-Fluorapatite mixture	dp-ap-31 mix (64.79 %), KCl (31.87 %), KBr (3.34 %)	1270 to 1220 ^{o}C @ 5 ^{o}C /hr	3	Failed (leak)
dp-ap-32	Fluorapatite mixture	CaO (32.50 %), P_2O_5 (27.53 %) CaF_2 (39.97 %)			
dp-ap-32a	Br-Cl-Fluorapatite mixture	dp-ap-32 mixture (93.54 %) KCl (3.26 %) KBr (3.20 %)	1450 to 1400 ^{o}C @ 2 ^{o}C /hr	3	Fine-grained apatite crystals + melt
dp-ap-33	Fluorapatite mixture	CaO (23.99 %), P_2O_5 (19.43 %) CaF_2 (57.58 %)			
dp-ap-33a	Br-Fluorapatite mixture	dp-ap-33 mixture (94.53 %) NaBr (5.47 %)	1300 to 1220 ^{o}C @ 5 ^{o}C /hr	6	Very fine-grained, needle-shaped apatite crystal + melt
dp-ap-33b	Br-Fluorapatite mixture	dp-ap-33 mixture (88.45 %) NaBr (11.55 %)	1300 to 1220 ^{o}C @ 5 ^{o}C /hr	6	Very fine-grained, needle-shaped apatite crystal + melt
dp-ap-34	Fluorapatite mixture	CaO (30.01 %), P_2O_5 (25.35 %) CaF_2 (44.64 %)			

Run No.	Description	Composition	Run Temperatures & Cooling Rate	Duration (Days)	Products
dp-ap-34a	Br-Cl-Fluorapatite mixture	dp-ap-34 mixture (82.36 %), NaBr (5.67 %), $CaCl_2$ (11.97 %)	1420 to 1330 ^oC @ 1 ^oC /hr	6	Fine-grained apatite crystals + melt
dp-ap-34b	Br-Cl-Fluorapatite mixture	dp-ap-34 mixture (91.18 %), NaBr (2.76 %), $CaCl_2$ (6.06 %)	1420 to 1330 ^oC @ 1 ^oC /hr	6	Fine-grained apatite crystals + melt
dp-ap-34c	Br-Cl-Fluorapatite mixture	dp-ap-34 mixture (95.59 %), NaBr (2.49 %), CaCl2(1.92 %)	1420 to 1330 ^oC @ 1 ^oC /hr	6	Failed (leak)
dp-ap-34d	Br-Cl-Fluorapatite mixture	dp-ap-34 mixture (98.03 %), NaBr (1.21 %), $CaCl_2$ (0.77 %)	1420 to 1330 ^oC @ 1 ^oC /hr	6	Apatite fragments + melt
dp-ap-35	Chlorapatite mixture	CaO (14.59 %), P_2O_5 (12.34 %) $CaCl_2$ (73.07 %)			
dp-ap-35a	Br-Chlorapatite mixture	dp-ap-35 mixture (92.79 %) NaBr (7.21 %)	1300 to 1220 ^oC @ 5 ^oC /hr	6	Fine-grained apatite + melt
dp-ap-36	Chlorapatite mixture	CaO (21.52 %), $CaCl_2$ (60.07), P_2O_5 (18.41 %)			
dp-ap-36a	Br-F-Chlorapatite mixture	dp-ap-36 mixture (96.96 %) NaBr (0.76 %) CaF_2 (2.28 %)	1420 to 1330 ^oC @ 1 ^oC /hr	6	Fine-grained apatite crystals + melt
dp-ap-36b	Br-F-Chlorapatite mixture	dp-ap-36 mixture (90.13 %) NaBr (1.47 %) CaF_2 (8.39 %)	1420 to 1330 ^oC @ 1 ^oC /hr	6	Fine-grained apatite crystals + melt

Appendix 2a Micro XRF Analytical Results of Synthetic Chlorapatite

Run No.	Analyse No.	Starting Material			Apatite
		Br (wt %)	Cl (wt %)	F (wt %)	Br (ppm)
ap-28-a	28-a-1-1	0.97	41.7	0	364
ap-28-a	28-a-1-2	0.97	41.7	0	359
ap-28-a	28-a-1-3	0.97	41.7	0	348
ap-28-a	28-a-2-1	0.97	41.7	0	307
ap-28-a	28-a-2-2	0.97	41.7	0	312
ap-28-a	28-a-2-3	0.97	41.7	0	315
ap-28-a	28-a-3-1	0.97	41.7	0	284
ap-28-a	28-a-3-2	0.97	41.7	0	315
ap-28-a	Average	**0.97**	**41.7**	**0**	**325**
	STDEV				28
ap-28-a(R)	28-a(R)-1-1	1.09	41.4	0	456
ap-28-a(R)	28-a(R)-1-2	1.09	41.4	0	500
ap-28-a(R)	28-a(R)-1-3	1.09	41.4	0	401
ap-28-a(R)	28-a(R)-2-1	1.09	41.4	0	455
ap-28-a(R)	28-a(R)-2-2	1.09	41.4	0	481
ap-28-a(R)	28-a(R)-3-1	1.09	41.4	0	546
ap-28-a(R)	28-a(R)-3-2	1.09	41.4	0	459
ap-28-a(R)	28-a(R)-4-1	1.09	41.4	0	427
ap-28-a(R)	28-a(R)-4-2	1.09	41.4	0	431
ap-28-a(R)	28-a(R)-4-3	1.09	41.4	0	423
ap-28-a(R)	28-a(R)-5-1	1.09	41.4	0	464
ap-28-a(R)	28-a(R)-5-2	1.09	41.4	0	437
ap-28-a(R)	28-a(R)-5-3	1.09	41.4	0	491
ap-28-a(R)	28-a(R)-6-1	1.09	41.4	0	425
ap-28-a(R)	28-a(R)-6-2	1.09	41.4	0	417
ap-28-a(R)	28-a(R)-6-3	1.09	41.4	0	448
ap-28-a(R)	Average	**1.09**	**41.4**	**0**	**454**
	STDEV				**37**
ap-28-b	28-b-1-1	0.10	42.3	0	76
ap-28-b	28-b-1-2	0.10	42.3	0	80
ap-28-b	28-b-1-3	0.10	42.3	0	69
ap-28-b	28-b-2-1	0.10	42.3	0	69
ap-28-b	28-b-2-2	0.10	42.3	0	66
ap-28-b	28-b-2-3	0.10	42.3	0	65
ap-28-b	28-b-3-1	0.10	42.3	0	64
ap-28-b	28-b-3-2	0.10	42.3	0	52
ap-28-b	28-b-3-3	0.10	42.3	0	56
ap-28-b	Average	**0.10**	**42.3**	**0**	**66**
	STDEV				9
ap-28-b (R)	28-b(R)-1-1	0.14	41.9	0	72
ap-28-b (R)	28-b(R)-1-2	0.14	41.9	0	66
ap-28-b (R)	28-b(R)-2-1	0.14	41.9	0	89
ap-28-b (R)	28-b(R)-2-2	0.14	41.9	0	101
ap-28-b (R)	28-b(R)-2-3	0.14	41.9	0	91
ap-28-b (R)	28-b(R)-3-1	0.14	41.9	0	75
ap-28-b (R)	28-b(R)-3-2	0.14	41.9	0	85
ap-28-b (R)	28-b(R)-3-3	0.14	41.9	0	84

Run No.	Analyse No.	Starting Material			Apatite
		Br (wt %)	Cl (wt %)	F (wt %)	Br (ppm)
ap-28-b (R)	28-b(R)-4-1	0.14	41.9	0	107
ap-28-b (R)	28-b(R)-4-2	0.14	41.9	0	94
ap-28-b (R)	Average	**0.14**	**41.9**	**0**	**86**
	STDEV				13
ap-28-c	28-c-1-1	0.01	42.3	0	5
ap-28-c	28-c-1-2	0.01	42.3	0	9
ap-28-c	28-c-1-3	0.01	42.3	0	7
ap-28-c	28-c-1-4	0.01	42.3	0	7
ap-28-c	28-c-2-1	0.01	42.3	0	6
ap-28-c	28-c-2-2	0.01	42.3	0	6
ap-28-c	28-c-2-3	0.01	42.3	0	6
ap-28-c	28-c-3-1	0.01	42.3	0	5
ap-28-c	28-c-3-2	0.01	42.3	0	8
ap-28-c	28-c-3-3	0.01	42.3	0	4
ap-28-c	Average	**0.01**	**42.3**	**0**	**6**
	STDEV				**2**
ap-28-e	28-e-1-1	2.54	40.1	0.9	973
ap-28-e	28-e-1-2	2.54	40.1	0.9	977
ap-28-e	28-e-3-1	2.54	40.1	0.9	735
ap-28-e	28-e-3-2	2.54	40.1	0.9	741
ap-28-e	28-e-4-1	2.54	40.1	0.9	591
ap-28-e	28-e-7-1	2.54	40.1	0.9	676
ap-28-e	Average	**2.54**	**40.1**	**0.9**	**782**
	STDEV				159
ap-28-f	28-f-1-1	9.06	35.5	2.2	1647
ap-28-f	28-f-1-2	9.06	35.5	2.2	1978
ap-28-f	28-f-1-3	9.06	35.5	2.2	2058
ap-28-f	28-f-2-1	9.06	35.5	2.2	1937
ap-28-f	28-f-2-2	9.06	35.5	2.2	1809
ap-28-f	28-f-3-1	9.06	35.5	2.2	1809
ap-28-f	28-f-3-2	9.06	35.5	2.2	1945
ap-28-f	28-f-4-1	9.06	35.5	2.2	1536
ap-28-f	28-f-4-4	9.06	35.5	2.2	1508
ap-28-f	Average	**9.06**	**35.5**	**2.2**	**1803**
	STDEV				199
ap-28-g	28-g-1-1	3.22	38.6	1.9	1245
ap-28-g	28-g-1-2	3.22	38.6	1.9	1386
ap-28-g	28-g-1-3	3.22	38.6	1.9	1667
ap-28-g	28-g-2-1	3.22	38.6	1.9	1303
ap-28-g	28-g-2-2	3.22	38.6	1.9	1417
ap-28-g	28-g-2-3	3.22	38.6	1.9	1598
ap-28-g	28-g-3-1	3.22	38.6	1.9	1307
ap-28-g	28-g-3-2	3.22	38.6	1.9	1358
ap-28-g	28-g-3-3	3.22	38.6	1.9	1191
ap-28-g	Average	**3.22**	**38.6**	**1.9**	**1386**
	STDEV				157
ap-28-h	28-h-1-1	3.35	39.2	1.1	1909
ap-28-h	28-h-1-2	3.35	39.2	1.1	1357

Run No.	Analyse No.	Starting Material			Apatite
		Br (wt %)	Cl (wt %)	F (wt %)	Br (ppm)
ap-28-h	28-h-2-1	3.35	39.2	1.1	1413
ap-28-h	28-h-2-2	3.35	39.2	1.1	1698
ap-28-h	28-h-2-3	3.35	39.2	1.1	1723
ap-28-h	28-h-3-1	3.35	39.2	1.1	1297
ap-28-h	28-h-3-2	3.35	39.2	1.1	1993
ap-28-h	28-h-4-1	3.35	39.2	1.1	1819
ap-28-h	28-h-4-2	3.35	39.2	1.1	1816
ap-28-h	28-h-4-3	3.35	39.2	1.1	1345
ap-28-h	28-h-4-4	3.35	39.2	1.1	1952
ap-28-h	28-h-4-5	3.35	39.2	1.1	1268
ap-28-h	Average	**3.35**	**39.2**	**1.1**	**1632**
	STDEV				277
ap-35-a	35-a-1-1	5.60	43.4	0.0	1863
ap-35-a	35-a-1-2	5.60	43.4	0.0	2055
ap-35-a	35-a-3-1	5.60	43.4	0.0	2142
ap-35-a	35-a-3-2	5.60	43.4	0.0	1802
ap-35-a	35-a-4-1	5.60	43.4	0.0	2184
ap-35-a	35-a-4-2	5.60	43.4	0.0	2180
ap-35-a	Average	**5.60**	**43.4**	**0.0**	**2038**
	STDEV				167
ap-36-a	36-a-1-1	0.59	37.2	1.1	404
ap-36-a	36-a-1-2	0.59	37.2	1.1	477
ap-36-a	36-a-2-1	0.59	37.2	1.1	415
ap-36-a	36-a-2-2	0.59	37.2	1.1	463
ap-36-a	36-a-3-1	0.59	37.2	1.1	392
ap-36-a	36-a-3-2	0.59	37.2	1.1	447
ap-36-a	36-a-4-1	0.59	37.2	1.1	380
ap-36-a	36-a-4-2	0.59	37.2	1.1	397
ap-36-a	36-a-5-1	0.59	37.2	1.1	406
ap-36-a	36-a-5-2	0.59	37.2	1.1	386
ap-36-a	36-a-6-1	0.59	37.2	1.1	451
ap-36-a	36-a-6-2	0.59	37.2	1.1	441
ap-36-a	36-a-7-1	0.59	37.2	1.1	475
ap-36-a	36-a-7-2	0.59	37.2	1.1	449
ap-36-a	36-a-8-1	0.59	37.2	1.1	441
ap-36-a	36-a-8-2	0.59	37.2	1.1	436
ap-36-a	36-a-9-1	0.59	37.2	1.1	418
ap-36-a	36-a-9-2	0.59	37.2	1.1	400
ap-36-a	36-a-10-1	0.59	37.2	1.1	439
ap-36-a	36-a-10-2	0.59	37.2	1.1	425
ap-36-a	Average	**0.59**	**37.2**	**1.1**	**427**
	STDEV				29
ap-36-b	36-b-4-1	1.14	34.6	4.1	675
ap-36-b	36-b-4-2	1.14	34.6	4.1	787
ap-36-b	36-b-5-1	1.14	34.6	4.1	884
ap-36-b	36-b-5-2	1.14	34.6	4.1	712
ap-36-b	36-b-6-1	1.14	34.6	4.1	618
ap-36-b	36-b-6-2	1.14	34.6	4.1	755
ap-36-b	36-b-7-1	1.14	34.6	4.1	623
ap-36-b	36-b-7-2	1.14	34.6	4.1	725
ap-36-b	Average	**1.14**	**34.6**	**4.1**	**722**
	STDEV				88

Appendix 2b Micro XRF Analytical Results of Synthetic Fluorapatite

Run No.	Analyse No.	Starting Material			Apatite
		Br (wt %)	Cl (wt %)	F (wt %)	Br (ppm)
ap-29-a	29-a-1-1	2.2	1.8	23.9	41
ap-29-a	29-a-1-2	2.2	1.8	23.9	44
ap-29-a	29-a-1-3	2.2	1.8	23.9	41
ap-29-a	29-a-2-1	2.2	1.8	23.9	56
ap-29-a	29-a-2-3	2.2	1.8	23.9	43
ap-29-a	29-a-2-4	2.2	1.8	23.9	48
ap-29-a	29-a-3-1	2.2	1.8	23.9	51
ap-29-a	29-a-3-2	2.2	1.8	23.9	51
ap-29-a	29-a-3-3	2.2	1.8	23.9	49
ap-29-a	29-a-4-1	2.2	1.8	23.9	41
ap-29-a	29-a-4-2	2.2	1.8	23.9	39
ap-29-a	29-a-4-3	2.2	1.8	23.9	45
ap-29-a	29-a-4-4	2.2	1.8	23.9	40
ap-29-a	29-a-4-5	2.2	1.8	23.9	44
ap-29-a	29-a-4-6	2.2	1.8	23.9	51
ap-29-a	Average	**2.2**	**1.8**	**23.9**	**46**
	STDEV				5
ap-29-b	some analyses are under detect limit				
ap-29-b	29-b-1-2	0.4	0.3	25.1	3
ap-29-b	29-b-1-3	0.4	0.3	25.1	3
ap-29-b	29-b-1-4	0.4	0.3	25.1	4
ap-29-b	29-b-1-5	0.4	0.3	25.1	3
ap-29-b	Average	**0.4**	**0.3**	**25.1**	**3**
	STDEV				0.4
ap-29-h	some analyses are under detect limit				
ap-29-h	29-h-1-1	1.1	0	25.0	27
ap-29-h	29-h-1-2	1.1	0	25.0	38
ap-29-h	29-h-2-1	1.1	0	25.0	43
ap-29-h	29-h-2-2	1.1	0	25.0	50
ap-29-h	29-h-2-3	1.1	0	25.0	43
ap-29-h	29-h-2-4	1.1	0	25.0	38
ap-29-h	29-h-3-1	1.1	0	25.0	37
ap-29-h	29-h-3-2	1.1	0	25.0	50
ap-29-h	29-h-3-3	1.1	0	25.0	36
ap-29-h	29-h-3-4	1.1		25.0	40
ap-29-h	Average	**1.1**	**0.0**	**25.0**	**40**
	STDEV				7
ap-29-c	29-c-1-1	4.9	0	23.7	623
ap-29-c	29-c-1-2	4.9	0	23.7	413
ap-29-c	29-c-1-3	4.9	0	23.7	887

Run No.	Analyse No.	Starting Material			Apatite
		Br (wt %)	Cl (wt %)	F (wt %)	Br (ppm)
ap-29-c	29-c-1-4	4.9	0	23.7	654
ap-29-c	29-c-2-1	4.9	0	23.7	456
ap-29-c	29-c-2-2	4.9	0	23.7	501
ap-29-c	29-c-3-1	4.9	0	23.7	263
ap-29-c	29-c-3-2	4.9	0	23.7	285
ap-29-c	29-c-3-3	4.9	0	23.7	262
ap-29-c	29-c-3-4	4.9	0	23.7	238
ap-29-c	29-c-4-1	4.9	0	23.7	634
ap-29-c	29-c-4-2	4.9	0	23.7	314
ap-29-c	29-c-4-3	4.9	0	23.7	325
ap-29-c	29-c-5-1	4.9	0	23.7	401
ap-29-c	29-c-5-2	4.9	0	23.7	368
ap-29-c	29-c-5-3	4.9	0	23.7	460
ap-29-c	Average	**4.9**	**0**	**23.7**	**443**
	STDEV				180
ap-29-c(R)	29-c-(R)-1-1	4.9	0	23.7	915
ap-29-c(R)	29-c-(R)-2-1	4.9	0	23.7	281
ap-29-c(R)	29-c-(R)-2-2	4.9	0	23.7	258
ap-29-c(R)	29-c-(R)-2-3	4.9	0	23.7	255
ap-29-c(R)	29-c-(R)-3-1	4.9	0	23.7	340
ap-29-c(R)	29-c-(R)-3-2	4.9	0	23.7	680
ap-29-c(R)	29-c-(R)-4-1	4.9	0	23.7	414
ap-29-c(R)	29-c-(R)-4-2	4.9	0	23.7	575
ap-29-c(R)	29-c-(R)-4-3	4.9	0	23.7	603
ap-29-c(R)	29-c-(R)-5-1	4.9	0	23.7	665
ap-29-c(R)	29-c-(R)-5-2	4.9	0	23.7	825
ap-29-c(R)	29-c-(R)-5-3	4.9	0	23.7	739
ap-29-c(R)	Average	**4.9**	**0**	**23.7**	**546**
	STDEV				231
ap-29-d	29-d-1-1	10.0	0	22.0	317
ap-29-d	29-d-1-2	10.0	0	22.0	547
ap-29-d	29-d-1-3	10.0	0	22.0	426
ap-29-d	29-d-2-1	10.0	0	22.0	395
ap-29-d	29-d-2-2	10.0	0	22.0	405
ap-29-d	29-d-2-3	10.0	0	22.0	410
ap-29-d	29-d-3-1	10.0	0	22.0	310
ap-29-d	29-d-3-2	10.0	0	22.0	369
ap-29-d	29-d-3-3	10.0	0	22.0	290
ap-29-d	29-d-4-1	10.0	0	22.0	219
ap-29-d	29-d-4-2	10.0	0	22.0	193
ap-29-d	Average	**10.0**	**0**	**22.0**	**353**
	STDEV				101
ap-29-d(R)	29-d(R)-1-1	10.0	0	22.0	195.8
ap-29-d(R)	29-d(R)-1-2	10.0	0	22.0	138.8

Run No.	Analyse No.	Starting Material			Apatite
		Br (wt %)	Cl (wt %)	F (wt %)	Br (ppm)
ap-29-d(R)	29-d(R)-1-3	10.0	0	22.0	174
ap-29-d(R)	29-d(R)-1-4	10.0	0	22.0	536
ap-29-d(R)	29-d(R)-2-1	10.0	0	22.0	582
ap-29-d(R)	29-d(R)-3-1	10.0	0	22.0	245
ap-29-d(R)	29-d(R)-3-2	10.0	0	22.0	508
ap-29-d(R)	29-d(R)-3-3	10.0	0	22.0	239
ap-29-d(R)	Average	**10.0**	**0**	**22.0**	**327**
	STDEV				182
ap-29-e	29-E-1-1	19.4	0	19.0	567
ap-29-e	29-E-1-2	19.4	0	19.0	792
ap-29-e	29-E-2-2	19.4	0	19.0	729
ap-29-e	29-E-3-1	19.4	0	19.0	467
ap-29-e	29-E-4-1	19.4	0	19.0	542
ap-29-e	Average	**19.4**	**0**	**19.0**	**619**
	STDEV				136
ap-30-a	30-a-1-1	1.8	1.2	24.9	42
ap-30-a	30-a-1-2	1.8	1.2	24.9	45
ap-30-a	30-a-2-1	1.8	1.2	24.9	44
ap-30-a	30-a-2-2	1.8	1.2	24.9	41
ap-30-a	30-a-3-1	1.8	1.2	24.9	46
ap-30-a	30-a-3-2	1.8	1.2	24.9	48
ap-30-a	Average	**1.8**	**1.2**	**24.9**	**44**
	STDEV				2
ap-30-a(R)	ap30aR3a	1.8	1.2	24.9	46
ap-30-a(R)	ap30aR3b	1.8	1.2	24.9	34
ap-30-a(R)	Average	**0.7**	**0.5**	**10.0**	**40**
	STDEV				8
ap-30-b	30-b-1-1	3.1	2.3	23.8	81
ap-30-b	30-b-1-2	3.1	2.3	23.8	90
ap-30-b	30-b-1-3	3.1	2.3	23.8	73
ap-30-b	30-b-2-1	3.1	2.3	23.8	43
ap-30-b	30-b-2-2	3.1	2.3	23.8	44
ap-30-b	Average	**3.1**	**2.3**	**23.8**	**66**
	STDEV				**22**
ap-30-c	30-c-1-1	5.7	4.0	21.8	55
ap-30-c	30-c-1-2	5.7	4.0	21.8	39
ap-30-c	30-c-2-1	5.7	4.0	21.8	70
ap-30-c	30-c-2-2	5.7	4.0	21.8	50
ap-30-c	30-c-3-1	5.7	4.0	21.8	39
ap-30-c	30-c-3-2	5.7	4.0	21.8	56
ap-30-c	Average	**5.7**	**4.0**	**21.8**	**52**
	STDEV				12

Run No.	Analyse No.	Starting Material			Apatite
		Br (wt %)	Cl (wt %)	F (wt %)	Br (ppm)
ap-32-a	32-a-1-1	2.1	1.6	18.2	260
ap-32-a	32-a-2-1	2.1	1.6	18.2	233
ap-32-a	32-a-2-2	2.1	1.6	18.2	181
ap-32-a	32-a-3-1	2.1	1.6	18.2	207
ap-32-a	32-a-3-2	2.1	1.6	18.2	204
ap-32-a	32-a-4-1	2.1	1.6	18.2	184
ap-32-a	32-a-4-2	2.1	1.6	18.2	248
ap-32-a	32-a-4-3	2.1	1.6	18.2	170
ap-32-a	32-a-5-1	2.1	1.6	18.2	212
ap-32-a	32-a-5-2	2.1	1.6	18.2	136
ap-32-a	32-a-5-3	2.1	1.6	18.2	160
ap-32-a	Average	**2.1**	**1.6**	**18.2**	**200**
	STDEV				38
ap-33-a	33-a-1-1	4.3	0.0	26.5	4443
ap-33-a	33-a-1-2	4.3	0.0	26.5	4309
ap-33-a	33-a-3-1	4.3	0.0	26.5	5020
ap-33-a	33-a-3-2	4.3	0.0	26.5	4046
ap-33-a	33-a-4-1	4.3	0.0	26.5	6508
ap-33-a	Average	**4.3**	**0.0**	**26.5**	**4865**
	STDEV				985
ap-33-b	33-b-1-1	0.5	0.0	24.8	178
ap-33-b	33-b-1-2	0.5	0.0	24.8	143
ap-33-b	33-b-2-1	0.5	0.0	24.8	191
ap-33-b	33-b-2-2	0.5	0.0	24.8	224
ap-33-b	33-b-3-1	0.5	0.0	24.8	198
ap-33-b	33-b-3-2	0.5	0.0	24.8	184
ap-33-b	33-b-4-1	0.5	0.0	24.8	265
ap-33-b	33-b-4-2	0.5	0.0	24.8	242
ap-33-b	Average	**0.5**	**0.0**	**24.8**	**203**
	STDEV				39

Appendix 2c EMPA Results of Synthetic Apatites (wt %)

Run No.	Analyse No.	CaO	P_2O_5	Na_2O	K_2O	F	Cl	Br	Total
Chlorapatite									
ap-28-a	28-a-1-1	55.33	40.03	0.00	0.01	0.00	6.45	0.005	101.82
ap-28-a	28-a-1-2	54.76	39.44	0.00	0.02	0.00	5.88	0.025	100.12
ap-28-a	28-a-1-3	56.11	40.15	0.00	0.01	0.00	5.19	0.012	101.47
ap-28-a	28-a-1-4	55.53	40.79	0.00	0.04	0.00	6.95	0.012	103.33
ap-28-a	28-a-2-1	55.68	40.43	0.00	0.00	0.00	2.51	0.008	98.63
ap-28-a	28-a-2-2	55.43	39.96	0.00	0.00	0.00	3.05	0.004	98.45
ap-28-a	28-a-2-3	54.34	39.87	0.00	0.00	0.00	3.52	0.010	97.74
ap-28-a	28-a-3-1	55.63	40.60	0.00	0.00	0.01	2.64	0.015	98.88
	Average	55.35	40.16	0.00	0.01	0.00	4.52	0.011	100.06
	STDEV	0.56	0.43	0.00	0.01	0.00	1.80	0.006	1.97
ap-28-a(R)	28-a(R)-1-1	55.14	39.33	0.01	0.00	0.00	6.52	0.019	101.01
ap-28-a(R)	28-a(R)-1-2	56.30	39.34	0.00	0.00	0.00	5.10	0.035	100.78
ap-28-a(R)	28-a(R)-1-3	55.98	38.66	0.01	0.00	0.00	5.83	0.034	100.51
ap-28-a(R)	28-a(R)-2-1	57.04	38.78	0.00	0.00	0.00	3.04	0.001	98.86
ap-28-a(R)	28-a(R)-2-2	55.56	38.23	0.00	0.00	0.00	4.11	0.015	97.92
ap-28-a(R)	28-a(R)-2-3	56.52	38.82	0.00	0.00	0.00	4.50	0.013	99.85
ap-28-a(R)	28-a(R)-3-1	55.77	38.47	0.00	0.01	0.00	4.72	0.028	99.00
ap-28-a(R)	28-a(R)-3-2	56.18	39.54	0.02	0.01	0.00	5.23	0.019	100.99
ap-28-a(R)	28-a(R)-3-3	56.03	39.32	0.00	0.00	0.00	5.79	0.015	101.15
ap-28-a(R)	28-a(R)-4-1	55.19	40.41	0.00	0.00	0.00	5.67	0.017	101.29
ap-28-a(R)	28-a(R)-4-2	55.54	39.51	0.00	0.03	0.00	5.75	0.040	100.86
ap-28-a(R)	28-a(R)-4-3	55.17	39.85	0.02	0.01	0.00	6.16	0.040	101.24
ap-28-a(R)	28-a(R)-5-1	56.15	39.89	0.00	0.00	0.00	6.23	0.018	102.29
ap-28-a(R)	28-a(R)-5-2	55.65	38.67	0.00	0.00	0.00	5.57	0.028	99.92
ap-28-a(R)	28-a(R)-5-3	55.77	38.96	0.00	0.00	0.00	5.17	0.033	99.93
ap-28-a(R)	28-a(R)-6-1	55.86	38.86	0.01	0.01	0.00	6.21	0.014	100.96
ap-28-a(R)	28-a(R)-6-2	56.50	38.20	0.00	0.00	0.00	5.43	0.025	100.15
ap-28-a(R)	28-a(R)-6-3	56.05	38.54	0.00	0.00	0.00	5.91	0.007	100.50
	Average	55.91	39.08	0.00	0.00	0.00	5.39	0.022	100.40
	STDEV	0.51	0.61	0.01	0.01	0.00	0.86	0.011	1.04
ap-28-b	28-b-1-1	55.09	39.76	0.00		0.00	5.64		100.49
ap-28-b	28-b-1-2	54.74	39.48	0.00	0.01	0.00	6.35	0.007	100.59
ap-28-b	28-b-3-1	56.52	38.94	0.00	0.01	0.00	4.92	0.007	100.40
ap-28-b	28-b-3-2	53.33	39.88	0.00		0.00	4.96	0.006	98.18
ap-28-b	28-b-4-2	54.97	40.86	0.00	0.08	0.00	6.84	0.039	102.79
	Average	54.93	39.78		0.03	0.00	5.74	0.015	100.49
	STDEV	1.13	0.70		0.04	0.00	0.85	0.016	1.63
ap-28-b(R)	28-b(R)-1-1	55.34	39.50	0.00	0.01	0.00	5.40		100.24
ap-28-b(R)	28-b(R)-1-2	56.28	39.61	0.00	0.00	0.00	5.49	0.005	101.39
ap-28-b(R)	28-b(R)-1-3	56.08	39.93	0.00	0.00	0.00	5.33	0.010	101.35
ap-28-b(R)	28-b(R)-3-1	55.17	40.06	0.00	0.00	0.00	4.98	0.012	100.22
ap-28-b(R)	28-b(R)-3-2	56.26	39.51	0.00	0.02	0.00	6.49	0.013	102.29
ap-28-b(R)	28-b(R)-3-3	55.35	40.20	0.00	0.02	0.00	5.55	0.007	101.13
ap-28-b(R)	28-b(R)-5-1	56.07	39.13	0.00	0.03	0.00	4.07		99.31
	Average	55.79	39.71	0.00	0.01	0.00	5.33	0.009	100.85
	STDEV	0.48	0.37	0.00	0.01	0.00	0.72	0.003	0.99

Run No.	Analyse No.	CaO	P_2O_5	Na_2O	K_2O	F	Cl	Br	Total
ap-28-c	28-c-1-1	53.85	39.86	0.00	0.00	0.00	5.85	0.002	99.57
ap-28-c	28-c-1-2	56.08	38.83	0.00	0.00	0.00	5.58	0.015	100.50
ap-28-c	28-c-2-1	54.28	39.03	0.00	0.01	0.00	5.37		98.68
ap-28-c	28-c-2-2	55.43	38.80	0.00	0.01	0.00	5.12	0.003	99.36
ap-28-c	28-c-3-1	54.34	39.69	0.00	0.00	0.00	5.49	0.006	99.53
ap-28-c	28-c-3-2	55.35	40.01	0.01	0.00	0.00	5.50	0.010	100.90
	Average	54.89	39.37	0.00	0.00	0.00	5.49	0.007	99.76
	STDEV	0.86	0.54	0.00	0.00	0.00	0.24	0.005	0.81
ap-28-e	28-e-1-1	50.28	44.42	0.10	0.05	0.00	6.58	0.085	101.52
ap-28-e	28-e-1-2	49.84	45.08	0.05	0.01	0.00	6.52	0.068	101.56
ap-28-e	28-e-1-3	52.77	41.55	0.04	0.01	0.00	5.91	0.073	100.42
ap-28-e	28-e-2-1	54.44	40.66	0.03	0.01	0.00	3.56	0.048	98.79
ap-28-e	28-e-2-2	54.52	41.00	0.05	0.00	0.00	5.33	0.052	101.41
ap-28-e	28-e-2-3	51.15	43.82	0.05	0.02	0.00	4.78	0.067	99.89
ap-28-e	28-e-2-4	52.87	41.93	0.07	0.02	0.00	5.21	0.065	100.22
ap-28-e	28-e-2-5	56.19	39.41	0.03	0.00	0.00	4.46	0.026	100.12
ap-28-e	28-e-2-6	54.65	44.93	0.04	0.01	0.00	4.00	0.035	103.68
ap-28-e	28-e-2-7	55.16	40.19	0.09	0.04	0.00	3.97	0.038	99.48
ap-28-e	28-e-2-8	54.67	41.05	0.04	0.04	0.00	4.53	0.071	100.46
	Average	53.32	42.19	0.05	0.02	0.00	4.99	0.057	100.69
	STDEV	2.11	2.02	0.02	0.02	0.00	1.02	0.018	1.31
ap-28-f	28-f-1-1	51.92	46.61	0.07	0.03	0.00	2.67	0.111	101.44
ap-28-f	28-f-1-2	53.80	42.67	0.04	0.00	0.62	2.65	0.128	99.91
ap-28-f	28-f-1-3	54.57	43.06	0.05	0.01	0.83	2.44	0.073	101.05
ap-28-f	28-f-1-4	54.27	40.62	0.06	0.00	0.54	2.47	0.102	98.10
ap-28-f	28-f-2-1	55.21	40.05	0.10	0.00	1.18	2.28	0.160	99.01
ap-28-f	28-f-2-2	53.18	43.58	0.05	0.01	0.72	2.27	0.104	99.95
ap-28-f	28-f-2-3	54.40	41.73	0.01	0.03	1.47	2.19	0.106	99.96
ap-28-f	28-f-3-1	54.15	43.06	0.05	0.01	0.81	2.26	0.133	100.52
ap-28-f	28-f-3-2	52.30	46.49	0.04	0.02	0.99	2.15	0.129	102.13
ap-28-f	28-f-3-3	52.66	43.80	0.01	0.02	0.18	2.50	0.110	99.28
ap-28-f	28-f-3-4	52.49	45.14	0.03	0.01	0.00	2.54	0.103	100.39
ap-28-f	28-f-4-1	50.68	46.84	0.05	0.00	0.00	2.37	0.088	100.04
ap-28-f	28-f-4-2	51.51	46.84	0.04	0.00	0.03	2.19	0.061	100.69
ap-28-f	28-f-4-3	54.36	41.10	0.01	0.01	0.62	2.12	0.080	98.30
ap-28-f	28-f-4-4	51.88	44.97	0.06	0.00	0.61	2.33	0.130	100.07
	Average	53.16	43.77	0.04	0.01	0.72	2.36	0.108	100.06
	STDEV	1.34	2.31	0.02	0.01	0.46	0.18	0.026	1.09
ap-28-g	28-g-1-1	50.68	41.50	0.12	0.01	0.76	4.70	0.109	97.87
ap-28-g	28-g-1-2	51.35	41.02	0.09	0.01	0.05	4.60	0.097	97.23
ap-28-g	28-g-1-3	50.15	42.38	0.11	0.01	0.09	4.62	0.093	97.51
ap-28-g	28-g-1-4	50.20	41.67	0.11	0.00	0.43	4.58	0.075	97.05
ap-28-g	28-g-1-5	49.53	42.64	0.08	0.00	0.99	5.51	0.095	98.87

Run No.	Analyse No.	CaO	P_2O_5	Na_2O	K_2O	F	Cl	Br	Total
ap-28-g	28-g-2-1	51.49	41.93	0.09	0.02	0.82	3.08	0.071	97.53
ap-28-g	28-g-2-2	49.28	43.67	0.10	0.00	0.48	3.38	0.112	97.03
ap-28-g	28-g-2-3	49.64	42.74	0.09	0.01	0.80	3.31	0.081	96.73
ap-28-g	28-g-2-4	52.95	40.48	0.06	0.00	0.69	3.04	0.065	97.30
ap-28-g	28-g-2-5	55.21	39.34	0.09	0.01	0.74	2.20	0.051	97.67
ap-28-g	28-g-2-6	49.38	45.93	0.11	0.01	0.00	2.19	0.049	97.69
ap-28-g	28-g-3-1	51.26	42.12	0.12	0.02	0.51	3.07	0.084	97.22
ap-28-g	28-g-3-2	50.21	43.88	0.11	0.00	0.60	3.26	0.069	98.19
ap-28-g	28-g-3-3	51.52	42.73	0.10	0.00	0.89	3.11	0.069	98.45
ap-28-g	28-g-3-4	50.85	40.86	0.13	0.05	0.97	3.31	0.064	96.24
ap-28-g	28-g-3-5	55.99	38.98	0.08	0.00	0.69	2.25	0.045	98.07
ap-28-g	28-g-4-1	50.76	43.10	0.07	0.00	0.45	3.44	0.076	97.94
ap-28-g	28-g-4-2	51.90	40.48	0.13	0.01	0.25	3.43	0.094	96.31
ap-28-g	28-g-4-3	53.49	41.39	0.08	0.02	0.00	2.52	0.055	97.56
ap-28-g	28-g-4-4	53.77	42.55	0.08	0.02	0.46	2.18	0.062	99.12
	Average	51.48	41.97	0.10	0.01	0.59	3.39	0.076	97.58
	STDEV	1.91	1.60	0.02	0.01	0.32	0.96	0.019	0.75
ap-28-h	28-h-1-1	48.34	41.92	0.10	0.01	0.00	5.68	0.120	96.20
ap-28-h	28-h-1-2	49.11	41.43	0.10	0.00	0.00	5.85	0.148	96.64
ap-28-h	28-h-1-3	50.64	41.10	0.10	0.02	0.00	5.65	0.135	97.66
ap-28-h	28-h-1-4	48.51	42.50	0.08	0.01	0.00	5.62	0.112	96.89
ap-28-h	28-h-1-5	51.85	43.68	0.09	0.02	0.00	4.32	0.096	100.07
ap-28-h	28-h-1-6	50.79	44.02	0.07	0.02	0.00	4.00	0.109	99.01
ap-28-h	28-h-1-7	55.64	37.88	0.11	0.03	0.00	4.13	0.107	97.93
ap-28-h	28-h-2-1	52.11	39.00	0.10	0.00	0.00	5.82	0.170	97.23
ap-28-h	28-h-2-2	48.59	42.23	0.13	0.01	0.00	5.81	0.155	96.95
ap-28-h	28-h-2-3	51.55	38.91	0.13	0.00	0.00	5.94	0.117	96.68
ap-28-h	28-h-2-4	50.42	40.43	0.09	0.01	0.00	5.93	0.132	97.04
ap-28-h	28-h-2-5	50.34	44.26	0.12	0.03	0.00	4.36	0.127	99.30
ap-28-h	28-h-2-6	54.60	37.82	0.14	0.01	0.00	4.16	0.114	96.87
ap-28-h	28-h-2-7	50.52	44.23	0.11	0.01	0.00	4.48	0.100	99.45
ap-28-h	28-h-3-1	52.95	36.51	0.11	0.01	0.00	5.94	0.126	95.64
ap-28-h	28-h-3-2	48.74	41.27	0.10	0.01	0.00	5.81	0.144	96.13
ap-28-h	28-h-3-3	49.34	40.32	0.11	0.01	0.00	5.82	0.148	95.74
ap-28-h	28-h-3-4	52.38	37.40	0.09	0.00	0.00	6.02	0.129	96.05
ap-28-h	28-h-3-5	50.10	44.19	0.10	0.02	0.00	4.61	0.123	99.17
ap-28-h	28-h-3-6	53.45	37.83	0.11	0.02	0.00	4.52	0.105	96.04
ap-28-h	28-h-4-1	53.65	40.06	0.09	0.02	0.00	5.02	0.088	98.93
ap-28-h	28-h-4-2	50.35	44.24	0.08	0.03	0.00	6.24	0.093	101.06
ap-28-h	28-h-4-3	50.32	46.28	0.09	0.01	0.00	5.14	0.145	102.00
ap-28-h	28-h-4-4	52.30	43.18	0.09	0.03	0.00	4.69	0.098	100.44
	Average	51.11	41.28	0.10	0.01	0.00	5.23	0.123	97.88
	STDEV	1.98	2.69	0.02	0.01	0.00	0.74	0.022	1.82
ap35a-3	35-a-1-1	55.79	40.64	0.03	0.03	0.00	3.81	0.076	100.37
ap35a-3	35-a-1-2	55.34	40.23	0.00	0.01	0.00	4.71	0.082	100.38
ap35a-3	35-a-1-3	56.13	40.73	0.02	0.04	0.00	3.41	0.054	100.38
ap35a-2	35-a-2-1	55.90	40.07	0.00	0.00	0.00	6.10	0.096	102.16
ap35a-2	35-a-2-2	54.49	39.37	0.00	0.03	0.00	5.24	0.100	99.22

Run No.	Analyse No.	CaO	P_2O_5	Na_2O	K_2O	F	Cl	Br	Total
ap35a-2	35-a-2-3	55.20	39.65	0.00	0.00	0.00	5.76	0.087	100.70
ap35a-1	35-a-3-1	57.83	38.47	0.00	0.02	0.00	3.12	0.085	99.53
ap35a-1	35-a-3-2	55.49	39.90	0.02	0.01	0.00	3.28	0.051	98.75
ap35a-4	35-a-4-1	55.41	41.32	0.04	0.02	0.00	3.18	0.080	100.04
ap35a-4	35-a-4-2	56.06	40.08	0.06	0.01	0.02	3.40	0.060	99.69
	Average	55.76	40.05	0.02	0.02	0.00	4.20	0.077	100.12
	STDEV	0.87	0.79	0.02	0.01	0.01	1.15	0.017	0.94
ap-36-a	36-a-1-1	52.07	41.83	0.06	0.00	0.60	5.33	0.035	99.92
ap-36-a	36-a-1-2	51.56	42.97	0.06	0.02	0.56	5.14	0.035	100.35
ap-36-a	36-a-1-3	52.26	41.87	0.08	0.00	0.56	5.29	0.025	100.10
ap-36-a	36-a-2-1	51.43	43.17	0.07	0.01	0.46	5.69	0.048	100.87
ap-36-a	36-a-2-2	52.25	41.66	0.07	0.02	0.46	5.66	0.030	100.15
ap-36-a	36-a-2-3	51.90	41.81	0.04	0.00	0.47	5.69	0.026	99.93
ap-36-a	36-a-3-1	51.63	41.03	0.06	0.00	0.75	4.52	0.027	98.02
ap-36-a	36-a-3-2	51.49	41.44	0.07	0.00	0.79	5.80	0.025	99.62
ap-36-a	36-a-3-3	51.65	39.08	0.08	0.01	0.77	6.09	0.033	97.72
ap-36-a	36-a-4-1	51.66	43.55	0.08	0.00	0.78	5.50	0.030	101.60
ap-36-a	36-a-4-2	51.92	41.21	0.06	0.00	0.77	4.26	0.025	98.26
ap-36-a	36-a-4-3	52.39	43.06	0.04	0.00	0.75	4.03	0.021	100.29
ap-36-a	36-a-5-1	51.41	42.53	0.07	0.01	0.75	3.62	0.026	98.43
ap-36-a	36-a-5-2	52.11	40.96	0.04	0.01	0.58	5.47	0.027	99.20
ap-36-a	36-a-6-1	51.99	42.94	0.08	0.01	0.93	2.94	0.045	98.93
ap-36-a	36-a-6-2	50.26	41.78	0.06	0.01	0.96	4.59	0.036	97.70
ap-36-a	36-a-7-1	51.65	42.24	0.04	0.02	0.92	4.32	0.014	99.19
ap-36-a	36-a-7-2	51.48	40.75	0.06	0.00	0.94	4.73	0.014	97.98
ap-36-a	36-a-8-1	51.90	42.64	0.06	0.00	0.81	4.80	0.033	100.24
ap-36-a	36-a-8-2	52.09	41.54	0.07	0.01	0.78	5.08	0.021	99.60
ap-36-a	36-a-9-1	51.60	43.11	0.10	0.00	1.00	3.92	0.022	99.74
ap-36-a	36-a-9-2	51.61	41.53	0.03	0.01	0.80	4.46	0.010	98.45
ap-36-a	36-a-10-1	51.06	41.53	0.06	0.02	0.86	4.58	0.025	98.14
ap-36-a	36-a-10-2	51.31	41.30	0.07	0.01	0.88	5.37	0.031	98.97
ap-36-a	36-a-11-1	51.83	40.66	0.05	0.00	0.48	5.75	0.022	98.80
ap-36-a	36-a-11-2	51.96	43.21	0.03	0.00	0.49	5.62	0.037	101.36
ap-36-a	36-a-11-3	51.99	41.86	0.10	0.01	0.47	5.73	0.018	100.19
ap-36-a	36-a-12-1	51.03	42.54	0.07	0.00	0.95	3.79	0.006	98.38
ap-36-a	36-a-12-2	51.98	41.17	0.09	0.00	0.77	4.01	0.009	98.02
ap-36-a	36-a-12-3	51.65	41.70	0.04	0.01	0.81	4.78	0.022	99.02
	Average	51.70	41.89	0.06	0.01	0.73	4.89	0.026	99.31
	STDEV	0.43	0.97	0.02	0.01	0.17	0.78	0.010	1.08
ap-36b	36-b-1-1	52.94	42.78	0.02	0.00	2.28	2.34	0.036	100.39
ap-36b	36-b-1-2	53.11	42.93	0.03	0.00	2.32	2.30	0.035	100.73
ap-36b	36-b-1-3	53.15	43.07	0.01	0.00	2.35	2.30	0.021	100.90
ap-36b	36-b-2-1	52.73	43.11	0.04	0.00	2.60	2.26	0.012	100.76
ap-36b	36-b-2-2	52.92	44.17	0.00	0.00	2.64	2.23	0.038	102.01
ap-36b	36-b-3-1	52.25	43.23	0.02	0.02	2.33	2.34	0.019	100.21
ap-36b	36-b-3-2	52.99	42.82	0.00	0.00	2.29	2.32	0.026	100.45
ap-36b	36-b-3-3	51.79	42.61	0.00	0.00	2.27	2.23	0.039	98.94
ap-36b	36-b-3-4	52.57	43.40	0.02	0.01	3.11	1.95	0.018	101.08

Run No.	Analyse No.	CaO	P_2O_5	Na_2O	K_2O	F	Cl	Br	Total
ap-36b	36-b-4-1	53.30	42.96	0.06	0.00	3.03	2.00	0.027	101.39
ap-36b	36-b-4-2	53.12	43.21	0.07	0.00	3.25	1.89	0.017	101.55
ap-36b	36-b-4-3	52.21	44.07	0.00	0.00	2.97	1.93	0.000	101.18
ap-36b	36-b-5-1	53.44	43.18	0.03	0.03	2.37	2.35	0.032	101.43
ap-36b	36-b-5-2	53.26	42.59	0.05	0.00	2.32	2.29	0.017	100.54
ap-36b	36-b-5-3	53.68	43.75	0.04	0.00	2.25	2.30	0.031	102.06
ap-36b	36-b-6-1	53.58	43.21	0.02	0.00	2.90	2.08	0.028	101.83
ap-36b	36-b-6-2	53.32	43.27	0.02	0.01	2.89	2.03	0.020	101.56
ap-36b	36-b-6-3	52.40	43.02	0.02	0.00	2.83	2.07	0.024	100.36
ap-36b	36-b-7-1	53.40	41.71	0.02	0.00	2.41	2.25	0.021	99.81
ap-36b	36-b-7-2	53.01	42.97	0.02	0.00	2.37	2.30	0.046	100.72
ap-36b	36-b-7-3	53.18	42.44	0.00	0.00	2.40	2.23	0.023	100.26
ap-36b	36-b-8-1	52.46	42.59	0.02	0.01	0.17	2.04	0.002	97.29
ap-36b	36-b-8-2	52.76	41.21	0.03	0.00	0.01	1.92	0.034	95.97
ap-36b	36-b-8-3	52.76	40.09	0.02	0.00	0.00	2.02	0.006	94.89
ap-36b	36-b-9-1	52.86	41.76	0.05	0.02	2.28	2.27	0.031	99.27
ap-36b	36-b-9-2	52.86	41.55	0.03	0.00	2.37	2.25	0.034	99.09
ap-36b	36-b-9-3	52.37	41.78	0.02	0.00	2.92	2.03	0.017	99.15
ap-36b	36-b-9-4	53.48	41.44	0.04	0.00	0.19	2.07	0.028	97.24
	Average	52.93	42.68	0.03	0.00	2.57	2.16	0.024	100.04
	STDEV	0.46	0.91	0.02	0.01	0.93	0.15	0.011	1.79
Fluorapatite									
ap-29-a	29-a-1-1	54.11	41.70	0.00	0.03	4.20	0.03	0.004	100.07
ap-29-a	29-a-1-2	54.48	41.39	0.00	0.00	4.23	0.01	0.002	100.11
ap-29-a	29-a-1-3	54.59	42.53	0.00	0.00	4.13	0.02		101.26
ap-29-a	29-a-1-4	54.47	42.26	0.00	0.00	4.21	0.02	0.009	100.98
ap-29-a	29-a-1-5	54.87	41.65	0.00	0.00	5.30	0.03		101.85
ap-29-a	29-a-1-6	54.53	42.47		0.05	3.98	0.01		101.05
ap-29-a	29-a-2-1	54.41	42.73	0.00	0.00	6.05	0.02	0.015	103.23
ap-29-a	29-a-2-2	55.01	42.03	0.00	0.01	5.60	0.04	0.007	102.70
ap-29-a	29-a-2-3	55.04	42.41	0.00	0.00	5.98	0.03		103.46
ap-29-a	29-a-2-4	55.23	41.73	0.00	0.01	5.47	0.04	0.009	102.49
ap-29-a	29-a-2-5	57.56	42.43		0.08	4.30	0.01	0.032	104.41
ap-29-a	29-a-2-6	57.87	42.62		0.01	4.33	0.03	0.030	104.90
ap-29-a	29-a-3-1	58.28	42.40	0.00	0.00	4.21	0.01	0.009	104.91
ap-29-a	29-a-3-2	58.46	41.88	0.00	0.01	4.13	0.01	0.013	104.50
ap-29-a	29-a-3-3	58.69	42.76	0.00	0.00	4.29	0.01	0.002	105.75
ap-29-a	29-a-3-4	55.17	42.32	0.00	0.00	5.30	0.01		102.81
ap-29-a	29-a-3-5	54.76	41.96		0.03	4.12	0.05		100.91
	Average	55.74	42.19	0.00	0.01	4.70	0.03	0.012	102.67
	STDEV	1.66	0.41	0.00	0.02	0.73	0.01	0.010	1.79
ap-29-b	29-b-1-1	54.35	41.88		0.00	3.88	0.00		100.10
ap-29-b	29-b-1-2	55.05	42.07	0.00	0.00	5.61	0.00		102.73
ap-29-b	29-b-1-3	55.39	41.83	0.00	0.00	5.49	0.01	0.006	102.73
ap-29-b	29-b-1-4	54.09	42.25	0.00	0.00	6.36	0.01		102.71
ap-29-b	29-b-1-5	54.26	42.70	0.00	0.00	6.12	0.00	0.013	103.10
ap-29-b	29-b-2-1	56.80	42.20		0.00	4.61	0.01	0.027	103.65
ap-29-b	29-b-2-2	56.87	42.59		0.00	4.38	0.00	0.034	103.87
ap-29-b	29-b-2-3	56.60	41.70		0.05	5.50	0.00		103.86

Run No.	Analyse No.	CaO	P_2O_5	Na_2O	K_2O	F	Cl	Br	Total
ap-29-b	29-b-3-1	54.70	42.24		0.00	4.34	0.00	0.010	101.30
ap-29-b	29-b-3-2	54.61	42.62		0.00	3.66	0.00	0.023	100.91
ap-29-b	29-b-3-3	55.79	41.89		0.04	4.45	0.00	0.005	102.18
ap-29-b	29-b-4-1	55.35	42.20		0.01	4.35	0.01	0.004	101.93
ap-29-b	29-b-4-2	55.79	42.10		0.01	4.45	0.01	0.025	102.38
ap-29-b	29-b-4-3	55.53	42.76	0.00	0.00	6.07	0.01		104.37
ap-29-b	29-b-4-4	55.11	42.38	0.00	0.01	5.60	0.00		103.10
ap-29-b	29-b-4-5	55.14	43.11	0.00	0.00	5.53	0.01	0.011	103.80
	Average	55.34	42.28	0.00	0.01	5.03	0.01	0.016	102.67
	STDEV	0.87	0.39	0.00	0.02	0.85	0.01	0.011	1.18
ap-29-c	29-c-1-1	54.19	42.33	0.00	0.00	5.96	0.01	0.021	102.52
ap-29-c	29-c-1-2	54.44	42.85	0.00	0.01	5.38	0.01		102.69
ap-29-c	29-c-1-3	54.10	41.93	0.00	0.01	5.70	0.00		101.76
ap-29-c	29-c-2-1	54.29	41.50	0.00	0.00	5.59	0.01	0.016	101.41
ap-29-c	29-c-2-2	53.97	42.71	0.00	0.00	5.55	0.01	0.021	102.26
ap-29-c	29-c-2-3	53.92	41.98	0.00	0.00	5.49	0.01	0.008	101.41
ap-29-c	Average	54.15	42.22	0.00	0.00	5.61	0.01	0.016	102.01
	STDEV	0.20	0.51	0.00	0.01	0.20	0.00	0.006	0.56
ap-29-c(R)	29-c-r-1-1	56.80	42.95	0.04	0.01	4.58	0.00	0.025	104.40
ap-29-c(R)	29-c-r-1-2	56.92	41.82	0.06	0.00	4.27	0.00	0.030	103.11
ap-29-c(R)	29-c-r-1-3	56.95	42.20	0.02	0.00	4.34	0.01	0.016	103.52
ap-29-c(R)	29-c-r-1-4	57.36	42.44	0.03	0.00	4.53	0.00	0.012	104.38
ap-29-c(R)	29-c-r-2-1	58.04	35.92	0.02	0.01	4.05	0.00	0.010	98.05
ap-29-c(R)	29-c-r-2-2	58.10	37.87	0.03	0.00	3.72	0.00	0.022	99.74
ap-29-c(R)	29-c-r-2-3	57.88	36.10	0.00	0.00	3.31	0.00	0.010	97.30
ap-29-c(R)	29-c-r-3-1	58.31	41.77	0.00	0.00	3.14	0.00	0.014	103.23
ap-29-c(R)	29-c-r-3-2	57.62	42.95	0.02	0.00	4.10	0.00	0.024	104.72
ap-29-c(R)	29-c-r-3-3	57.77	43.33	0.02	0.00	4.38	0.00	0.012	105.51
ap-29-c(R)	29-c-r-3-4	57.39	42.29	0.02	0.00	3.92	0.00	0.012	103.64
ap-29-c(R)	29-c-r-3-5	57.84	43.14	0.02	0.00	2.89	0.01	0.020	103.91
ap-29-c(R)	29-c-r-3-6	57.86	43.35	0.01	0.00	3.16	0.01	0.004	104.39
ap-29-c(R)	29-c-r-3-7	53.44	43.69	0.42	0.00	4.64	0.02	0.017	102.23
	Average	57.31	41.42	0.05	0.00	3.93	0.00	0.016	103.63
	STDEV	1.21	2.69	0.11	0.00	0.59	0.01	0.007	2.54
ap-29-d	29-d-1-1	54.62	42.08	0.00	0.02	5.78	0.00	0.036	102.54
ap-29-d	29-d-1-2	54.62	42.68	0.00	0.00	5.87	0.00	0.028	103.20
ap-29-d	29-d-1-3	55.83	42.13	0.00	0.00	5.74	0.00	0.008	103.71
ap-29-d	29-d-2-1	54.05	43.04	0.00	0.00	4.34	0.00	0.013	101.45
ap-29-d	29-d-2-2	54.28	42.60	0.00	0.02	4.16	0.01	0.018	101.09
ap-29-d	29-d-2-3	53.69	43.66	0.00	0.00	4.11	0.00	0.024	101.48
ap-29-d	29-d-3-1	56.95	42.04	0.00	0.01	4.08	0.01	0.011	103.10
ap-29-d	29-d-3-2	53.86	43.83	0.03	0.00	5.16	0.01	0.048	102.93
ap-29-d	29-d-3-3	56.49	43.76	0.03	0.01	3.86	0.01	0.012	104.18
ap-29-d	29-d-4-1	55.88	43.95	0.10	0.00	2.42	0.00	0.025	102.39
ap-29-d	29-d-5-1	53.71	43.59	0.09	0.00	4.44	0.00	0.024	101.86
	Average	54.91	43.03	0.02	0.01	4.54	0.00	0.022	102.54
	STDEV	1.17	0.76	0.04	0.01	1.03	0.00	0.012	0.99

Run No.	Analyse No.	CaO	P_2O_5	Na_2O	K_2O	F	Cl	Br	Total
ap-29-d(R)	29-d-R-1-1	53.80	41.97	0.00	0.00	4.19	0.00	0.001	99.96
ap-29-d(R)	29-d-R-1-2	53.67	41.61	0.00	0.00	4.03	0.01	0.000	99.32
ap-29-d(R)	29-d-R-1-3	54.14	40.74	0.00	0.00	4.12	0.00	0.000	99.00
ap-29-d(R)	29-d-R-2-1	58.12	42.06	0.11	0.00	4.40	0.01	0.000	104.71
ap-29-d(R)	29-d-R-2-2	57.75	41.48	0.00	0.01	4.85	0.00	0.000	104.08
ap-29-d(R)	29-d-R-2-3	58.04	42.03	0.01	0.00	5.63	0.01	0.008	105.74
ap-29-d(R)	29-d-R-3-1	57.53	41.46	0.00	0.00	4.01	0.01	0.007	103.02
ap-29-d(R)	29-d-R-3-2	57.55	41.40	0.00	0.00	5.67	0.00	0.002	104.63
ap-29-d(R)	29-d-R-3-3	58.30	40.89	0.00	0.00	3.89	0.01	0.000	103.09
ap-29-d(R)	29-d-R-4-1	55.41	41.37	0.00	0.00	5.12	0.00	0.003	101.91
ap-29-d(R)	29-d-R-4-2	55.68	41.21	0.00	0.00	4.71	0.01	0.015	101.63
ap-29-d(R)	29-d-R-4-3	56.18	41.39	0.01	0.00	4.54	0.00	0.000	102.12
	Average	56.35	41.47	0.01	0.00	4.60	0.01	0.006	102.43
	STDEV	1.77	0.41	0.03	0.00	0.62	0.01	0.005	2.20
ap-29-e	29-e-1-1	57.49	40.46	0.00	0.00	3.94	0.00	0.008	101.91
ap-29-e	29-e-1-2	57.63	41.67	0.00	0.02	3.96	0.00	0.012	103.30
ap-29-e	29-e-1-3	56.56	40.81	0.00	0.00	4.13	0.00	0.025	101.53
ap-29-e	29-e-2-1	56.62	40.07	0.00	0.00	5.20	0.01	0.016	101.93
ap-29-e	29-e-2-2	55.47	41.07	0.00	0.00	4.45	0.00	0.010	101.00
ap-29-e	29-e-2-3	55.61	42.33	0.00	0.00	4.17	0.00	0.020	102.12
	Average	56.56	41.07	0.00	0.00	4.31	0.01	0.015	101.97
	STDEV	0.91	0.82	0.00	0.01	0.47	0.01	0.006	0.77
ap-29-h	29-h-1-1	56.90	41.99	0.00	0.01	3.86	0.01	0.000	102.77
ap-29-h	29-h-2-1	54.92	41.17	0.00	0.00	5.37	0.01	0.000	101.46
ap-29-h	29-h-2-2	55.40	41.28	0.00	0.00	5.61	0.00	0.000	102.28
ap-29-h	29-h-2-3	54.82	41.01	0.00	0.01	5.84	0.00	0.001	101.69
ap-29-h	29-h-3-1	55.32	40.60	0.00	0.01	5.39	0.01	0.008	101.33
ap-29-h	29-h-3-2	54.01	40.08	0.00	0.00	5.39	0.00	0.000	99.48
ap-29-h	29-h-3-3	55.22	39.81	0.00	0.00	5.67	0.00	0.010	100.71
ap-29-h	29-h-3-4	54.37	40.89	0.00	0.00	5.68	0.00	0.011	100.95
ap-29-h	29-h-4-1	57.31	41.01	0.00	0.00	3.93	0.01	0.000	102.26
ap-29-h	29-h-4-2	57.84	40.90	0.00	0.00	3.87	0.00	0.013	102.63
ap-29-h	29-h-4-3	57.90	41.60	0.00	0.00	4.27	0.01	0.007	103.79
ap-29-h	29-h-4-4	57.74	41.14	0.00	0.00	3.89	0.00	0.010	102.79
	Average	55.98	40.96	0.00	0.00	4.90	0.01	0.009	101.85
	STDEV	1.45	0.59	0.00	0.00	0.84	0.00	0.005	1.15
ap-30-a	30-a-1-1	52.55	46.15	0.00	0.01	3.73	0.02	0.014	102.49
ap-30-a	30-a-1-2	50.67	47.49	0.00	0.01	4.29	0.02	0.010	102.49
ap-30-a	30-a-1-3	54.95	41.81	0.02	0.02	5.39	0.02	0.000	102.22
ap-30-a	30-a-2-1	56.38	40.67	0.02	0.00	4.38	0.02	0.014	101.49
ap-30-a	30-a-2-2	56.45	40.35	0.01	0.00	2.31	0.02	0.002	99.18
ap-30-a	30-a-2-3	55.00	45.20	0.00	0.01	5.85	0.03	0.010	106.12
ap-30-a	30-a-3-1	55.04	42.39	0.01	0.02	5.09	0.02	0.018	102.59
ap-30-a	30-a-3-2	50.58	48.06	0.00	0.00	4.51	0.01	0.006	103.19
ap-30-a	30-a-3-3	53.37	44.59	0.00	0.00	4.58	0.02	0.000	102.58
	Average	53.89	44.08	0.01	0.01	4.46	0.02	0.010	102.48
	STDEV	2.23	2.89	0.01	0.01	1.02	0.01	0.006	1.79

Run No.	Analyse No.	CaO	P_2O_5	Na_2O	K_2O	F	Cl	Br	Total
ap-30-a(R)	30-a-R-1-1	52.66	47.30	0.01	0.01	4.13	0.02	0.013	104.14
ap-30-a(R)	30-a-R-1-2	50.80	48.15	0.02	0.00	4.69	0.02	0.000	103.71
ap-30-a(R)	30-a-R-1-3	51.60	47.96	0.00	0.01	3.53	0.02	0.001	103.14
ap-30-a(R)	30-a-R-2-1	54.75	44.92	0.00	0.01	4.02	0.00	0.000	103.73
ap-30-a(R)	30-a-R-2-2	55.13	41.35	0.03	0.00	5.59	0.02	0.020	102.14
ap-30-a(R)	30-a-R-3-1	54.60	43.87	0.01	0.22	4.71	0.02	0.006	103.43
ap-30-a(R)	30-a-R-3-2	56.77	41.07	0.03	0.18	3.82	0.03	0.000	101.93
	Average	53.76	44.95	0.01	0.06	4.36	0.02	0.010	103.17
	STDEV	2.13	3.00	0.01	0.10	0.69	0.01	0.008	0.84
ap-30-b	30-b-1-1	51.56	45.59	0.02	0.02	2.66	0.03	0.000	99.89
ap-30-b	30-b-1-2	52.66	43.74	0.01	0.01	5.30	0.04	0.000	101.79
ap-30-b	30-b-1-3	50.64	47.15	0.06	0.20	4.31	0.06	0.003	102.46
ap-30-b	30-b-2-1	55.62	40.66	0.02	0.04	4.18	0.05	0.010	100.60
ap-30-b	30-b-2-2	49.62	47.09	0.02	0.02	4.21	0.05	0.002	101.02
ap-30-b	30-b-2-3	51.97	44.62	0.02	0.03	6.46	0.04	0.005	103.15
ap-30-b	30-b-2-4	53.31	43.54	0.00	0.02	4.66	0.03	0.001	101.58
ap-30-b	30-b-2-5	52.74	44.49	0.00	0.05	4.47	0.06	0.000	101.87
ap-30-b	30-b-2-6	50.22	46.92	0.00	0.03	4.53	0.04	0.000	101.79
ap-30-b	30-b-3-1	54.56	43.24	0.03	0.01	4.66	0.02	0.000	102.52
ap-30-b	30-b-3-2	51.79	47.34	0.00	0.00	3.72	0.04	0.000	102.93
ap-30-b	30-b-3-3	52.94	44.45	0.00	0.00	2.11	0.04	0.000	99.57
	Average	52.30	44.90	0.02	0.04	4.27	0.04	0.003	101.60
	STDEV	1.73	2.02	0.02	0.05	1.12	0.01	0.003	1.14
ap-30-b(R)	30-b-R-1-1	50.19	47.74	0.00	0.04	2.13	0.04	0.012	100.15
ap-30-b(R)	30-b-R-1-2	54.76	42.92	0.00	0.04	4.03	0.04	0.000	101.78
ap-30-b(R)	30-b-R-1-3	54.20	42.20	0.01	0.05	4.45	0.05	0.018	101.02
ap-30-b(R)	30-b-R-2-1	52.05	45.54	0.00	0.00	4.50	0.04	0.000	102.14
ap-30-b(R)	30-b-R-2-2	55.48	41.83	0.01	0.00	2.41	0.03	0.009	99.77
ap-30-b(R)	30-b-R-2-3	50.98	46.86	0.02	0.01	2.11	0.04	0.019	100.04
ap-30-b(R)	30-b-R-3-1	52.23	45.59	0.00	0.03	4.45	0.04	0.008	102.35
ap-30-b(R)	30-b-R-3-2	51.58	46.43	0.01	0.05	6.77	0.05	0.006	104.90
ap-30-b(R)	30-b-R-3-3	52.55	46.84	0.01	0.13	3.20	0.04	0.000	102.76
ap-30-b(R)	30-b-R-3-4	52.06	47.28	0.03	0.04	5.07	0.03	0.000	104.50
ap-30-b(R)	30-b-R-3-5	51.41	46.96	0.02	0.05	5.52	0.05	0.001	104.03
	Average	52.50	45.47	0.01	0.04	4.06	0.04	0.010	102.13
	STDEV	1.64	2.14	0.01	0.03	1.48	0.01	0.007	1.80
ap-30-c	30-c--1-1	53.89	43.89	0.00	0.02	3.92	0.04	0.000	101.77
ap-30-c	30-c--1-2	54.23	43.04	0.00	0.02	3.89	0.04	0.004	101.23
ap-30-c	30-c--1-3	54.17	43.38	0.09	0.03	3.85	0.05	0.008	101.58
ap-30-c	30-c--1-4	56.38	42.38		0.04	4.70	0.07		103.57
ap-30-c	30-c--2-1	56.16	43.36	0.00	0.01	2.72	0.03	0.002	102.29
ap-30-c	30-c--2-2	55.05	43.79	0.01	0.01	2.88	0.03	0.007	101.78
ap-30-c	30-c--2-3	55.81	44.31	0.01	0.01	2.89	0.03	0.005	103.07
ap-30-c	30-c--3-1	53.97	43.14	0.00	0.01	4.18	0.05	0.012	101.36
ap-30-c	30-c--3-2	53.97	43.52	0.01	0.01	4.00	0.04	0.007	101.56
ap-30-c	30-c--3-3	54.10	44.19	0.01	0.02	3.91	0.04	0.002	102.27
	Average	54.77	43.50	0.01	0.02	3.69	0.04	0.006	102.05
	STDEV	0.99	0.58	0.03	0.01	0.65	0.01	0.004	0.76

Run No.	Analyse No.	CaO	P_2O_5	Na_2O	K_2O	F	Cl	Br	Total
ap-30-c(R)	30-c-R-1-1	53.50	43.59	0.00	0.01	4.07	0.04	0.004	101.22
ap-30-c(R)	30-c-R-1-2	53.90	42.81	0.01	0.01	4.03	0.04	0.005	100.82
ap-30-c(R)	30-c-R-1-3	53.88	43.56	0.01	0.02	4.05	0.05	0.004	101.57
ap-30-c(R)	30-c-R-2-1	54.16	43.14	0.00	0.02	4.43	0.05	0.002	101.79
ap-30-c(R)	30-c-R-2-2	53.73	43.43	0.00	0.01	4.97	0.04	0.000	102.18
ap-30-c(R)	30-c-R-2-3	53.80	43.22	0.00	0.01	4.46	0.04	0.006	101.55
ap-30-c(R)	30-c-R-3-1	54.43	43.43	0.00	0.01	4.47	0.04	0.006	102.39
ap-30-c(R)	30-c-R-3-2	54.34	43.33	0.01	0.02	4.50	0.04	0.003	102.23
ap-30-c(R)	30-c-R-3-3	54.23	43.07	0.05	0.02	4.44	0.08	0.012	101.91
	Average	54.00	43.29	0.01	0.01	4.38	0.05	0.005	101.74
	STDEV	0.31	0.25	0.02	0.00	0.30	0.01	0.003	0.51
ap-32-a	32-a-1-4	49.63	41.85	0.07	0.02	4.57	0.03	0.004	96.18
ap-32-a	32-a-1-5	57.65	38.50	0.01	0.03	2.70	0.04	0.010	98.95
ap-32-a	32-a-1-6	57.66	42.12	0.02	0.03	2.19	0.03	0.003	102.05
ap-32-a	32-a-1-7	56.84	38.09	0.01	0.02	2.88	0.02	0.003	97.86
ap-32-a	32-a-2-4	56.58	36.72	0.01	0.01	3.53	0.02	0.007	96.90
ap-32-a	32-a-2-5	58.77	38.79	0.00	0.02	3.87	0.03	0.016	101.51
ap-32-a	32-a-2-6	56.98	35.90	0.01	0.01	3.80	0.02	0.010	96.73
ap-32-a	32-a-3-4	58.95	43.65	0.00	0.01	2.87	0.03	0.001	105.51
ap-32-a	32-a-3-5	59.30	40.97	0.00	0.02	3.58	0.02	0.010	103.89
ap-32-a	32-a-3-6	59.39	41.57	0.01	0.02	3.21	0.03	0.000	104.22
ap-32-a	32-a-3-7	59.20	40.32	0.00	0.02	3.29	0.02	0.000	102.86
ap-32-a	32-a-4-1	58.11	44.16	0.02	0.01	2.38	0.03	0.009	104.72
ap-32-a	32-a-4-2	56.70	41.40	0.00	0.01	4.09	0.04	0.000	102.25
ap-32-a	32-a-4-3	57.09	42.63	0.01	0.02	3.72	0.04	0.010	103.51
ap-32-a	32-a-4-4	58.38	41.96	0.01	0.00	2.77	0.00	0.005	103.12
ap-32-a	32-a-4-5	58.77	41.35	0.03	0.00	3.33	0.00	0.008	103.50
ap-32-a	32-a-4-6	58.48	37.97	0.03	0.00	3.88	0.00	0.002	100.36
ap-32-a	32-a-4-7	58.87	37.14	0.03	0.00	3.75	0.00	0.008	99.80
ap-32-a	32-a-4-8	57.92	38.82	0.00	0.00	3.76	0.00	0.000	100.50
ap-32-a	32-a-4-9	58.25	39.28	0.03	0.00	3.25	0.00	0.003	100.82
	Average	57.68	40.16	0.02	0.01	3.37	0.03	0.006	101.26
	STDEV	2.10	2.35	0.02	0.01	0.60	0.02	0.004	2.80
ap-33-a	33-a-1-1	55.17	41.96	0.00	0.01	4.85	0.00	0.008	102.00
ap-33-a	33-a-1-2	55.15	41.76	0.02	0.00	5.67	0.01	0.020	102.62
ap-33-a	33-a-1-3	55.00	41.05	0.04	0.02	5.70	0.00	0.011	101.81
ap-33-a	33-a-2-1	57.09	41.87	0.00	0.01	4.49	0.00	0.019	103.48
ap-33-a	33-a-2-2	54.81	40.78	0.00	0.00	6.28	0.00	0.005	101.88
ap-33-a	33-a-2-3	55.45	40.93	0.12	0.00	6.26	0.00	0.009	102.78
ap-33-a	33-a-2-4	54.86	41.59	0.10	0.00	5.95	0.00	0.015	102.51
ap-33-a	33-a-2-5	56.80	40.83	0.00	0.00	5.01	0.01	0.019	102.67
ap-33-a	Average	55.54	41.35	0.03	0.01	5.53	0.00	0.013	102.47
	STDEV	0.89	0.50	0.05	0.01	0.67	0.00	0.006	0.56
ap-33-b	33-b-1-1	54.80	43.73	0.00	0.00	4.81	0.01	0.013	103.37
ap-33-b	33-b-1-2	54.49	43.55	0.03	0.00	4.81	0.01	0.004	102.90
ap-33-b	33-b-1-3	54.67	43.27	0.00	0.00	5.52	0.01	0.000	103.47
ap-33-b	33-b-2-1	52.94	42.40	0.03	0.00	4.52	0.05	0.002	99.95
ap-33-b	33-b-3-1	53.56	43.16	0.02	0.00	5.33	0.01	0.000	102.07
	Average	54.09	43.22	0.02	0.00	5.00	0.02	0.006	102.35
	STDEV	0.81	0.51	0.02	0.00	0.41	0.02	0.006	1.45

Appendix 3a Micro XRF Analytical Results of Aoshan Apatite (ppm)

Sample No.	Analyse No.	Mn	Fe (wt %)	Zn	Sr	Y	Ce	Pb	Th	Ni	Cu	Br
99-6-3	3-a-1	201	0.089	7	506	521	2	6	230			
99-6-3	3-b-1	289	0.169	11	555	580	2	10	259			
99-6-3	3-d-1	193	0.098	3	545	569	2	8	249			
99-6-3	3-d-2	169	0.097	3	550	575	2	9	258			
99-6-3	3-d-3	196	0.105	5	542	565	2	8	248			
99-6-3	**Average**	**210**	**0.111**	**6**	**540**	**562**	**2**	**8**	**249**			
	STDEV	46	0.033	3	19	24	0	2	12			
99-6-4	4-a-1	155	0.107	9	503	625	2	19	302			
99-6-4	4-a-2	268	0.144	13	529	633	3	21	326			
99-6-4	4-a-3	153	0.122	8	505	613	2	20	289			
99-6-4	4-b-1	221	0.285	11	557	626	2	20	323			
99-6-4	4-b-2	298	0.148	11	557	616	3	20	302			
99-6-4	4-b-3	222	0.156	9	540	600	3	19	313			
99-6-4	4-c-1	149	0.188	9	515	575	2	14	271			
99-6-4	4-c-2	178	0.188	5	528	591	2	13	278			
99-6-4	4-c-3	178	0.162	10	542	600	2	13	293			
99-6-4	**Average**	**202**	**0.167**	**9**	**531**	**609**	**2**	**18**	**300**			
	STDEV	53	0.052	2	20	19	0	3	19			
99-6-5	5-a-1	271	0.156	8	506	611	2	18	255			
99-6-5	5-a-2	329	0.145	6	535	610	2	17	259			
99-6-5	5-a-3	331	0.246	12	483	607	2	21	251			
99-6-5	5-b-1	268	0.187	8	508	615	2	17	251			
99-6-5	5-b-2	225	0.180	9	469	617	2	28	251			
99-6-5	5-b-3	250	0.200	6	543	614	2	17	248			
99-6-5	5-c-1	440	0.193	8	519	595	2	14	232			
99-6-5	5-c-2	475	0.215	8	528	600	2	14	231			
99-6-5	5-c-3	390	0.173	5	527	602	2	16	234			
99-6-5	5-d-1	415	0.149	36	519	595	2	20	243			

Sample No.	Analyse No.	Mn	Fe (wt %)	Zn	Sr	Y	Ce	Pb	Th	Ni	Cu	Br
99-6-5	5-d-2	334	0.154	48	490	602	2	22	244			
99-6-5	5-e-1	286	0.130	21	519	592	2	16	230			2
99-6-5	5-e-2	388	0.134	7	502	572	2	11	238			
99-6-5	5-e-3	260	0.128	58	512	577	2	23	220		18	8
99-6-5	5-e-4	304	0.127	45	500	578	2	22	230		10	10
99-6-5	5-f-1	242	0.128	56	507	571	2	23	225		21	10
99-6-5	5-f-2	237	0.115	9	521	589	2	16	245			
99-6-5	5-f-3	206	0.103	3	521	590	2	12	239			
99-6-5	5-f-4	289	0.116	2	533	614	2	13	250			
99-6-5	5-g-1	492	0.129	10	533	598	2	15	248			
99-6-5	5-g-2	423	0.133	17	498	596	2	20	261			
99-6-5	5-g-3	552	0.179	12	533	600	2	18	248			
99-6-5	**Average**	**337**	**0.155**	**18**	**514**	**598**	**2**	**18**	**242**		**16**	**7**
	STDEV	97	0.037	18	19	14	0	4	11		6	4
99-6-6	6-a-1	162	0.089	7	536	536	1	12	201			
99-6-6	6-a-2	180	0.115	8	539	556	2	16	219			
99-6-6	6-a-3	205	0.112	10	533	538	1	19	187			
99-6-6	6-b-1	217	0.157	30	529	604	2	14	285			
99-6-6	6-b-2	252	0.116	27	524	611	2	13	288			
99-6-6	6-b-3	300	0.152	36	517	593	2	13	287			
99-6-6	6-c-1	212	0.126	11	537	554	2	13	248			
99-6-6	6-c-2	206	0.123	11	541	544	2	13	240			
99-6-6	6-c-3	232	0.139	9	541	556	2	15	248			
99-6-6	6-c-4	211	0.117	12	543	549	2	13	242			
99-6-6	**Average**	**217**	**0.125**	**16**	**534**	**564**	**2**	**14**	**245**			
	STDEV	38	0.020	11	8	28	0	2	35			
99-6-7	7-a-1	211	0.136	13	535	679	3	16	320			
99-6-7	7-a-2	257	0.216	26	521	676	3	23	346			
99-6-7	7-a-3	206	0.170	13	533	685	3	19	326			
99-6-7	7-b-1	240	0.158	455	507	659	2	18	315			
99-6-7	7-b-2	249	0.167	102	538	681	3	20	337			

Sample No.	Analyse No.	Mn	Fe (wt %)	Zn	Sr	Y	Ce	Pb	Th	Ni	Cu	Br
99-6-7	7-b-3	213	0.170	367	493	652	3	18	318			
99-6-7	7-c-1	274	0.169	13	577	675	3	21	320			
99-6-7	7-c-2	196	0.133	7	555	640	2	14	303			
99-6-7	7-c-3	260	0.151	9	562	644	3	16	303			
99-6-7	**Average**	**234**	**0.163**	**112**	**536**	**666**	**3**	**18**	**321**			
	STDEV	28	0.024	174	27	17	0	3	14			
996-8	8-a-1	248	0.116	3	554	585	2	11	251			
996-8	8-a-2	230	0.113	7	549	581	2	12	258			
996-8	8-a-3	203	0.123	5	542	573	2	11	250			
996-8	8-a-4	241	0.120	9	559	587	2	14	249			
996-8	8-b-1	126	0.103	16	451	571	1	17	222			
996-8	8-b-2	179	0.124	18	493	583	2	17	237			
996-8	8-b-3	140	0.105	16	462	568	1	15	221			
996-8	8-c-1	187	0.106	3	555	590	2	16	256			
996-8	8-c-2	203	0.112	3	545	579	2	14	260			
996-8	8-c-3	222	0.108	5	551	592	2	14	252			
996-8	**Average**	**198**	**0.113**	**8**	**526**	**581**	**2**	**14**	**246**			
	STDEV	41	0.008	6	41	8	0	2	14			
99-6-9	9-a-1	262	0.157	25	478	481	2	18	244			
99-6-9	9-a-2	238	0.162	19	476	479	2	18	242			
99-6-9	9-a-3	234	0.147	39	444	452	2	17	231			
99-6-9	9-b-1	180	0.113	9	522	618	2	15	318			
99-6-9	9-b-2	204	0.130	10	520	623	2	15	312			
99-6-9	9-b-3	204	0.140	9	506	587	2	15	308			
99-6-9	9-c-1	253	0.162	9	479	598	2	19	292			
99-6-9	9-c-2	274	0.154	9	473	592	2	20	291			
99-6-9	9-c-3	246	0.183	10	476	604	2	19	313			
99-6-9	**Average**	**233**	**0.150**	**15**	**486**	**559**	**2**	**17**	**283**			
	STDEV	31	0.020	11	25	68	0	2	35			
99-6-11	11-a-1		0.105	61	482	433		40	151		76	18

Sample No.	Analyse No.	Mn	Fe (wt %)	Zn	Sr	Y	Ce	Pb	Th	Ni	Cu	Br
99-6-11	11-a-2	224	0.130	85	533	449	2	11	163	29	80	21
99-6-11	11-a-3	59	0.107	66	469	417	1	60	144	58	83	18
99-6-11	11-a-4	184	0.116	83	510	439	1	12	158	47	90	20
99-6-11	11-b-1		0.074	45				10			53	12
99-6-11	11-b-2		0.061	39				8		26	46	10
99-6-11	11-c-1		0.085	56	365	332		52	112	36	57	10
99-6-11	11-c-2	26	0.148	7	517	496	2	41	227	4		
99-6-11	11-f-1	21	0.140	6	500	450	1	29	168			
99-6-11	11-g-1		0.164	4	498	445	1	33	165	6		1
99-6-11	11-g-2		0.189	3	515	482	1	38	205	6		
99-6-11	11-g-3	344	0.244		656	668	2	50	285	9		
99-6-11	11-h-1	346	0.210		656	668	2	48	294	2		3
99-6-11	11-h-2	234	0.166	2	566	510	2	19	239			4
99-6-11	11-h-3	340	0.227	1	648	656	2	48	283	2		4
99-6-11	11-h-4	234	0.183	4	566	505	2	19	233			3
99-6-11	11-h-5	401	0.214		644	648	2	52	281	2		2
99-6-11	11-h-6	285	0.173	3	571	505	2	20	236			2
99-6-11	11-i-1	206	0.223	7	510	433	1	22	186			5
99-6-11	11-i-2	231	0.229		520	442	1	19	187			6
99-6-11	11-i-3	253	0.221	2	506	423	2	20	175			9
99-6-11	**Average**	**226**	**0.162**	**28**	**487**	**495**	**2**	**31**	**205**	**19**	**69**	**9**
	STDEV	116	0.056	32	74	97	0	16	54	20	17	7
99-6-12	12-a-1		0.099	40	466	521	1	11	223	21	51	11
99-6-12	12-b-1		0.137	312	419	461	2	16	214	258	331	86
99-6-12	12-b-2		0.126	376	393	441	2	18	198	223	420	99
99-6-12	12-b-3		0.131	388	399	438	2	21	190	329	439	105
99-6-12	12-c-1		0.117	141	431	494	1	11	190	77	154	36
99-6-12	12-c-2		0.110	79	435	500	1	9	199	44	82	21
99-6-12	12-c-3		0.109	72	432	493	1	7	194	44	83	20
99-6-12	12-c-4		0.119	147	432	494	1	11	187	78	155	38
99-6-12	12-d-1		0.099	23	444	506	1	9	196	15	22	

Sample No.	Analyse No.	Mn	Fe (wt %)	Zn	Sr	Y	Ce	Pb	Th	Ni	Cu	Br
99-6-12	12-d-2		0.110	37	448	506	1	12	200	28	38	
99-6-12	12-d-3		0.112	24	446	513	1	12	199	20	24	
99-6-12	12-e-1		0.102	6	462	523	2	8	224	6		
99-6-12	12-e-2		0.118	4	456	523	1	11	223	6		
99-6-12	**Average**		**0.114**	**127**	**436**	**493**	**1**	**12**	**203**	**88**	**163**	**52**
	STDEV		0.012	140	22	29	0	4	13	108	158	38
99-6-14	14-a-1		0.280	108	462	601	3	29	315	83	67	20
99-6-14	14-a-2		0.283	172	436	573	3	30	300	141	112	29
99-6-14	14-a-3		0.338	86	455	597	2	31	304	71	52	18
99-6-14	14-b-1		0.129	39	486	617	2	22	305	27	21	8
99-6-14	14-b-2		0.129	21	483	617	2	19	310	8	7	3
99-6-14	14-b-3		0.151	65	478	598	2	28	300	44	55	15
99-6-14	14-c-1		0.256	20	513	615	4	29	315	18		3
99-6-14	14-c-2		0.237	27	519	612	4	33	327	15		2
99-6-14	14-d-1		0.232	87	485	598	4	31	351	76	58	18
99-6-14	**Average**		**0.226**	**70**	**480**	**603**	**3**	**28**	**314**	**54**	**53**	**13**
	STDEV		0.074	50	26	14	1	4	16	43	34	10
99-6-15	15-a-1		0.110	14	469	531	1	15	225	9	24	2
99-6-15	15-a-2		0.107	11	493	545	2	12	236	11	1	0
99-6-15	15-a-3		0.169	32	495	535	2	15	250	12	11	7
99-6-15	15-b-1		0.119	17	413	482	2	6	221	5	15	2
99-6-15	15-b-2		0.124	29	410	472	2	9	214	15	21	5
99-6-15	15-b-3		0.126	18	411	474	1	8	215	5	10	2
99-6-15	15-c-1		0.141	34	393	457	1	12	207	15	30	8
99-6-15	15-c-2		0.149	27	318	364	1	8	190	10	33	9
99-6-15	15-c-3		0.211	40	323	354	2	6	195	8	33	5
99-6-15	15-d-1		0.096	9	468	541	1	8	227	9	5	0
99-6-15	15-d-2		0.108	11	476	538	2	8	229	13	6	1
99-6-15	15-d-3		0.106	11	485	562	2	13	246	6	1	0
99-6-15	15-e-1		0.134	7	474	574	2	14	244	5		
99-6-15	15-e-2		0.126	8	483	568	2	16	234	7		

Sample No.	Analyse No.	Mn	Fe (wt %)	Zn	Sr	Y	Ce	Pb	Th	Ni	Cu	Br
99-6-15	15-e-3		0.204	9	495	584	2	20	264	5		
99-6-15	**Average**		**0.135**	**18**	**441**	**505**	**2**	**11**	**227**	**9**	**16**	**4**
	STDEV		0.035	11	60	71	0	4	20	3	12	3
99-6-16	16-a-1			30	435	517	1	39	218	14	16	3
99-6-16	16-a-2			27	456	526	2	30	228	10	6	3
99-6-16	16-b-1	95	0.110	39	517	557	2	25	251	15	59	8
99-6-16	16-b-2	173	0.128	114	499	551	2	39	243	53	175	29
99-6-16	16-c-1	117	0.134	96	432	517	1	51	221	63	147	25
99-6-16	16-d-1	48	0.114	52	328	459	1	94	201	37	80	15
99-6-16	16-d-2	107	0.104	86	367	469	1	74	208	51	148	24
99-6-16	16-d-3	116	0.141	149	415	478	1	55	223	108	238	37
99-6-16	16-e-1	133	0.130	109	456	498	1	33	235	73	128	24
99-6-16	16-e-2	164	0.144	219	458	504	1	71	218	84	168	27
99-6-16	16-e-3	147	0.138	80	453	506	2	45	239	45	92	21
99-6-16	16-f-1	142	0.157	104	451	483	1	26	212	64	133	23
99-6-16	16-f-2	135	0.164	128	446	482	1	34	235	87	149	27
99-6-16	16-f-3	140	0.177	126	480	494	1	26	239	96	164	27
99-6-16	**Average**	**126**	**0.137**	**97**	**442**	**503**	**1**	**46**	**227**	**57**	**122**	**21**
	STDEV	33	0.022	52	48	29	0	21	15	31	64	10
99-6-17	17-a-1	172	0.535	61	467	512	2	41	222	47	90	19
99-6-17	17-a-2	235	0.277	58	501					33	103	13
99-6-17	17-a-3	87	0.348	63	492					53	138	19
99-6-17	17-b-1	158	0.176	5	513	537	2	26	281			6
99-6-17	17-b-2	198	0.173	9	509	518	2	24	268			5
99-6-17	17-b-3	168	0.167	7	499	516	2	23	265	1		8
99-6-17	17-c-1	105	0.343	9	417	509	2	93	257	10		
99-6-17	17-c-2	90	0.186	15	397	502	2	89	265			
99-6-17	17-c-3	121	0.217	11	467	535	2	46	252	10		
99-6-17	17-c-4	133	0.243	14	503	538	2	21	266	6		
99-6-17	17-d-1	143	0.329	33	392	511	2	108	242	14	11	5
99-6-17	17-d-2	252	0.336	39	383	512	1	113	237	25	20	6

Sample No.	Analyse No.	Mn	Fe (wt %)	Zn	Sr	Y	Ce	Pb	Th	Ni	Cu	Br
99-6-17	17-d-3	227	0.293	28	403	510	1	101	227	15	11	6
99-6-17	17-e-1	187	0.159	10	515	563	2	23	279			
99-6-17	17-e-2	375	0.291	7	516	564	2	22	266			
99-6-17	17-e-3	194	0.152	10	516	561	2	25	284			
99-6-17	17-f-1	241	0.155	6	517	565	2	23	279			
99-6-17	17-f-2	241	0.186	10	520	558	2	24	279	4		
99-6-17	17-f-3	247	0.162	6	513	559	2	29	277	2		
99-6-17	17-g-1	193	0.507	8	518	548	1	30	230	5		
99-6-17	17-g-2	216	0.461	3	516	547	1	32	231	2		
99-6-17	17-g-3	235	0.485	7	513	541	1	33	230	8		
99-6-17	17-h-1	236	0.197	10	486	547	1	34	234	3		10
99-6-17	17-h-2	179	0.197	12	493	566	1	33	239	8		7
99-6-17	**Average**	**193**	**0.274**	**18**	**482**	**537**	**2**	**45**	**255**	**15**	**62**	**9**
	STDEV	64	0.121	19	46	22	0	32	21	16	55	5
99-6-18	18-a-1	161	1.032	45	503	513	1	18	204	33	34	8
99-6-18	18-a-2	256	1.049	71	286	279	1	18	149	37	70	14
99-6-18	18-a-3	242	0.446	47	281	276	1	14	158	33	48	10
99-6-18	18-b-1	371	0.585	26	506	504	1	18	219	14	13	3
99-6-18	18-b-2	197	0.323	18	515	522	1	13	218	25		
99-6-18	18-b-3	168	0.265	9	516	517	1	15	213	8		
99-6-18	18-c-1	160	0.739	37	497	505	1	16	202	27	31	9
99-6-18	18-c-2	207	0.273	36	500	524	1	29	240	19	30	8
99-6-18	18-c-3	191	0.258	42	496	522	1	38	246	27	38	5
99-6-18	**Average**	**217**	**0.552**	**37**	**456**	**462**	**1**	**20**	**205**	**25**	**38**	**8**
	STDEV	67	0.321	18	98	105	0	8	33	9	18	3
99-6-19	19-a-1	174	0.117	30	499	558	1	42	217	17	16	
99-6-19	19-a-2	137	0.140	58	474	559	1	66	221	38	42	6
99-6-19	19-a-3	212	0.130	18	511	567	2	41	232	11	4	
99-6-19	19-b-1	153	0.138	16	502	581	1	50	240	10	5	
99-6-19	19-b-2	228	0.137	12	522	579	2	35	256	4		
99-6-19	19-b-3	232	0.120	32	511	570	1	34	227	5	15	5

Sample No.	Analyse No.	Mn	Fe (wt %)	Zn	Sr	Y	Ce	Pb	Th	Ni	Cu	Br
99-6-19	19-b-4	203	0.186	32	506	600	2	54	251	21	13	5
99-6-19	19-c-1	166	0.158	36	496	560	2	35	234	31	27	6
99-6-19	19-c-2	191	0.161	44	480	555	2	68	242	35	35	7
99-6-19	19-c-3	197	0.151	31	510	565	2	33	240	18	22	5
99-6-19	**Average**	**189**	**0.144**	**31**	**501**	**569**	**1**	**46**	**236**	**19**	**20**	**6**
	STDEV	31	0.021	14	15	14	0	13	12	12	13	1
99-6-20	20-a-1	169	0.115	9	527	422	1	26	271	5		
99-6-20	20-a-2	165	0.139	13	520	414	1	26	267	11	5	
99-6-20	20-a-3	150	0.104	7	537	427	1	27	284	6		
99-6-20	20-b-1	139	0.104	4	529	464	1	22	280	4	10	
99-6-20	20-b-2	193	0.115	10	533	510	1	36	201	7	2	
99-6-20	20-b-3	190	0.133	1	556	473	1	34	310	6		
99-6-20	20-c-1	142	0.220	6	448	571	1	138	281			
99-6-20	20-c-2	155	0.127	5	466	581	2	160	295	7		1
99-6-20	20-c-3	157	0.315	12	441	561	1	132	280	2		1
99-6-20	**Average**	**162**	**0.153**	**7**	**506**	**491**	**1**	**67**	**274**	**6**	**6**	**1**
	STDEV	19	0.071	4	42	67	0	58	30	3	4	1
Sample #	Analyse #	Mn	Fe	Zn	Sr	Y	Ce	Pb	Th	Ni	Cu	Br
99-6-21	21-a-1	149	0.095	4	498	522	1	17	225			
99-6-21	21-a-2	156	0.105	7	498	523	1	17	229			
99-6-21	21-a-3	142	0.095	7	498	528	1	18	234			
99-6-21	21-b-1	165	0.084	12	511	530	1	18	226	11		
99-6-21	21-b-2	137	0.119	9	514	543	1	17	235			
99-6-21	21-b-3	181	0.087	12	489	525	1	41	232	6	2	1
99-6-21	21-c-1	156	0.087	7	475	521	1	42	230	4	1	
99-6-21	21-c-2	201	0.092	5	487	535	1	47	234			
99-6-21	21-c-3	167	0.092	9	483	510	1	33	223	10	0	
99-6-21	**Average**	**162**	**0.095**	**8**	**495**	**527**	**1**	**28**	**230**	**8**	**1**	**1**
	STDEV	20	0.011	3	13	9	0	13	4	3	1	
99-6-22	22-a-1	125	0.100	4	530	608	1	58	88	3		
99-6-22	22-a-2	154	0.085	5	519	591	1	70	81			

Sample No.	Analyse No.	Mn	Fe (wt %)	Zn	Sr	Y	Ce	Pb	Th	Ni	Cu	Br
99-6-22	22-a-3	162	0.098	3	523	591	1	56	88	3		
99-6-22	22-b-1	213	0.109	5	517	576	1	75	79	7		
99-6-22	22-b-2	187	0.130	7	490	557	1	94	80	5		0
99-6-22	22-b-3	122	0.091	4	496	573	1	83	82	2		0
99-6-22	22-c-1	184	0.163	11	485	566	2	35	245	6		
99-6-22	22-c-2	156	0.205	8	481	545	1	39	247	0	0	
99-6-22	22-c-3	183	0.165	7	493	574	2	41	258	1		
99-6-22	**Average**	**165**	**0.127**	**6**	**504**	**576**	**1**	**61**	**139**	**3**	**0**	**0**
	STDEV	30	0.042	2	19	19	0	21	84	3		0
99-6-23	23-a-1	700	0.150	7	487	546	1	34	269	3	0	
99-6-23	23-a-2	341	0.206	10	494	562	2	55	302		1	
99-6-23	23-a-3	643	0.162	10	500	549	2	35	277	1		
99-6-23	23-b-1	770	0.256	7	447	501	1	105	250	2		
99-6-23	23-b-2	796	0.412	9	455	497	2	107	235			1
99-6-23	23-b-3	695	0.299	11	430	489	2	126	252	2		
99-6-23	23-c-1	164	0.149	13	473	532	1	69	234	9	2	
99-6-23	23-c-2	212	0.167	15	473	516	1	67	229	11	8	1
99-6-23	23-c-3	182	0.151	10	470	521	1	55	242	7		
99-6-23	**Average**	**500**	**0.217**	**10**	**470**	**524**	**1**	**73**	**254**	**5**	**3**	**1**
	STDEV	270	0.090	3	23	26	0	33	24	4	3	0
99-6-24	24-a-1	452	0.122	13	476	532	2	36	241	0	1	1
99-6-24	24-a-2	432	0.302	14	474	533	1	48	239		1	2
99-6-24	24-a-3	855	0.124	23	464	518	1	29	233	0	3	3
99-6-24	24-b-1	175	0.152	12	485	534	1	30	240	4		
99-6-24	24-b-2	185	0.135	14	487	538	2	38	246	7		
99-6-24	24-b-3	175	0.168	10	472	523	2	36	238	5	1	
99-6-24	24-c-1	185	0.113	8	495	518	2	9	224			
99-6-24	24-c-2	311	0.211	13	500	531	2	12	256			
99-6-24	24-c-3	208	0.139	7	495	523	2	10	237			
99-6-24	**Average**	**331**	**0.163**	**13**	**483**	**528**	**2**	**27**	**239**	**3**	**2**	**2**
	STDEV	225	0.060	5	12	7	0	14	9	3	1	1

Appendix 3b EMPA Results of Aoshan Apatite (wt %)

Sample No.	Analyse No.	CaO	SiO_2	MnO	FeO	Na_2O	P_2O_5	Cl	F	Br	O=(Cl+F)	Total
99-6-3	6-3-1	55.53	0.20	0.00	0.14	0.13	40.92	0.63	3.20		1.49	99.26
99-6-3	6-3-2	55.98	0.21	0.05	0.19	0.23	41.45	0.78	3.22		1.53	100.58
99-6-3	6-3-3	55.67	0.26	0.02	0.17	0.27	41.24	0.95	3.47		1.67	100.39
99-6-3	6-3-4	55.13	0.29	0.00	0.19	0.22	41.16	0.88	3.10		1.50	99.47
99-6-3	6-3-5	55.80	0.21	0.02	0.23	0.24	41.60	0.84	3.13		1.50	100.56
99-6-3	6-3-6	54.89	0.24	0.03	0.14	0.26	40.85	0.93	3.14		1.53	98.95
99-6-3	6-3-7	55.79	0.21	0.00	0.13	0.24	41.24	0.87	2.86		1.40	99.94
99-6-3	6-3-8	55.34	0.24	0.00	0.13	0.31	41.83	1.00	2.81		1.40	100.26
99-6-3	6-3-9	55.65	0.21	0.02	0.06	0.23	41.31	0.84	3.47		1.65	100.14
99-6-3	6-3-10	55.72	0.23	0.02	0.19	0.24	41.15	0.95	3.18		1.55	100.12
99-6-3	6-3-11	55.05	0.22	0.01	0.21	0.27	41.62	0.79	3.28		1.56	99.89
99-6-3	6-3-12	55.59	0.23	0.07	0.10	0.28	41.09	0.96	3.03		1.49	99.85
99-6-3	6-3-13	55.55	0.21	0.00	0.05	0.00	41.76	0.18	3.14		1.36	99.52
99-6-3	6-3-14	55.75	0.15	0.00	0.00	0.00	42.55	0.31	2.58		1.16	100.19
99-6-3	6-3-15	56.70	0.07	0.00	0.00	0.00	42.02	0.18	2.70		1.17	100.50
99-6-3	6-3-16	55.57	0.18	0.00	0.10	0.00	41.37	0.16	2.74		1.19	98.93
99-6-3	6-3-17	56.20	0.27	0.00	0.12	0.00	41.86	0.16	2.75		1.19	100.17
99-6-3	6-3-18	56.42	0.15	0.02	0.00	0.00	41.44	0.31	2.52		1.13	99.74
99-6-3	6-3-19	49.60	0.19	0.01	0.14	0.30	47.82	0.78	2.36	0.001	1.17	100.04
99-6-3	6-3-20	53.09	0.19	0.03	0.29	0.23	44.46	0.72	2.22		1.10	100.14
99-6-3	6-3-21	49.86	0.26	0.00	0.15	0.28	47.03	0.77	2.37		1.17	99.56
99-6-3	6-3-22	49.06	0.18	0.04	0.12	0.32	47.19	1.13	2.23	0.002	1.19	99.07
99-6-3	6-3-23	52.93	0.22	0.00	0.19	0.25	40.32	1.16	2.04			95.99
99-6-3	6-3-24	53.06	0.20	0.07	0.17	0.25	41.99	1.05	2.08	0.011	1.11	97.77
99-6-3	6-3-25	49.40	0.25	0.02	0.15	0.21	47.97	0.84	2.41	0.024	1.20	100.08
99-6-3	6-3-26	52.97	0.21	0.04	0.15	0.31	41.42	0.85	2.27	0.027	1.15	97.10
99-6-3	6-3-27	50.12	0.20	0.08	0.10	0.31	45.84	0.79	2.39	0.005	1.18	98.66
	Average	54.16	0.21	0.02	0.13	0.20	42.61	0.73	2.77	0.012	1.33	99.52
	STDEV	2.44	0.04	0.02	0.07	0.12	2.35	0.31	0.44	0.011	0.19	1.09
99-6-4	6-4-1	53.85	0.32	0.02	0.10	0.35	40.37	0.98	2.70		1.35	97.33
99-6-4	6-4-2	54.60	0.28	0.02	0.11	0.38	40.36	1.10	2.68		1.37	98.17
99-6-4	6-4-3	54.14	0.20	0.05	0.12	0.24	40.56	1.04	2.69		1.37	97.68
99-6-4	6-4-4	54.13	0.29	0.08	0.26	0.46	40.93	0.99	2.50		1.27	98.37
99-6-4	6-4-5	54.06	0.30	0.02	0.38	0.38	40.54	1.00	2.60		1.32	97.97
99-6-4	6-4-6	54.44	0.18	0.00	0.20	0.15	40.92	0.83	2.70		1.32	98.10
99-6-4	6-4-7	54.88	0.14	0.03	0.13	0.18	41.72	0.84	2.82		1.37	99.36
99-6-4	6-4-8	54.49	0.29	0.01	0.19	0.20	41.75	0.87	2.70		1.33	99.17
99-6-4	6-4-9	54.65	0.16	0.00	0.26	0.21	40.89	0.95	2.30		1.18	98.24
99-6-4	6-4-10	52.93	0.33	0.02	0.00	0.10	41.24	0.35	2.31	0.012	1.05	96.24
99-6-4	6-4-11	52.02	0.35	0.00	0.08	0.38	40.82	1.28	2.02		1.14	95.81
99-6-4	6-4-12	50.13	0.29	0.02	0.09	0.44	43.95	1.28	2.00	0.028	1.13	97.10
99-6-4	6-4-13	50.22	0.76	0.08	0.09	0.38	44.15	0.81	2.06	0.012	1.05	97.51
99-6-4	6-4-14	53.13	0.31	0.02	0.06	0.38	42.51	0.69	2.22	0.030	1.09	98.26
99-6-4	6-4-15	49.44	0.34	0.01	0.06	0.41	46.36	0.48	2.16	0.009	1.01	98.26
99-6-4	6-4-16	52.52	0.28	0.11	0.17	0.45	43.85	0.77	2.12	0.006	1.06	99.21

Sample No.	Analyse No.	CaO	SiO_2	MnO	FeO	Na_2O	P_2O_5	Cl	F	Br	O= (Cl+F)	Total
99-6-4	6-4-17	51.60	0.27	0.00	0.15	0.38	44.01	0.87	2.36		1.18	98.46
99-6-4	6-4-18	51.97	0.28	0.04	0.18	0.39	44.24	0.75	2.29	0.039	1.13	99.06
	Average	52.96	0.30	0.03	0.15	0.32	42.18	0.88	2.40	0.019	1.21	98.03
	STDEV	1.72	0.13	0.03	0.09	0.11	1.80	0.24	0.27	0.014	0.13	0.97
99-6-5	6-5-1	53.95	0.17	0.06	0.02	0.00	41.91	0.12	2.74		1.18	97.79
99-6-5	6-5-2	49.36	0.27	0.00	0.10	0.34	44.47	1.20	2.10		1.15	96.70
99-6-5	6-5-3	48.92	0.28	0.02	0.21	0.30	46.23	1.19	2.01		1.11	98.04
99-6-5	6-5-4	50.78	0.02	0.00	0.00	0.06	46.88	0.14	2.24	0.036	0.97	99.19
99-6-5	6-5-5	49.42	0.21	0.08	0.16	0.27	44.44	0.76	2.45		1.20	96.60
99-6-5	6-5-6	49.73	0.23	0.00	0.10	0.30	45.41	0.74	2.22		1.10	97.63
99-6-5	6-5-7	48.91	0.25	0.04	0.16	0.26	45.15	0.79	2.41		1.19	96.79
99-6-5	6-5-8	55.27	0.25	0.04	0.15	0.28	39.45	0.72	3.33		1.56	97.93
99-6-5	6-5-9	55.68	0.25	0.06	0.12	0.36	37.52	0.72	3.44	0.009	1.61	96.56
99-6-5	6-5-10	55.22	0.26	0.09	0.14	0.26	38.58	0.75	3.25	0.006	1.53	97.02
99-6-5	6-5-11	56.16	0.28	0.00	0.19	0.28	37.88	0.73	3.15	0.004	1.49	97.19
99-6-5	6-5-12	55.56	0.29	0.02	0.08	0.28	37.40	0.70	3.19	0.008	1.50	96.03
99-6-5	6-5-13	56.43	0.26	0.00	0.16	0.27	36.89	0.74	3.32		1.56	96.51
99-6-5	6-5-14	56.17	0.28	0.03	0.19	0.26	38.06	0.74	3.62	0.020	1.69	97.69
	Average	52.97	0.24	0.03	0.13	0.25	41.45	0.72	2.82	0.014	1.35	97.27
	STDEV	3.18	0.07	0.03	0.06	0.10	3.81	0.30	0.56	0.012	0.24	0.83
99-6-6	6-6-1	56.73	0.12	0.01	0.08	0.00	42.72	0.14	3.16		1.36	101.60
99-6-6	6-6-2	56.64	0.03	0.12	0.04	0.07	42.80	0.16	3.63		1.56	101.94
99-6-6	6-6-3	55.00	0.22	0.06	0.09	0.19	41.08	0.80	2.89		1.40	98.94
99-6-6	6-6-4	55.30	0.14	0.00	0.02	0.20	42.12	0.76	3.03		1.44	100.13
99-6-6	6-6-5	55.71	0.24	0.02	0.06	0.18	41.73	0.84	3.12		1.50	100.41
99-6-6	6-6-6	55.64	0.30	0.02	0.13	0.23	41.07	0.86	2.83		1.38	99.69
99-6-6	6-6-7	55.58	0.30	0.03	0.11	0.23	41.24	0.93	2.86		1.41	99.88
99-6-6	6-6-8	56.17	0.16	0.00	0.00	0.00	41.67	0.16	3.17		1.37	99.97
99-6-6	6-6-9	56.46	0.13	0.00	0.00	0.00	41.98	0.12	3.06		1.31	100.44
99-6-6	6-6-10	56.59	0.26	0.00	0.00	0.00	41.78	0.07	3.43		1.46	100.68
99-6-6	6-6-11	55.87	0.28	0.00	0.17	0.20	38.84	0.77	2.82		1.36	97.59
99-6-6	6-6-12	52.81	0.21	0.05	0.13	0.19	42.84	0.76	2.80	0.016	1.35	98.46
99-6-6	6-6-13	55.32	0.23	0.00	0.13	0.20	40.51	0.65	2.95	0.011	1.39	98.61
99-6-6	6-6-14	53.49	0.30	0.06	0.06	0.44	40.56	0.89	3.48		1.66	97.63
99-6-6	6-6-15	52.81	0.33	0.08	0.05	0.43	41.12	0.93	3.21		1.56	97.40
99-6-6	6-6-16	54.42	0.27	0.04	0.10	0.46	39.14	0.82	3.30		1.57	96.98
99-6-6	6-6-17	52.77	0.36	0.02	0.13	0.38	40.93	1.32	3.61		1.81	97.71
99-6-6	6-6-18	53.83	0.27	0.02	0.12	0.28	40.86	1.25	3.79	0.027	1.87	98.56
99-6-6	6-6-19	53.70	0.26	0.01	0.13	0.24	38.57	1.15	3.79		1.85	96.00
	Average	54.99	0.23	0.03	0.08	0.21	41.13	0.71	3.21	0.018	1.51	99.10
	STDEV	1.38	0.08	0.03	0.05	0.15	1.24	0.39	0.33	0.008	0.18	1.62
99-6-7	6-7-1	53.81	0.22	0.00	0.06	0.30	40.59	1.13	2.59		1.34	97.35
99-6-7	6-7-2	54.66	0.26	0.01	0.15	0.25	40.68	0.91	2.57		1.28	98.21
99-6-7	6-7-3	53.05	2.26	0.00	0.00	0.02	42.58	0.92	2.83		1.39	100.27
99-6-7	6-7-4	54.54	0.26	0.06	0.01	0.25	41.74	1.12	2.59		1.34	99.22

Sample No.	Analyse No.	CaO	SiO_2	MnO	FeO	Na_2O	P_2O_5	Cl	F	Br	O= (Cl+F)	Total
99-6-7	6-7-5	54.91	0.22	0.06	0.09	0.06	41.87	0.94	2.50		1.26	99.39
99-6-7	6-7-6	54.70	0.21	0.00	0.09	0.25	42.47	1.18	2.75		1.42	100.24
99-6-7	6-7-7	54.87	0.22	0.04	0.12	0.23	41.52	1.07	2.75		1.40	99.42
99-6-7	6-7-8	54.57	0.28	0.00	0.10	0.28	41.23	1.19	2.55		1.34	98.87
99-6-7	6-7-9	54.53	0.21	0.00	0.00	0.29	41.78	1.15	2.49		1.30	99.15
99-6-7	6-7-10	53.50	0.30	0.00	0.21	0.34	41.44	1.14	2.51		1.31	98.12
99-6-7	6-7-11	54.57	0.25	0.02	0.16	0.30	41.82	1.05	2.43		1.26	99.35
99-6-7	6-7-12	54.03	0.27	0.06	0.07	0.28	41.25	1.21	2.69		1.40	98.45
99-6-7	6-7-13	54.89	0.31	0.04	0.14	0.34	41.37	1.13	2.47		1.29	99.40
99-6-7	6-7-14	54.40	0.30	0.03	0.22	0.28	41.25	1.02	2.44		1.25	98.69
99-6-7	6-7-15	54.76	0.24	0.06	0.18	0.29	41.09	0.97	2.95		1.46	99.08
99-6-7	6-7-16	54.40	0.23	0.02	0.08	0.33	41.24	1.02	2.62		1.33	98.61
99-6-7	6-7-17	55.55	0.20	0.01	0.00	0.00	42.96	0.11	3.23		1.38	100.68
99-6-7	6-7-18	54.94	0.26	0.02	0.07	0.07	41.62	0.45	2.93		1.33	99.02
99-6-7	6-7-19	54.19	0.24	0.08	0.08	0.26	40.86	1.01	2.83		1.41	98.14
99-6-7	6-7-20	54.28	0.25	0.03	0.20	0.29	41.44	0.91	2.96		1.45	98.91
	Average	54.46	0.35	0.03	0.10	0.24	41.54	0.98	2.68		1.35	99.03
	STDEV	0.55	0.45	0.03	0.07	0.11	0.61	0.27	0.22		0.06	0.80
99-6-8	6-8-1	54.12	0.26	0.04	0.09	0.28	37.46	1.12	3.56	0.010	1.75	95.20
99-6-8	6-8-2	54.62	0.28	0.10	0.19	0.35	36.99	1.19	3.66	0.049	1.81	95.63
99-6-8	6-8-3	54.20	0.25	0.00	0.18	0.24	38.47	1.20	3.50	0.013	1.74	96.31
99-6-8	6-8-4	54.64	0.24	0.04	0.07	0.30	37.31	1.15	3.69	0.040	1.81	95.67
99-6-8	6-8-5	54.66	0.26	0.01	0.09	0.30	39.87	0.72	3.23		1.52	97.62
99-6-8	6-8-6	54.83	0.30	0.02	0.07	0.25	39.68	0.69	3.41	0.002	1.59	97.66
99-6-8	6-8-7	54.93	0.28	0.02	0.04	0.28	39.85	0.77	3.62		1.69	98.10
99-6-8	6-8-8	52.57	0.27	0.02	0.11	0.29	43.54	0.66	2.84		1.34	98.95
99-6-8	6-8-9	54.39	0.28	0.00	0.17	0.29	40.69	0.67	2.75	0.009	1.31	97.94
99-6-8	6-8-10	56.09	0.22	0.00	0.18	0.34	40.89	0.74	2.90		1.38	99.97
	Average	54.51	0.26	0.02	0.12	0.29	39.48	0.89	3.32	0.020	1.59	97.31
	STDEV	0.87	0.02	0.03	0.06	0.03	2.01	0.24	0.36	0.019	0.20	1.56
99-6-9	6-9-1	55.98	0.19	0.03	0.24	0.00	42.37	0.13	2.75		1.19	100.51
99-6-9	6-9-2	56.50	0.18	0.02	0.07	0.01	42.39	0.27	2.43		1.08	100.79
99-6-9	6-9-3	55.17	0.16	0.00	0.02	0.00	42.49	0.39	2.62		1.19	99.66
99-6-9	6-9-4	54.48	0.26	0.00	0.13	0.27	41.47	1.08	2.37		1.24	98.83
99-6-9	6-9-5	54.85	0.20	0.05	0.21	0.18	41.59	0.99	2.49		1.27	99.28
99-6-9	6-9-6	56.51	0.05	0.08	0.07	0.00	43.08	0.07	2.60		1.11	101.35
99-6-9	6-9-7	54.16	0.14	0.06	0.14	0.19	42.55	0.99	2.24		1.16	99.30
99-6-9	6-9-8	56.10	0.10	0.00	0.03	0.00	42.92	0.07	2.50		1.07	100.65
99-6-9	6-9-9	55.71	0.06	0.00	0.09	0.00	42.31	0.13	2.97		1.28	99.99
99-6-9	6-9-10	55.78	0.15	0.05	0.24	0.00	42.34	0.16	2.65		1.15	100.22
99-6-9	6-9-11	56.64	0.08	0.02	0.00	0.00	42.69	0.08	3.67		1.56	101.62
99-6-9	6-9-12	55.44	0.24	0.04	0.12	0.30	41.71	0.75	2.94		1.40	100.13
99-6-9	6-9-13	55.66	0.20	0.00	0.13	0.22	41.57	0.91	2.73		1.35	100.07
99-6-9	6-9-14	55.67	0.20	0.04	0.04	0.19	41.86	0.79	2.86		1.38	100.27
99-6-9	6-9-15	55.27	0.25	0.03	0.18	0.24	41.59	0.96	2.81		1.39	99.93
99-6-9	6-9-16	55.32	0.20	0.07	0.10	0.22	41.99	1.00	2.56		1.30	100.17

Sample No.	Analyse No.	CaO	SiO_2	MnO	FeO	Na_2O	P_2O_5	Cl	F	Br	O= (Cl+F)	Total
99-6-9	6-9-17	54.90	0.34	0.04	0.17	0.34	41.16	0.72	2.72	0.021	1.31	99.10
99-6-9	6-9-18	54.32	0.29	0.05	0.09	0.18	41.95	0.71	3.52		1.64	99.48
99-6-9	6-9-19	52.70	0.30	0.02	0.13	0.37	43.32	0.71	2.99	0.004	1.41	99.12
	Average	55.32	0.19	0.03	0.12	0.14	42.18	0.58	2.76	0.013	1.29	100.04
	STDEV	0.96	0.08	0.02	0.07	0.13	0.59	0.38	0.36	0.012	0.16	0.76
99-6-11	6-11-1	50.65	0.15	0.00	0.19	0.18	45.67	0.61	2.38	0.020	1.14	98.72
99-6-11	6-11-2	50.62	0.17	0.01	0.20	0.18	45.42	0.63	1.91	0.007	0.94	98.21
99-6-11	6-11-3	50.60	0.22	0.01	0.11	0.21	46.23	0.63	1.95		0.96	99.00
99-6-11	6-11-4	53.75	0.20	0.00	0.08	0.24	42.36	0.61	2.10	0.054	1.02	98.38
99-6-11	6-11-5	54.37	0.23	0.11	0.16	0.23	41.88	0.66	2.69		1.28	99.06
99-6-11	6-11-6	52.30	0.18	0.00	0.00	0.16	46.96	0.65	2.42		1.16	101.51
99-6-11	6-11-7	50.91	0.22	0.04	0.20	0.19	45.23	0.74	2.53	0.020	1.23	98.84
99-6-11	6-11-8	50.79	0.21	0.07	0.06	0.23	45.33	0.74	2.71	0.002	1.31	98.83
99-6-11	6-11-9	54.57	0.18	0.00	0.18	0.21	39.47	0.72	2.57		1.24	96.66
99-6-11	6-11-10	52.73	0.21	0.06	0.13	0.22	41.61	0.64	3.40		1.57	97.43
99-6-11	6-11-11	55.91	0.20	0.05	0.10	0.18	37.38	0.66	2.71		1.29	95.90
99-6-11	6-11-12	53.40	0.23	0.05	0.14	0.24	42.84	0.65	3.07	0.027	1.44	99.21
99-6-11	6-11-13	54.61	0.25	0.00	0.17	0.15	39.10	0.78	3.44		1.62	96.88
99-6-11	6-11-14	53.32	0.21	0.07	0.12	0.22	40.81	0.73	3.40		1.59	97.28
99-6-11	6-11-15	53.91	0.22	0.03	0.15	0.22	39.75	0.74	3.11	0.020	1.47	96.68
99-6-11	6-11-16	56.68	0.22	0.08	0.11	0.21	37.80	0.66	3.75	0.028	1.72	97.81
99-6-11	6-11-17	55.84	0.21	0.02	0.23	0.18	38.90	0.64	3.64		1.67	98.00
99-6-11	6-11-18	54.70	0.21	0.03	0.11	0.15	40.60	0.62	3.54	0.015	1.63	98.35
99-6-11	6-11-19	53.91	0.22	0.00	0.16	0.15	39.03	1.00	3.61		1.74	96.33
99-6-11	6-11-20	53.95	0.22	0.03	0.20	0.18	38.70	1.10	3.46	0.020	1.70	96.16
99-6-11	6-11-21	51.77	0.16	0.01	0.14	0.20	40.49	1.14	3.54	0.029	1.74	95.74
	Average	53.30	0.21	0.03	0.14	0.20	41.69	0.73	2.95	0.022	1.40	97.87
	STDEV	1.87	0.02	0.03	0.06	0.03	3.02	0.16	0.60	0.015	0.27	1.40
99-6-12	6-12-1	54.63	0.28	0.13	0.14	0.33	40.87	0.94	3.28		1.59	99.01
99-6-12	6-12-2	54.73	0.27	0.00	0.17	0.36	40.76	0.82	2.73		1.33	98.51
99-6-12	6-12-3	55.23	0.23	0.00	0.21	0.47	41.19	0.84	3.03		1.46	99.75
99-6-12	6-12-4	55.30	0.19	0.04	0.17	0.28	41.44	0.84	3.24		1.55	99.96
99-6-12	6-12-5	55.37	0.21	0.08	0.11	0.22	40.70	0.76	3.21		1.52	99.15
99-6-12	6-12-6	55.62	0.26	0.07	0.26	0.27	41.13	0.78	3.46		1.63	100.22
99-6-12	6-12-7	55.76	0.27	0.01	0.14	0.23	41.64	0.87	3.40		1.62	100.70
99-6-12	6-12-8	52.94	0.21	0.00	0.15	0.16	43.00	0.78	2.35	0.009	1.16	98.45
99-6-12	6-12-9	53.02	0.25	0.04	0.25	0.25	42.25	1.00	2.21		1.15	98.11
99-6-12	6-12-10	51.67	0.26	0.00	0.14	0.23	45.22	1.05	2.71		1.38	99.91
99-6-12	6-12-11	53.40	0.24	0.00	0.18	0.31	44.07	0.72	1.93		0.98	99.89
99-6-12	6-12-12	51.25	0.26	0.00	0.17	0.32	45.10	0.64	1.85		0.92	98.66
99-6-12	6-12-13	54.52	0.23	0.07	0.12	0.29	41.31	0.68	1.73		0.88	98.06
99-6-12	6-12-14	54.78	0.26	0.00	0.22	0.28	39.19	0.70	2.29		1.12	96.60
99-6-12	6-12-15	50.54	0.16	0.06	0.67	0.34	46.47	0.67	2.16	0.001	1.06	100.01
99-6-12	6-12-16	52.62	0.28	0.00	0.18	0.30	41.81	0.78	2.18	0.019	1.09	97.08
99-6-12	6-12-17	50.65	0.27	0.00	0.15	0.33	44.75	0.78	2.48	0.020	1.22	98.20
99-6-12	6-12-18	52.84	0.22	0.04	0.23	0.30	43.83	0.74	2.22		1.10	99.31

Sample No.	Analyse No.	CaO	SiO_2	MnO	FeO	Na_2O	P_2O_5	Cl	F	Br	O= (Cl+F)	Total
99-6-12	6-12-19	51.31	0.22	0.00	0.15	0.33	43.30	0.75	2.37		1.16	97.27
	Average	53.48	0.24	0.03	0.20	0.29	42.53	0.80	2.57	0.012	1.26	98.90
	STDEV	1.77	0.03	0.04	0.12	0.07	1.93	0.11	0.55	0.008	0.24	1.15
99-6-14	6-14-1	56.33	0.07	0.02	0.01	0.00	41.39	0.11	3.28		1.40	99.81
99-6-14	6-14-2	55.68	0.16	0.05	0.00	0.00	42.06	0.04	2.94		1.24	99.69
99-6-14	6-14-3	54.61	0.29	0.03	0.22	0.31	40.54	1.01	3.02		1.50	98.54
99-6-14	6-14-4	55.34	0.25	0.01	0.10		40.94	0.96	3.14		1.53	99.20
99-6-14	6-14-5	55.52	0.27	0.00	0.17	0.18	41.42	0.86	2.86		1.39	99.88
99-6-14	6-14-6	54.81	0.27	0.09	0.19	0.23	40.51	0.98	2.70		1.36	98.44
99-6-14	6-14-7	55.37	0.32	0.01	0.18	0.11	40.98	0.93	3.13		1.52	99.51
99-6-14	6-14-8	55.16	0.28	0.02	0.17	0.36	40.81	0.93	2.91		1.43	99.20
99-6-14	6-14-9	55.27	0.28	0.10	0.14	0.22	41.31	0.84	3.07		1.48	99.75
99-6-14	6-14-10	55.38	0.32	0.00	0.19	0.26	41.41	0.92	3.02		1.47	100.03
99-6-14	6-14-11	56.86	0.12	0.05	0.02	0.02	42.10	0.15	3.31		1.42	101.21
99-6-14	6-14-12	55.60	0.07	0.04	0.01	0.02	42.75	0.07	2.65		1.13	100.07
99-6-14	6-14-13	55.31	0.17	0.10	0.00	0.07	42.04	0.38	2.83		1.27	99.63
99-6-14	6-14-14	55.75	0.03	0.06	0.02	0.00	43.09	0.13	2.84		1.22	100.71
99-6-14	6-14-15	55.98	0.07	0.00	0.01	0.00	43.09	0.05	3.24		1.37	101.07
99-6-14	6-14-16	55.74	0.00	0.00	0.04	0.00	42.47	0.45	2.43		1.12	100.01
99-6-14	6-14-17	55.35	0.08	0.07	0.01	0.04	42.65	0.13	2.81		1.21	99.92
99-6-14	6-14-18	55.22	0.23	0.00	0.06	0.10	41.57	0.36	2.92	0.020	1.31	99.18
99-6-14	6-14-19	50.95	0.27	0.01	0.10	0.18	44.16	0.71	2.48	0.008	1.20	97.67
99-6-14	6-14-20	52.64	0.29	0.00	0.25	0.32	41.61	0.76	2.05		1.03	96.90
99-6-14	6-14-21	49.45	0.28	0.03	0.10	0.27	42.86	1.18	2.11	0.026	1.15	95.15
99-6-14	6-14-22	52.77	0.31	0.00	0.08	0.47	39.37	1.25	1.95	0.004	1.10	95.10
99-6-14	6-14-23	52.65	0.19	0.02	0.12	0.27	41.67	1.22	2.15	0.013	1.18	97.11
99-6-14	6-14-24	54.23	0.30	0.00	0.15	0.31	40.14	0.79	2.30		1.14	97.08
99-6-14	6-14-25	53.32	0.21	0.04	0.23	0.13	40.83	0.75	2.44		1.19	96.76
99-6-14	6-14-26	53.41	0.23	0.09	0.17	0.21	41.00	0.73	2.16	0.034	1.07	96.96
	Average	54.57	0.21	0.03	0.11	0.16	41.65	0.64	2.72	0.017	1.29	98.81
	STDEV	1.72	0.10	0.03	0.08	0.14	1.07	0.40	0.41	0.013	0.15	1.69
99-6-15	6-15-1	53.67	0.24	0.01	0.13	0.30	41.05	0.80	2.39	0.008	1.19	97.43
99-6-15	6-15-2	52.95	0.18	0.02	0.26	0.29	41.72	0.81	2.44		1.21	97.47
99-6-15	6-15-3	54.01	0.22	0.00	0.20	0.36	40.43	0.76	2.61		1.27	97.32
99-6-15	6-15-4	51.51	0.24	0.00	0.25	0.25	43.77	0.98	2.24	0.011	1.16	98.09
99-6-15	6-15-5	48.79	0.24	0.00	0.22	0.27	45.63	1.03	2.30		1.20	97.28
99-6-15	6-15-6	50.59	0.26	0.03	0.08	0.38	45.70	0.92	2.33		1.19	99.10
99-6-15	6-15-7	50.61	0.23	0.00	0.15	0.32	44.60	0.75	2.53	0.035	1.23	97.99
99-6-15	6-15-8	52.67	0.23	0.02	0.14	0.37	40.83	0.77	2.47	0.004	1.21	96.29
99-6-15	6-15-9	49.65	0.30	0.07	0.13	0.33	45.31	0.78	2.51		1.23	97.85
99-6-15	6-15-10	51.97	0.26	0.00	0.19	0.29	43.00	1.11	2.20		1.17	97.85
99-6-15	6-15-11	53.28	0.26	0.05	0.17	0.32	40.99	1.11	2.25	0.011	1.19	97.24
99-6-15	6-15-12	51.25	0.23	0.06	0.08	0.32	46.13	1.23	2.07		1.15	100.22
99-6-15	6-15-13	50.88	0.20	0.00	0.15	0.17	47.11	0.71	2.42		1.17	100.46
99-6-15	6-15-14	51.22	0.20	0.00	0.15	0.33	46.49	0.67	2.47		1.19	100.35
99-6-15	6-15-15	53.31	0.27	0.08	0.22	0.29	43.74	0.71	2.69		1.29	100.02

Sample No.	Analyse No.	CaO	SiO_2	MnO	FeO	Na_2O	P_2O_5	Cl	F	Br	O= (Cl+F)	Total
99-6-15	6-15-16	51.11	0.20	0.02	0.04	0.28	47.21	0.74	2.47	0.043	1.20	100.92
99-6-15	6-15-17	50.71	0.24	0.00	0.15	0.28	46.38	0.79	2.55		1.25	99.85
99-6-15	6-15-18	50.84	0.25	0.02	0.12	0.37	45.35	0.80	2.56	0.025	1.26	99.07
	Average	51.61	0.24	0.02	0.16	0.31	44.19	0.86	2.42	0.019	1.21	98.61
	STDEV	1.44	0.03	0.03	0.06	0.05	2.33	0.16	0.16	0.013	0.04	1.40
99-6-16	6-16-1	54.94	0.24	0.06	0.15	0.23	42.88	1.12	2.58		1.33	100.86
99-6-16	6-16-2	54.29	0.21	0.05	0.18	0.28	40.96	0.92	3.17		1.54	98.53
99-6-16	6-16-3	54.48	0.23	0.04	0.17	0.25	41.32	1.01	3.13		1.54	99.09
99-6-16	6-16-4	54.61	0.26	0.01	0.17	0.23	41.91	1.09	2.54		1.31	99.51
99-6-16	6-16-5	54.69	0.21	0.08	0.16	0.28	41.43	1.20	2.55		1.34	99.26
99-6-16	6-16-6	54.43	0.22	0.02	0.15	0.16	41.59	1.09	2.69		1.38	98.97
99-6-16	6-16-7	55.58	0.06	0.04	0.06	0.08	42.20	0.41	3.16		1.42	100.17
99-6-16	6-16-8	54.77	0.20	0.02	0.20	0.19	40.72	1.10	2.50		1.30	98.41
99-6-16	6-16-9	53.62	0.30	0.00	0.16	0.27	40.02	0.70	2.98	0.014	1.41	96.64
99-6-16	6-16-10	55.96	0.28	0.02	0.21	0.21	38.53	0.64	3.16	0.024	1.47	97.56
99-6-16	6-16-11	54.55	0.27	0.06	0.16	0.27	39.53	0.69	2.52	0.032	1.22	96.88
99-6-16	6-16-12	53.38	0.25	0.00	0.19	0.25	42.54	0.66	2.91		1.37	98.80
99-6-16	6-16-13	53.68	0.29	0.00	0.14	0.27	41.64	0.63	2.73	0.016	1.29	98.10
99-6-16	6-16-14	56.11	0.24	0.03	0.21	0.30	37.24	0.66	2.91		1.37	96.32
99-6-16	6-16-15	54.89	0.28	0.07	0.24	0.29	39.73	0.72	3.96	0.024	1.82	98.38
99-6-16	6-16-16	53.59	0.24	0.07	0.13	0.28	41.29	0.76	2.85		1.37	97.85
99-6-16	6-16-17	56.78	0.17	0.04	0.13	0.13	37.66	0.21	4.61		1.98	97.75
	Average	54.73	0.23	0.04	0.17	0.23	40.66	0.80	3.00	0.022	1.44	98.43
	STDEV	0.94	0.06	0.03	0.04	0.06	1.65	0.27	0.55	0.013	0.20	1.21
99-6-17	6-17-1	53.60	0.27	0.00	0.18	0.27	40.26	0.94	3.39		1.64	97.27
99-6-17	6-17-2	54.03	0.30	0.05	0.15	0.32	38.55	0.91	3.31		1.60	96.03
99-6-17	6-17-3	54.57	0.28	0.00	0.19	0.28	38.80	0.94	3.05		1.49	96.63
99-6-17	6-17-4	53.50	0.22	0.06	0.14	0.34	41.25	1.03	2.29	0.022	1.19	97.66
99-6-17	6-17-5	52.11	0.22	0.06	0.21	0.37	42.41	1.08	2.13	0.009	1.14	97.47
99-6-17	6-17-6	50.06	0.22	0.04	0.18	0.26	47.07	1.02	2.14		1.13	99.86
99-6-17	6-17-7	53.59	0.24	0.07	0.12	0.26	40.96	1.04	3.60		1.75	98.13
99-6-17	6-17-8	54.73	0.26	0.02	0.13	0.27	39.30	1.08	3.53	0.016	1.72	97.60
99-6-17	6-17-9	53.84	0.24	0.08	0.15	0.31	39.20	1.23	3.35	0.003	1.68	96.71
99-6-17	6-17-10	53.73	0.25	0.03	0.21	0.20	43.55	0.68	3.39		1.58	100.46
99-6-17	6-17-11	52.96	0.27	0.04	0.12	0.23	42.81	0.72	2.91	0.002	1.38	98.68
99-6-17	6-17-12	54.39	0.30	0.01	0.18	0.27	41.43	0.68	3.40		1.58	99.07
	Average	53.43	0.26	0.04	0.16	0.28	41.30	0.95	3.04	0.011	1.49	97.97
	STDEV	1.28	0.03	0.03	0.03	0.05	2.44	0.17	0.55	0.008	0.23	1.34
99-6-18	6-18-1	56.13	0.00	0.00	0.25	0.00	42.36	1.24	0.00		0.28	99.70
99-6-18	6-18-2	57.11	0.00	0.07	0.26	0.00	41.87	1.23	0.11		0.32	100.33
99-6-18	6-18-3	55.05	0.00	0.06	0.19	0.00	41.20	1.15	0.11		0.31	97.46
99-6-18	6-18-4	56.98	0.00	0.01	0.14	0.01	42.67	1.22	0.45		0.46	101.01
99-6-18	6-18-5	55.09	0.00	0.05	0.08	0.00	40.71	1.10	0.57		0.48	97.11
99-6-18	6-18-6	56.65	0.00	0.05	0.05	0.00	42.54	1.05	1.41		0.83	100.92
99-6-18	6-18-7	54.60	0.00	0.02	0.15	0.00	40.83	1.00	1.61		0.90	97.31

Sample No.	Analyse No.	CaO	SiO_2	MnO	FeO	Na_2O	P_2O_5	Cl	F	Br	O= (Cl+F)	Total
99-6-18	6-18-8	56.15	0.22	0.09	0.03	0.15	43.46	1.16	2.78		1.43	102.60
99-6-18	6-18-9	54.26	0.22	0.00	0.22	0.23	40.97	1.03	3.14		1.55	98.52
99-6-18	6-18-10	56.92	0.20	0.10	0.06	0.11	43.88	1.02	2.09		1.11	103.28
99-6-18	6-18-11	54.78	0.15	0.03	0.21	0.16	41.13	1.01	2.67		1.35	98.79
99-6-18	6-18-12	54.68	0.12	0.01	0.20	0.14	41.49	1.07	2.66		1.36	99.01
99-6-18	6-18-13	57.87	0.07	0.00	0.04	0.00	43.17	0.15	2.59		1.12	102.76
99-6-18	6-18-14	56.97	0.10	0.05	0.00	0.00	42.47	0.10	2.10		0.90	100.88
99-6-18	6-18-15	50.74	0.20	0.08	0.07	0.17	42.65	1.27	2.08		1.16	96.10
99-6-18	6-18-16	52.18	0.23	0.07	0.12	0.27	42.31	0.88	2.34		1.18	97.22
99-6-18	6-18-17	52.79	0.19	0.07	0.12	0.24	40.86	0.96	2.28	0.029	1.17	96.37
99-6-18	6-18-18	54.42	0.23	0.04	0.10	0.21	39.86	0.63	2.60	0.006	1.24	96.87
99-6-18	6-18-19	53.98	0.22	0.01	0.13	0.33	40.30	0.69	2.40		1.16	96.90
99-6-18	6-18-20	50.42	0.24	0.00	0.07	0.23	44.79	0.73	2.57	0.027	1.24	97.83
	Average	54.89	0.12	0.04	0.13	0.11	41.98	0.93	1.83	0.021	0.98	99.07
	STDEV	2.10	0.10	0.03	0.08	0.11	1.28	0.33	1.02	0.010	0.40	2.26
99-6-19	6-19-1	54.38	0.25	0.07	0.20	0.18	41.01	1.10	2.61		1.35	98.46
99-6-19	6-19-2	56.13	0.06	0.00	0.05	0.00	42.31	0.20	2.97		1.29	100.42
99-6-19	6-19-3	54.62	0.21	0.00	0.11	0.20	41.79	1.04	2.49		1.28	99.18
99-6-19	6-19-4	54.80	0.28	0.10	0.15	0.23	41.54	1.01	2.94		1.46	99.58
99-6-19	6-19-5	50.97	0.22	0.00	0.06	0.33	46.12	0.83	2.30	0.013	1.16	99.70
99-6-19	6-19-6	49.67	0.25	0.09	0.17	0.28	46.39	0.82	2.54		1.25	98.95
99-6-19	6-19-7	53.59	0.26	0.00	0.17	0.55	40.97	0.90	2.05		1.06	97.43
99-6-19	6-19-8	54.32	0.25	0.03	0.19	0.39	43.74	0.68	2.03	0.019	1.00	100.64
99-6-19	6-19-9	49.44	0.25	0.00	0.18	0.32	46.90	1.03	2.14	0.040	1.13	99.18
99-6-19	6-19-10	53.13	0.29	0.05	0.23	0.27	42.17	0.82	2.40	0.039	1.19	98.22
99-6-19	6-19-11	54.82	0.25	0.03	0.13	0.31	41.32	0.70	2.44		1.18	98.81
99-6-19	6-19-12	54.43	0.26	0.00	0.18	0.31	41.46	0.61	2.56		1.21	98.60
99-6-19	6-19-13	51.11	0.26	0.01	0.16	0.34	45.55	0.73	2.45		1.20	99.43
99-6-19	6-19-14	50.31	0.24	0.00	0.14	0.24	46.74	0.72	2.22	0.015	1.09	99.53
99-6-19	6-19-15	52.23	0.25	0.00	0.22	0.31	44.07	0.67	2.35		1.14	98.96
99-6-19	6-19-16	51.60	0.20	0.00	0.11	0.09	46.72	0.13	2.67	0.026	1.15	100.39
99-6-19	6-19-17	51.34	0.25	0.00	0.19	0.29	45.15	0.79	2.50		1.23	99.28
99-6-19	6-19-18	51.28	0.24	0.04	0.16	0.25	45.00	0.83	2.42	0.001	1.20	99.02
99-6-19	6-19-19	53.91	0.24	0.00	0.12	0.19	42.21	0.84	2.48	0.034	1.23	98.79
99-6-19	6-19-20	53.53	0.27	0.06	0.17	0.33	43.09	0.77	2.32		1.15	99.39
99-6-19	6-19-21	53.43	0.20	0.02	0.09	0.38	43.26	0.74	2.55		1.24	99.43
99-6-19	6-19-22	49.97	0.24	0.01	0.20	0.25	46.34	0.82	2.40		1.19	99.04
	Average	52.68	0.24	0.02	0.15	0.27	43.81	0.76	2.45	0.023	1.20	99.22
	STDEV	1.95	0.05	0.03	0.05	0.11	2.14	0.23	0.24	0.015	0.10	0.73
99-6-20	6-20-1	54.95	0.08	0.00	0.04	0.00	43.29	0.19	2.80		1.22	100.14
99-6-20	6-20-2	55.59	0.01	0.00	0.01	0.00	41.83	0.02	3.25		1.37	99.35
99-6-20	6-20-3	55.20	0.10	0.00	0.03	0.00	42.48	0.18	2.93		1.27	99.65
99-6-20	6-20-4	55.01	0.04	0.03	0.01	0.00	42.06	0.03	3.24		1.37	99.04
99-6-20	6-20-5	53.21	0.19	0.01	0.37	0.00	41.53	0.13	2.65		1.14	96.95
99-6-20	6-20-6	55.25	0.14	0.04	0.07	0.01	41.98	0.07	2.86		1.22	99.21
99-6-20	6-20-7	54.36	0.12	0.00	0.15	0.09	41.61	0.46	2.93		1.33	98.38

Sample No.	Analyse No.	CaO	SiO_2	MnO	FeO	Na_2O	P_2O_5	Cl	F	Br	O= (Cl+F)	Total
99-6-20	6-20-8	53.37	0.15	0.01	0.11	0.15	41.31	1.05	2.67		1.36	97.47
99-6-20	6-20-9	54.30	0.20	0.00	0.36	0.00	41.19	0.18	3.06		1.33	97.96
99-6-20	6-20-10	55.30	0.09	0.00	0.04	0.00	42.17	0.20	2.80		1.22	99.37
99-6-20	6-20-11	53.76	0.16	0.06	0.13	0.11	41.38	0.74	2.74		1.32	97.75
99-6-20	6-20-12	52.94	0.21	0.01	0.22	0.08	41.21	0.39	2.36		1.08	96.33
99-6-20	6-20-13	54.85	0.12	0.01	0.03	0.00	42.15	0.06	2.80		1.19	98.82
99-6-20	6-20-14	55.41	0.05	0.00	0.00	0.00	42.08	0.08	3.00		1.28	99.34
99-6-20	6-20-15	54.16	0.10	0.00	0.11	0.20	41.53	0.71	2.64		1.27	98.18
99-6-20	6-20-16	54.54	0.28	0.00	0.10	0.16	41.31	0.65	3.37	0.007	1.56	98.86
99-6-20	6-20-17	56.17	0.26	0.05	0.02	0.17	39.05	0.67	3.05	0.020	1.43	98.03
99-6-20	6-20-18	54.44	0.24	0.00	0.08	0.11	40.51	0.34	3.09		1.37	97.45
99-6-20	6-20-19	54.77	0.74	0.05	0.34	0.17	40.09	0.56	3.54	0.007	1.61	98.65
99-6-20	6-20-20	55.67	0.23	0.02	0.11	0.20	39.16	0.66	3.05		1.43	97.66
99-6-20	6-20-21	53.51	0.28	0.03	0.13	0.15	42.00	0.67	2.74		1.30	98.20
99-6-20	6-20-22	51.65	0.35	0.04	0.15	0.27	40.38	0.88	3.45	0.011	1.65	95.53
99-6-20	6-20-23	51.18	0.32	0.00	0.08	0.25	41.52	0.80	3.44	0.007	1.62	95.98
99-6-20	6-20-24	54.74	0.34	0.04	0.14	0.27	37.64	0.94	3.12	0.010	1.52	95.72
	Average	54.35	0.20	0.02	0.12	0.10	41.23	0.44	2.98	0.010	1.35	98.09
	STDEV	1.22	0.15	0.02	0.11	0.10	1.24	0.33	0.30	0.007	0.15	1.27
99-6-21	6-21-1	54.33	0.29	0.03	0.09	0.00	41.66	0.44	2.63		1.20	98.27
99-6-21	6-21-2	54.57	0.08	0.00	0.09	0.00	42.63	0.08	3.02		1.29	99.18
99-6-21	6-21-3	55.64	0.04	0.01	0.00	0.00	42.39	0.05	3.14		1.33	99.94
99-6-21	6-21-4	55.29	0.04	0.00	0.03	0.00	42.53	0.03	3.31		1.40	99.84
99-6-21	6-21-5	53.97	0.17	0.00	0.00	0.00	42.80	0.11	3.02		1.29	98.78
99-6-21	6-21-6	55.06	0.16	0.00	0.00	0.00	41.85	0.13	3.15		1.35	99.00
99-6-21	6-21-7	54.87	0.09	0.00	0.00	0.01	41.76	0.09	3.19		1.36	98.65
99-6-21	6-21-8	54.48	0.18	0.01	0.03	0.00	41.90	0.10	3.32		1.42	98.61
99-6-21	6-21-9	55.14	0.09	0.06	0.00	0.00	42.60	0.07	2.78		1.19	99.56
99-6-21	6-21-10	55.63	0.10	0.03	0.07	0.01	42.50	0.14	3.37		1.45	100.39
99-6-21	6-21-11	55.20	0.06	0.03	0.01	0.00	42.45	0.18	3.30		1.43	99.80
99-6-21	6-21-12	53.93	0.10	0.00	0.00	0.00	42.58	0.16	3.17		1.37	98.57
99-6-21	6-21-13	54.63	0.11	0.00	0.03	0.00	41.36	0.20	3.09		1.34	98.08
99-6-21	6-21-14	54.50	0.10	0.04	0.09	0.00	42.27	0.04	3.37		1.42	98.98
99-6-21	6-21-15	55.39	0.09	0.03	0.05	0.00	42.48	0.04	3.23		1.37	99.95
99-6-21	6-21-16	54.62	0.15	0.00	0.05	0.01	41.80	0.23	3.21		1.40	98.67
99-6-21	6-21-17	55.11	0.14	0.00	0.00	0.00	42.01	0.16	2.29		1.00	98.71
99-6-21	6-21-18	55.24	0.01	0.02	0.00	0.06	42.27	0.23	3.16		1.38	99.61
99-6-21	6-21-19	54.57	0.21	0.00	0.11	0.23	41.23	1.07	2.70		1.37	98.75
99-6-21	6-21-20	54.27	0.26	0.00	0.09	0.28	42.03	1.05	2.53		1.30	99.20
99-6-21	6-21-21	54.40	0.23	0.04	0.18	0.24	41.38	1.01	2.53		1.29	98.72
99-6-21	6-21-22	54.73	0.23	0.01	0.09	0.28	41.07	1.03	2.55		1.30	98.69
99-6-21	6-21-23	54.18	0.24	0.02	0.15	0.27	41.80	1.09	2.68		1.37	99.06
99-6-21	6-21-24	55.00	0.28	0.06	0.12	0.28	36.60	1.08	3.65	0.020	1.78	95.30
99-6-21	6-21-25	55.37	0.27	0.08	0.16	0.30	39.49	0.65	3.21	0.003	1.49	98.03
	Average	54.80	0.15	0.02	0.06	0.08	41.74	0.38	3.02	0.012	1.35	98.90
	STDEV	0.49	0.08	0.02	0.06	0.12	1.28	0.41	0.34	0.012	0.13	0.97

Sample No.	Analyse No.	CaO	SiO_2	MnO	FeO	Na_2O	P_2O_5	Cl	F	Br	O= (Cl+F)	Total
99-6-22	6-21-1	51.99	0.22	0.02	0.12	0.20	39.93	0.89	3.38	0.005	1.62	95.13
99-6-22	6-21-2	55.20	0.23	0.02	0.11	0.26	35.96	0.81	3.53		1.66	94.45
99-6-22	6-21-3	52.85	0.21	0.04	0.06	0.25	39.34	0.88	3.52		1.68	95.47
99-6-22	6-21-4	53.92	0.28	0.00	0.13	0.22	38.76	0.87	3.63	0.024	1.72	96.11
99-6-22	6-21-5	56.48	0.17	0.01	0.08	0.20	38.37	0.74	3.24		1.53	97.77
99-6-22	6-21-6	56.01	0.13	0.01	0.06	0.26	38.19	0.78	3.01	0.009	1.44	97.01
99-6-22	6-21-7	56.01	0.15	0.02	0.09	0.16	38.49	0.72	2.85		1.36	97.14
99-6-22	6-21-8	56.14	0.29	0.00	0.14	0.24	36.90	0.66	3.84	0.001	1.76	96.44
99-6-22	6-21-9	54.49	0.33	0.00	0.17	0.28	39.10	0.66	3.59		1.66	96.96
99-6-22	6-21-10	55.00	0.27	0.00	0.19	0.29	38.99	0.66	3.86	0.005	1.77	97.49
	Average	54.81	0.23	0.01	0.11	0.24	38.40	0.77	3.45	0.011	1.62	96.40
	STDEV	1.50	0.06	0.01	0.04	0.04	1.18	0.09	0.33	0.008	0.14	1.09
99-6-23	6-23-1	53.47	0.28	0.00	0.12	0.32	41.04	1.04	2.38		1.23	97.41
99-6-23	6-23-2	54.00	0.20	0.00	0.12	0.11	41.68	1.14	2.43		1.28	98.41
99-6-23	6-23-3	54.04	0.34	0.06	0.15	0.38	40.20	1.15	2.31		1.23	97.40
99-6-23	6-23-4	56.05	0.11	0.01	0.03	0.00	42.04	0.09	2.81		1.20	99.94
99-6-23	6-23-5	55.21	0.12	0.07	0.00	0.03	41.99	0.15	2.62		1.13	99.05
99-6-23	6-23-6	56.00	0.09	0.00	0.01	0.00	42.24	0.08	2.78		1.18	100.01
99-6-23	6-23-7	55.01	0.04	0.01	0.00	0.00	42.72	0.15	2.87		1.24	99.56
99-6-23	6-23-8	53.62	0.30	0.00	0.18	0.31	40.48	1.03	2.46		1.27	97.12
99-6-23	6-23-9	55.53	0.26	0.00	0.03	0.02	42.00	0.24	2.77		1.22	99.62
99-6-23	6-23-10	54.72	0.08	0.01	0.23	0.13	41.93	0.86	3.21		1.54	99.63
99-6-23	6-23-11	55.89	0.03	0.02	0.12	0.00	43.36	0.03	3.48		1.47	101.46
99-6-23	6-23-12	55.27	0.25	0.06	0.01	0.07	41.39	0.41	2.81		1.27	98.98
99-6-23	6-23-13	53.95	0.24	0.00	0.18	0.11	42.23	0.93	2.96		1.45	99.15
99-6-23	6-23-14	56.33	0.03	0.00	0.11	0.00	41.80	0.08	3.52		1.50	100.37
99-6-23	6-23-15	54.95	0.11	0.00	0.01	0.00	42.77	0.07	3.37		1.43	99.85
99-6-23	6-23-16	54.58	0.21	0.06	0.08	0.11	41.90	0.93	3.05		1.49	99.41
99-6-23	6-23-17	55.00	0.32	0.06	0.13	0.23	41.23	0.90	2.89		1.41	99.33
99-6-23	6-23-18	55.33	0.23	0.00	0.02	0.03	41.79	0.48	3.28		1.48	99.66
99-6-23	6-23-19	54.37	0.27	0.02	0.19	0.15	41.90	0.92	2.89		1.42	99.29
99-6-23	6-23-20	53.98	0.25	0.00	0.15	0.12	42.19	0.99	3.02		1.49	99.21
99-6-23	6-23-21	54.49	0.22	0.00	0.08	0.22	42.25	0.65	2.91		1.37	99.45
99-6-23	6-23-22	55.86	0.26	0.02	0.04	0.00	42.45	0.03	3.39		1.43	100.62
99-6-23	6-23-23	54.54	0.25	0.00	0.22	0.25	41.93	0.70	2.47		1.19	99.17
99-6-23	6-23-24	52.32	0.24	0.02	0.12	0.24	45.22	0.64	1.81	0.028	0.90	99.74
99-6-23	6-23-25	52.07	0.22	0.00	0.12	0.26	45.04	0.66	1.69		0.86	99.21
99-6-23	6-23-26	51.71	0.31	0.14	0.11	0.21	46.87	0.67	1.75	0.004	0.89	100.88
	Average	54.55	0.20	0.02	0.10	0.13	42.33	0.58	2.77	0.016	1.29	99.40
	STDEV	1.21	0.09	0.03	0.07	0.12	1.44	0.40	0.50	0.014	0.19	0.99
99-6-24	6-24-1	53.94	0.22	0.02	0.21	0.27	40.47	1.05	3.32		1.63	97.87
99-6-24	6-24-2	53.81	0.28	0.00	0.16	0.26	41.04	0.99	2.92		1.45	98.02
99-6-24	6-24-3	53.81	0.23	0.04	0.11	0.23	41.21	0.89	2.27		1.15	97.64
99-6-24	6-24-4	52.64	0.21	0.00	0.14	0.32	41.10	0.97	2.24		1.16	96.46
99-6-24	6-24-5	53.00	0.27	0.04	0.16	0.26	41.12	1.01	2.57		1.31	97.12
99-6-24	6-24-6	53.36	0.16	0.06	0.18	0.15	41.37	0.65	2.81		1.33	97.41

Sample No.	Analyse No.	CaO	SiO_2	MnO	FeO	Na_2O	P_2O_5	Cl	F	Br	O= (Cl+F)	Total
99-6-24	6-24-7	54.73	0.08	0.03	0.03	0.00	41.51	0.28	2.47		1.10	98.03
99-6-24	6-24-8	53.44	0.17	0.00	0.11	0.25	41.41	0.98	2.53		1.28	97.61
99-6-24	6-24-9	53.80	0.08	0.00	0.00	0.00	42.14	0.14	2.75		1.19	97.72
99-6-24	6-24-10	53.32	0.23	0.05	0.14	0.27	40.88	1.06	2.48		1.28	97.14
99-6-24	6-24-11	53.08	0.26	0.00	0.18	0.20	40.73	1.10	2.36		1.24	96.67
99-6-24	6-24-12	53.13	0.23	0.01	0.10	0.28	40.82	0.99	3.19		1.56	97.19
99-6-24	6-24-13	53.05	0.19	0.05	0.03	0.07	41.51	0.33	2.55		1.14	96.62
99-6-24	6-24-14	54.09	0.16	0.02	0.05	0.00	41.84	0.13	2.84		1.22	97.92
99-6-24	6-24-15	52.41	0.26	0.00	0.15	0.31	40.30	1.11	2.22	0.040	1.18	95.62
99-6-24	6-24-16	52.46	0.30	0.00	0.18	0.30	40.02	1.05	2.07	0.008	1.11	95.28
99-6-24	6-24-17	49.99	0.24	0.06	0.09	0.32	43.51	1.18	2.26	0.012	1.21	96.44
99-6-24	6-24-18	50.02	0.23	0.05	0.17	0.31	45.27	1.13	2.10	0.026	1.14	98.16
99-6-24	6-24-19	52.38	0.22	0.01	0.07	0.32	40.65	1.10	2.38	0.057	1.25	95.95
99-6-24	6-24-20	52.37	0.28	0.00	0.13	0.25	39.73	1.20	2.15	0.014	1.17	94.96
99-6-24	6-24-21	51.92	0.20	0.00	0.15	0.47	40.35	1.18	2.15	0.013	1.17	95.26
99-6-24	6-24-22	50.07	0.24	0.00	0.16	0.24	43.50	1.10	2.12	0.014	1.14	96.31
99-6-24	6-24-23	51.17	0.21	0.12	0.25	0.27	42.58	1.15	2.08	0.053	1.13	96.75
	Average	52.70	0.22	0.02	0.13	0.23	41.44	0.90	2.47	0.026	1.24	96.89
	STDEV	1.31	0.06	0.03	0.06	0.12	1.28	0.34	0.36	0.019	0.14	0.97
99-6-26	6-26-1	53.29	0.15	0.04	0.15	0.17	41.03	0.69	2.77		1.32	96.97
99-6-26	6-26-2	53.13	0.03	0.06	0.09	0.16	41.50	0.75	2.82		1.35	97.19
99-6-26	6-26-3	53.17	0.00	0.03	0.22	0.15	41.84	0.71	2.73		1.31	97.54
99-6-26	6-26-4	53.28	0.01	0.00	0.09	0.22	41.53	0.74	2.75		1.32	97.30
99-6-26	6-26-5	54.03	0.03	0.01	0.12	0.24	41.49	0.74	2.59		1.26	98.00
99-6-26	6-26-6	52.20	0.04	0.03	0.12	0.21	41.50	0.77	2.83		1.36	96.33
99-6-26	6-26-7	53.63	0.16	0.00	0.24	0.24	41.35	0.77	2.79		1.34	97.83
99-6-26	6-26-8	53.07	0.18	0.05	0.17	0.18	41.33	0.79	2.80		1.35	97.21
99-6-26	6-26-9	53.16	0.17	0.03	0.19	0.18	41.44	0.74	2.52		1.22	97.21
99-6-26	6-26-10	54.03	0.02	0.00	0.04	0.12	40.37	0.01	3.39		1.43	96.55
99-6-26	6-26-11	53.27	0.20	0.04	0.15	0.26	41.14	0.69	2.84		1.35	97.25
99-6-26	6-26-12	53.72	0.00	0.09	0.13	0.22	41.65	0.74	3.18		1.50	98.22
99-6-26	6-26-13	53.49	0.01	0.00	0.18	0.36	41.31	0.67	3.20		1.50	97.72
99-6-26	6-26-14	54.19	0.05	0.01	0.21	0.28	41.37	0.71	3.14		1.48	98.48
99-6-26	6-26-15	53.76	0.00	0.00	0.22	0.20	42.00	0.72	3.06		1.45	98.52
99-6-26	6-26-16	52.94	0.09	0.04	0.56	0.23	42.05	0.70	3.20		1.50	98.31
99-6-26	6-26-17	54.78	0.06	0.00	0.72	0.07	42.04	0.37	3.37		1.50	99.92
99-6-26	6-26-18	53.04	0.06	0.01	0.12	0.14	41.71	0.66	3.01		1.41	97.34
99-6-26	6-26-19	54.33	0.02	0.00	0.06	0.12	41.50	0.71	2.85		1.36	98.24
99-6-26	6-26-20	54.52	0.00	0.01	0.19	0.22	42.17	0.71	3.10		1.46	99.46
99-6-26	6-26-21	54.26	0.09	0.05	0.10	0.11	41.95	0.71	3.20		1.50	98.96
99-6-26	6-26-22	53.06	0.11	0.02	0.16	0.19	41.80	0.71	3.24		1.52	97.76
99-6-26	6-26-23	53.94	0.10	0.03	0.11	0.13	41.81	0.72	3.00		1.42	98.42
99-6-26	6-26-24	53.51	0.24	0.00	0.17	0.16	41.78	0.71	3.00		1.42	98.14
99-6-26	6-26-25	53.08	0.06	0.06	0.14	0.31	41.30	0.69	2.44		1.18	96.90
99-6-26	6-26-26	52.65	0.02	0.03	0.12	0.36	41.32	0.76	2.56		1.25	96.58
99-6-26	6-26-27	52.94	0.00	0.00	0.17	0.33	41.58	0.79	2.66		1.30	97.18
99-6-26	6-26-28	52.44	0.01	0.09	0.12	0.35	41.75	0.77	2.70		1.31	96.93

Sample No.	Analyse No.	CaO	SiO_2	MnO	FeO	Na_2O	P_2O_5	Cl	F	Br	O= (Cl+F)	Total
99-6-26	6-26-29	52.81	0.03	0.09	0.18	0.29	42.07	0.75	2.72		1.31	97.63
99-6-26	6-26-30	53.47	0.01	0.05	0.14	0.15	41.89	0.67	2.78		1.32	97.84
99-6-26	6-26-31	53.23	0.12	0.00	0.29	0.11	41.66	0.75	2.77		1.33	97.59
99-6-26	6-26-32	53.41	0.18	0.06	0.24	0.19	41.22	0.69	2.66		1.27	97.36
	Average	53.43	0.07	0.03	0.18	0.21	41.58	0.69	2.90		1.37	97.72
	STDEV	0.60	0.07	0.03	0.13	0.08	0.37	0.14	0.25		0.09	1.58

Appendix 4a Micro XRF Analytical Results of Oka Apatite (ppm)

Sample No.	Analyse No.	Mn	Fe (wt %)	Br	Sr	Y	Ce	Nd
9718	9718-1		0.029	19	9574	428	7	3
9718	9718-2		0.032	16	9243	418	7	3
9718	9718-3		0.017	14	8051	390	10	2
9718	9718-4		0.008	13	8256	410	9	3
9718	9718-5		0.132	22	8457	482	9	4
9718	9718-6		0.097	28	8192	463	8	4
9718	9718-7		0.133	34	7236	314	8	3
9718	9718-8	390	0.150	39	7569	313	8	3
9718	9718-9	880	0.030	56	7138	386	9	5
9718	9718-10	631	0.037	90	6615	357	10	4
9718	9718-11	523	0.040	126	5143	253	9	3
9718	9718-12	266	0.012	147	4671	240	7	3
9718	9718-13	525	0.035	134	4829	229	9	3
	Average	536	0.058	57	7306	360	9	3
	STDEV	211	0.051	50	1602	84	1	1
9719	9719-1			35	9063	207		
9719	9719-2			40	8723	200		
9719	9719-3			20	8938	186		
9719	9719-4			28	8951	181		
9719	9719-5			19	9756	203		
9719	9719-6			15	9170	191		
9719	9719-7			81	7946	166		
9719	9719-8			66	8469	185		
9719	9719-9			77	8624	203		
9719	9719-10			67	8259	190		
9719	9719-11			24	10159	213		
9719	9719-12			25	9729	201		
	Average			41	8982	194		
	STDEV			25	650	13		
9723	9723-1	678	0.043	43	5095	224	5	2
9723	9723-2	827	0.071	38	5084	209	6	3
9723	9723-3	682	0.005	37	5101	187	7	3
9723	9723-4	929	0.063	16	5532	188	7	3
9723	9723-5	865	0.018	19	5547	197	7	3
9723	9723-6	531	0.017	21	4315	157	7	2
9723	9723-7	1351	0.020	2	4754	180	9	5
9723	9723-8	1048	0.018	13	5158	198	6	2
9723	9723-9	807	0.012	26	6465	267	8	3
9723	9723-10	776	0.002	21	5410	225	7	5
9723	9723-11	584	0.015	10	3257	130	4	1
9723	9723-12	696	0.011	4	6777	260	7	3
9723	9723-13	769	0.017	10	6787	261	7	4
	Average	811	0.024	20	5329	206	7	3
	STDEV	213	0.022	13	977	41	1	1

Sample No.	Analyse No.	Mn	Fe (wt %)	Br	Sr	Y	Ce	Nd
9729	9729-1	684	0.034	27	7177	403	9	4
9729	9729-2	672	0.049	16	8017	450	10	4
9729	9729-3	458	0.042	30	8186	469	11	5
9729	9729-4	445	0.035	5	8900	502	10	4
9729	9729-5	446	0.034	4	8774	496	11	5
9729	9729-6	792	0.450	10	8562	452	12	4
9729	9729-7	735	0.916	9	8219	449	12	5
9729	9729-8	640	0.940	9	8288	447	11	6
9729	9729-9	607	1.059	8	8152	443	10	5
9729	9729-10	788	0.031	37	6229	355	10	3
9729	9729-11	501	0.041	27	6762	379	8	5
9729	9729-12	808	0.035	42	6313	373	9	4
9729	9729-13	791	0.045	11	8212	469	12	5
9729	9729-14	782	0.034	4	7693	444	10	4
	Average	653	0.268	17	7820	438	10	4
	STDEV	140	0.398	13	868	44	1	1
9730	9730-1	797	0.196	11	4885	416	15	5
9730	9730-2	759	0.171	8	4829	387	15	5
	Average	778	0.183	9	4857	401	15	5
	STDEV	27	0.018	3	40	21	0	0

Appendix 4b EMPA Results of Apatite from Oka Carbonatite (wt %)

Sample No.	Analyse No.	CaO	FeO	MnO	SrO	Na_2O	K_2O	P_2O_5	Cl	F	Br	Total
8718	9718-1	48.83	0.05	0.07	0.73	0.14		41.49	0.01	2.51	0.007	93.84
8718	9718-2	52.03	0.04	0.11	0.81	0.14	0.01	38.71	0.02	2.62		94.49
8718	9718-3	48.56	0.03	0.11	0.72	0.14	0.00	40.34	0.01	2.58		92.48
8718	9718-4	48.56	0.03	0.10	0.87	0.12	0.01	43.72	0.00	2.64	0.013	96.06
8718	9718-5	49.96	0.07		0.82	0.14		42.00	0.02	2.74	0.001	95.75
8718	9718-6	50.88	0.02	0.09	0.84	0.15		42.61	0.01	2.61	0.007	97.23
8718	9718-7	51.32		0.02	0.81	0.19	0.02	39.28	0.01	2.56		94.21
8718	9718-8	48.21		0.09	0.85	0.16		43.81	0.01	2.55	0.005	95.68
8718	9718-9	51.15	0.00	0.04	0.87	0.10		40.21	0.01	2.52	0.020	94.91
8718	9718-10	53.03		0.12	0.87	0.07		40.16	0.01	2.01	0.006	96.28
8718	9718-11	51.41	0.01	0.04	0.85	0.15		39.42	0.00	1.95	0.005	93.83
8718	9718-12	49.75		0.11	0.87	0.10		41.59	0.00	1.87		94.28
8718	9718-13	49.56	0.01	0.10	0.85	0.13		43.40	0.01	1.92		95.99
8718	9718-14	50.26	0.02	0.02		0.15	0.02	43.25	0.00	0.53	0.004	94.26
8718	9718-15	49.29		0.02		0.09	0.01	44.77	0.01	0.41	0.005	94.60
	Average	50.19	0.03	0.07	0.83	0.13	0.01	41.65	0.01	2.13	0.007	94.93
	STDEV	1.42	0.02	0.04	0.05	0.03	0.01	1.90	0.01	0.74	0.006	1.22
9719	9719-1	52.89				0.23		43.58	0.25	3.05		100.08
9719	9719-2	54.17				0.23		41.36	0.40	2.96		99.20
9719	9719-3	49.97		0.11	0.73	0.17		45.63	0.00	3.43	0.013	100.06
9719	9719-4	50.15		0.09	0.79	0.25	0.01	44.89		3.72	0.022	99.92
9719	9719-5	55.80		0.06	1.03	0.27		41.64	0.00	1.47		100.27
9719	9719-6	53.55	0.05	0.09	0.84	0.19	0.02	41.65		2.44		98.83
9719	9719-7	51.16		0.12	0.98	0.26	0.01	43.62	0.00	3.45		99.61
9719	9719-8	52.54		0.04	1.00	0.29		42.32	0.00	2.12	0.011	98.32
9719	9719-9	48.32		0.12	0.77	0.20	0.01	45.78	0.01	3.53	0.010	98.74
9719	9719-10	48.60		0.10	0.76	0.21		46.67		3.38	0.002	99.73
9719	9719-11	48.46		0.08	0.91	0.22		45.88	0.00	3.34	0.019	98.91
9719	9719-12	51.83	0.01	0.14	0.94	0.28		41.76	0.01	3.68	0.003	98.65
9719	9719-13	52.80	0.03	0.15	0.73	0.22		39.39	0.00	3.39		96.71
9719	9719-14	52.87	0.02	0.06	0.73	0.18		41.58	0.02	3.49		98.95
9719	9719-15	49.10	0.02	0.12	0.92	0.18	0.01	46.18	0.00	3.56		100.09
9719	9719-16	52.22	0.06	0.02	0.92	0.28		42.12		3.35	0.025	98.98
9719	9719-17	50.15	0.05	0.02	0.94	0.25		45.65	0.00	3.28		100.35
9719	9719-18	50.29		0.16		0.31	0.01	45.30	0.01	2.38	0.006	98.46
	Average	51.38	0.03	0.08	0.87	0.23	0.01	43.61	0.05	3.11	0.012	99.21
	STDEV	2.14	0.02	0.04	0.11	0.04	0.00	2.18	0.12	0.61	0.008	0.91
9723	9723-4	50.98	0.04	0.01	0.16	0.03	0.02	46.15	5.69		0.029	103.10
9723	9723-5	53.42			0.19	0.00	0.04	43.49	5.47		0.025	102.64
9723	9723-6	51.08	0.01	0.02	0.16	0.04		47.04	5.10		0.043	103.49
9723	9723-1	52.59	0.01	0.05	0.68	0.13		42.33		2.83		98.61
9723	9723-2	53.39	0.05	0.03	0.61	0.14		41.22	0.01	4.35		99.81
9723	9723-3	53.75		0.02	0.74	0.10		39.68	0.01	3.13	0.019	97.45

Sample No.	Analyse No.	CaO	FeO	MnO	SrO	Na_2O	K_2O	P_2O_5	Cl	F	Br	Total
9723	9723-7	51.70	0.02	0.12	0.68	0.16		41.76	0.01	3.53		97.97
9723	9723-8	49.06	0.03		0.74	0.17	0.00	45.64	0.01	3.72		99.36
9723	9723-9	49.98		0.14	0.69	0.11	0.00	42.35		3.68		96.94
	Average	51.77	0.02	0.05	0.46	0.09	0.00	43.30	0.01	3.54	0.029	99.93
	STDEV	1.89	0.02	0.05	0.05	0.03	0.00	1.97	0.00	0.53	0.010	2.53
9729	9729-1	49.03	0.06	0.08	0.85	0.12		42.81	0.01	2.51		95.47
9729	9729-2	51.61	0.01	0.11	0.81	0.10	0.00	39.00	0.01	2.75		94.39
9729	9729-3	49.89		0.06	0.80	0.11	0.02	41.95	0.00	2.66		95.49
9729	9729-4	50.51		0.05	0.80	0.12	0.02	41.85	0.00	1.89	0.006	95.24
9729	9729-5	49.63		0.09	0.86	0.12	0.01	43.19	0.02	1.87		95.79
9729	9729-6	52.39		0.04	0.88	0.13	0.02	37.82	0.01	2.54		93.83
9729	9729-7	49.68	0.02	0.06	0.84	0.13		43.63	0.01	2.70		97.06
9729	9729-8	49.16	0.02	0.02	0.84	0.11		43.59	0.01	2.71		96.45
	Average	50.24	0.02	0.06	0.83	0.12	0.01	41.73	0.01	2.45	0.006	95.47
	STDEV	1.20	0.02	0.03	0.03	0.01	0.01	2.18	0.01	0.36		1.04
9730	9730-1	51.57		0.09	0.61	0.07	0.01	39.57	0.02	2.19		94.12
9730	9730-2	49.29		0.07	0.66	0.11	0.00	42.63	0.01	2.10	0.006	94.86
	Average	50.43		0.08	0.63	0.09	0.01	41.10	0.01	2.15	0.006	94.49
	STDEV	1.61		0.02	0.04	0.03	0.00	2.16	0.01	0.06		0.52

Appendix 5a Micro XRF Analytical Results of Scapolite (ppm)

Sample No.	Analyse No.	Fe	Mn	Cu	Zn	Ga	Sr	Br	Location
99-1-1	99-1-1 a	6466	93	9	27	32	2196	75	Tieshan, China
99-1-1	99-1-1 b	6588	441	60	39	38	3122	12	Tieshan, China
99-1-1	99-1-1 c	3777	61	27	21	33	1351	5	Tieshan, China
	Average	5610	198	32	29	34	2223	31	Tieshan, China
	STDEV	1589	211	26	9	3	886	39	
99-1-3	99-1-3 a	3396	129	5	31	10	1706	35	Tieshan, China
99-1-3	99-1-3 b	4638	58	49	27	16	1524	45	Tieshan, China
99-1-3	99-1-3 c	2258	57	27	23	28	1967	52	Tieshan, China
	Average	3431	81	27	27	18	1733	44	Tieshan, China
	STDEV	1190	41	22	4	9	222	9	
99-1-5	99-1-5 a	6120	94	104	52	28	2123	64	Tieshan, China
99-1-5	99-1-5 b	7712	63	49	41	38	1983	86	Tieshan, China
99-1-5	99-1-5 c	2629	19	37	8	16	1295	56	Tieshan, China
	Average	5487	59	64	34	27	1800	68	Tieshan, China
	STDEV	2600	38	36	23	11	443	15	
99-1-6	99-1-6 a	3452	22	123	22	11	3666	64	Tieshan, China
99-1-6	99-1-6 b	2551	17	108	9	28	1567	44	Tieshan, China
99-1-6	99-1-6 c	3387	26	14	20	29	1380	42	Tieshan, China
	Average	3130	22	82	17	23	2204	50	Tieshan, China
	STDEV	502	4	59	7	10	1269	12	
99-1-7	99-1-7 a	5431	246	33	41	24	12122	41	Tieshan, China
99-1-7	99-1-7 b	4651	89	48	14	25	7201	47	Tieshan, China
99-1-7	99-1-7 c	4435	106	124	18	39	5180	60	Tieshan, China
	Average	4839	147	68	24	29	8168	49	Tieshan, China
	STDEV	524	86	49	14	8	3570	10	
99-1-9	99-1-9 a	6651	183	16	34	11	1065	43	Tieshan, China
99-1-9	99-1-9 b	12268	147	10	38	10	981	39	Tieshan, China
99-1-9	99-1-9 c	7539	132	10	38	17	981	44	Tieshan, China
	Average	8819	154	12	37	13	1009	42	Tieshan, China
	STDEV	3019	26	4	3	4	48	3	
99-1-12	99-1-12 a	3898	64	38	56	24	1530	40	Tieshan, China
99-1-12	99-1-12 b	2473	29	47	36	15	1601	40	Tieshan, China
99-1-12	99-1-12 c	9509	67	185	136	23	1545	39	Tieshan, China
	Average	5293	53	90	76	21	1559	40	Tieshan, China
.	STDEV	3720	21	83	53	5	37	0	
99-1-13	99-1-13 a	15585	131	3	125	6	1340	47	Tieshan, China
99-1-13	99-1-13 b	3228	113		29	14	1486	40	Tieshan, China
99-1-13	99-1-13 c	4273	44	7	40	10	1361	42	Tieshan, China
99-1-13	99-1-13 d	8462	219		66	9	1436	51	Tieshan, China
	Average	7887	127	5	65	10	1406	45	Tieshan, China
	STDEV	5608	72	3	43	3	68	5	

Sample No.	Analyse No.	Fe	Mn	Cu	Zn	Ga	Sr	Br	Location
99-1-14	99-1-14 a	10457	235	104	46	4	1650	113	Tieshan, China
99-1-14	99-1-14 b	12533	113	41	46	8	1372	64	Tieshan, China
99-1-14	99-1-14 c	21498	120	88	113		1021	43	Tieshan, China
99-1-14	99-1-14 d	19057	-60	124	21		554	19	Tieshan, China
	Average	15886	102	89	56	6	1149	60	Tieshan, China
	STDEV	5237	122	36	40	2	473	40	
99-1-15	99-1-15 a	16876	289	8	45	11	1190	46	Tieshan, China
99-1-15	99-1-15 b	22947	266	8	72	12	831	31	Tieshan, China
99-1-15	99-1-15 c	19067	150	112	84	2	1278	46	Tieshan, China
	Average	19630	235	43	67	8	1100	41	Tieshan, China
	STDEV	3074	74	60	20	5	237	9	
99-1-16	99-1-16 a	4200	56	4	15	31	1114	53	Tieshan, China
99-1-16	99-1-16 b	3241		2	21	41	1105	56	Tieshan, China
99-1-16	99-1-16 c	2715	17	8	13	16	1280	52	Tieshan, China
99-1-16	99-1-16 d	4260	31	7	21	16	1223	57	Tieshan, China
	Average	3604	35	5	18	26	1181	55	Tieshan, China
	STDEV	754	20	3	4	12	85	2	
99-1-17	99-1-17 a	5714	56	7	20	19	1183	49	Tieshan, China
99-1-17	99-1-17 b	12732	195	45	35	20	1728	58	Tieshan, China
99-1-17	99-1-17 c	11666	150		16	8	1478	58	Tieshan, China
99-1-17	99-1-17 d	16509		28	30		1008	36	Tieshan, China
99-1-17	99-1-17 e	5950	62	22	24	22	1184	51	Tieshan, China
	Average	10514	116	25	25	17	1316	50	Tieshan, China
	STDEV	4638	68	16	8	6	285	9	
99-1-19	99-1-19 a	2554	56	67	12	14	1791	61	Tieshan, China
99-1-19	99-1-19 b	3097	116	15	13	16	3415	55	Tieshan, China
99-1-19	99-1-19 c	9059	128	9	27	10	2126	43	Tieshan, China
	Average	4903	100	30	17	13	2444	53	Tieshan, China
	STDEV	3609	38	32	8	3	857	10	
99-1-20	99-1-20 a	41117	557	132	101	22	1203	55	Tieshan, China
99-1-20	99-1-20b	21100	228	32	39	17	2378	39	Tieshan, China
99-1-20	99-1-20 c	14695	143	16	21	13	1399	49	Tieshan, China
	Average	25637	309	60	54	17	1660	47	Tieshan, China
	STDEV	13783	219	63	42	5	629	8	
99-1-21	99-1-21 a	14151	230	84	23		963	31	Tieshan, China
99-1-21	99-1-21 b	20941	192	6	28		1112	33	Tieshan, China
99-1-21	99-1-21 c	10509	67	56	18	22	1275	60	Tieshan, China
99-1-21	99-1-21 d	8810	235	2	31	3	1392	51	Tieshan, China
	Average	13603	181	37	25	12	1185	44	Tieshan, China
	STDEV	5376	78	40	6	13	188	14	
99-1-22	99-1-22 a	19593	170	23	33	32	1455	43	Tieshan, China
99-1-22	99-1-22 b	19175	402	122	106	28	1054	52	Tieshan, China
99-1-22	99-1-22 c	43745	557	49	29	18	1339	54	Tieshan, China
99-1-22	99-1-22 d	11252	230	54	28	13	1143	56	Tieshan, China
99-1-22	99-1-22 e	10339	145	10	23	4	1821	126	Tieshan, China

Sample No.	Analyse No.	Fe	Mn	Cu	Zn	Ga	Sr	Br	Location
99-1-22	99-1-22 f	45507	526	47	63	7	1532	22	Tieshan, China
	Average	24935	338	51	47	17	1391	59	Tieshan, China
	STDEV	15742	181	39	32	11	278	35	
H-2	H-2 a	11541	284		49	22	1017	131	Tieshan, China
H-2	H-2 b	12732	270		53	19	1195	79	Tieshan, China
H-2	H-2 c	11112	236	3	49	27	1381	96	Tieshan, China
	Average	11795	263	1	50	23	1198	102	Tieshan, China
	STDEV	839	25		3	4	182	27	
S88-DL-6C	DL-6C a	11676	1457		87		105	3	Grenville, QC/ON
S88-DL-6C	DL-6C b	12111	1369		100	3	96	1	Grenville, QC/ON
S88-DL-6C	DL-6C c	11076	1220		82		88		Grenville, QC/ON
	Average	11621	1349		90	3	97	2	Grenville, QC/ON
	STDEV	520	120		9		9	1	
S88-DL-9L	DL-9L a	107	144	4	8	34	3332	8	Grenville, QC/ON
S88-DL-9L	DL-9L b	189	246	5	1	30	3214	6	Grenville, QC/ON
S88-DL-9L	DL-9L c	107	112	6	6	34	3158	9	Grenville, QC/ON
	Average	134	167	5	5	32	3234	8	Grenville, QC/ON
	STDEV	47	69	1	4	2	89	1	
S88-DL-22B	DL-22B a	6515	175	8	48	39	1473	121	Grenville, QC/ON
S88-DL-22B	DL-22B b	3391	219		89	35	1423	100	Grenville, QC/ON
S88-DL-22B	DL-22B c	2034	110		46	48	1391	103	Grenville, QC/ON
	Average	3980	168	8	61	41	1429	108	Grenville, QC/ON
	STDEV	2298	55		24	7	41	11	
S88-DL-26A	DL-26A a	2436	194		29	40	2421	33	Grenville, QC/ON
S88-DL-26A	DL-26A b	5844	119		40	29	2319	28	Grenville, QC/ON
S88-DL-26A	DL-26A c	7279	101	0	44	32	2552	32	Grenville, QC/ON
	Average	5186	138	0	38	34	2430	31	Grenville, QC/ON
	STDEV	2488	49		8	6	117	3	
S88-DL-27C	DL-27C a	6960	146		5	39	42		Grenville, QC/ON
S88-DL-27C	DL-27C b	2982		3	7	29	138		Grenville, QC/ON
S88-DL-27C	DL-27C c	6643	4		7	21	26	2	Grenville, QC/ON
	Average	5528	75	3	6	30	69	2	Grenville, QC/ON
	STDEV	2211	100		1	9	60		
S88-DL-28A	DL-28A a	2731	145	9	24	28	1745	152	Grenville, QC/ON
S88-DL-28A	DL-28A b	2693	181	6	32	31	2243	126	Grenville, QC/ON
S88-DL-28A	DL-28A c	2212	140	4	38	38	1394	153	Grenville, QC/ON
	Average	2545	155	6	31	32	1794	144	Grenville, QC/ON
	STDEV	289	22	2	7	6	427	15	
S88-DL-30A	DL-30A a	1979	56		17	60	817		Grenville, QC/ON
S88-DL-30A	DL-30A b	1259	67		42	42	743	3	Grenville, QC/ON
S88-DL-30A	DL-30A c	2683	19	3	33	46	824	7	Grenville, QC/ON
	Average	1974	47	3	31	49	795	5	Grenville, QC/ON
	STDEV	712	25		13	9	45	3	

Sample No.	Analyse No.	Fe	Mn	Cu	Zn	Ga	Sr	Br	Location
S88-DL-36B	DL-36B a	10580	1542		65		385		Grenville, QC/ON
S88-DL-36B	DL-36B b	9313	1365		60		317		Grenville, QC/ON
S88-DL-36B	DL-36B c	7576	1045		47		327		Grenville, QC/ON
	Average	9156	1317	0	57	0	343	0	Grenville, QC/ON
	STDEV	1508	252		9		37		
S88-DL-45D	DL-45D a	2612	148	5	19	112	527	113	Grenville, QC/ON
S88-DL-45D	DL-45D b	1807	150	2	25	104	563	109	Grenville, QC/ON
S88-DL-45D	DL-45D c	5928	179	23	23	110	566	89	Grenville, QC/ON
	Average	3449	159	10	22	109	552	104	Grenville, QC/ON
	STDEV	2184	18	11	3	5	22	13	
S88-DL-60A	DL-60A a	1107	96		73	57	2893	79	Grenville, QC/ON
S88-DL-60A	DL-60A b	1469	61		65	48	2748	76	Grenville, QC/ON
S88-DL-60A	DL-60A c	7109	1830		19		2152	2	Grenville, QC/ON
	Average	3228	662		52	53	2598	53	Grenville, QC/ON
	STDEV	3366	1012		29	7	393	44	
S88-DL-61A	DL-61A a	306	155	7	19	32	4362	14	Grenville, QC/ON
S88-DL-61A	DL-61A b	684	998		2		2514	0	Grenville, QC/ON
S88-DL-61A	DL-61A c	749	176	10	11	21	4263	25	Grenville, QC/ON
	Average	580	443	9	11	27	3713	19	Grenville, QC/ON
	STDEV	239	481	3	8	8	1039	13	
S88-DL-62C-1	DL-62C-1 a	484	53		25	47	3915	77	Grenville, QC/ON
S88-DL-62C-1	DL-62C-1 b	448	147	4	33	61	3782	96	Grenville, QC/ON
S88-DL-62C-1	DL-62C-1 c	1740	79		60	68	2055	102	Grenville, QC/ON
	Average	891	93	5	39	59	3251	91	Grenville, QC/ON
	STDEV	736	48		18	11	1038	13	
S88-DL-62F-1	DL-62f-1 a	15963	1025		71		108	0	Grenville, QC/ON
S88-DL-62F-1	DL-62f-1 b	23950	1396	9	97		114		Grenville, QC/ON
S88-DL-62F-1	DL-62f-1 c	19971	1149		68		104	0	Grenville, QC/ON
	Average	19961	1190	9	79		109	0	Grenville, QC/ON
	STDEV	3994	189		16		5	0	
S88-DL-66E	DL-66E a	8646	197	36	24	39	2764	76	Grenville, QC/ON
S88-DL-66E	DL-66E b	5765	217		33	40	2658	78	Grenville, QC/ON
S88-DL-66E	DL-66E c	4738	222		39	44	2759	82	Grenville, QC/ON
	Average	6383	212	36	32	41	2727	79	Grenville, QC/ON
	STDEV	2026	13		7	2	60	3	
S88-DL-60G	60G-a	3183	1500		3		2365	4	Grenville, QC/ON
S88-DL-60G	60G-b	7251	2149		7		2898	7	Grenville, QC/ON
S88-DL-60G	60G-c	3009	122	6	76	51	3144	70	Grenville, QC/ON
	Average	4481	1257	6	29	51	2802	27	Grenville, QC/ON
	STDEV	2400	1036		41		398	37	

Sample No.	Analyse No.	Fe	Mn	Cu	Zn	Ga	Sr	Br	Location
S88-DL-70K	70ka	4782			47	22	1627	83	Grenville, QC/ON
S88-DL-70K	70k b	7385	195		62	33	2094	162	Grenville, QC/ON
S88-DL-70K	70k c	2191	93		50	37	1902	177	Grenville, QC/ON
S88-DL-70K	70k d	3311	223	7	39	35	1696	127	Grenville, QC/ON
	Average	4417	170	7	50	32	1830	155	Grenville, QC/ON
	STDEV	2245	68		9	7	211	42	
S88-DL-70M	70M a	2674	233		66	30	2540	71	Grenville, QC/ON
S88-DL-70M	70M b	1941	149		74	46	2839	58	Grenville, QC/ON
S88-DL-70M	70M c	1267	131		52	28	1940	57	Grenville, QC/ON
	Average	1961	171		64	35	2440	62	Grenville, QC/ON
	STDEV	704	54		12	10	458	8	
S88-DL-70N	70N a	2298	173	4	141	30	3220	94	Grenville, QC/ON
S88-DL-70N	70N b	640	92		45	38	3071	92	Grenville, QC/ON
S88-DL-70N	70N c	535	79		49	35	3413	92	Grenville, QC/ON
	Average	1158	115	4	78	34	3235	93	Grenville, QC/ON
	STDEV	989	51		54	4	172	1	
HD-55	HD-55 a	1824	225	0	226	57	323	121	Nickel Plate, BC
HD-55	HD-55 b	45475	1410	36	223	46	790	134	Nickel Plate, BC
	Average	23650	818	18	225	51	557	128	Nickel Plate, BC
	STDEV	30866	838	25	2	8	330	9	
GR-91-130	GR-91-130 a	2647	279		252	70	252	136	Nickel Plate, BC
GR-91-130	GR-91-130 b	2492	460	1	168	76	231	142	Nickel Plate, BC
GR-91-130	GR-91-130 c	1678	138	7	149	57	210	137	Nickel Plate, BC
	Average	2272	293	3	190	68	231	138	Nickel Plate, BC
	STDEV	521	161	4	55	10	21	4	

Appendix 5b EMPA Results of Scapolite (wt %)

Sample No.	Location	SiO_2	Al_2O_3	FeO[a]	MnO	CaO	SrO	BaO	Na_2O	K_2O	SO_3	Cl	Total
99-1-1	Tieshan, China	58.56	22.81	0.22	0.00	6.38	0.31	0.00	9.52	0.75	0.27	3.21	102.04
99-1-1	Tieshan, China	59.50	22.81	0.10	0.00	5.48	0.24	0.01	10.14	0.83	0.14	3.59	102.85
99-1-1	Tieshan, China	57.56	21.91	0.23	0.00	5.82	0.23	0.05	9.50	1.26	0.31	3.27	100.13
99-1-1	Tieshan, China	58.37	22.77	0.22	0.02	6.16	0.27	0.00	9.64	1.20	0.27	3.21	102.14
	Average	58.50	22.58	0.19	0.01	5.96	0.26	0.01	9.70	1.01	0.25	3.32	101.79
	STDEV	0.80	0.44	0.06	0.01	0.39	0.04	0.02	0.30	0.26	0.07	0.18	1.16
99-1-3	Tieshan, China	55.45	23.41	0.12	0.00	8.14	0.08	0.05	8.62	0.81	0.46	2.91	100.02
99-1-3	Tieshan, China	54.28	23.72	0.13	0.00	8.94	0.16	0.06	8.10	0.76	0.48	2.78	99.39
99-1-3	Tieshan, China	51.91	24.50	0.20	0.01	10.39	0.14	0.01	7.07	0.96	0.62	2.34	98.14
99-1-3	Tieshan, China	55.04	23.95	0.18	0.00	8.34	0.09	0.03	8.48	0.98	0.46	3.03	100.57
99-1-3	Tieshan, China	55.13	23.36	0.13	0.00	8.12	0.18	0.05	8.46	0.66	0.45	2.80	99.33
99-1-3	Tieshan, China	55.43	23.84	0.18	0.02	8.64	0.11	0.00	8.50	0.82	0.50	2.85	100.90
	Average	54.54	23.80	0.16	0.00	8.76	0.13	0.03	8.21	0.83	0.49	2.78	99.73
	STDEV	1.36	0.42	0.03	0.01	0.86	0.04	0.02	0.58	0.12	0.06	0.24	1.00
99-1-5	Tieshan, China	56.01	23.41	0.06	0.00	7.06	0.25	0.02	9.09	0.82	0.33	3.38	100.43
99-1-5	Tieshan, China	55.83	23.11	0.07	0.02	7.49	0.22	0.02	9.09	0.70	0.28	3.35	100.17
99-1-5	Tieshan, China	58.19	23.25	0.14	0.00	5.94	0.21	0.00	9.07	0.59	0.27	2.98	100.65
99-1-5	Tieshan, China	56.69	22.92	0.09	0.00	7.08	0.14	0.00	8.81	0.72	0.32	3.12	99.89
99-1-5	Tieshan, China	57.25	22.36	0.14	0.00	6.45	0.23	0.00	9.52	0.68	0.27	3.18	100.08
99-1-5	Tieshan, China	57.17	22.69	0.16	0.00	6.57	0.19	0.03	9.50	0.95	0.32	3.27	100.85
	Average	56.86	22.96	0.11	0.00	6.77	0.21	0.01	9.18	0.74	0.30	3.21	100.35
	STDEV	0.88	0.39	0.04	0.01	0.55	0.04	0.01	0.28	0.13	0.03	0.15	0.36
99-1-6	Tieshan, China	57.65	23.52	0.09	0.00	4.15	0.09	0.00	10.59	0.59	0.21	2.21	99.12
99-1-6	Tieshan, China	59.88	22.19	0.12	0.00	4.86	0.12	0.02	10.19	0.87	0.17	3.80	102.23
99-1-6	Tieshan, China	57.80	22.56	0.15	0.02	6.20	0.09	0.04	9.79	0.95	0.26	3.51	101.37
99-1-6	Tieshan, China	55.86	22.77	0.13	0.00	6.07	0.10	0.04	9.35	0.63	0.31	3.12	98.38

Sample No.	Location	SiO_2	Al_2O_3	FeO[a]	MnO	CaO	SrO	BaO	Na_2O	K_2O	SO_3	Cl	Total
99-1-6	Tieshan, China	60.03	22.10	0.16	0.00	4.82	0.19	0.07	10.22	0.81	0.29	3.85	102.53
99-1-6	Tieshan, China	57.42	22.77	0.12	0.00	6.59	0.15	0.07	9.79	0.75	0.32	3.50	101.48
99-1-6	Tieshan, China	57.92	22.81	0.12	0.00	6.36	0.12	0.04	9.53	0.74	0.29	3.39	101.32
	Average	58.08	22.67	0.13	0.00	5.58	0.12	0.04	9.92	0.76	0.27	3.34	100.92
	STDEV	1.45	0.47	0.02	0.01	0.95	0.04	0.03	0.43	0.13	0.05	0.55	1.56
99-1-7	Tieshan, China	55.09	23.93	0.10	0.04	8.70	0.17	0.00	8.52	0.75	0.46	2.92	100.68
99-1-7	Tieshan, China	57.85	22.75	0.06	0.00	6.06	0.19	0.00	9.44	0.61	0.31	3.53	100.81
99-1-7	Tieshan, China	59.65	21.46	0.16	0.00	4.76	0.11	0.00	9.38	0.75	0.19	3.30	99.74
	Average	57.53	22.71	0.11	0.01	6.51	0.15	0.00	9.11	0.71	0.32	3.25	100.41
	STDEV	2.30	1.24	0.05	0.02	2.01	0.04	0.00	0.51	0.08	0.14	0.31	0.58
99-1-9	Tieshan, China	51.95	24.32	0.09	0.00	11.11	0.09	0.01	6.95	0.63	0.50	2.22	97.86
99-1-9	Tieshan, China	52.35	25.09	0.10	0.00	11.10	0.06	0.07	7.09	0.88	0.57	2.10	99.42
99-1-9	Tieshan, China	52.95	24.18	0.08	0.05	10.76	0.12	0.00	7.16	0.66	0.45	2.33	98.75
99-1-9	Tieshan, China	52.71	24.45	0.08	0.00	10.61	0.05	0.02	7.30	0.60	0.53	2.21	98.57
99-1-9	Tieshan, China	53.07	24.22	0.08	0.00	10.43	0.04	0.03	7.23	0.97	0.46	2.28	98.81
99-1-9	Tieshan, China	52.96	24.63	0.08	0.06	10.67	0.11	0.01	7.05	0.74	0.51	2.23	99.03
99-1-9	Tieshan, China	51.11	24.57	0.10	0.06	11.75	0.06	0.00	6.62	0.69	0.56	2.00	97.52
	Average	52.44	24.49	0.09	0.02	10.92	0.07	0.02	7.06	0.74	0.51	2.20	98.57
	STDEV	0.71	0.31	0.01	0.03	0.44	0.03	0.02	0.22	0.14	0.04	0.11	0.66
99-1-12	Tieshan, China	55.65	23.51	0.10	0.00	8.19	0.12	0.02	8.85	0.67	0.37	2.82	100.30
99-1-12	Tieshan, China	55.11	23.97	0.08	0.01	8.70	0.19	0.01	8.35	0.65	0.38	2.82	100.27
99-1-12	Tieshan, China	54.60	23.47	0.10	0.05	8.45	0.14	0.00	8.13	0.94	0.39	2.78	99.03
99-1-12	Tieshan, China	54.55	23.21	0.12	0.00	8.52	0.12	0.00	8.20	1.09	0.40	2.78	98.99
99-1-12	Tieshan, China	55.03	23.83	0.13	0.00	8.71	0.17	0.00	8.64	0.64	0.37	2.67	100.19
99-1-12	Tieshan, China	55.22	23.18	0.18	0.01	8.01	0.19	0.06	9.00	0.85	0.48	3.08	100.26
99-1-12	Tieshan, China	54.71	23.45	0.14	0.00	7.85	0.14	0.00	8.79	0.90	0.48	3.07	99.53
	Average	54.98	23.52	0.12	0.01	8.35	0.15	0.01	8.57	0.82	0.41	2.86	99.80
	STDEV	0.39	0.29	0.03	0.02	0.34	0.03	0.02	0.34	0.17	0.05	0.16	0.60

Sample No.	Location	SiO_2	Al_2O_3	FeO[a]	MnO	CaO	SrO	BaO	Na_2O	K_2O	SO_3	Cl	Total
99-1-13	Tieshan, China	55.12	23.37	0.08	0.00	8.49	0.10	0.02	8.51	0.76	0.29	2.88	99.62
99-1-13	Tieshan, China	55.14	23.72	0.11	0.04	8.50	0.12	0.07	8.56	0.82	0.28	2.83	100.20
99-1-13	Tieshan, China	59.21	22.21	0.17	0.00	5.57	0.19	0.03	9.86	0.92	0.21	3.73	102.10
99-1-13	Tieshan, China	60.07	22.23	0.18	0.02	4.91	0.14	0.10	10.23	0.97	0.27	3.81	102.92
99-1-13	Tieshan, China	60.09	22.96	0.14	0.00	5.46	0.16	0.07	9.77	0.85	0.23	3.78	103.50
99-1-13	Tieshan, China	54.36	23.97	0.09	0.04	8.80	0.13	0.07	8.41	0.62	0.26	2.76	99.52
99-1-13	Tieshan, China	54.62	23.77	0.10	0.00	8.86	0.10	0.00	8.56	0.64	0.34	2.77	99.75
	Average	56.94	23.18	0.12	0.02	7.23	0.14	0.05	9.13	0.80	0.27	3.22	101.09
	STDEV	2.69	0.73	0.04	0.02	1.81	0.03	0.04	0.79	0.13	0.04	0.52	1.70
99-1-14	Tieshan, China	54.51	23.87	0.11	0.00	9.47	0.13	0.00	7.76	0.60	0.36	2.53	99.33
99-1-14	Tieshan, China	54.03	24.16	0.14	0.00	9.38	0.12	0.00	8.00	0.68	0.36	2.48	99.36
99-1-14	Tieshan, China	54.90	23.75	0.11	0.00	8.02	0.14	0.00	8.45	0.80	0.72	3.02	99.89
99-1-14	Tieshan, China	55.23	22.67	0.15	0.00	6.70	0.13	0.03	8.76	0.89	0.38	3.37	98.30
99-1-14	Tieshan, China	54.79	23.73	0.12	0.00	8.63	0.13	0.00	8.37	0.78	0.33	2.72	99.60
99-1-14	Tieshan, China	54.88	23.78	0.10	0.00	9.27	0.10	0.00	8.02	0.00	0.31	2.64	99.11
99-1-14	Tieshan, China	55.63	23.63	0.11	0.00	7.90	0.16	0.04	8.87	0.68	0.34	3.00	100.36
	Average	54.85	23.66	0.12	0.00	8.48	0.13	0.01	8.32	0.63	0.40	2.82	99.42
	STDEV	0.51	0.47	0.02	0.00	1.01	0.02	0.02	0.41	0.29	0.14	0.32	0.65
99-1-15	Tieshan, China	55.94	23.44	0.14	0.00	7.48	0.19	0.00	8.85	0.67	0.53	3.24	100.48
99-1-15	Tieshan, China	55.60	23.70	0.13	0.00	7.69	0.15	0.00	9.00	0.67	0.42	3.22	100.58
99-1-15	Tieshan, China	55.89	23.53	0.13	0.00	7.70	0.10	0.02	8.86	0.68	0.52	3.17	100.60
99-1-15	Tieshan, China	56.23	23.88	0.17	0.00	8.01	0.13	0.00	8.95	0.61	0.62	3.11	101.72
99-1-15	Tieshan, China	54.96	24.31	0.11	0.01	9.22	0.13	0.06	7.99	0.57	0.92	2.75	101.02
99-1-15	Tieshan, China	57.06	23.32	0.22	0.00	7.17	0.07	0.00	9.64	0.70	0.56	3.37	102.10
99-1-15	Tieshan, China	53.42	23.97	0.13	0.00	9.17	0.12	0.00	7.10	0.71	0.56	2.52	97.70
	Average	55.59	23.74	0.15	0.00	8.06	0.13	0.01	8.63	0.66	0.59	3.05	100.60
	STDEV	1.15	0.34	0.04	0.01	0.81	0.04	0.02	0.83	0.05	0.16	0.31	1.42
99-1-16	Tieshan, China	58.49	22.90	0.18	0.00	5.67	0.06	0.01	9.89	0.84	0.42	3.82	102.30
99-1-16	Tieshan, China	58.13	22.77	0.17	0.00	5.54	0.12	0.01	9.97	0.96	0.42	3.66	101.76

Sample No.	Location	SiO_2	Al_2O_3	FeO[a]	MnO	CaO	SrO	BaO	Na_2O	K_2O	SO_3	Cl	Total
99-1-16	Tieshan, China	57.98	22.50	0.17	0.02	6.01	0.10	0.00	9.43	1.32	0.36	3.55	101.43
99-1-16	Tieshan, China	57.31	22.82	0.20	0.00	5.98	0.12	0.00	9.36	1.36	0.38	3.69	101.22
99-1-16	Tieshan, China	60.42	22.27	0.15	0.04	4.68	0.06	0.02	10.35	1.00	0.24	3.92	103.15
99-1-16	Tieshan, China	59.02	22.17	0.21	0.00	5.30	0.11	0.00	9.98	1.21	0.28	3.69	101.96
99-1-16	Tieshan, China	58.65	22.86	0.15	0.02	5.91	0.08	0.01	8.63	0.84	0.36	3.69	101.19
	Average	58.57	22.61	0.18	0.01	5.58	0.09	0.01	9.66	1.08	0.35	3.72	101.86
	STDEV	0.98	0.30	0.02	0.02	0.47	0.03	0.01	0.57	0.22	0.07	0.12	0.70
99-1-17	Tieshan, China	57.09	22.40	0.11	0.00	6.36	0.13	0.01	9.69	0.83	0.23	3.46	100.30
99-1-17	Tieshan, China	58.64	23.19	0.14	0.00	5.90	0.15	0.00	10.05	0.79	0.21	3.49	102.57
99-1-17	Tieshan, China	58.49	23.14	0.16	0.00	6.23	0.10	0.05	9.52	0.79	0.31	3.48	102.27
99-1-17	Tieshan, China	57.59	22.89	0.07	0.00	6.37	0.15	0.00	9.63	0.76	0.28	3.53	101.28
99-1-17	Tieshan, China	57.28	22.91	0.17	0.04	6.40	0.12	0.00	9.79	0.71	0.29	3.47	101.18
99-1-17	Tieshan, China	57.57	22.45	0.16	0.00	6.56	0.15	0.04	9.54	0.77	0.27	3.52	101.03
	Average	57.78	22.83	0.14	0.01	6.30	0.13	0.02	9.70	0.78	0.26	3.49	101.44
	STDEV	0.64	0.34	0.04	0.02	0.22	0.02	0.02	0.20	0.04	0.04	0.03	0.84
99-1-19	Tieshan, China	56.03	23.58	0.16	0.07	7.88	0.14	0.06	8.59	0.67	0.35	2.92	100.44
99-1-19	Tieshan, China	55.49	23.69	0.12	0.00	7.86	0.06	0.07	8.58	0.77	0.28	3.18	100.09
99-1-19.	Tieshan, China	55.70	23.56	0.08	0.02	8.11	0.22	0.00	8.46	0.92	0.40	2.75	100.20
99-1-19	Tieshan, China	55.64	23.68	0.14	0.00	8.38	0.15	0.07	8.53	0.86	0.45	2.77	100.67
99-1-19	Tieshan, China	56.19	24.05	0.14	0.01	7.66	0.17	0.00	8.84	0.69	0.40	2.96	101.12
99-1-19	Tieshan, China	56.92	23.27	0.12	0.00	7.37	0.14	0.03	8.76	0.70	0.29	3.15	100.74
	Average	56.00	23.64	0.13	0.02	7.88	0.15	0.04	8.63	0.77	0.36	2.95	100.54
	STDEV	0.52	0.25	0.03	0.03	0.35	0.05	0.03	0.14	0.10	0.07	0.18	0.38
99-1-20	Tieshan, China	54.36	23.65	0.11	0.00	8.73	0.12	0.00	8.42	0.82	0.32	2.78	99.31
99-1-20	Tieshan, China	53.77	24.07	0.14	0.01	8.94	0.04	0.09	8.16	0.86	0.34	2.86	99.29
99-1-20	Tieshan, China	54.62	23.79	0.19	0.00	8.76	0.08	0.02	8.43	0.74	0.38	2.79	99.81
99-1-20	Tieshan, China	55.26	23.25	0.18	0.02	8.01	0.11	0.00	8.86	0.80	0.36	3.08	99.94
99-1-20.	Tieshan, China	54.21	23.49	0.06	0.04	7.64	0.12	0.00	8.60	0.78	0.34	3.02	98.30
99-1-20	Tieshan, China	54.66	23.63	0.11	0.00	8.69	0.13	0.00	8.28	0.75	0.34	2.87	99.46

Sample No.	Location	SiO_2	Al_2O_3	FeO[a]	MnO	CaO	SrO	BaO	Na_2O	K_2O	SO_3	Cl	Total
99-1-20	Tieshan, China	58.53	22.68	0.12	0.02	6.28	0.08	0.00	9.53	0.89	0.19	3.37	101.69
99-1-20.	Tieshan, China	57.38	22.75	0.20	0.01	6.27	0.10	0.05	9.37	0.86	0.19	3.31	100.48
	Average	55.35	23.41	0.14	0.01	7.92	0.10	0.02	8.71	0.81	0.31	3.01	99.79
	STDEV	1.69	0.49	0.05	0.01	1.10	0.03	0.03	0.51	0.06	0.08	0.23	0.99
99-1-21	Tieshan, China	53.80	24.13	0.14	0.06	9.42	0.13	0.04	7.88	0.74	0.54	2.70	99.55
99-1-21	Tieshan, China	61.57	21.61	0.15	0.00	4.53	0.12	0.00	10.18	0.73	0.16	3.83	102.89
99-1-21	Tieshan, China	57.16	23.29	0.09	0.00	6.67	0.07	0.00	9.69	0.91	0.23	3.32	101.43
99-1-21	Tieshan, China	56.87	22.42	0.11	0.04	6.70	0.11	0.03	9.20	0.89	0.22	3.28	99.88
99-1-21	Tieshan, China	52.74	23.47	0.09	0.00	8.83	0.12	0.00	8.19	0.68	0.40	2.72	97.25
99-1-21	Tieshan, China	52.24	24.41	0.05	0.02	10.80	0.14	0.00	6.97	0.63	0.51	2.17	97.94
99-1-21	Tieshan, China	55.36	23.49	0.09	0.00	8.13	0.13	0.00	8.51	0.66	0.32	2.87	99.55
	Average	55.68	23.26	0.10	0.02	7.87	0.12	0.01	8.66	0.75	0.34	2.98	99.78
	STDEV	3.23	0.97	0.03	0.02	2.08	0.02	0.02	1.11	0.11	0.15	0.54	1.93
99-1-22	Tieshan, China	55.59	23.08	0.16	0.00	7.03	0.21	0.03	8.78	1.09	0.29	3.12	99.38
99-1-22	Tieshan, China	55.98	22.57	0.14	0.00	7.06	0.19	0.06	8.85	1.16	0.32	3.05	99.38
99-1-22	Tieshan, China	57.48	22.93	0.12	0.01	6.41	0.15	0.08	9.39	0.96	0.26	3.18	100.98
99-1-22	Tieshan, China	56.58	23.57	0.17	0.00	7.27	0.16	0.00	9.15	0.61	0.27	3.09	100.88
99-1-22	Tieshan, China	54.61	23.13	0.11	0.00	8.05	0.16	0.03	8.40	0.73	0.30	2.87	98.41
99-1-22	Tieshan, China	56.97	22.87	0.09	0.00	6.90	0.20	0.03	9.46	0.84	0.38	3.19	100.94
	Average	56.20	23.03	0.13	0.00	7.12	0.18	0.04	9.01	0.90	0.30	3.08	100.00
	STDEV	1.03	0.33	0.03	0.00	0.54	0.02	0.03	0.40	0.21	0.04	0.12	1.09
H-2	Tieshan, China	51.70	22.03	0.11	0.02	8.25	0.09	0.01	8.43	0.66	0.36	2.59	94.25
H-2	Tieshan, China	55.32	23.96	0.14	0.00	8.93	0.11	0.02	8.41	0.66	0.36	2.78	100.68
H-2	Tieshan, China	54.96	23.14	0.10	0.00	8.82	0.07	0.04	8.11	0.64	0.34	2.74	98.97
H-2	Tieshan, China	55.19	23.97	0.05	0.04	8.98	0.10	0.05	8.15	0.66	0.37	2.80	100.37
H-2	Tieshan, China	58.82	25.38	0.06	0.00	7.13	0.14	0.06	7.06	0.13	0.01	0.01	98.80
H-2	Tieshan, China	58.65	26.49	0.07	0.06	7.44	0.15	0.01	7.17	0.03	0.00	0.01	100.07
H-2	Tieshan, China	55.20	23.94	0.13	0.02	8.17	0.12	0.00	8.68	0.73	0.55	2.98	100.52
	Average	55.69	24.13	0.10	0.02	8.25	0.11	0.03	8.00	0.50	0.29	1.99	99.09
	STDEV	2.44	1.45	0.03	0.02	0.73	0.03	0.02	0.64	0.29	0.20	1.36	2.26

Sample No.	Location	SiO_2	Al_2O_3	FeO[a]	MnO	CaO	SrO	BaO	Na_2O	K_2O	SO_3	Cl	Total
S88-DL-22B	Grenville, QC/ON	52.73	24.55	0.12	0.05	10.89	0.10	0.00	6.91	1.14	0.19	2.09	98.79
S88-DL-22B	Grenville, QC/ON	53.45	24.57	0.05	0.01	10.48	0.16	0.00	7.25	1.12	0.30	2.22	99.61
S88-DL-22B	Grenville, QC/ON	51.78	24.59	0.17	0.00	11.40	0.13	0.08	6.52	0.92	0.17	1.98	97.74
S88-DL-22B	Grenville, QC/ON	52.03	24.22	0.04	0.02	11.43	0.15	0.00	6.88	0.97	0.19	1.92	97.84
S88-DL-22B	Grenville, QC/ON	52.93	24.22	0.08	0.00	11.07	0.10	0.00	6.74	1.14	0.14	2.03	98.45
S88-DL-22B	Grenville, QC/ON	53.24	24.28	0.08	0.00	11.16	0.12	0.02	6.94	1.18	0.11	2.10	99.22
	Average	52.69	24.41	0.09	0.01	11.07	0.12	0.02	6.87	1.08	0.18	2.06	98.61
	STDEV	0.66	0.18	0.05	0.02	0.35	0.02	0.03	0.24	0.11	0.06	0.11	0.75
S88-DL-26A	Grenville, QC/ON	50.70	24.60	0.07	0.01	12.79	0.17	0.00	5.86	0.46	1.58	1.20	97.43
S88-DL-26A	Grenville, QC/ON	50.46	24.93	0.05	0.00	12.88	0.13	0.00	5.91	0.44	1.47	1.22	97.51
S88-DL-26A	Grenville, QC/ON	50.87	24.40	0.04	0.02	12.79	0.16	0.00	6.02	0.43	1.46	1.20	97.39
S88-DL-26A	Grenville, QC/ON	50.66	24.78	0.07	0.01	12.73	0.15	0.00	5.93	0.50	1.43	1.23	97.48
S88-DL-26A	Grenville, QC/ON	50.52	24.31	0.05	0.00	13.12	0.10	0.03	5.87	0.32	1.55	1.11	96.98
S88-DL-26A	Grenville, QC/ON	50.29	24.35	0.07	0.00	13.05	0.20	0.00	5.94	0.49	1.64	1.15	97.18
S88-DL-26A	Grenville, QC/ON	51.18	24.96	0.01	0.00	12.65	0.18	0.00	6.44	0.45	1.45	1.21	98.54
	Average	50.67	24.62	0.05	0.01	12.86	0.16	0.00	6.00	0.44	1.51	1.19	97.50
	STDEV	0.29	0.28	0.02	0.01	0.17	0.03	0.01	0.20	0.06	0.08	0.04	0.50
S88-DL-28A	Grenville, QC/ON	50.86	25.29	0.09	0.00	12.21	0.14	0.06	6.29	0.97	1.01	1.68	98.60
S88-DL-28A	Grenville, QC/ON	51.21	24.96	0.05	0.00	12.08	0.16	0.01	6.05	1.04	0.97	1.61	98.11
S88-DL-28A	Grenville, QC/ON	51.36	25.01	0.05	0.00	12.06	0.09	0.07	6.43	0.88	1.06	1.64	98.66
S88-DL-28A	Grenville, QC/ON	49.89	24.94	0.14	0.06	12.47	0.11	0.08	6.03	0.91	1.19	1.53	97.34
S88-DL-28A	Grenville, QC/ON	50.74	24.93	0.07	0.00	12.43	0.13	0.04	5.88	0.85	1.37	1.48	97.93
S88-DL-28A	Grenville, QC/ON	50.99	24.77	0.02	0.00	11.86	0.20	0.03	6.38	0.93	1.04	1.83	98.06
S88-DL-28A	Grenville, QC/ON	51.53	24.41	0.00	0.08	11.66	0.23	0.06	6.59	0.97	1.26	1.79	98.59
S88-DL-28A	Grenville, QC/ON	52.35	24.93	0.06	0.00	11.19	0.22	0.05	6.82	1.03	1.30	1.92	99.86
S88-DL-28A	Grenville, QC/ON	51.00	24.77	0.09	0.00	12.02	0.12	0.02	6.29	0.91	1.12	1.68	98.02
	Average	51.10	24.89	0.06	0.02	12.00	0.16	0.05	6.31	0.94	1.15	1.68	98.35
	STDEV	0.66	0.24	0.04	0.03	0.40	0.05	0.03	0.29	0.06	0.14	0.14	0.70

Sample No.	Location	SiO_2	Al_2O_3	FeO[a]	MnO	CaO	SrO	BaO	Na_2O	K_2O	SO_3	Cl	Total
S88-DL-30A	Grenville, QC/ON	50.30	24.67	0.09	0.00	11.68	0.18	0.06	5.09	1.05	1.17	1.34	95.62
S88-DL-30A	Grenville, QC/ON	57.05	23.64	0.05	0.03	6.60	0.27	0.01	8.06	0.42	0.45	2.19	98.77
	Average	**53.68**	**24.16**	**0.07**	**0.01**	**9.14**	**0.23**	**0.03**	**6.58**	**0.74**	**0.81**	**1.76**	**97.20**
	STDEV	4.77	0.73	0.02	0.02	3.59	0.06	0.04	2.10	0.44	0.51	0.60	2.23
	Grenville, QC/ON												
S88-DL-60A	Grenville, QC/ON	51.89	24.95	0.07	0.02	12.19	0.23	0.00	6.20	1.02	1.10	1.63	99.32
S88-DL-60A	Grenville, QC/ON	52.20	24.12	0.09	0.00	11.76	0.27	0.00	6.30	0.92	1.14	1.70	98.49
S88-DL-60A	Grenville, QC/ON	52.92	24.21	0.07	0.01	11.03	0.22	0.02	6.82	1.03	0.88	1.97	99.18
S88-DL-60A	Grenville, QC/ON	52.68	23.88	0.08	0.00	10.76	0.22	0.00	6.95	1.11	0.91	2.00	98.60
S88-DL-60A	Grenville, QC/ON	52.97	24.35	0.04	0.00	10.64	0.25	0.01	7.28	0.94	1.15	1.92	99.56
S88-DL-60A	Grenville, QC/ON	51.70	23.94	0.14	0.00	11.41	0.29	0.00	6.51	1.02	1.20	1.73	97.95
	Average	52.39	24.24	0.08	0.01	11.30	0.25	0.00	6.68	1.01	1.07	1.83	98.85
	STDEV	0.54	0.39	0.03	0.01	0.60	0.03	0.01	0.41	0.07	0.14	0.16	0.61
S88-DL-60G	Grenville, QC/ON	53.16	24.20	0.11	0.04	10.64	0.24	0.00	6.65	0.92	1.10	1.92	98.97
S88-DL-60G	Grenville, QC/ON	53.80	24.01	0.07	0.00	10.62	0.27	0.11	7.05	1.05	1.12	2.02	100.13
	Average	53.48	24.11	0.09	0.02	10.63	0.26	0.06	6.85	0.98	1.11	1.97	99.55
	STDEV	0.45	0.13	0.03	0.03	0.01	0.02	0.08	0.28	0.09	0.01	0.07	0.82
S88-DL-61A	Grenville, QC/ON	42.87	29.02	0.00	0.00	19.29	0.34	0.02	2.39	0.07	1.76	0.20	95.94
S88-DL-61A	Grenville, QC/ON	42.40	28.96	0.01	0.00	19.00	0.38	0.00	2.28	0.04	1.86	0.20	95.14
S88-DL-61A	Grenville, QC/ON	42.68	28.83	0.03	0.04	19.28	0.44	0.01	2.29	0.02	1.80	0.20	95.62
S88-DL-61A	Grenville, QC/ON	42.94	29.43	0.03	0.01	19.13	0.37	0.00	2.32	0.07	1.98	0.15	96.42
S88-DL-61A	Grenville, QC/ON	42.08	28.93	0.03	0.00	19.30	0.40	0.02	2.26	0.10	1.87	0.17	95.15
S88-DL-61A	Grenville, QC/ON	45.96	30.76	0.04	0.00	18.30	0.41	0.01	2.86	0.11	1.43	0.29	100.17
	Average	43.16	29.32	0.02	0.01	19.05	0.39	0.01	2.40	0.07	1.78	0.20	96.41
	STDEV	1.41	0.73	0.01	0.01	0.39	0.03	0.01	0.23	0.03	0.19	0.05	1.91
S88-DL-62C	Grenville, QC/ON	51.15	25.01	0.03	0.01	12.37	0.30	0.04	6.24	0.55	1.10	1.59	98.38
S88-DL-62C	Grenville, QC/ON	51.59	24.69	0.04	0.00	12.13	0.34	0.00	6.40	0.54	1.17	1.73	98.64
S88-DL-62C	Grenville, QC/ON	50.73	25.09	0.03	0.00	12.75	0.23	0.00	5.99	0.66	0.97	1.47	97.92

Sample No.	Location	SiO_2	Al_2O_3	FeO[a]	MnO	CaO	SrO	BaO	Na_2O	K_2O	SO_3	Cl	Total
S88-DL-62C	Grenville, QC/ON	50.75	24.87	0.05	0.04	12.46	0.30	0.07	6.19	0.61	1.00	1.57	97.89
S88-DL-62C	Grenville, QC/ON	50.16	25.22	0.01	0.02	13.06	0.23	0.01	5.72	0.65	1.25	1.37	97.70
S88-DL-62C	Grenville, QC/ON	49.30	25.44	0.04	0.00	13.44	0.31	0.04	5.44	0.48	1.26	1.28	97.03
	Average	50.61	25.05	0.03	0.01	12.70	0.29	0.03	6.00	0.58	1.12	1.50	97.93
	STDEV	0.80	0.26	0.01	0.01	0.48	0.04	0.03	0.36	0.07	0.12	0.16	0.56
S88-DL-66E	Grenville, QC/ON	56.93	23.20	0.05	0.02	8.17	0.21	0.00	8.79	0.80	0.72	2.65	101.53
S88-DL-66E	Grenville, QC/ON	56.55	22.86	0.08	0.01	8.13	0.22	0.00	8.30	0.88	0.76	2.55	100.35
S88-DL-66E	Grenville, QC/ON	57.79	23.78	0.11	0.00	8.05	0.26	0.05	8.36	0.61	0.70	2.63	102.34
S88-DL-66E	Grenville, QC/ON	57.42	23.31	0.12	0.00	7.69	0.23	0.03	8.57	0.57	0.69	2.65	101.27
S88-DL-66E	Grenville, QC/ON	57.53	23.44	0.07	0.04	8.01	0.23	0.00	8.88	0.69	0.64	2.67	102.20
S88-DL-66E	Grenville, QC/ON	57.88	23.21	0.05	0.00	7.84	0.25	0.04	8.92	0.72	0.68	2.62	102.22
	Average	57.35	23.30	0.08	0.01	7.98	0.23	0.02	8.64	0.71	0.70	2.63	101.65
	STDEV	0.52	0.30	0.03	0.02	0.18	0.02	0.02	0.27	0.12	0.04	0.04	0.77
s88-DL-66H	Grenville, QC/ON	54.93	23.12	0.12	0.00	8.78	0.27	0.05	7.94	1.01	0.48	2.41	99.10
S88-DL-66H	Grenville, QC/ON	55.24	23.04	0.09	0.00	8.75	0.25	0.03	7.85	0.94	0.50	2.46	99.15
S88-DL-66H	Grenville, QC/ON	54.63	23.20	0.11	0.02	8.74	0.21	0.05	8.02	1.12	0.45	2.47	99.03
S88-DL-66H	Grenville, QC/ON	52.86	22.05	2.57	0.02	8.02	0.18	0.00	7.38	0.90	0.51	2.33	96.83
S88-DL-66H	Grenville, QC/ON	54.85	23.57	0.13	0.02	8.87	0.18	0.00	7.79	1.02	0.66	2.38	99.46
S88-DL-66H	Grenville, QC/ON	53.91	23.23	0.14	0.03	8.67	0.24	0.00	7.74	1.02	0.51	2.45	97.94
S88-DL-66H	Grenville, QC/ON	54.88	23.26	0.13	0.08	8.77	0.17	0.01	8.08	1.02	0.51	2.48	99.39
S88-DL-66H	Grenville, QC/ON	54.44	23.36	0.11	0.00	8.69	0.24	0.00	7.87	0.95	0.56	2.45	98.66
S88-DL-66H	Grenville, QC/ON	54.52	22.77	0.21	0.00	8.56	0.22	0.00	7.95	1.11	0.44	2.46	98.23
S88-DL-66H	Grenville, QC/ON	55.35	23.40	0.14	0.01	8.76	0.14	0.00	8.16	0.87	0.65	2.46	99.94
S88-DL-66H	Grenville, QC/ON	54.55	23.22	0.13	0.02	8.76	0.27	0.03	7.78	1.07	0.54	2.50	98.87
	Average	54.56	23.11	0.35	0.02	8.67	0.21	0.02	7.87	1.00	0.53	2.44	98.78
	STDEV	0.69	0.41	0.74	0.02	0.23	0.04	0.02	0.21	0.08	0.07	0.05	0.86
S88-DL-70M	Grenville, QC/ON	47.41	26.60	0.07	0.00	15.49	0.29	0.03	4.18	0.64	1.64	0.89	97.25
S88-DL-70M	Grenville, QC/ON	47.41	26.38	0.04	0.01	15.39	0.34	0.00	4.21	0.64	1.75	0.83	97.00
S88-DL-70M	Grenville, QC/ON	49.78	25.76	0.07	0.00	13.69	0.21	0.00	5.14	0.88	1.58	1.18	98.30

Sample No.	Location	SiO_2	Al_2O_3	FeO[a]	MnO	CaO	SrO	BaO	Na_2O	K_2O	SO_3	Cl	Total
S88-DL-70M	Grenville, QC/ON	49.09	25.85	0.04	0.00	14.04	0.31	0.00	5.18	0.66	1.41	1.15	97.73
S88-DL-70M	Grenville, QC/ON	48.47	25.68	0.09	0.01	13.86	0.28	0.00	5.12	0.44	1.36	1.27	96.57
	Average	48.43	26.05	0.06	0.00	14.49	0.29	0.01	4.77	0.65	1.55	1.06	97.37
	STDEV	1.04	0.41	0.02	0.01	0.87	0.05	0.02	0.52	0.15	0.16	0.19	0.67
S88-DL-70K	Grenville, QC/ON	49.75	25.61	0.05	0.01	13.43	0.13	0.08	5.46	0.71	1.50	1.28	98.01
S88-DL-70K	Grenville, QC/ON	50.06	25.03	0.04	0.03	13.55	0.18	0.00	5.45	0.80	1.43	1.33	97.90
S88-DL-70K	Grenville, QC/ON	51.63	24.51	0.06	0.00	11.46	0.26	0.00	6.50	0.81	1.26	1.73	98.22
S88-DL-70K	Grenville, QC/ON	53.43	24.35	0.07	0.00	10.15	0.25	0.00	7.63	0.84	0.80	2.33	99.85
S88-DL-70K	Grenville, QC/ON	49.73	25.41	0.08	0.00	13.65	0.21	0.03	5.44	0.54	1.50	1.20	97.80
S88-DL-70K	Grenville, QC/ON	50.09	25.34	0.05	0.00	13.67	0.18	0.00	5.44	0.63	1.66	1.28	98.35
	Average	50.78	25.04	0.06	0.01	12.65	0.20	0.02	5.99	0.72	1.36	1.53	98.36
	STDEV	1.48	0.51	0.01	0.01	1.49	0.05	0.03	0.91	0.12	0.30	0.43	0.76
S88-DL-70N	Grenville, QC/ON	48.78	25.35	0.00	0.04	14.39	0.32	0.00	5.07	0.77	1.64	1.14	97.51
S88-DL-70N	Grenville, QC/ON	48.57	25.67	0.00	0.00	14.18	0.33	0.00	5.15	0.75	1.73	1.19	97.57
S88-DL-70N	Grenville, QC/ON	47.70	26.72	0.07	0.04	15.51	0.24	0.00	4.40	0.60	1.68	0.86	97.83
S88-DL-70N	Grenville, QC/ON	47.11	25.64	0.03	0.05	14.71	0.14	0.00	4.53	0.65	1.59	0.94	95.39
S88-DL-70N	Grenville, QC/ON	47.51	26.76	0.06	0.00	15.36	0.18	0.00	4.38	0.73	1.74	0.95	97.68
S88-DL-70N	Grenville, QC/ON	47.66	26.18	0.06	0.00	14.96	0.21	0.00	4.53	0.72	1.68	0.93	96.93
	Average	47.89	26.05	0.04	0.02	14.85	0.24	0.00	4.68	0.70	1.68	1.00	97.15
	STDEV	0.65	0.60	0.03	0.02	0.53	0.08	0.00	0.34	0.06	0.06	0.13	0.92
S88-DL-450	Grenville, QC/ON	58.40	22.48	0.01	0.01	7.22	0.05	0.06	8.46	1.03	0.00	3.23	100.94
S88-DL-450	Grenville, QC/ON	59.89	22.76	0.02	0.00	6.32	0.02	0.01	9.17	1.00	0.01	3.36	102.57
S88-DL-450	Grenville, QC/ON	58.07	22.24	0.39	0.03	6.29	0.04	0.05	9.03	0.85	0.04	3.23	100.26
S88-DL-450	Grenville, QC/ON	58.06	22.35	0.02	0.01	7.39	0.00	0.00	8.34	1.16	0.02	3.10	100.45
S88-DL-450	Grenville, QC/ON	58.89	22.56	0.00	0.02	6.63	0.02	0.02	9.13	0.97	0.00	3.39	101.62
S88-DL-450	Grenville, QC/ON	59.84	22.46	0.01	0.03	6.11	0.05	0.01	9.18	1.03	0.00	3.28	101.99
S88-DL-450	Grenville, QC/ON	58.79	22.39	0.00	0.02	6.88	0.03	0.01	8.63	1.07	0.00	3.28	101.10
	Average	58.85	22.46	0.06	0.02	6.69	0.03	0.02	8.85	1.02	0.01	3.27	101.28
	STDEV	0.76	0.17	0.15	0.01	0.49	0.02	0.02	0.36	0.10	0.02	0.10	0.83

Sample No.	Location	SiO_2	Al_2O_3	FeO[a]	MnO	CaO	SrO	BaO	Na_2O	K_2O	SO_3	Cl	Total
HD-55	Nickel Plate, BC	50.25	24.38	0.09	0.00	13.27	0.05	0.03	5.42	0.78	0.00	1.40	95.67
HD-55	Nickel Plate, BC	50.20	25.21	0.11	0.00	13.57	0.06	0.00	5.37	0.70	0.05	1.38	96.66
HD-55	Nickel Plate, BC	51.28	24.58	0.08	0.03	11.93	0.06	0.03	6.29	0.96	0.00	2.01	97.24
HD-55	Nickel Plate, BC	50.75	25.08	0.07	0.00	12.16	0.05	0.03	6.20	0.94	0.00	1.92	97.20
HD-55	Nickel Plate, BC	49.62	25.17	0.07	0.00	13.20	0.08	0.01	5.54	0.81	0.05	1.62	96.16
	Average	50.42	24.88	0.08	0.01	12.83	0.06	0.02	5.76	0.84	0.02	1.66	96.59
	STDEV	0.63	0.38	0.02	0.01	0.73	0.01	0.01	0.44	0.11	0.03	0.29	0.68
GR-91-130	Nickel Plate, BC	49.07	26.03	0.14	0.08	14.04	0.02	0.00	5.13	0.76	0.01	1.39	96.67
GR-91-130	Nickel Plate, BC	49.62	25.01	0.17	0.02	13.44	0.03	0.00	5.25	0.77	0.01	1.47	95.79
GR-91-130	Nickel Plate, BC	48.76	25.74	0.12	0.00	14.35	0.00	0.01	4.75	0.77	0.04	1.31	95.84
GR-91-130	Nickel Plate, BC	48.08	26.16	0.16	0.01	14.93	0.00	0.00	4.49	0.73	0.00	1.25	95.81
GR-91-130	Nickel Plate, BC	49.55	25.10	0.11	0.00	13.57	0.00	0.00	5.39	0.81	0.01	1.51	96.05
GR-91-130	Nickel Plate, BC	49.24	25.56	0.08	0.02	13.85	0.00	0.00	5.26	0.78	0.00	1.37	96.16
GR-91-130	Nickel Plate, BC	50.21	25.64	0.13	0.01	13.46	0.01	0.00	5.41	0.52	0.01	1.47	96.89
GR-91-130	Nickel Plate, BC	51.43	24.75	0.12	0.02	12.98	0.01	0.00	5.77	0.56	0.02	1.43	97.09
	Average	**49.50**	**25.50**	**0.13**	**0.02**	**13.83**	**0.01**	**0.00**	**5.18**	**0.71**	**0.01**	**1.40**	**96.29**
	STDEV	1.00	0.50	0.03	0.02	0.61	0.01	0.00	0.40	0.11	0.01	0.09	0.52